

Transmembrane Model Peptides – A Powerful Tool to Investigate Protein-Lipid Interactions

**Transmembraan Modelpeptiden – een Krachtig
Instrument voor Onderzoek aan Eiwit-Lipide Interacties**
(met een samenvatting in het Nederlands)

Proefschrift

ter verkrijging van de graad van doctor aan de Universiteit Utrecht
op gezag van de rector magnificus, prof. dr. J.C. Stoof, ingevolge het
besluit van het college voor promoties in het openbaar te verdedigen
op maandag 24 augustus 2009 des ochtends te 10.30 uur

door

Andrea Holt

geboren op 4 augustus 1977 te Lingen, Duitsland

Promotor: Prof. dr. J. A. Killian

The research described in this Ph.D. thesis has been supported by a Marie Curie Early Stage Research Training Fellowship for 36 months from the European Community's Sixth Framework Program under contract number Biomem-MEST-CT 2004-007931.

*The outcome of any serious research can only be to make
two questions grow where only one grew before.*

Thorstein Bunde Veblen (1857-1929)

ISBN: 978-90-393-5112-3

Drukwerk: Ridderprint Offsetdrukkerij BV, Ridderkerk

Table of Contents

	Abstract of the Thesis	1
Chapter 1	General Introduction	3
Chapter 2	Is there a Preferential Interaction between Cholesterol and Tryptophan Residues in Membrane Proteins?	27
Chapter 3	Orientation and Dynamical Properties of a Transmembrane Model Peptide as Studied by a New Strategy Based on Solid-State NMR Methods	49
Chapter 4	Tilt and Rotation Angles of a Transmembrane Model Peptide as Studied by Fluorescence Spectroscopy	71
Chapter 5	Influence of Hydrophobic Mismatch and Peptide Composition on the Diffusion of Transmembrane Model Peptides	93
Chapter 6	Summarizing Discussion	109
	Nederlandstalige samenvatting	119
	Zusammenfassung in deutscher Sprache	121
	Dankwoord – Danksagung – Acknowledgments	123
	List of Publications	126
	Curriculum Vitae	127
	Abbreviations	129

Abstract of the Thesis

The function of membrane proteins depends in many cases on the properties of the surrounding lipid environment, including the membrane thickness, fluidity and composition. Still, it is not completely understood how membrane proteins are influenced by the membrane, which is for a large part due to the difficulties to study these hydrophobic systems. This has initiated the use of synthetic transmembrane model peptides mimicking transmembrane segments of membrane proteins, which offers several advantages. The structure of these model peptides can be varied systematically and any labels needed for investigation using biophysical techniques can be easily incorporated during peptide synthesis. Such designed transmembrane peptides are increasingly being used for the systematic investigations on how membrane properties and peptide composition influence the orientation and dynamics of transmembrane segments. Frequently used model peptides are the WALP and KALP peptides, consisting of a hydrophobic stretch of alternating leucines and alanines flanked at both ends by a pair of tryptophans and lysines, respectively.

Chapter 1 contains a general introduction to biomembranes, the use and design of transmembrane model peptides and an overview of results obtained using model peptides. In **chapter 2**, a study aiming at elucidation of the nature of the previously suggested preferential interaction between tryptophans and cholesterol is presented. ^2H NMR (Nuclear Magnetic Resonance) and FRET (Förster resonance energy transfer) experiments on WALP containing bilayers indicated no general tendency for a preferential interaction between cholesterol and tryptophans located at the membrane interface, which is an important finding for understanding the processes involved in the partitioning behavior of membrane proteins to cholesterol-rich liquid-ordered domains in membranes. In **chapter 3**, a new approach for the investigation of the orientation and dynamics of transmembrane peptides based on well-established solid-state NMR techniques called MACADAM (Multiple Anisotropic Constraints and Dynamic Analysis of Membrane peptides) is described. Using this advanced approach a much larger tilt angle was determined for the WALP peptide as compared to the previously employed ^2H NMR experiments in combination with GALA (Geometric Analysis of Labeled Alanines). The evident conclusion is that peptide dynamics has to be taken into account explicitly when interpreting NMR results for determination of the orientation of transmembrane peptides. In **chapter 4**, an alternative, complementary approach based on steady-state fluorescence experiments was used to determine the orientation of transmembrane peptides in bilayers with different thickness. The results were consistent with those obtained in **chapter 3** by NMR methods. In addition, these studies showed only incomplete compensation for the changes in bilayer thickness by helix tilting, which is in agreement with previous findings that other mismatch adaptations occur simultaneously. **Chapter 5** reports on the results of a fluorescence correlation spectroscopy study using model peptides with different hydrophobic lengths, flanking residues and hydrophobic stretches incorporated into different types of bilayers are described. A model explaining the differences observed in diffusion behavior of the model peptides especially for large hydrophobic mismatch was developed. **Chapter 6** contains a summarizing discussion that places the results obtained in this thesis into a broader context and indicates future perspectives for the use of transmembrane model peptides.

Chapter 1

General Introduction

Biological membranes are diverse and complex systems

The formation of membranes is one of the most important steps in evolution of life. Cells of all kingdoms of life are enclosed by a more or less complex membrane, which functions as a semi-permeable barrier that protects the cell, allows uptake of nutrients and keeps essential molecules inside the cell. In addition, many cell types contain organelles that are also surrounded by membranes. Here, membranes create specialized compartments which for example store nutrients, separate waste and harmful molecules, or create special chemical environments.

Probably the most important feature of biological membranes is the selective permeability to solutes. Only few solutes can freely pass the membrane, others can only pass with assistance of transporters and channels, whereas some cannot pass the membrane at all. The barrier properties of membranes are mainly due to the particular arrangement of the major membrane building blocks, the lipids. Biological membranes are almost exclusively bilayers composed of two opposed leaflets of lipids which are amphipathic molecules with hydrophilic headgroups and hydrophobic tails. Upon contact with water the hydrophobic tails cluster together and the hydrophilic headgroups face the aqueous phase. For most lipid species this leads to spontaneous formation of lipid bilayers. In these lipid bilayers membrane proteins with diverse functions and structures are embedded that carry out specialized functions. These proteins will be discussed later.

Biological membranes contain a large variety of different lipids with greatly varying abundance and properties. The majority of the lipids in biological membranes are phospholipids, which can be divided into phosphoglycerides and sphingolipids (see Figure 1A and 1B for representative examples). In some types of eukaryotic membranes also cholesterol, a steroid alcohol, is present in major amounts (Figure 1C). Phosphoglycerides contain a phosphorylated glycerol, and the different types of phosphoglycerides are distinguished by the moiety attached to the phosphate, e.g. phosphatidylcholine (PC), phosphatidylethanolamine (PE), or phosphatidic acid (PA). Sphingolipids contain a phosphorylated sphingosine which is an amino alcohol with a long, mono-unsaturated hydrocarbon chain, and the head group almost exclusively consists of a phosphorylcholine group (sphingomyelin).

In addition to the variation in headgroups also differences in the hydrophobic tails are present. In phosphoglycerides fatty acids are attached to the glycerol by esterification, and in sphingolipids the fatty acid is attached via an amide bond. These fatty acids can differ in length and usually contain an even number of carbons, typically between 14 and 24. These hydrocarbon chains can be fully saturated or include one or more unsaturated bonds (compare Figure 1A), mostly in *cis*-configuration. Other lipids present in the membrane, but usually at lower amounts, are for example ceramide, the simplest sphingosine-derived lipid, and the greatly varying members of the class of glycolipids which are sphingosine-derived lipids with one or more sugars attached.

Already in the early days of membrane research it was recognized that biological membranes are very dynamical structures. According to the Fluid-Mosaic model of Singer and Nicholson dating 1972, a biological membrane can be considered as a two-dimensional liquid where all lipids and integral membrane proteins diffuse more or less freely along the membrane plane [1]. From time to time lipids may also traffic to the opposite leaflet of the membrane by a process called lipid flip-flop. The diversity in components in biological

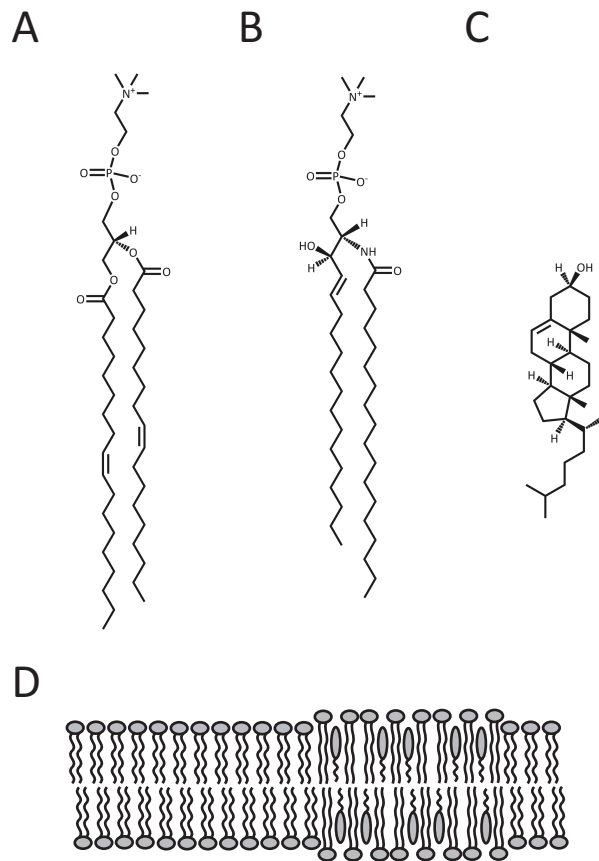


Figure 1: Chemical structures of typical membrane lipids: (A) Phosphatidylcholine, (B) Sphingomyelin, and (C) Cholesterol. (D) Schematic drawing of domain formation in membranes. The thinner liquid-disordered domains contain mainly lipids with unsaturated hydrocarbon chains, and the cholesterol-rich liquid-ordered domains contain predominantly saturated (sphingo)lipids.

membranes forms the basis for lateral heterogeneity in biological membranes. Combined with the dynamic character of most membrane components it feeds the formation of membrane microdomains with lipid compositions different from that of the bulk membrane and of which the size and the lifetime may vary. The material properties of such membrane microdomains can differ in hydrophobic thickness, curvature and rigidity. Membrane microdomains enriched in cholesterol, so-called lipid rafts, are liquid-ordered membrane domains that are more rigid than the bulk membrane (see Figure 1D). There is much evidence now that such lipid rafts have functional importance to cells (reviewed in [2-4]) and, in addition, different subtypes of lipid rafts have been described and identified [5-8].

Cholesterol, a lipid with special properties

The obvious importance of lipid rafts has initiated many studies on the basic principles underlying the formation of membrane microdomains, and in the past decades, model membrane systems including cholesterol have been investigated in great detail. Cholesterol contains a complex 4-ring system with an attached branched hydrocarbon chain and has a small hydroxyl head group. Mixtures of cholesterol and saturated phospholipids were found to phase separate into a cholesterol-rich liquid-ordered phase and a liquid-disordered phase with low cholesterol content. Nowadays, many of such binary and also ternary lipid systems have been characterized with different biophysical techniques (an extensive summary up to the year 2002 can be found in [9]) in order to learn about their phase behavior and to understand general principles underlying phase separation. From these studies it is well known that addition of cholesterol increases the lipid acyl chain order and reduces the area per lipid head group, as shown with experimental methods [10-13] and supported by molecular dynamics (MD) simulations [14-16].

Ternary lipid systems composed of cholesterol, unsaturated phospholipids and sphingomyelin are now frequently used to model lipid rafts (reviewed in [17]). Such model systems were extensively studied to better understand the process of formation of lipid rafts. Domain formation can be promoted by favorable interactions among the different types of lipids present in the membrane [18], but also proteins were suggested to facilitate domain formation by preferential interaction with certain lipid species. For example, the presence of an α -helical apolipoprotein AI mimetic peptide in a cholesterol containing phospholipid bilayer was found to promote the formation of cholesterol-rich domains by interacting with phospholipids and stabilizing domains devoid of cholesterol [19]. However, knowledge on the processes and mechanisms involved in membrane microdomain formation, and how membrane proteins and peptides sense and respond to lipid micro-environments is still relatively sparse.

Membrane proteins - essential for cell survival

During evolution, transmembrane proteins with highly specific and often essential functions for the cell emerged. They fulfill cellular key functions such as signaling, cell-cell recognition, cell adhesion, enzymatic activities, transduction of energy, and nutrient/waste transport across the membrane. The transport functions provided by membrane proteins are indispensable for the cell since intact membranes are virtually impermeable to most soluble molecules due to the hydrophobic core of the lipid bilayer. Small molecules like water can pass the hydrophobic barrier to a small extent, mainly driven by (large) osmotic gradients. In presence of intact membranes, large-rate transfer of water, transport of all ions and most of the larger molecules can only take place through channels or via active transport by (co)transporters.

In such a way, membrane proteins provide a directed transport of nutrients into the cell and of waste molecules to the outside, maintaining a healthy chemical environment inside the cells and the organelles. Absence, failure or impaired function of membrane proteins can have serious implications for the cell as was shown in many deletion and mutation studies. In fact, many diseases can be linked to malfunctioning of membrane proteins. In order to learn how membrane proteins work and also to better understand the reasons for (mal)functioning, knowledge on the structure of membrane proteins and their integration into the membrane is crucially needed.

Membrane proteins interact with the lipid environment

Often membrane proteins are assembled from several subunits to build a functional unit. It was suggested that membrane microdomains may favor such specific protein-protein interactions by concentrating certain proteins in these microdomains while excluding others [2]. A recent analysis of bitopic membrane proteins, composed of a single transmembrane α -helix connecting two extra-membranous domains, showed that the transmembrane domains of such proteins were highly conserved compared to other parts of the protein [20]. In particular, one face of the transmembrane segment was found to be more conserved than the other, suggesting a participation in specific interactions. Such specific interactions may be modulated by the lipid microenvironment in vicinity to the transmembrane segments.

The outer hydrophobic regions of a multi-spanning transmembrane protein or of a protein complex are exposed to the lipids, which can influence the stability of membrane proteins. For example, stabilizing effects of the membrane have been observed for the tetrameric potassium channel KcsA, which was found to be more stable in the presence of anionic lipids [21]. In many cases, also the function of membrane proteins itself was shown to depend on properties of the membrane such as membrane fluidity and membrane thickness. Both properties are coupled to temperature and strongly depend on the length and degree of saturation of the hydrocarbon chains. At physiological temperatures biological membranes are generally in a fluid state, which is required for normal cell functioning. An example of a protein affected by membrane fluidity is the thermosensor protein DesK [22,23]. This integral membrane protein is part of the signaling cascade regulating fatty acid desaturation and initiates the production of lipids with higher level of unsaturation in case of cold-shocks, which helps the membrane to sustain its fluidity.

The membrane fluidity and thickness are also influenced by the sterol concentration in the membrane. The rigidity of the membrane increases with increasing sterol concentration due to the condensing effect of cholesterol on the lipid acyl chains. In particular, the effect of cholesterol on membrane fluidity is believed to affect the activity of some membrane proteins. For the cholecystokinin receptor it was found that the ligand-binding to the receptor was strongly dependent on the sterol concentration in the membrane [24]. In this case, the effect of different sterol species correlated well with their capacity to affect the membrane fluidity, indicating no specificity to the nature of sterol. However, in contrast to such unspecific effects, it is also possible that membrane proteins interact directly with sterols present in the membrane. The structurally related oxytocin receptor was found to exhibit specificity to the nature of the sterols present in the membrane, and showed highest ligand-binding in the presence of cholesterol and weaker binding for closely related sterols, suggesting a specific cholesterol-receptor interaction in this case [25,26]. The nature of interactions between cholesterol and membrane proteins is not elucidated yet. From several studies it was suggested that an interaction of cholesterol with specific protein side chains e.g. tryptophans might play a role [27-31].

Other membrane proteins can sense tensions in the membrane, and changes in the membrane tension can modulate the activity of these proteins. A well-studied example of such membrane proteins is the mechanosensitive channel MscL. These channels prevent bacterial cells from bursting in case of osmotic down-shocks as a result of water transport into the cell (reviewed in [32,33]). The regulation of MscL was shown to arise from changes in the lateral pressure of the membrane, which is mediated by hydrophobic coupling between the lipids and the hydrophobic segments of membrane protein, and results in the conformational changes needed to switch the channels to open state. The decrease in lateral pressure is accompanied with thinning of the membrane which may also affect the tilt angles of transmembrane segments of the protein.

Finally, bilayer thickness itself was shown to be an important determinant for the function of membrane proteins. Several reconstitution studies suggested a strong effect of the bilayer thickness on the activity of membrane proteins. For different ATPases, cytochrome c oxidase or melibiose permease the activity was found to highest for proteins reconstituted in bilayers with matching hydrophobic thickness [34-37]. Most probably, the activity of these membrane proteins is altered by small changes in the structure of the proteins, including changes in the tilt angle of transmembrane segments.

Functional importance of helix tilting in membrane proteins

By definition, membrane proteins need to undergo conformational changes to perform their function. These changes can include internal motion like turning, tilting or shifting of one or more α -helices or whole domains with respect to one another, (partial) folding/unfolding or adaptation of secondary structure elements, or simple reorientation of one or more amino acid residues. In addition, all these changes can be accompanied by a (partial) reorientation of the protein within the membrane. In case of MscL, bilayer deformation initiates major structural rearrangements. When switching to the open state, MscL undergoes a large concerted iris-like expansion combined with flattening of the whole channel (see Figure 2), which involves large reorientations of the transmembrane α -helices [38].

In other proteins, small changes in the orientation of one or more α -helices are sufficient to properly function. For sensory rhodopsin II a small outward tilting of TM6 (helix F) was observed [39], which initiates a 20-30° turning of helix TM2 of the neighboring transducer complex [40]. For the related bacteriorhodopsin an outward movement of TM6 (helix F) and a subsequent approach of TM7 (helix G) toward the proton channel were observed during the photo cycle [41]. For melibiose permease, a symporter coupling uphill transport of sugars and various other galactosides to the downhill transport of Na^+ , Li^+ and H^+ ions, changes in the average helix tilt were observed during substrate binding [42]. FTIR experiments on the reconstructed protein indicated an increase in average helix tilt of the putative 12 TM segment protein upon sodium binding and a subsequent decrease upon melibiose binding. However, high-resolution structures are needed to fully understand the structural changes required for functioning of these and other membrane proteins.

Orientation of transmembrane segments in membranes

The examples given above demonstrate the importance of the orientation of transmembrane segments for the function of membrane proteins. A recent empirical study reported an average tilt angle of $24 \pm 14^\circ$ for the transmembrane α -helices of polytopic membrane proteins based on 46 qualified high resolution structures available in 2006 [43], which agree well with earlier reported values of $22 \pm 12^\circ$ based on 15 structures in 2001 [44] and $21 \pm 10^\circ$ based on only two structures, bacteriorhodopsin and cytochrome c oxidase in 1997 [45]. The low number of high resolution structures available for membrane proteins is mainly due to the difficulties to grow crystals of these hydrophobic structures that are needed for structure elucidation using x-ray-crystallography, one of the standard techniques

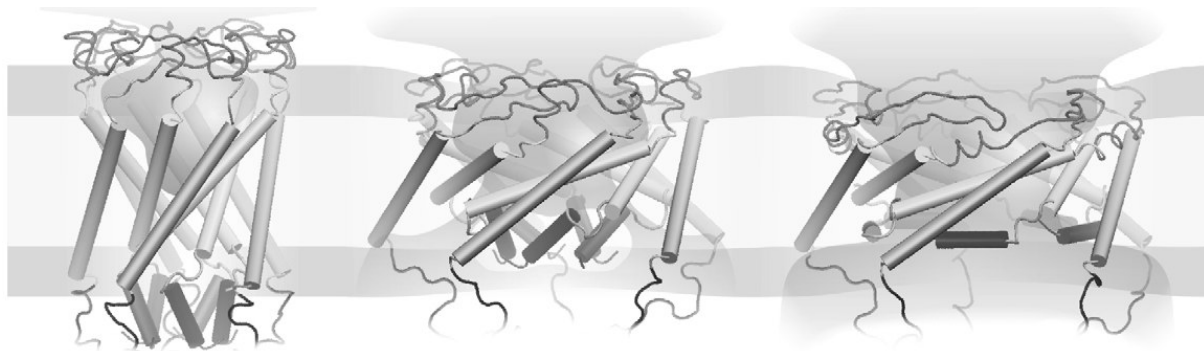


Figure 2: Gating transition of MscL (adapted from [33]).

for structure elucidation of soluble proteins. Alternative methods are used to study structural properties of membrane proteins, including solid-state NMR spectroscopy, EPR spectroscopy, CD spectroscopy, ATR-FTIR spectroscopy and Fluorescence spectroscopy. Using such alternative biophysical techniques, for several natural transmembrane peptides, most of which are believed to form oligomers in membranes, tilt angles of the transmembrane α -helices with respect to the membrane have been determined. These tilt angles were found to vary significantly.

From solid-state NMR measurements using the PISEMA (polarization inversion with spin exchange at magic angle) method, a tilt angle of 38° was reported for the influenza A M2 channel in di-C14:OPC [46], 26° for the membrane conformation of the major pVIII coat protein of fd filamentous bacteriophage in C16:0,C18:1PC/C16:0,C18:1PG (4:1) [47], and 13° for wild-type phospholamban in C16:0,C18:1PC [48]. For the channel-lining M2 segments from the d-subunit of the nicotinic acetylcholine receptor in di-C14:OPC a tilt angle of 12° was reported from PISEMA experiments [49] and a tilt angle of 14° from EPR studies [50]. For phospholemman in di-C14:OPC a tilt angle of 17° was found using ATR-FTIR spectroscopy on the full length protein [51], and a tilt angle of 7° was reported from NMR experiments on a phospholemman transmembrane region in di-C16:OPC [52]. Using fluorescence techniques, a tilt angle of 18° was determined for major coat protein from bacteriophage M13 in di-C18:1PC/di-C18:1PG (4:1) [53]. This variation in tilt angles raises questions about the determinants for the tilt of transmembrane helices. Is helix tilt an intrinsic property of transmembrane helices, or is the tilt imposed from the membrane, or a combination of both?

Importance of the peptide composition

The structure, and therefore the behavior and the orientation of transmembrane peptides in the membrane are determined by their sequence. Empirical analysis of the amino acid structure in putative transmembrane segments of α -helical single-span proteins showed a non-random distribution of amino acids in transmembrane segments [54,55]. The hydrophobic stretch is to a large percentage composed of hydrophobic residues like isoleucine, leucine, valine and alanine, with leucine being the most common residue. Putative helix initiating residues like proline, asparagine and serine were found to be enriched at the N-terminus of transmembrane segments. Aromatic residues like tryptophan and tyrosine as well as charged residues like lysine and arginine were found to have a positional preference for the interface region. In particular these residues at the interface can be expected to have a large influence on the orientation of transmembrane segments, because these interactions will be much more specific than those between hydrophobic amino acids in the lipid acyl chain region.

A common motif observed in many membrane proteins is a belt of aromatic residues located at the membrane-water interface; examples for this structural motif can be found in the α -helical potassium channel KcsA [56,57] (see Figure 3A) and the β -barrel maltoporin [58]. Interfacial tryptophans are believed to anchor membrane proteins in the membrane, where interaction with the surrounding lipids will help the proteins to adopt the proper orientation in the membrane. For free indole groups incorporated into phosphocholine membranes a bimodal indole distribution was observed, with the first group residing at the upper hydrocarbon chain/glycerol region of the lipid and the second near the choline group [59].

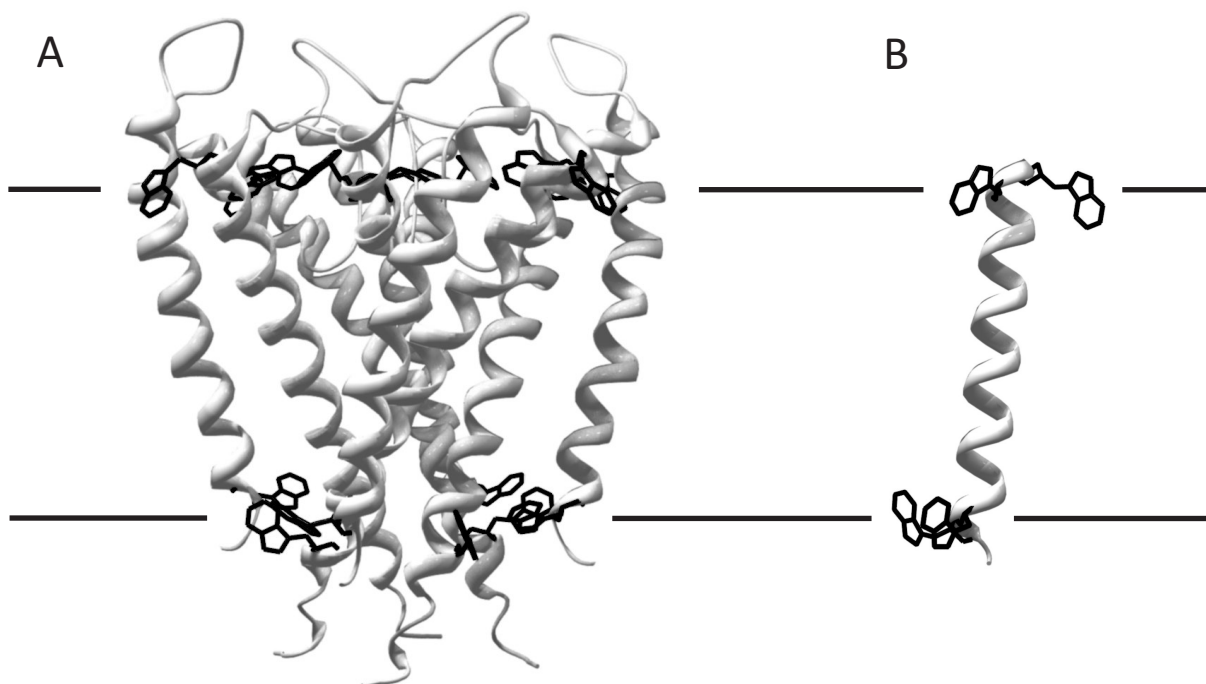


Figure 3: Structures of (A) the transmembrane parts of the potassium channel KcsA (PDB entry 1J95) and (B) the transmembrane model peptide WALP23, which is used to mimic transmembrane segments of membrane proteins; only tryptophans are shown with explicit side chains. This nicely illustrates the belt of aromatic residues present in KcsA.

From molecular modeling studies it was found that the tryptophan indole amide hydrogen atoms form stable hydrogen bonds to the phosphate oxygen of the phospholipid head groups, which may be another reason for the preferential location at the membrane interface [60]. However, another study proposed that dipole-dipole interactions and steric constraints in the membrane hydrocarbon region determine positioning and orientation of tryptophans, whereas hydrogen bonding and cation- π interactions with lipid head groups were thought to be less important [61].

Charged amino acids like lysines and arginines are another category of residues that is frequently found at the membrane-water interface. Indeed, belts of charged residues are present in KcsA and maltoporin, which are located more towards the aqueous phase with respect to the belts of aromatic residues on the two sides of the membrane [57,58], with positive charges mainly occurring at the side of biosynthetic insertion according to the positive-inside rule [62,63]. Like aromatic residues, charged residues are thought to anchor membrane proteins to the membrane interface. However, the long side chains in this case would allow a more flexible anchoring. For positively charged residues like lysine and arginine electrostatic protein-lipid interactions with anionic lipids can occur. More specific interactions also may occur, for example the formation of particularly favorable hydrogen bonds between the side chains of lysine and the phosphate of phosphatidic acid [64].

Use & Design of transmembrane model peptides

The structural elements characteristic for membrane proteins were used to design transmembrane model peptides. Such model peptides offer the advantages that their structure can be varied systematically and that labels can be incorporated easily during peptide synthesis. Furthermore, these synthetic peptides have proven exceptionally useful in

development and improvement of biophysical techniques to characterize membrane proteins and peptides [65,66]. Frequently used model peptides are the WALP (depicted in Figure 3B) and KALP peptides which are composed of a hydrophobic stretch of alternating leucines and alanines flanked at both ends by a pair of tryptophans and lysines, respectively. A summary of transmembrane model peptides used in literature is given in Table 1.

Such designed transmembrane peptides are increasingly being used to understand the basic principles for the organization of peptide/protein-lipid complexes [67-71]. An important parameter for the structural organization is the orientation of transmembrane segments within the membrane. Analysis of the tilt angle with respect to the membrane may yield an answer to the question to what extent the orientation of transmembrane segments is an intrinsic property or is being imposed from the membrane. WALP/KALP and WLP/KLP peptides have been investigated using ^2H NMR spectroscopy in combination with GALA (geometric analysis of labeled alanines), which yielded relatively small tilt angles ranging from 5-11° [72,73]. In a recent study, the very similar model peptide GWALP23 which is flanked with a single tryptophan at each end, was studied with different solid-state NMR methods, yielding comparable tilt angles of 12.6° from ^2H NMR experiments combined with GALA and 10.8° for PISEMA (polarization inversion with spin exchange at magic angle) experiments when incorporated into bilayers of di-C12:0PC [74]. The influence of the lipid environment on membrane proteins can be studied in more detail by analyzing the effects of hydrophobic mismatch on the tilt angles of transmembrane segments.

Hydrophobic mismatch as driving force for reorientation

Hydrophobic mismatch occurs if the hydrophobic length of the membrane protein does not match the hydrophobic thickness of the membrane. To be more specific, positive hydrophobic mismatch describes situations with too thin membranes, and negative mismatch situations with too thick membranes. It has been shown for a number of membrane proteins that their activity depends strongly on the hydrophobic thickness of the bilayer and is decreased in non-matching situation (for reviews see [75,76]). To relieve the mismatch situation in case of positive mismatch, a logical response seems adaptation of the tilt of the helix.

Table 1: Amino acid sequences of transmembrane model peptides.

Model peptide	Amino acid sequence	
WALP13/17/19/21/23/27/31	Acetyl-GWW(LA) _{3/5/6/7/8/10/12} LWWA-amide ^a	[27,72,73,77-92]
WALP16	Acetyl-GWW(LA) ₈ WWA-amide	[78,82-84,86,87,92]
WLP23	Acetyl-GWWL ₁₇ WWA-amide	[73,93]
KALP19/23/27/31	Acetyl-GKK(LA) _{6/8/10/12} LWWA-amide	[27,73,80,82,84,94]
KLP23	Acetyl-GKKL ₁₇ KKA-amide	[73,93]
GWALP23	Acetyl-GGALW(LA) ₆ LWLAGA-ethanolamine	[74]
KWALP23	Acetyl-GKALW(LA) ₆ LWLAKA-amide	[95]
pL _{12/14/16}	Acetyl-KKGL _{6/7/8} WL _{6/7/8} KKA-amide	[96]
p(LA) _{6/8}	Acetyl-KKG(LA) _{3/4} LW(LA) _{3/4} LKKA-amide	[96]
pL _{6/7/8} A _{6/7/8}	Acetyl-KKGL _{6/7/8} WA _{6/7/8} KKA-amide	[96]
WL22	Acetyl-WWL ₁₈ WW-amide	[97]
WA22	Acetyl-WWA ₁₈ WW-amide	[97]

^a In some cases ethanolamine is used instead

The response of transmembrane peptides to hydrophobic mismatch has been studied for a number of natural peptides and model peptides. From ^2H NMR experiments using different transmembrane model peptides a small but systematic increase in tilt angle was observed when inserting the peptides into lipid bilayers with decreasing chain length. For example, the tilt angle for WALP23 peptides increased from 5.2° in di-C14:OPC to 8.1° in di-C12:OPC, and for KALP23 peptides from 7.6° to 11.2° [72,73]. Considering geometrics, the change in tilt angle for these peptides does not compensate for the changes in bilayer thickness. Perhaps these transmembrane peptides tolerate hydrophobic mismatch within a certain range to preserve a possible intrinsic tilt. On the other hand, it was postulated that the tilt angles could have been underestimated due to extensive motional averaging on the time scale of the ^2H NMR experiments [91,93].

Yet similar results with incomplete compensation have been obtained for several natural peptides using techniques with much shorter time scales. For M13 coat protein, an increase from 18° in di-C20:1PC to 33° in di-14:1PC was determined from fluorescence experiments using IAEDANS labeled peptides [98]. For alamethicin, a peptide antibiotic building pores in cell membranes, a decrease in tilt angle from 23° in di-C10:OPC to 13° in di-C18:OPC was found from EPR experiments employing the TOAC-label [99]. For both natural peptides, the changes in tilt angle are insufficient to compensate for changes in bilayer thickness. These findings suggest that the tilt of a protein transmembrane segment may be a result of a combination of an intrinsic property and being imposed from the membrane.

However, there is also one example of a natural peptide for which full compensation for hydrophobic mismatch has been observed. Using PISEMA experiments, for virus protein U (Vpu) from HIV-1 incorporated into bilayers of ether-linked di-C10:OPC/di-C10:OPG (9:1) a tilt angle of 51° was found, which systematically decreased upon increasing the bilayer thickness to 18° in ether-linked di-C18:1PC/di-C18:1PG [100]. In this case, the change in tilt angle fully compensates for the change in bilayer thickness. Considering these large changes in tilt angle, we can clearly note that the membrane has an influence on the tilt of transmembrane segments. The reasons for the differences in adaptation to hydrophobic mismatch are not clear yet. The question remains of what determines the type of response to hydrophobic mismatch and what particular features of the transmembrane segment allow complete adaptation by tilting.

Alternative/additional mechanisms to adapt to mismatch

A complicating factor to the issue of adaptation is the consideration that a change in the tilt angle of transmembrane segments is not the only possible mechanism to compensate for hydrophobic mismatch. If such additional mechanisms occur, there is no reason to expect complete adaptation just by changing the tilt angle of the transmembrane segment. Figure 4 illustrates several possible adaptations for negative mismatch situations (top panel) and for positive mismatch situations (bottom panel). In case of a too thick bilayer, the lipid acyl chains in direct vicinity to the peptide could be squeezed, or in case of a too thin bilayer be stretched to accommodate the peptide. Another possible adaptation may be deformation of the peptide backbone, like formation of the extended 3_{10} -helix in too thick bilayers or formation of a π -helix in too thin bilayers. When considering peptide backbone deformation, another possible adaptation in case of positive hydrophobic mismatch could be kinking or flexing of the transmembrane helix. ^2H NMR results on WALP peptides and analogues

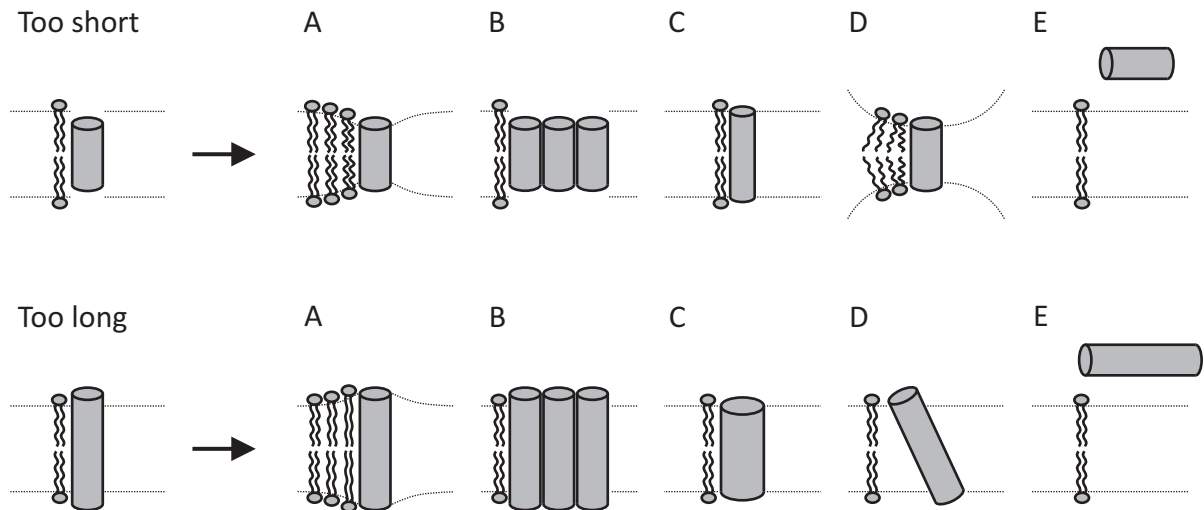


Figure 4: Schematic representation of possible adaptations in case of a too short transmembrane segment (top row) i.e. negative hydrophobic mismatch conditions: (A) acyl chain squeezing, (B) oligomerization, (C) backbone deformation/distortion, (D) non-lamellar phase formation, (E) exclusion from the membrane; and in case of a too long transmembrane segment (bottom row) i.e. positive hydrophobic mismatch conditions: (A) acyl chain stretching, (B) oligomerization, (C) backbone deformation/distortion, (D) tilting, (E) exclusion from the membrane (figure adapted from [101]).

thereof that were incorporated into too thin bilayers indicated a kink in the helix as response to the too thin bilayer [72,95]. A similar reaction was found for the TM1 segment of lactose permease, which was observed to flex in addition to tilting to satisfy the hydrophobic mismatch [102].

Another logical consequence to extreme mismatch conditions could be that at normal conditions transmembrane peptides are even excluded from the membrane. Such a relationship between the hydrophobic length of a transmembrane segment and the thickness of the bilayer required for transmembrane insertion of the peptide into the bilayers has been studied extensively using lysine-flanked model peptides of different hydrophobic lengths and compositions [96]. Peptide aggregation could be yet another possibility to alleviate the consequences of positive as well as negative hydrophobic mismatch. Indeed, this behavior was observed for WALP peptides in much too thin and in much too thick bilayers [89]. Thus, it is likely that WALP peptides show incomplete adaptation by tilting to compensate for hydrophobic mismatch. It is still far from clear at this moment what determines the extent of tilting of transmembrane segments, whether other adaptations occur and to what extent these occur.

Lateral diffusion in membranes

Hydrophobic mismatch can also influence lateral diffusion of proteins and lipids in membranes. Because of the many possible consequences of mismatch it may do so in different ways, which will be discussed below. Lateral diffusion is an important determinant since many biological processes rely on lateral diffusion of molecules in the membrane in order to find the “right” spot for proper functioning. Consequently, the inherent mobility of molecules in the membrane also renders membrane microdomains unstable in time and location, they may even disappear and reappear somewhere else. A recent MD simulation

study suggests that lateral diffusion in membranes is the result of collective flows, in which the movements of neighboring lipids were found to be strongly correlated with loosely defined clusters of lipids moving together [103].

The consequences of hydrophobic mismatch, which can include tilting and aggregation of peptides as well as stretching or disordering of surrounding lipids, are all expected to change the hydrodynamic radius of the diffusing molecules. Already in the 1970's, Saffman and Delbrück proposed that lateral diffusion of integral membrane proteins in bilayers follows a weak logarithmic i.e. $\ln(1/R)$ dependence on the hydrodynamic radius of the diffusing object [104]. A study summing up experimental data on protein diffusion from different sources proposed a stronger $1/R$ relationship between the hydrodynamic radius and the diffusion speed [105]. The apparent discrepancies between theory and experiment were suggested to be due to protein-induced membrane deformations [106].

From a study on the diffusion behavior of selectively aggregated transmembrane peptides different diffusion regimes were found, with monomers and dimers to diffuse according to the free area model, and larger aggregates according to the hydrodynamic continuum model [107]. In biological membranes, the diffusion speed is most probably influenced by many parameters, for example hydrophobic mismatch, preferential interactions between lipid and proteins, membrane fluidity and curvature. Diffusion in biological membranes crowded with proteins was found to be much slower compared to (artificial) membranes devoid of proteins [108]. Model peptides are ideal to investigate how lateral diffusion can be affected by mismatch and how different parameters may contribute.

Methods for the investigation of transmembrane peptides

Compared to the number of structures available for soluble proteins, the number of elucidated structures of membrane proteins is rather small, which is mostly due to the difficulties to study these hydrophobic molecules using conventional experimental techniques for structure elucidation of proteins. For this reason, alternative approaches were developed to study structural properties of membrane proteins, including approaches based on solid-state NMR (nuclear magnetic resonance) spectroscopy and fluorescence spectroscopy approaches. Below, the experimental techniques employed in this thesis are briefly introduced.

Solid-state NMR spectroscopy

Solid-state NMR spectroscopy is a versatile technique for the investigation of solid or solid-like materials, which is sensitive to the orientation and motion of molecules. It complements liquid-state NMR spectroscopy, which is used to investigate molecules in solution. The definition of solid materials can be extended to lipid bilayers in the sense of being two-dimensional quasi-solid materials.

^2H NMR spectroscopy

^2H NMR spectroscopy is a valuable tool for the investigation of biological molecules like lipids and proteins/peptides. In case of peptides, the deuterons required for ^2H NMR experiments can be selectively and easily introduced by using ^2H labeled amino acids during

peptide synthesis. ^2H NMR spectroscopy is a very sensitive NMR method since the fast intranuclear relaxation allows faster pulsing and therefore accelerated acquisition of ^2H NMR spectra compared to ^{13}C and ^{15}N NMR experiments. From the technical point of view, ^2H NMR experiments are more straightforward to perform and require less sophisticated equipment than ^{13}C and ^{15}N NMR techniques, which often employ CP (cross-polarization) methods to transfer magnetization from an abundant nucleus like ^1H to the nucleus in question. Cross-polarization enhances the sensitivity but also introduces issues with heat dissipation in the sample.

In powder samples, the size of the quadrupolar splitting of a C- ^2H bond depending on the angle ϑ of the bond with respect to the magnetic field is given by [109]

$$(1) \quad \Delta\nu_Q = \frac{3}{2} \left(\frac{e^2 q Q}{h} \right) \cdot \left\{ \frac{1}{2} (3 \cos^2 \vartheta - 1) + \eta \sin^2 \vartheta \cos(2\varphi) \right\},$$

where eq corresponds to the electric field gradient at the nucleus, Q is the nuclear quadrupolar momentum, h is Planck's constant, and η is the asymmetry parameter. The orientation of the principal axis frame of the interaction tensor is given by the Euler angle φ .

^2H NMR experiments allow determination of the quadrupolar splittings of the C- ^2H bonds (or C $_{\alpha}$ -C $_{\beta}$ bonds in case of methyl-deuterated alanines), which yields information on the direction of the nuclear interaction with respect to the magnetic field. Transmembrane peptides inserted into bilayers undergo fast motional averaging around the bilayer normal. In this case, the quadrupolar splittings yield information on the direction with respect to the axis of motional averaging, making interpretation of ^2H NMR spectra relatively straightforward. In the absence of such motional averaging one needs to use oriented bilayers to derive information on the orientation of the peptide. In either case, a set of quadrupolar splittings obtained from peptides with ^2H labeled alanines introduced in different positions can then be analyzed using the GALA (geometric analysis of labeled alanines) method, yielding the orientation of the transmembrane peptide with respect to the bilayer [72,73,85].

Magic Angle Spinning techniques

In liquid-state NMR spectroscopy, fast isotropic tumbling of the molecules solved in liquids leads to complete averaging of the line broadening arising from anisotropic interactions, which include chemical shift tensors and dipolar couplings. In solid-state NMR spectroscopy, which deals with "powdered samples", the anisotropic nuclear interactions are not averaged out and lead to broadened NMR spectra due to overlapping powder spectrums. It should be noted here, that these spectra actually contain an overload of information, which is almost impossible to interpret. An elegant solution to this problem is the MAS (magic angle spinning) technique.

Fast rotation of the whole sample at frequencies in the kHz range around an axis inclined at an angle of 54.7° with respect to the magnetic field, often referred to as the magic angle, leads to averaging of any second-rank tensor interaction to zero, and concentrates the NMR signal into peaks of narrow line width. The static spectral line shape is now simplified into a spectrum with a central peak and neighboring spinning side bands separated by the rotation frequency. When using low rotation frequencies the envelope over the sideband pattern

describes the shape of the static spectral pattern. The sideband patterns observed can be used for spinning side band analysis, yielding the anisotropy and asymmetry parameter of the nuclear interaction in question. REDOR (Rotational-echo double resonance) experiments can be used to reintroduce specific anisotropic interactions like dipolar couplings between ^{13}C and ^{15}N nuclei.

Similar to the quadrupolar splittings described above, experimental NMR parameters like chemical shift anisotropies and dipolar couplings can be used to retrieve structural information about transmembrane segments [110,111]. In addition, the isotropic chemical shift position obtained from MAS experiments can be used directly for determination of the secondary structure of proteins and peptides [112-114].

Fluorescence spectroscopy

Förster resonance energy transfer

FRET (Förster resonance energy transfer) is a non-radiative energy transfer mechanism based on a long-range dipole-dipole coupling of two chromophores. The energy transfer only occurs if there is a spectral overlap between the emission spectrum of the donor and the absorption spectrum of the acceptor (Figure 5).

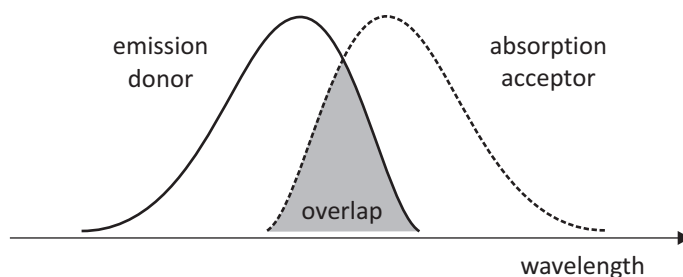


Figure 5: Schematic representation of the spectral overlap needed for Förster resonance energy transfer.

The efficiency E of the energy transfer strongly depends on the distance r between donor and acceptor

$$(2) \quad E = \frac{1}{1 + (r/R_0)^6},$$

where R_0 is the Förster distance that defines the distance at which 50% of the donor energy is transferred to the acceptor. The Förster distance R_0 depends on the quantum yield of the donor, the spectral overlap and the orientation of the donor dipole and the acceptor dipole with respect to each other. The theoretical Förster distance (in Å) can be calculated from [115]

$$(3) \quad R_0 = 0.2108 \left[\kappa^2 n^{-4} \Phi_D \int_0^\infty I_D(\lambda) \epsilon_A(\lambda) \lambda^4 d\lambda \right]^{\frac{1}{6}},$$

Where κ is the orientation factor for the dipole-dipole coupling of donor and acceptor, n is the refractive index of the medium, Φ_D is the quantum yield of the donor in absence of any acceptor, $I_D(\lambda)$ is the normalized emission spectrum of the donor depending on the wavelength λ , and $\epsilon_A(\lambda)$ is the molar absorption spectrum of the acceptor (in $\text{M}^{-1}\text{cm}^{-1}$).

FRET is a versatile tool for the investigation of membrane proteins, and can, for example, be used to probe whether two molecules are in close proximity, to measure distances between the two chromophores in the range of up to 10 nm, or to investigate the distribution of molecules in membranes. For the experiments only small amounts of fluorescently labeled peptides or lipids are required since fluorescence spectroscopy is a very sensitive technique, also allowing the use of relatively low peptide/lipid ratios of 1:500 or even lower. The preferred bilayer systems for this technique are LUVs (large unilamellar vesicles) which are sufficiently small to avoid or minimize scattering artifacts and large enough to avoid artifacts due to a high surface curvature, as may occur in Small Unilamellar vesicles usually prepared by sonication. LUVs are fairly easy to prepare by extrusion through inorganic membranes with suitable pore sizes and usually remain stable for a few hours. Similar to other fluorescence techniques, the experiments are usually performed on quite dilute samples which typically contain the labeled material at μM concentration.

Fluorescence correlation spectroscopy

FCS (fluorescence correlation spectroscopy) experiments can be used to determine diffusion times of fluorescent molecules. Figure 6 shows a schematic drawing of a FCS setup. Via a dichroic mirror a laser is focused to the sample through the objective of the confocal microscope. Fluorescent molecules located in the excitation volume (magnification in Figure 6, indicated by conic lines) are excited by the laser light. The fluorescence emission is collected from the objective and passes the dichroic mirror towards the detection system.

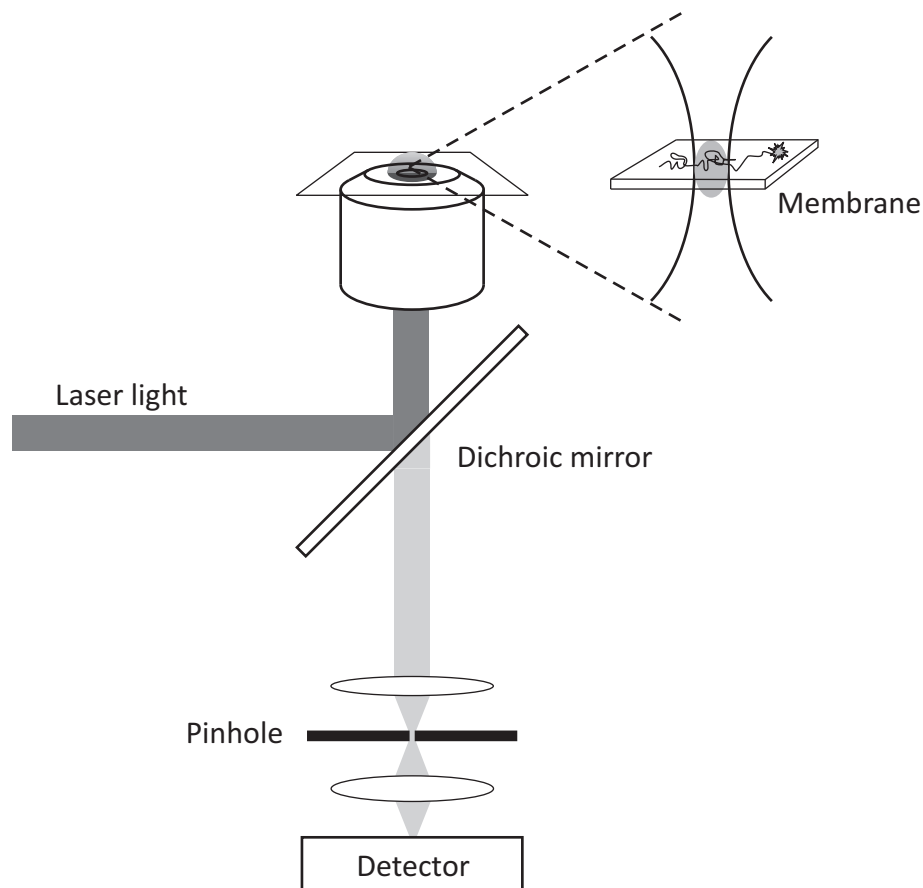


Figure 6: Schematic drawing of a confocal laser scanning setup used for fluorescence correlation spectroscopy.

Fluorescent molecules diffusing through the confocal volume cause temporal fluctuations in the fluorescence intensity (Figure 7, left panel). These fluctuations are statistically analyzed using the auto-correlation function

$$(4) \quad G(\tau) = \frac{\langle \delta F(t) \delta F(t + \tau) \rangle}{\langle F(t) \rangle^2},$$

where the square brackets denote the temporal average.

In a next step, the experimentally determined auto-correlation curves (Figure 7, right panel) are analyzed with using a theoretical model function to extract the parameters of interest. For the determination of diffusion coefficients of molecules in solution, the correlation function describing the Brownian diffusion through the detection volume is [116]

$$(5) \quad G(\tau) = \frac{1}{N} \left(1 + \frac{\tau}{\tau_D} \right)^{-1} \left(1 + \frac{\tau}{S^2 \tau_D} \right)^{-\frac{1}{2}},$$

where τ_D denote the diffusion time and N the number of particles in the detection volume $V_{eff} = S \pi^{\frac{3}{2}} d_{xy}^2$. The geometry of the elliptic detection volume is defined by the form factor $S = d_z / d_{xy}$ (see magnification in Figure 6).

FCS experiments can be used for the investigation of the diffusion of soluble molecules i.e. three-dimensional diffusion, as well as for membrane-bound molecules i.e. two-dimensional diffusion. For molecules confined to a lipid bilayer, the detection volume reduces to a “disc” of membrane and the correlation function reduces to

$$(6) \quad G(\tau) = \frac{1}{N} \left(1 + \frac{\tau}{\tau_D} \right)^{-1}.$$

Finally, the diffusion coefficient in membranes can then be calculated from

$$(7) \quad D = \frac{d_{xy}^2}{4 \tau_D}.$$

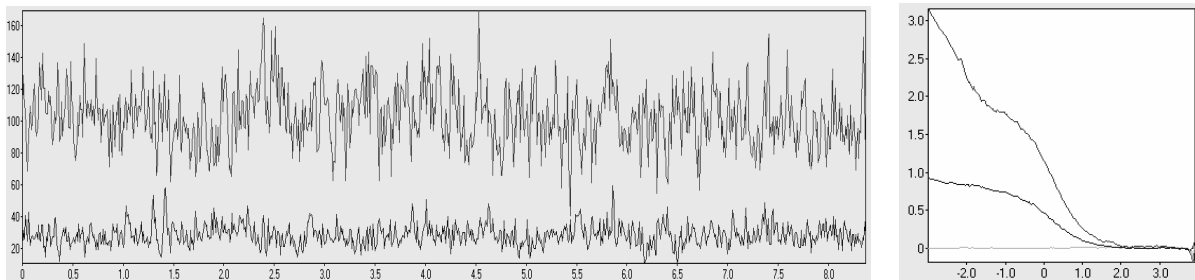


Figure 7: Left panel: Typical examples of fluorescence fluctuations recorded on Giant Unilamellar Vesicles (GUVs) containing fluorescently labeled transmembrane peptides and lipid markers. Right panel: Auto- and cross-correlation curves derived from the fluorescence fluctuating curves.

FCS is suitable for the investigation of the diffusion of membrane proteins/peptides in membranes with different compositions. The molecules in question need to be labeled with photo-stable fluorophores, for example the commercially available Alexa labels, to prevent photo-bleaching during the long exposures to intense laser light needed to record the fluorescence fluctuations. FCS experiments require only tiny amounts of labeled material, also allowing studies on membrane proteins with difficult expression and purification. Labeled molecules are typically present in the samples at nM concentrations to achieve labeled molecules in the range of 0.1 and 100 in the detection volume i.e. the focal volume.

FCS experiments require the use of GUVs (Giant Unilamellar Vesicles), also described as free-standing spherical lipid bilayers with diameters ranging from 10 - 100 μm that are visible under the microscope. GUVs can be obtained using well-established electroformation protocols [117,118]. These procedures usually provide large numbers of homogeneous liposomes and were recently adapted to allow the use of physiological salt concentrations [119]. Another possibility for the preparation of GUVs is spontaneous formation in the presence of charged phospholipids or the use of buffers that contain Mg^{2+} -ions.

Scope of the thesis

Protein-lipid interactions are important determinants for the function of membrane proteins and their integration into the membrane. Several indications have been found for a preferential interaction between interfacial tryptophans and membrane bound cholesterol. Such an interaction could place membrane proteins including interfacial tryptophans into cholesterol rich domains like lipid rafts, which could have functional importance. In **chapter 2**, we answered the question whether tryptophans located at the membrane interface have a general tendency to interact with membrane bound cholesterol. Here, the tryptophan-flanked model peptide WALP23 was used to mimic transmembrane segments of membrane proteins. Solid-state ^2H NMR experiments were performed to investigate the orientation and dynamics of interfacial tryptophans and cholesterol. For both molecules these parameters were found to be unaffected in the presence of the putative interaction partner. Additionally, FRET experiments were performed to obtain information on the distribution of peptides and cholesterol in the membrane. These experiments showed a random distribution of cholesterol in the membrane. Both findings suggest no preferential interaction between cholesterol and interfacial tryptophans.

Interfacial tryptophans were also suggested to anchor membrane proteins to the membrane interface. Such anchoring can be expected to play an important role for the orientation of membrane proteins in the membrane. From ^2H NMR experiments relatively small tilt angles were found for the tryptophan-flanked model peptide WALP23. Recent MD simulations on the same peptide indicated much larger tilt angles and it was suggested, that insufficient accounting for peptide motion in the model used for analysis of ^2H NMR data could result in too small tilt angles. In **chapter 3**, a new approach based on solid-state NMR techniques called MACADAM (Multiple Anisotropic Constraints and Dynamic Analysis of Membrane peptides) is presented, which allows the determination of orientational as well as dynamical parameters for transmembrane peptides. Indeed, important motions were observed for the WALP peptides and a much larger tilt angle was determined.

NMR methods for analysis of orientation of transmembrane segments are complicated by motional averaging. We therefore explored another method to derive tilt angles. Fluorescence techniques have the advantage of short time scales, sufficiently fast to neglect peptide motions. In **chapter 4**, we report on fluorescence experiments using the environment-sensitive fluorescent label BADAN to investigate the response of the WALP23 peptide to bilayers with different thickness and containing different amounts of cholesterol. The fluorescence data obtained was used to determine the orientation of the WALP23 peptide in the membrane. The tilt angles obtained from this fluorescence approach agree well with the results of the solid-state NMR approach presented in chapter 3. We observed only small changes in tilt angle as response to mismatch situations, which were not sufficient to compensate for the change in bilayer thickness. This is consistent with the occurrence of other additional mechanisms to adapt to hydrophobic mismatch, as reported in literature.

Finally, hydrophobic mismatch can influence the lateral diffusion of membrane proteins in the membrane. Model peptides allow systematic studies on the influence of the structure of transmembrane segments of membrane proteins on the lateral diffusion. In **chapter 5**, we present the results of a FCS study using model peptides with different hydrophobic lengths, flanking residues and hydrophobic stretch incorporated into different types of bilayers. A model was developed to explain the change in diffusion behavior of the model peptides especially for large hydrophobic mismatch.

References

1. Singer SJ and Nicolson GL (1972) The fluid mosaic model of the structure of cell membranes. *Science*, 175:720–731.
2. Simons K and Toomre D (2000) Lipid rafts and signal transduction. *Nat Rev Mol Cell Biol*, 1:31–39.
3. Edidin M (2003) The state of lipid rafts: from model membranes to cells. *Annu Rev Biophys Biomol Struct*, 32:257–283.
4. Hanzal-Bayer MF and Hancock JF (2007) Lipid rafts and membrane traffic. *FEBS Lett*, 581:2098–2104.
5. Zurzolo C, van Meer G, and Mayor S (2003) The order of rafts. *EMBO Rep*, 4:1117–1121.
6. Pike LJ (2003) Lipid rafts: bringing order to chaos. *J Lipid Res*, 44:655–667.
7. Pike LJ (2004) Lipid rafts: heterogeneity on the high seas. *Biochem J*, 378:281–292.
8. Asano A, Selvaraj V, Buttke DE, Nelson JL, Green KM, Evans JE, and Travis AJ (2009) Biochemical characterization of membrane fractions in murine sperm: identification of three distinct sub-types of membrane rafts. *J Cell Physiol*, 218:537–548.
9. Koynova R and Caffrey M (2002) An index of lipid phase diagrams. *Chem Phys Lipids*, 115:107–219.
10. Dufourc EJ, Parish EJ, Chitrakorn S, and Smith ICP (1984) Structural and dynamical details of cholesterol-lipid interaction as revealed by deuterium NMR. *Biochemistry*, 23:6062–6071.
11. Davies MA, Schuster HF, Brauner JW, and Mendelsohn R (1990) Effects of cholesterol on conformational disorder in dipalmitoylphosphatidylcholine bilayers. A quantitative IR study of the depth dependence. *Biochemistry*, 29:4368–4373.
12. Kurad D, Jeschke G, and Marsh D (2004) Lateral ordering of lipid chains in cholesterol-containing membranes: high-field spin-label EPR. *Biophys J*, 86:264–271.
13. Tiburu EK, Dave PC, and Lorigan GA (2004) Solid-state 2H NMR studies of the effects of cholesterol on the acyl chain dynamics of magnetically aligned phospholipid bilayers. *Magn Reson Chem*, 42:132–138.
14. Robinson AJ, Richards WG, Thomas PJ, and Hann MM (1995) Behavior of cholesterol and its effect on head group and chain conformations in lipid bilayers: a molecular dynamics study. *Biophys J*, 68:164–170.
15. Hofsaef C, Lindahl E, and Edholm O (2003) Molecular dynamics simulations of phospholipid bilayers with cholesterol. *Biophys J*, 84:2192–2206.
16. Martinez-Seara H, Róg T, Pasenkiewicz-Gierula M, Vattulainen I, Karttunen M, and Reigada R (2008) Interplay of unsaturated phospholipids and cholesterol in membranes: effect of the double-bond position. *Biophys J*, 95:3295–3305.
17. Goñi FM, Alonso A, Bagatolli LA, Brown RE, Marsh D, Prieto M, and Thewalt JL (2008) Phase diagrams of lipid mixtures relevant to the study of membrane rafts. *Biochim Biophys Acta*, 1781:665–684.
18. Zheng L, McQuaw CM, Ewing AG, and Winograd N (2007) Sphingomyelin/phosphatidylcholine and cholesterol interactions studied by imaging mass spectrometry. *J Am Chem Soc*, 129:15730–15731.
19. Epand RM, Epand RF, Sayer BG, Melacini G, Palgulachari MN, Segrest JP, and Anantharamaiah GM (2004) An apolipoprotein AI mimetic peptide: membrane interactions and the role of cholesterol. *Biochemistry*, 43:5073–5083.
20. Zviling M, Kochva U, and Arkin IT (2007) How important are transmembrane helices of bitopic membrane proteins? *Biochim Biophys Acta*, 1768:387–392.
21. van Dalen A, Hegger S, Killian JA, and de Kruijff B (2002) Influence of lipids on membrane assembly and stability of the potassium channel KcsA. *FEBS Lett*, 525:33–38.
22. Cybulski LE, Albanesi D, Mansilla MC, Altabe S, Aguilar PS, and de Mendoza D (2002) Mechanism of membrane fluidity optimization: isothermal control of the *Bacillus subtilis* acyl-lipid desaturase. *Mol Microbiol*, 45:1379–1388.
23. Aguilar PS, Hernandez-Arriaga AM, Cybulski LE, Erazo AC, and de Mendoza D (2001) Molecular basis of thermosensing: a two-component signal transduction thermometer in *Bacillus subtilis*. *EMBO J*, 20:1681–1691.
24. Gimpl G, Burger K, and Fahrenholz F (1997) Cholesterol as modulator of receptor function. *Biochemistry*, 36:10959–10974.
25. Burger K, Gimpl G, and Fahrenholz F (2000) Regulation of receptor function by cholesterol. *Cell Mol Life Sci*, 57:1577–1592.

26. Gimpl G and Fahrenholz F (2001) The oxytocin receptor system: structure, function, and regulation. *Physiol Rev*, 81:629–683.
27. van Duyl BY, Meeldijk H, Verkleij AJ, Rijkers DTS, Chupin V, de Kruijff B, and Killian JA (2005) A synergistic effect between cholesterol and tryptophan-flanked transmembrane helices modulates membrane curvature. *Biochemistry*, 44:4526–4532.
28. Santiago J, Guzmán GR, Rojas LV, Marti R, Asmar-Rovira GA, Santana LF, McNamee M, and Lasalde-Dominicci JA (2001) Probing the effects of membrane cholesterol in the *Torpedo californica* acetylcholine receptor and the novel lipid-exposed mutation alphaC418W in *Xenopus* oocytes. *J Biol Chem*, 276:46523–46532.
29. Carozzi AJ, Roy S, Morrow IC, Pol A, Wyse B, Clyde-Smith J, Prior IA, Nixon SJ, Hancock JF, and Parton RG (2002) Inhibition of lipid raft-dependent signaling by a dystrophy-associated mutant of caveolin-3. *J Biol Chem*, 277(20):17944–17949.
30. Nakamura M, Sekino N, Iwamoto M, and Ohno-Iwashita Y (1995) Interaction of theta-toxin (perfringolysin o), a cholesterol-binding cytolysin, with liposomal membranes: change in the aromatic side chains upon binding and insertion. *Biochemistry*, 34:6513–6520.
31. Gasset M, Killian JA, Tournois H, and de Kruijff B (1988) Influence of cholesterol on gramicidin-induced H_{II} phase formation in phosphatidylcholine model membranes. *Biochim Biophys Acta*, 939:79–88.
32. Corry B and Martinac B (2008) Bacterial mechanosensitive channels: experiment and theory. *Biochim Biophys Acta*, 1778:1859–1870.
33. Sukharev S and Anishkin A (2004) Mechanosensitive channels: what can we learn from ‘simple’ model systems? *Trends Neurosci*, 27:345–351.
34. Johannsson A, Smith G, and Metcalfe J (1981) The effect of bilayer thickness on the activity of (Na⁺ + K⁺)-ATPase. *Biochim Biophys Acta*, 641:416–421.
35. Johannsson A, Keightley CA, Smith GA, Richards CD, Hesketh TR, and Metcalfe JC (1981) The effect of bilayer thickness and n-alkanes on the activity of the (Ca²⁺ + Mg²⁺)-dependent ATPase of sarcoplasmic reticulum. *J Biol Chem*, 256:1643–1650.
36. Montecucco C, Smith GA, Dabbeni-sala F, Johannsson A, Galante YM, and Bisson R (1982) Bilayer thickness and enzymatic activity in the mitochondrial cytochrome c oxidase and ATPase complex. *FEBS Lett*, 144:145–148.
37. Dumas F, Tocanne JF, Leblanc G, and Lebrun MC (2000) Consequences of hydrophobic mismatch between lipids and melibiose permease on melibiose transport. *Biochemistry*, 39:4846–4854.
38. Betanzos M, Chiang CS, Guy HR, and Sukharev S (2002) A large iris-like expansion of a mechanosensitive channel protein induced by membrane tension. *Nat Struct Biol*, 9:704–710.
39. Wegener AA, Chizhov I, Engelhard M, and Steinhoff HJ (2000) Time-resolved detection of transient movement of helix F in spin-labelled pharaonis sensory rhodopsin II. *J Mol Biol*, 301:881–891.
40. Wegener AA, Klare JP, Engelhard M, and Steinhoff HJ (2001) Structural insights into the early steps of receptor-transducer signal transfer in archaeal phototaxis. *EMBO J*, 20:5312–5319.
41. Radzwill N, Gerwert K, and Steinhoff HJ (2001) Time-resolved detection of transient movement of helices F and G in doubly spin-labeled bacteriorhodopsin. *Biophys J*, 80:2856–2866.
42. Dave N, Lórenz-Fonfría VA, Leblanc G, and Padrós E (2008) FTIR spectroscopy of secondary-structure reorientation of melibiose permease modulated by substrate binding. *Biophys J*, 94:3659–3670.
43. Ulmschneider MB, Sansom MS, and Di Nola A (2005) Properties of integral membrane protein structures: derivation of an implicit membrane potential. *Proteins: Struct, Funct, Bioinf*, 59:252–265.
44. Ulmschneider MB and Sansom MSP (2001) Amino acid distributions in integral membrane protein structures. *Biochim Biophys Acta*, 1512:1–14.
45. Bowie JU (1997) Helix packing in membrane proteins. *J Mol Biol*, 272:780–789.
46. Wang J, Kim S, Kovacs F, and Cross TA (2001) Structure of the transmembrane region of the M2 protein H⁺ channel. *Protein Sci*, 10:2241–2250.
47. Marassi FM and Opella SJ (2003) Simultaneous assignment and structure determination of a membrane protein from NMR orientational restraints. *Protein Sci*, 12:403–411.
48. Abu-Baker S, Lu JX, Chu S, Shetty KK, Gor'kov PL, and Lorigan GA (2007) The structural topology of wild-type phospholamban in oriented lipid bilayers using 15N solid-state NMR spectroscopy. *Protein Sci*, 16:2345–2349.

49. Opella SJ, Marassi FM, Gesell JJ, Valente AP, Kim Y, Oblatt-Montal M, and Montal M (1999) Structures of the M2 channel-lining segments from nicotinic acetylcholine and NMDA receptors by NMR spectroscopy. *Nat Struct Biol*, 6:374–379.
50. Inbaraj JJ, Laryukhin M, and Lorigan GA (2007) Determining the helical tilt angle of a transmembrane helix in mechanically aligned lipid bilayers using EPR spectroscopy. *J Am Chem Soc*, 129:7710–7711.
51. Beevers AJ and Kukol A (2006) Secondary structure, orientation, and oligomerization of phospholemman, a cardiac transmembrane protein. *Protein Sci*, 15:1127–1132.
52. Wong A, Beevers AJ, Kukol A, Dupree R, and Smith ME (2008) Solid-state 17O NMR spectroscopy of a phospholemman transmembrane domain protein: implications for the limits of detecting dilute 17O sites in biomaterials. *Solid State Nucl Magn Reson*, 33:72–75.
53. Nazarov PV, Koehorst RBM, Vos WL, Apanasovich VV, and Hemminga MA (2007) FRET study of membrane proteins: determination of the tilt and orientation of the N-terminal domain of M13 major coat protein. *Biophys J*, 92:1296–1305.
54. Landolt-Marticorena C, Williams KA, Deber CM, and Reithmeier RAF (1993) Nonrandom distribution of amino-acids in the transmembrane segments of human type I single span membrane proteins. *J Mol Biol*, 229:602–608.
55. Arkin IT and Brunger AT (1998) Statistical analysis of predicted transmembrane alpha-helices. *Biochim Biophys Acta*, 1429:113–128.
56. Doyle DA, Cabral JM, Pfuetzner RA, Kuo A, Gulbis JM, Cohen SL, Chait BT, and MacKinnon R (1998) The structure of the potassium channel: molecular basis of K⁺ conduction and selectivity. *Science*, 280:69–77.
57. Williamson IM, Alvis SJ, East JM, and Lee AG (2003) The potassium channel KcsA and its interaction with the lipid bilayer. *Cell Mol Life Sci*, 60:1581–1590.
58. Seshadri K, Garemyr R, Wallin E, von Heijne G, and Elofsson A (1998) Architecture of beta-barrel membrane proteins: analysis of trimeric porins. *Protein Sci*, 7:2026–2032.
59. Gaede HC, Yau WM, and Gawrisch K (2005) Electrostatic contributions to indole-lipid interactions. *J Phys Chem B*, 109:13014–13023.
60. Sanderson JM and Whelan EJ (2004) Characterisation of the interactions of aromatic amino acids with diacetyl phosphatidylcholine. *Phys Chem Chem Phys*, 6:1012–1017.
61. Esbjörner EK, Caesar CEB, Albinsson B, Lincoln P, and Nordén B (2007) Tryptophan orientation in model lipid membranes. *Biochem Biophys Res Commun*, 361:645–650.
62. von Heijne G and Gavel Y (1988) Topogenic signals in integral membrane proteins. *Eur J Biochem*, 174:671–678.
63. von Heijne G (1989) Control of topology and mode of assembly of a polytopic membrane protein by positively charged residues. *Nature*, 341:456–458.
64. Kooijman EE, Tieleman DP, Testerink C, Munnik T, Rijkers DTS, Burger KNJ, and de Kruijff B (2007) An electrostatic/hydrogen bond switch as the basis for the specific interaction of phosphatidic acid with proteins. *J Biol Chem*, 282:11356–11364.
65. Andronesi OC, Pfeifer JR, Al-Momani L, Özdirekcan S, Rijkers DTS, Angerstein B, Luca S, Koert U, Killian JA, and Baldus M (2004) Probing membrane protein orientation and structure using fast magic-angle-spinning solid-state NMR. *J Biomol NMR*, 30:253–265.
66. Lemaitre V, de Planque MRR, Howes AP, Smith ME, Dupree R, and Watts A (2004) Solid-state 17O NMR as a probe for structural studies of proteins in biomembranes. *J Am Chem Soc*, 126:15320–15321.
67. Killian JA and Nyholm TKM (2006) Peptides in lipid bilayers: the power of simple models. *Curr Opin Struct Biol*, 16:473–479.
68. Shahidullah K and London E (2008) Effect of lipid composition on the topography of membrane-associated hydrophobic helices: stabilization of transmembrane topography by anionic lipids. *J Mol Biol*, 379:704–718.
69. Mall S, Broadbridge R, Sharma RP, Lee AG, and East JM (2000) Effects of aromatic residues at the ends of transmembrane alpha-helices on helix interactions with lipid bilayers. *Biochemistry*, 39:2071–2078.
70. Yano Y, Takemoto T, Kobayashi S, Yasui H, Sakurai H, Ohashi W, Niwa M, Futaki S, Sugiura Y, and Matsuzaki K (2002) Topological stability and self-association of a completely hydrophobic model transmembrane helix in lipid bilayers. *Biochemistry*, 41:3073–3080.

71. Liu F, Lewis RNAH, Hodges RS, and McElhaney RN (2002) Effect of variations in the structure of a poly-leucine-based alpha-helical transmembrane peptide on its interaction with phosphatidylcholine bilayers. *Biochemistry*, 41:9197–9207.
72. Strandberg E, Özdirekcan S, Rijkers DTS, van der Wel PCA, Koeppe II RE, Liskamp RMJ, and Killian JA (2004) Tilt angles of transmembrane model peptides in oriented and non-oriented lipid bilayers as determined by 2H solid-state NMR. *Biophys J*, 86:3709–3721.
73. Özdirekcan S, Rijkers DTS, Liskamp RMJ, and Killian JA (2005) Influence of flanking residues on tilt and rotation angles of transmembrane peptides in lipid bilayers. A solid-state 2H NMR study. *Biochemistry*, 44:1004–1012.
74. Vostrikov VV, Grant CV, Daily AE, Opella SJ, and Koeppe II RE (2008) Comparison of “polarization inversion with spin exchange at magic angle” and “geometric analysis of labeled alanines” methods for transmembrane helix alignment. *J Am Chem Soc*, 130:12584–12585.
75. Andersen OS and Koeppe II RE (2007) Bilayer thickness and membrane protein function: an energetic perspective. *Annu Rev Biophys Biomol Struct*, 36:107–130.
76. Jensen M and Mouritsen OG (2004) Lipids do influence protein function - the hydrophobic matching hypothesis revisited. *Biochim Biophys Acta*, 1666:205–226.
77. Killian JA, Salemink I, de Planque MRR, Lindblom G, Koeppe II RE, and Greathouse DV (1996) Induction of nonbilayer structures in diacylphosphatidylcholine model membranes by transmembrane alpha-helical peptides: importance of hydrophobic mismatch and proposed role of tryptophans. *Biochemistry*, 35:1037–1045.
78. de Planque MRR, Greathouse DV, Koeppe II RE, Schäfer H, Marsh D, and Killian JA (1998) Influence of lipid/peptide hydrophobic mismatch on the thickness of diacylphosphatidylcholine bilayers. A 2H NMR and ESR study using designed transmembrane alpha-helical peptides and gramicidin A. *Biochemistry*, 37:9333–9345.
79. de Planque MRR, Kruijtz JAW, Liskamp RMJ, Marsh D, Greathouse DV, Koeppe II RE, de Kruijff B, and Killian JA (1999) Different membrane anchoring positions of tryptophan and lysine in synthetic transmembrane alpha-helical peptides. *J Biol Chem*, 274(30):20839–20846.
80. de Planque MRR, Goormaghtigh E, Greathouse DV, Koeppe II RE, Kruijtz JAW, Liskamp RMJ, de Kruijff B, and Killian JA (2001) Sensitivity of single membrane-spanning alpha-helical peptides to hydrophobic mismatch with a lipid bilayer: effects on backbone structure, orientation, and extent of membrane incorporation. *Biochemistry*, 40:5000–5010.
81. Rinia HA, Boots JWP, Rijkers DTS, Kik RA, Snel MME, Demel RA, Killian JA, van der Eerden JPJM, and de Kruijff B (2002) Domain formation in phosphatidylcholine bilayers containing transmembrane peptides: specific effects of flanking residues. *Biochemistry*, 41:2814–2824.
82. Strandberg E, Morein S, Rijkers DTS, Liskamp RMJ, van der Wel PCA, and Killian JA (2002) Lipid dependence of membrane anchoring properties and snorkeling behavior of aromatic and charged residues in transmembrane peptides. *Biochemistry*, 41:7190–7198.
83. Petrache HI, Zuckerman DM, Sachs JN, Killian JA, Koeppe II RE, and Woolf TB (2002) Hydrophobic matching mechanism investigated by molecular dynamics simulations. *Langmuir*, 18:1340–1351.
84. Morein S, Killian JA, and Sperotto MM (2002) Characterization of the thermotropic behavior and lateral organization of lipid-peptide mixtures by a combined experimental and theoretical approach: effects of hydrophobic mismatch and role of flanking residues. *Biophys J*, 82:1405–1417.
85. van der Wel PCA, Strandberg E, Killian JA, and Koeppe II RE (2002) Geometry and intrinsic tilt of a tryptophan-anchored transmembrane alpha-helix determined by 2H NMR. *Biophys J*, 83:1479–1488.
86. Weiss TM, van der Wel PCA, Killian JA, Koeppe II RE, and Huang HW (2003) Hydrophobic mismatch between helices and lipid bilayers. *Biophys J*, 84:379–385.
87. Im W and Brooks III CL (2005) Interfacial folding and membrane insertion of designed peptides studied by molecular dynamics simulations. *Proc Natl Acad Sci U S A*, 102:6771–6776.
88. Sparr E, Ganchev DN, Snel MME, Ridder ANJA, Kroon-Batenburg LMJ, Chupin V, Rijkers DTS, Killian JA, and de Kruijff B (2005) Molecular organization in striated domains induced by transmembrane alpha-helical peptides in dipalmitoyl phosphatidylcholine bilayers. *Biochemistry*, 44:2–10.
89. Sparr E, Ash WL, Nazarov PV, Rijkers DTS, Hemminga MA, Tieleman DP, and Killian JA (2005) Self-association of transmembrane alpha-helices in model membranes - importance of helix orientation and role of hydrophobic mismatch. *J Biol Chem*, 280:39324–39331.

90. Siegel DP, Cherezov V, Greathouse DV, Koeppe II RE, Killian JA, and Caffrey M (2006) Transmembrane peptides stabilize inverted cubic phases in a biphasic length-dependent manner: implications for protein-induced membrane fusion. *Biophys J*, 90(1):200–211.
91. Özdirekcan S, Etchebest C, Killian JA, and Fuchs PFJ (2007) On the orientation of a designed transmembrane peptide: toward the right tilt angle? *J Am Chem Soc*, 129:15174–15181.
92. van der Wel PCA, Reed ND, Greathouse DV, and Koeppe II RE (2007) Orientation and motion of tryptophan interfacial anchors in membrane-spanning peptides. *Biochemistry*, 46:7514–7524.
93. Esteban-Martin S and Salgado J (2007) The dynamic orientation of membrane-bound peptides: bridging simulations and experiments. *Biophys J*, 93:4278–4288.
94. Kandasamy SK and Larson RG (2006) Molecular dynamics simulations of model trans-membrane peptides in lipid bilayers: a systematic investigation of hydrophobic mismatch. *Biophys J*, 90:2326–2343.
95. Daily AE, Greathouse DV, van der Wel PCA, and Koeppe II RE (2008) Helical distortion in tryptophan- and lysine-anchored membrane-spanning alpha-helices as a function of hydrophobic mismatch: a solid-state deuterium NMR investigation using the geometric analysis of labeled alanines method. *Biophys J*, 94:480–491.
96. Krishnakumar SS and London E (2007) Effect of sequence hydrophobicity and bilayer width upon the minimum length required for the formation of transmembrane helices in membranes. *J Mol Biol*, 374:671–687.
97. Esteban-Martin S and Salgado J (2007) Self-assembling of peptide/membrane complexes by atomistic molecular dynamics simulations. *Biophys J*, 92:903–912.
98. Koehorst RBM, Spruijt RB, Vergeldt FJ, and Hemminga MA (2004) Lipid bilayer topology of the transmembrane alpha-helix of M13 major coat protein and bilayer polarity profile by site-directed fluorescence spectroscopy. *Biophys J*, 87:1445–1455.
99. Marsh D, Jost M, Peggion C, and Toniolo C (2007) Lipid chain-length dependence for incorporation of alamethicin in membranes: electron paramagnetic resonance studies on TOAC-spin labeled analogs. *Biophys J*, 92:4002–4011.
100. Park SH and Opella SJ (2005) Tilt angle of a trans-membrane helix is determined by hydrophobic mismatch. *J Mol Biol*, 350:310–318.
101. de Planque MRR and Killian JA (2003) Protein-lipid interactions studied with designed transmembrane peptides: role of hydrophobic matching and interfacial anchoring. *Mol Membr Biol*, 20:271–284.
102. Yeagle PL, Bennett M, Lemaître V, and Watts A (2007) Transmembrane helices of membrane proteins may flex to satisfy hydrophobic mismatch. *Biochim Biophys Acta*, 1768:530–537.
103. Falck E, Rog T, Karttunen M, and Vattulainen I (2008) Lateral diffusion in lipid membranes through collective flows. *J Am Chem Soc*, 130:44–45.
104. Saffman PG and Delbrück M (1975) Brownian motion in biological membranes. *Proc Natl Acad Sci U S A*, 72:3111–3113.
105. Gambin Y, Lopez-Esparza R, Reffay M, Sierrecki E, Gov NS, Genest M, Hodges RS, and Urbach W (2006) Lateral mobility of proteins in liquid membranes revisited. *Proc Natl Acad Sci U S A*, 103:2098–2102.
106. Naji A, Levine AJ, and Pincus PA (2007) Corrections to the Saffman-Delbrück mobility for membrane bound proteins. *Biophys J*, 93:L49–L51.
107. Lee CC and Petersen NO (2003) The lateral diffusion of selectively aggregated peptides in giant unilamellar vesicles. *Biophys J*, 84:1756–1764.
108. Frick M, Schmidt K, and Nichols BJ (2007) Modulation of lateral diffusion in the plasma membrane by protein density. *Curr Biol*, 17:462–467.
109. Seelig J (1977) Deuterium magnetic resonance: theory and application to lipid membranes. *Q Rev Biophys*, 10(3):353–418.
110. Drechsler A and Separovic F (2003) Solid-state NMR structure determination. *IUBMB Life*, 55(9):515–523.
111. Cady SD, Goodman C, Tatko CD, DeGrado WF, and Hong M (2007) Determining the orientation of uniaxially rotating membrane proteins using unoriented samples: a 2H, 13C, and 15N solid-state NMR investigation of the dynamics and orientation of a transmembrane helical bundle. *J Am Chem Soc*, 129:5719–5729.
112. Saito H (1986) Conformation-dependent carbon-13 chemical shifts: a new means of conformational characterization as obtained by high-resolution solid-state carbon-13 NMR. *Mag Res Chem*, 24:835–852.

113. Wishart DS, Sykes BD, and Richards FM (1991) Relationship between nuclear magnetic resonance chemical shift and protein secondary structure. *J Mol Biol*, 222:311–333.
114. Wishart DS and Sykes BD (1994) The ¹³C chemical-shift index: a simple method for the identification of protein secondary structure using ¹³C chemical-shift data. *J Biomol NMR*, 4:171–180.
115. Lakowicz JR (1999) Principles of Fluorescence Spectroscopy. Kluwer Academic / Plenum Publishers.
116. Elson EL and Magde D (1974) Fluorescence correlation spectroscopy. I. Conceptual basis and theory. *Biopolymers*, 13:1–27.
117. Angelova MI and Dimitrov DS (1986) Liposome electroformation. *Faraday Discuss Chem Soc*, 81:303–311.
118. Angelova MI, Soléau S, Méléard P, Faucon F, and Bothorel P (1992) Preparation of giant vesicles by external AC fields. Kinetics and application. *Prog Colloid Polym Sci*, 89:127–131.
119. Montes LR, Alonso A, Goñi FM, and Bagatolli LA (2007) Giant unilamellar vesicles electroformed from native membranes and organic lipid mixtures under physiological conditions. *Biophys J*, 93:3548–3554.

Chapter 2

Is there a Preferential Interaction between Cholesterol and Tryptophan Residues in Membrane Proteins?

Andrea Holt,[‡] Rodrigo F. M. de Almeida,[§] Thomas K. M. Nyholm,[‡] Luís M. S. Loura,[^]
Anna E. Daily,[#] Rutger W. H. M. Staffhorst,[‡] Dirk T. S. Rijkers,^{||} Roger E. Koeppe II,[#]
Manuel Prieto,[§] and J. Antoinette Killian[‡]

[‡]Chemical Biology & Organic Chemistry, Bijvoet Center for Biomolecular Research, Utrecht University, Utrecht, The Netherlands, and ^{||}Medicinal Chemistry & Chemical Biology, Utrecht Institute for Pharmaceutical Sciences, Utrecht University, Utrecht, The Netherlands, and [§]Centro de Química-Física Molecular, Complexo Interdisciplinar, Instituto Superior Técnico, Lisbon, Portugal, and [^]Faculdade de Farmácia da Universidade de Coimbra, Coimbra, Portugal, and [#]Department of Chemistry & Biochemistry, University of Arkansas, Fayetteville, USA.

Published in *Biochemistry* (2008), 47:2638-2649

Abstract

Recently several indications have been found that suggest a preferential interaction between cholesterol and tryptophan residues located near the membrane-water interface. The aim of the present study was to investigate by direct methods how tryptophan and cholesterol interact with each other and what the possible consequences are for membrane organization. For this purpose we used cholesterol containing model membranes of dimyristoylphosphatidylcholine (DMPC) in which a transmembrane model peptide with flanking tryptophans (Acetyl-GWW(LA)₈LWWA-amide), called WALP23 peptide was incorporated to mimic interfacial tryptophans of membrane proteins. These model systems were studied with two complementary methods. 1) Steady-state and time-resolved Förster resonance energy transfer (FRET) experiments employing the fluorescent cholesterol analogue dehydroergosterol (DHE) in combination with a competition experiment with cholesterol were used to obtain information about the distribution of cholesterol in the bilayer in the presence of WALP23. The results were consistent with a random distribution of cholesterol which indicates that cholesterol and interfacial tryptophans are not preferentially located next to each other in these bilayer systems. 2) Solid-state ²H NMR experiments employing either deuterated cholesterol or indole ring deuterated WALP23 peptides were performed to study the orientation and dynamics of both molecules. The results showed that the quadrupolar splittings of labeled cholesterol were not affected by an interaction with tryptophan-flanked peptides, and, vice versa, that the quadrupolar splittings of labeled indole rings in WALP23 are not significantly influenced by addition of cholesterol to the bilayer. Therefore, both NMR and fluorescence spectroscopy results independently show that, at least in the model systems studied here, there is no evidence for a preferential interaction between cholesterol and tryptophans located at the membrane-water interface.

Introduction

Biological membranes are composed of a variety of different lipids and contain a huge diversity of membrane proteins. They are very heterogeneous systems and often include membrane microdomains that can have compositions different from the bulk membrane and that are important for some membrane proteins to fulfill their functions [1]. Often the formation of these membrane microdomains involves local enrichment of cholesterol [2,3].

Cholesterol can be found in membranes of eukaryotic organisms and is a major constituent in some types of membranes [4]. It is thought to have a dual function in the membrane [5]. On the one hand it has an ordering effect on acyl chains of surrounding (phospho)lipids which results in a more condensed bilayer. Membrane domains with an increased cholesterol content, also referred to as lipid rafts, therefore have an increased bilayer thickness. On the other hand cholesterol introduces negative membrane curvature and is able to fill voids in the bilayer due to its bulky body. The presence of cholesterol thus affects several membrane properties which can also influence the function and distribution of membrane proteins.

Membrane proteins perform many essential functions in the cell such as transport, signaling, catalysis, and transduction of energy. The transmembrane domains of these proteins are hydrophobic and frequently include aromatic residues such as tryptophan and tyrosine located at the lipid-water interface [6,7]. In particular these interfacial tryptophans are

believed to anchor transmembrane domains of membrane proteins in the bilayer and to help them to adopt correct positioning needed for proper functioning [8,9]. Tryptophans at the membrane interface are also thought to have an important role in folding and assembly of transmembrane complexes of membrane proteins [7].

The indole ring makes tryptophan the bulkiest amino acid among all 20 amino acids naturally occurring in proteins and allows amphipathic interactions including imino group hydrogen bonding, specific dipolar interactions, cation- π interactions and hydrophobic interactions [7,10,11]. The special character of the indole ring provides the potential to interact with a variety of molecules. The rigid indole ring of tryptophan is often found stacking with other rigid ring structures as found in nucleic acids or other amino acids including phenylalanine or tyrosine.

Cholesterol also has a complex rigid ring structure which could favorably interact with the indole ring of tryptophans. If such an interaction occurs and if it is sufficiently favorable, it could lead to a preferential interaction between cholesterol and tryptophans located at the bilayer interface. Indeed, several indications have been found for such an interaction. In a study of Gasset *et al.* [12], the authors proposed the formation of a complex between cholesterol and the tryptophan-rich gramicidin A driven by hydrophobic interactions. Carozzi *et al.* [13] found that a cysteine to tryptophan mutation in the membrane protein caveolin-3 affects the cholesterol distribution in the membrane. This naturally occurring C71W mutation was observed to increase the affinity of caveolin-3 for cholesterol and thereby prevent the release of cholesterol from caveolae to noncaveolar membrane domains.

In another study Santiago *et al.* [14] found that a cysteine to tryptophan mutation alters the function of the nicotinic acetylcholine receptor AChR. This α C418W mutation which is located in a lipid exposed transmembrane segment dramatically enhanced the response of the receptor to cholesterol modulation. Finally, van Duyl *et al.* [5] observed a synergistic effect between cholesterol and tryptophan-flanked transmembrane peptides in lipid phase behavior. They found that model membranes composed of unsaturated phospholipids and cholesterol form an isotropic phase upon incorporation of tryptophan-flanked peptides. This was not observed for model peptides in which the flanking tryptophans had been replaced by lysines or histidines, and these results led the authors to propose a preferential interaction between cholesterol and interfacial tryptophans.

In spite of these indications for a preferential interaction between cholesterol and tryptophans there is little known about the interaction and the possible consequences for membrane organization. Here, we investigated this issue by employing tryptophan-flanked model peptides which were incorporated into bilayers of phospholipids containing varying amounts of cholesterol. These peptides, called WALP peptides, consist of a stretch of alternating leucines and alanines flanked on both sides by a pair of tryptophans. These transmembrane peptides have been designed as well-defined models to gain insight into basic principles of membrane organization and have been studied extensively throughout the last decade [9,15-17]. They have often been used to mimic transmembrane segments of membrane proteins [16] and readily integrate into bilayers under formation of stable transmembrane α -helices.

To study the interaction between cholesterol and the interfacial tryptophans of WALP peptides, we used a two-fold approach employing fluorescence spectroscopy and NMR spectroscopy. Fluorescence experiments using Förster resonance energy transfer (FRET)

between tryptophan and the fluorescent cholesterol analogue dehydroergosterol (DHE) were used to obtain information on the distribution of cholesterol in the bilayer with respect to the peptides. Solid-state ^2H NMR measurements using either deuterated cholesterol or tryptophan deuterated WALP peptides were performed to observe possible changes in motion and orientation of cholesterol and tryptophan. The results indicate that cholesterol remains homogeneously distributed in the bilayer in the presence of tryptophan-flanked peptides and that the dynamics and orientation of neither cholesterol nor of tryptophans located at the bilayer interface are influenced by the presence of the other molecule.

Materials and Methods

Materials

Unlabeled WALP23, KALP23, WLP23 and KLP23 peptides (for sequences see Table 1) were synthesized using Fmoc/tBu solid-phase synthesis as described elsewhere for related KALP peptides [18]. Deuterium labeled L-tryptophan (indole- d_5 , 98%) was purchased from Cambridge Isotopes Laboratories Inc. (Andover, MA, USA), and Fmoc (9-fluorenylmethyl-oxycarbonyl) was used to protect its amino functionality as described by ten Kortenaar *et al.* [19] before being used in the peptide synthesis. The deuterium labeled WALP23 peptides were synthesized according to the procedure described in [20] to avoid exchange of deuterons located at the indole ring against hydrogen's in the presence of TFA (trifluoroacetic acid) [21]. Due to the use of ethanolamine as cleavage agent the C-terminus of the deuterium labeled WALP23 peptide is capped by ethanolamine instead of an amide. Indole ring deuterated tryptophans were introduced either at position 2 or 3 of the WALP23 peptide. The identity of the synthesized peptides was verified by mass spectrometry and the purity was analyzed by HPLC using a C4 reverse phase HPLC column with an aqueous phosphorous acid/triethylamine buffer at pH 2.25, according to procedures described in [22]. The purity of peptides used in this study was generally better than 95%.

Cholesterol and 1,2-dimyristoyl-*sn*-glycero-3-phosphocholine (di-C14:0PC) were purchased from Avanti Polar Lipids Inc. (Alabaster, AL, USA); β -(d_6 -2,2,3,4,4,6)cholesterol was purchased from Medical Isotopes Inc. (Pelham, NH, USA); 2,2,2-trifluoroethanol (TFE) was obtained from Merck (Darmstadt, Germany); and ergosta-5,7,9(11),22-tetraen-3 β ol (DHE, >96%) was purchased from Sigma Aldrich. All lipids were used without further purification. All other chemicals used were of analytical grade. Deuterium-depleted water for NMR samples was obtained from Cambridge Isotope Laboratories, Inc. All other water used during sample preparation was deionized and purified with a Milli-Q Gradient Water purification system from Millipore Corporation (Billerica, MA, USA).

Table 1: Amino acid sequence of the model peptides

peptide	amino acid sequence
WALP23	Acetyl-GWWLALALALALALALALWWA-amide
KALP23	Acetyl-GKKLALALALALALALALKKA-amide
WLP23	Acetyl-GWWLLLLLLLLLLLLLLLLLWWA-amide
KLP23	Acetyl-GKKLLLLLLLLLLLLLLLLLKKA-amide
WALP23- d_5 -Trp2	Acetyl-GW*WLALALALALALALALWWA-ethanolamine
WALP23- d_5 -Trp3	Acetyl-GWW*LALALALALALALALWWA-ethanolamine

* positions labeled with indole-deuterated d_5 -Trp.

Methods

Fluorescence spectroscopy

Stock solutions of ca. 20 mM di-C14:0PC in chloroform were prepared and the lipid concentration was determined by a phosphorus assay [23]. Stock solutions of WALP23 and DHE were prepared with a concentration of ca. 200 μM in TFE respectively MeOH. The concentration of WALP23 and DHE was determined by absorption spectroscopy using an extinction coefficient of $22400 \text{ M}^{-1}\text{cm}^{-1}$ at 280 nm for WALP23 [24] and $10500 \text{ M}^{-1}\text{cm}^{-1}$ at 324 nm for DHE [25]. Cholesterol stock solutions were prepared by weight with a concentration of 5 mM in chloroform.

All fluorescence experiments were performed with a constant peptide/phospholipid molar ratio of 1/200 and a final peptide concentration of 5 μM . First, appropriate amounts of peptide and phospholipid were mixed in solution and distributed over a number of tubes. Then varying amounts of DHE (0 to 8 mol%) were added to the tubes. For competition experiments additionally equimolar amounts of cholesterol were added. After thorough mixing the organic solvents were evaporated under a nitrogen flow and were further removed under vacuum overnight (ca. $1 \cdot 10^{-2}$ mbar). Then the samples were hydrated with buffer (25 mM HEPES, 100 mM NaCl, pH 7.0) and incubated for about 30 minutes. Large Unilamellar Vesicles (LUVs) were produced by first freeze-thawing the samples at least 10 times and subsequent extrusion through inorganic membrane filters with a pore size of 200 nm (Anotop 10; Whatman International Ltd., Maidstone, England).

For steady-state fluorescence measurements the samples (1.2 ml) were directly after preparation transferred to a 10 mm quartz cuvette. All measurements were performed using a SLM-Aminco SPF-500 C fluorimeter (Jobin Yvon, Edison, NJ, USA) and were carried out at 30°C to ensure that the lipid bilayers are in fluid phase. The samples were allowed to equilibrate in the fluorimeter for at least 5 minutes under continuous stirring before measurements. The tryptophans of WALP23 were excited at 280 nm and emission from tryptophan and DHE was recorded from 300 to 525 nm using a bandwidth of 5 nm for both the excitation and emission channel. All emission spectra were corrected for instrument-specific deviations using a standard emission spectrum of L-tryptophan [26]. Samples without peptide and DHE were used to correct for light scattering of the vesicle suspensions.

Fluorescence decay measurements were carried out on a time-correlated single-photon timing system which is described elsewhere [27,28]. All time-resolved fluorescence measurements were performed at 30°C. For the FRET experiments, the donor (Trp in WALP23) was excited at 290 nm to minimize absorption of the acceptor (DHE). Tryptophan emission was collected at 330 nm using the magic angle relative to the vertically polarized excitation beam and to avoid scattered excitation a cutoff filter was added to the monochromator. The collection bandwidth was set to 20 nm to avoid that acceptor emission reaches the detector. The fluorescence decays were obtained with an accumulation of 20000 counts on the peak channel and timescales ranging from 22 ps/channel for donor only to 12 ps/channel for high acceptor concentrations.

Analysis of fluorescence data

Data analysis was carried out using a nonlinear, least-squares iterative convolution method based on the algorithm of Marquardt [29]. The decay curves obtained for different acceptor concentrations were analyzed using a global analysis approach with linkage of lifetimes and ratios of pre-exponential factors [27]. The quality of the fit was judged from χ^2 values of the individual experiment, the global χ^2 value (χ^2_G), and weighted residuals and autocorrelation plots.

The critical distance for FRET, the Förster distance (R_0) was calculated by

$$(1) \quad R_0 = 0.2108 \left[\kappa^2 n^{-4} \Phi_D \times \int_0^{\infty} \lambda^4 \times I(\lambda) \times \varepsilon(\lambda) d\lambda \right]^{\frac{1}{6}},$$

where κ is the orientation factor for dipole-dipole coupling of donor and acceptor, Φ_D is the quantum yield of the donor in absence of acceptor, n is the refractive index of the medium, λ is the wavelength expressed in nm, $I(\lambda)$ is the normalized emission spectrum of the donor, and $\varepsilon(\lambda)$ is the molar absorption spectrum of the acceptor in $M^{-1}cm^{-1}$ [30]. The resulting Förster distance has the unit Å. A refractive index of $n = 1.4$ was used for the bilayer interface [30,31] which is an average value between $n = 1.5$ for the bilayer interior [32] and $n = 1.33$ for aqueous environments. An orientation factor of $\kappa^2 = 2/3$ was used, which represents the dynamic isotropic limit i.e. donor and acceptor undergo fast reorientation during the lifetime of the excited state of the donor [31,33]. This value is commonly used for FRET experiments performed in bilayers [27,34].

For FRET within one leaflet of the bilayer the decay of donor fluorescence in the presence of acceptor for unlinked and randomly distributed donor and acceptor was derived in [35]

$$(2) \quad \rho_{cis}(t) = \exp \left\{ -\pi R_0^2 n \gamma \left[\frac{2}{3}, \left(\frac{R_0}{R_e} \right)^6 \left(\frac{t}{\langle \tau \rangle} \right) \right] \left(\frac{t}{\langle \tau \rangle} \right)^{\frac{1}{3}} + \pi R_e^2 c \left(1 - \exp \left[- \left(\frac{R_0}{R_e} \right)^6 \left(\frac{t}{\langle \tau \rangle} \right) \right] \right) \right\},$$

where n is the surface density of acceptors, R_e is the radius of exclusion of acceptors around the donor and the average lifetime $\langle \tau \rangle = \sum_i \alpha_i \tau_i^2 / \sum_i \alpha_i \tau_i$. For the calculations of the FRET efficiency between the tryptophans of WALP23 and DHE in di-C14:0PC bilayers, the radius of exclusion R_e was estimated to be 7.5 Å, being the sum of the radii of tryptophan and DHE calculated from the square root over the area of the molecules in the bilayer. The incomplete Gamma function γ is defined as $\gamma[x, y] = \int_0^y z^{x-1} \exp(-z) dz$.

For FRET to the opposing bilayer leaflet the decay of donor fluorescence was derived in [31]

$$(3) \quad \rho_{trans}(t) = \exp \left\{ -2 \pi w^2 n \cdot \int_0^{\frac{w}{\sqrt{w^2 + R_e^2}}} \left[1 - \exp \left\{ - \left(\frac{R_0}{R_e} \right)^6 \left(\frac{t}{\langle \tau \rangle} \right) \alpha^6 \right\} \right] \alpha^{-3} d\alpha \right\},$$

where w is the interplanar distance between donor and acceptor which was considered to be 23 Å based on molecular models.

The decay of donor fluorescence in presence of acceptor molecules in both leaflets is then described by

$$(4) \quad i_{DA}(t) = i_D(t) \cdot \rho_{cis}(t) \cdot \rho_{trans}(t).$$

Finally, the FRET efficiency is calculated by numerical integration of

$$(5) \quad E = 1 - \frac{\int_0^{\infty} i_D(t) \cdot \rho_{cis}(t) \cdot \rho_{trans}(t) dt}{\langle \tau \rangle_D},$$

where $i_D(t) = \sum_i \alpha_i \exp\left\{-\left(\frac{t}{\tau_{Di}}\right)\right\}$ describes the fluorescence decay of the donor in absence of acceptor and $\langle \tau \rangle_D = \sum_i \alpha_i \cdot \tau_i$ corresponds to the donor lifetime weighted by quantum yield.

NMR spectroscopy

Phospholipid and (deuterated) cholesterol stock solutions were prepared as described above. For NMR experiments employing deuterated cholesterol typically 2 μmol of deuterated cholesterol and 100 μmol of phospholipids were used per sample. The lipids were mixed in solution and organic solvents were removed as described above. Deuterium-depleted buffer was prepared by lyophilization of a small amount of buffer (25 mM HEPES, 100 mM NaCl, pH 7.0) prepared with Milli-Q water which was rehydrated with the same amount of deuterium-depleted water. The samples were first hydrated with Milli-Q water (1 ml) and lyophilized. Then the powder was transferred to the smaller NMR tubes and hydrated using 100 μl of deuterium-depleted buffer. The NMR tubes were sealed with a silicon stopper under a N_2 atmosphere and freeze-thawed 10 times to promote sample homogeneity. Samples with a higher cholesterol concentration in the bilayer were supplemented with undeuterated cholesterol. For peptide containing samples 1 μmol of the indicated peptide was weighed, dissolved in TFE (0.5 ml) and added to the lipid mixture.

The NMR experiments employing tryptophan deuterated WALP peptides were performed on oriented samples. Stock solutions of deuterated WALP peptides were prepared with a concentration of ca. 500 μM in TFE. For each oriented sample typically 2 μmol of deuterated peptide and 50 μmol of phospholipids were mixed in solution. For samples also containing cholesterol 2 μmol of the sterol was added to the mixture. Organic solvents were removed as described above and the sample was redissolved in a mixture of methanol and chloroform (1:1, v/v, 2 ml). This mixture was distributed over 50 glass platelets (4.8 x 23 x 0.06-0.08 mm; Marienfeld Laboratory Glassware, Lauda-Königshafen, Germany) and solvents were evaporated as described. Then the platelets were stacked into a square glass cuvette and if necessary supplemented with empty glass platelets to ensure a tight fit. The sample was hydrated with deuterium-depleted water to 40% hydration (w/w), and the cuvette was sealed immediately under nitrogen atmosphere using a glass plate and quick-drying epoxy glue. To promote alignment of the bilayers along the glass plates, the samples were incubated at 37°C for at least three days before NMR measurements.

NMR experiments were carried out on a Bruker Avance 500 MHz wide bore spectrometer (Bruker Biospin, Karlsruhe, Germany). All NMR measurements were performed at 40°C. The samples were allowed to equilibrate for at least 10 minutes before measurements. The bilayer alignment of the oriented samples was checked by ^{31}P NMR experiments as described in [36]. ^2H NMR experiments were performed at 76.78 MHz using a quadrupolar echo sequence [37], an echo delay of 50 μs and a relaxation time of 100 ms. For ^2H NMR measurements on the samples containing deuterated cholesterol 400 000 scans were acquired. For the oriented samples containing deuterated peptides $2.4 \cdot 10^6$ and $1.6 \cdot 10^6$ scans were acquired for the 0° and 90° orientation of the bilayer normal to the magnetic field, respectively.

Results

FRET experiments

FRET measurements were carried out to obtain information on the lateral distribution of sterols in the bilayer in the presence of tryptophan-flanked peptides. Since cholesterol itself is not fluorescent we used the fluorescent cholesterol analogue DHE. The fluorescence characteristics of WALP23 and DHE in bilayers of di-C14:0PC is shown in Figure 1. The emission of the tryptophans (solid line) overlaps with the absorbance of DHE (dashed line) in the range of 300 to 355 nm which allows FRET between these molecules, whereby the tryptophans of WALP23 serve as donor and DHE serves as acceptor. For DHE the maximal molar extinction coefficient in di-C14:0PC bilayers was determined to be $7300 \text{ M}^{-1}\text{cm}^{-1}$ at 324 nm by comparison with absorption of DHE in methanol using a molar extinction coefficient of $10,500 \text{ M}^{-1}\text{cm}^{-1}$ at 324 nm [25]. The overlap integral was solved based on the absorption spectrum of DHE and the normalized emission spectrum of WALP23 as shown in Figure 1. The quantum yield of the tryptophans of WALP23 in bilayers of di-C14:0PC was determined to be 0.106 using tryptophan in water as a standard [30] and an excitation wavelength of 280 nm. Based on these parameters, the characteristic Förster distance for the FRET pair WALP23 and DHE was calculated to be 20 Å according to equation 1.

Distribution of cholesterol in the membrane

Steady-state fluorescence spectra were recorded on di-C14:0PC bilayers containing WALP23 peptides and increasing concentrations of 0 mol% to 8 mol% DHE in the lipid fraction (see Figure 2A). From the spectral line shapes it is clear that as the surface density of DHE in the bilayer increases, the intensity of the emission due to the tryptophans of WALP23 (dashed lines top panel) decreases. A concomitant increase of the emission of acceptor is observed (solid lines bottom panel), which is mainly the sensitized emission of DHE (due to FRET from WALP23) and a minor contribution of the direct excitation of DHE at 280 nm. Because the emission spectra of WALP23 and DHE overlap to a great extent (see Figure 1), the recorded spectra need to be decomposed into emission of donor and emission of acceptor in order to calculate the FRET efficiency from the integrated area of the spectrum.

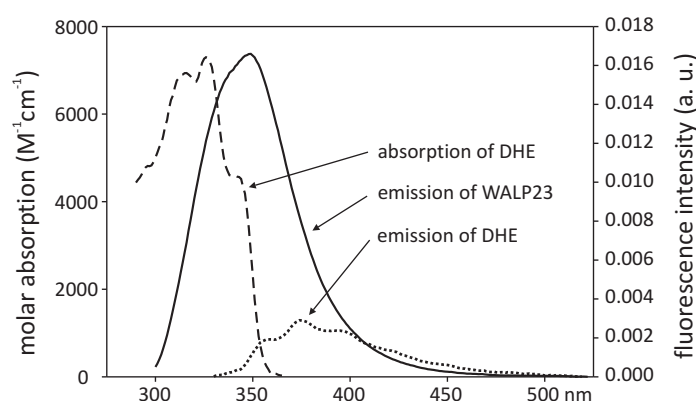


Figure 1: Spectral overlap for the FRET pair with WALP23 as the donor and DHE as the acceptor in LUVs of di-C14:0PC at pH 7.0. Dashed line: absorption spectrum of DHE with a molar absorption coefficient of $7300 \text{ M}^{-1}\text{cm}^{-1}$ at maximal absorption at 324 nm, solid line: fluorescence emission spectrum of WALP23, and dashed line: fluorescence emission spectrum of DHE. The spectra were recorded at a temperature of 30°C. The excitation wavelength was 280 nm for WALP23 and 324 nm for DHE.

In principle, the calculation could also be performed from the steady-state intensity at a given wavelength at which there is no emission from the acceptor. However, by decomposition of the spectra it is possible to check whether the shape of the emission spectra remains the same, ruling out the presence of other photophysical processes. In addition, the method is more reliable since the area under the spectrum is directly proportional to the quantum yield of fluorescence even if small spectral shifts are taking place. Since the emission in-between 300 and 330 nm originates exclusively from the tryptophans of WALP23, we fitted the emission spectrum of WALP23 in the absence of acceptor DHE in the range between 300 and 330 nm to the emission spectra for different concentrations of DHE. The FRET efficiency was then calculated from the area integral ratio between fitted spectrum and original spectrum for donor only as $E = 1 - (\Phi_{DA}/\Phi_D)$, where Φ is the quantum yield of the donor alone (D) or in the presence of acceptor (DA). Subtraction of the fitted spectrum from the total emission spectrum yielded the emission of DHE (Figure 2 B).

The FRET efficiencies are plotted in Figure 3 (open circles) as function of the surface density of DHE in the bilayer which was calculated from the mole fraction of DHE in the bilayer using an area per lipid molecule of 59.5 \AA^2 for di-C14:0PC [38] and 37.7 \AA^2 for DHE and cholesterol [39]. Condensation effects due to sterols present in the bilayer were assumed to be negligible at the low concentrations of sterols used here [39]. The FRET efficiency in a bilayer, a quasi two-dimensional system, depends on the Förster distance of the FRET pair, the exclusion radius of acceptor around the donor and the amount and distribution of acceptor in the bilayer. The theoretical FRET efficiency for a random distribution of WALP23 and DHE in both leaflets of the bilayer was calculated based on equations 2 and 3 computed into equation 5.

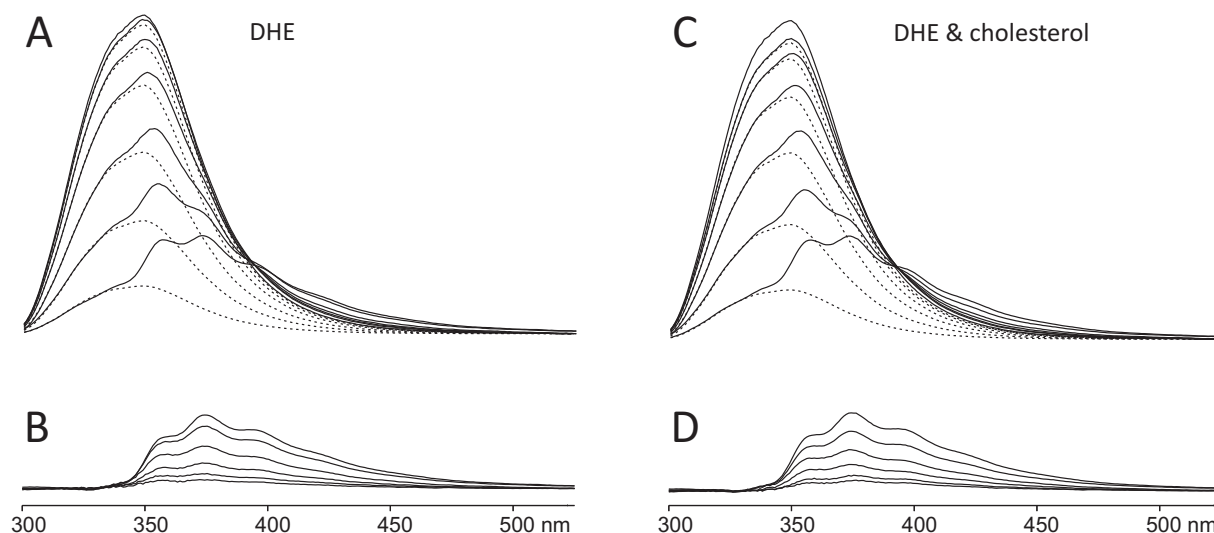


Figure 2: Fluorescence emission spectra of WALP23 and of DHE in bilayers of di-C14:0PC containing different concentrations of sterols at pH 7.0 and 30°C. (A) The solid lines are spectra from FRET experiments using increasing DHE concentrations (from top to bottom, 0, 0.25, 0.5, 1, 2, 4, and 8 mol%) added to the lipid fraction. The dashed lines show the fluorescence emission of the tryptophans of WALP23, obtained by decomposition. (B) Fluorescence emission of DHE (from top to bottom, 8, 4, 2, 1, 0.5, and 0.25 mol %), obtained by decomposition of the spectra in panel A. (C) Samples as in panel A but with equimolar amounts of DHE and cholesterol added to the lipid fraction. (D) Fluorescence emission of DHE in the presence of equimolar amounts of cholesterol, obtained by decomposition of the spectra in panel C. In all samples, the excitation wavelength was 280 nm and the final concentration of WALP23 was 5 μM using a peptide/lipid ratio of 1/200.

This curve is shown in Figure 3 (solid lines) for different theoretical values of the Förster distance. The experimentally determined FRET efficiencies for different surface densities of DHE match the theoretical FRET efficiency curve for the calculated Förster distance of 20 Å (circles in Figure 3). If the acceptor is excluded from the vicinity of the donor the experimental FRET efficiencies would be located below the theoretical FRET efficiency curve, (see [40] for a non-homogeneous distribution with acceptor excluded from donor). Alternatively, if the acceptor is attracted to the donor the experimental values would be located above the theoretical curve. Therefore, these results indicate that DHE is randomly distributed in the bilayer in the presence of tryptophan-flanked peptides.

As a complementary approach we also used time-resolved fluorescence techniques [41]. Fluorescence decays were recorded for the same samples compositions used for the steady-state measurements above (Figure 4A). With increasing DHE concentration in the lipid bilayer the intensity of tryptophan fluorescence is decaying faster due to increasing FRET from the tryptophans to DHE. The fluorescence decay of WALP23 in di-C14:0PC at 30°C shows multi-exponential behavior and can be described by a sum of three exponentials with the following parameters: $\tau_1 = 0.31$ ns (28%), $\tau_2 = 1.72$ ns (39%), and $\tau_3 = 5.24$ ns (33%), corresponding to an average lifetime of 4.12 ns. Both the average lifetime and the lifetime components are very similar to those obtained for the tryptophan-flanked γ M4 peptide, an α -helical transmembrane segment of the nicotinic acetylcholine receptor [40,42].

In a global analysis approach, the decay curves for different concentrations of DHE (shown in Figure 4A) were fitted simultaneously based on a FRET model for a single discrete concentration of acceptors according to equation 4. With exception of the varying acceptor density n , all other parameters (R_0 , R_e , $\langle \tau \rangle$ and w) were linked in the global analysis and therefore forced to have identical values for all decays i.e. the same values as for the integrated curve with $R_0 = 20$ Å shown in Figure 3. Good quality fits from global analysis are characterized by a low global χ^2_G , which is indicative for a good agreement with the underlying model of random distribution of acceptor molecules in the bilayer. The global analysis of the decay series for bilayers containing WALP23 and different concentrations of DHE yielded a low χ^2_G of 1.43 which indicates a homogeneous distribution of the acceptor DHE in the bilayer (compare [42]). This result confirms the findings from steady-state fluorescence experiments.

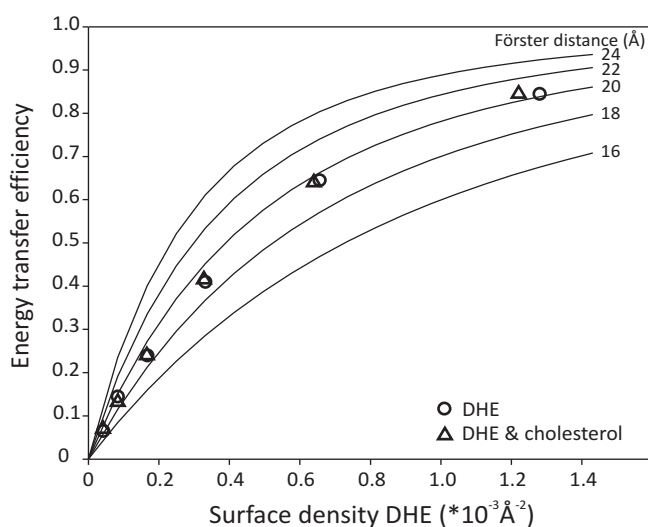


Figure 3: Theoretically calculated FRET efficiency curves (equation 5) for different Förster distances based on the model for a random distribution of acceptor taking into account transfer to both leaflets (equations 2 and 3) are shown as solid lines. FRET efficiencies calculated from steady-state data (Figure 2) with WALP23 as the donor and DHE as the acceptor depending on the surface density of the acceptor in the bilayer in the presence of only DHE (circles) and in the presence of the equimolar amounts of DHE and cholesterol (triangles).

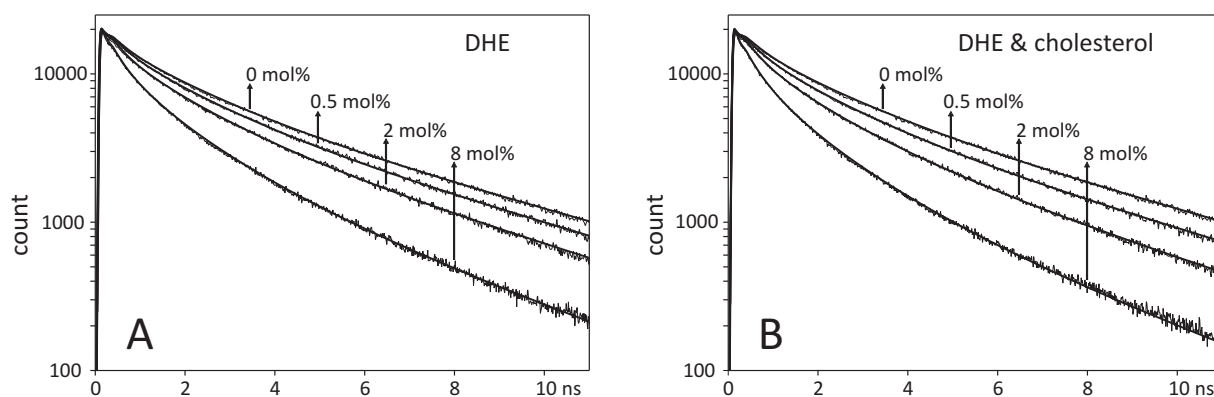


Figure 4: Fluorescence intensity decays of WALP23 in the presence of varying concentrations of DHE in bilayers of di-C14:0PC at pH 7.0 and 30 °C. The bilayers contained either no cholesterol (A) or equimolar amounts of cholesterol (B). Global analysis of the data according to the model for a random distribution of DHE (equations 2 and 3) resulted in the fitting curves shown, yielding global χ^2_G values of 1.43 for panel A and 1.35 for panel B.

Since the complex ring system of DHE has a different three-dimensional shape than the one of cholesterol, it is in principle possible that cholesterol, but not DHE interacts preferentially with the tryptophan-flanked peptide. This question was addressed by a competition experiment where also cholesterol is present in the bilayer. If cholesterol would also be randomly distributed in the bilayer, the FRET efficiency should stay unchanged, whereas if cholesterol is attracted towards the tryptophans, it pushes the acceptor DHE away from the tryptophans and lowers the effective acceptor surface density in the vicinity of the donor, which in turn lowers the FRET efficiency (see Figure 5).

Steady-state fluorescence spectra were recorded on samples containing equimolar concentrations of DHE and cholesterol in the lipid fraction (Figure 2C) and were analyzed as above. The results show that also in the presence of cholesterol the experimentally determined FRET efficiencies match the theoretical FRET efficiency curve for the Förster distance of 20 Å for the pair WALP23 and DHE (triangles in Figure 3). Thus, the competition experiments indicate a random distribution of cholesterol in the bilayer. This was supported by fluorescence decay measurements on samples containing equimolar amounts of DHE and

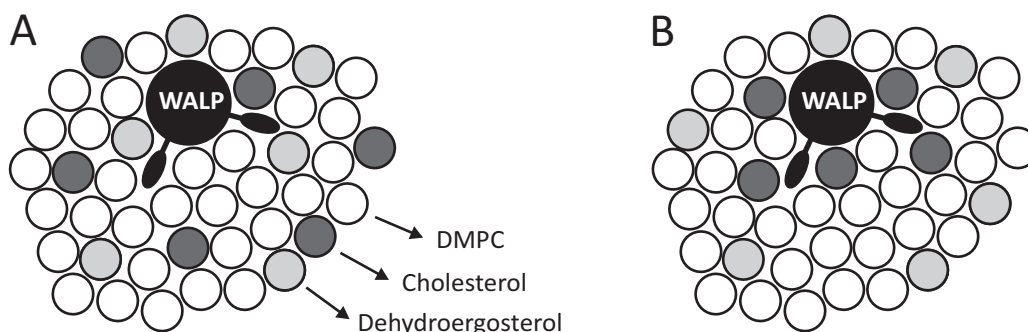


Figure 5: Schematic top view of the membrane illustrating two possible outcomes for the competition experiment using bilayers containing DHE and cholesterol. (A) Both DHE (gray circles) and cholesterol (black circles) are randomly distributed which leaves the FRET efficiency unchanged when compared to that from the experiment in the absence of cholesterol. (B) Cholesterol occupies the sites next to the tryptophans of WALP23 and pushes in turn DHE away which leads to a lower FRET efficiency.

cholesterol in the lipid fraction (Figure 4B). There is no significant change in decay behavior if also cholesterol is added to the bilayer compared to bilayers only containing DHE (Figure 4A). Global analysis of the decay series for different equimolar concentrations of DHE and cholesterol yielded a χ^2_G of 1.35, indicating a good agreement with the underlying model of random distribution of DHE (and therefore also of cholesterol) in the bilayer, which strongly supports the finding of a random distribution of both DHE and cholesterol in the bilayer.

^2H NMR results

All results obtained from fluorescence experiments indicate a random distribution of cholesterol in the bilayer in the presence of tryptophan-flanked peptides. Nevertheless, it is still possible that specific interactions occur between cholesterol and interfacial tryptophans which could influence the behavior of these molecules and thereby influence the properties of the membrane. Such an interaction could also be mediated via neighboring lipids. To investigate these possibilities, we performed ^2H NMR experiments on samples containing either deuterated cholesterol or tryptophan deuterated WALP peptides. ^2H NMR spectroscopy is a very sensitive tool to observe small changes in the dynamics and/or the orientational properties of molecules and does not rely on the use of a fluorescent cholesterol analogue. Any change in orientation and/or dynamics of labeled molecules leads to a change in ^2H NMR spectra since the average orientation of the C-D bonds with respect to the magnetic field is altered. ^2H NMR experiments can also be used to detect different populations of molecules that may occur if only parts of the population are influenced by specific interactions with other molecules. We investigated both the effect of WALP23 on deuterated cholesterol and the effect of cholesterol on tryptophan deuterated WALP23.

Influence of tryptophan-flanked peptides on deuterated cholesterol

For the ^2H NMR measurements we used β -(d_6 -2,2,3,4,4,6)cholesterol which has deuterons located near the hydroxyl head group. To investigate the influence of WALP23 peptides on deuterated cholesterol we incorporated 2 or 4 mol% of cholesterol into unoriented di-C14:0PC bilayers and compared the spectra in the presence and absence of 1 mol% of the tryptophan-flanked WALP23 peptide. To distinguish effects due to the presence of interfacial tryptophans from effects due to the incorporation of peptides into the cholesterol containing bilayers we used the lysine-flanked KALP23 peptide as a control peptide. At first glance the ^2H NMR spectra of all these samples (shown in Figure 6) look very similar, indicating that there are no large effects in the orientation and dynamics of cholesterol. However, some subtle but significant changes in the values of the quadrupolar splittings occur which will be discussed later.

The ^2H NMR spectrum for a bilayer containing 2 mol% of deuterated cholesterol in the absence of peptide (top row in Figure 6) is typical for β -(d_6 -2,2,3,4,4,6)cholesterol incorporated into fluid phase bilayers [43]. Knowing that the orientation of cholesterol in the bilayer is rather fixed along its long axis, the similarity of the ^2H NMR spectra suggests the same assignment of the splittings to the deuterons in all cases which allows direct comparison of the quadrupolar splittings summarized in Table 2.

Closer inspection of the quadrupolar splittings in the absence of peptides shows that addition of more cholesterol (4 mol%) leads to a small increase of 0.6 - 0.8 kHz in quadrupolar splittings. Cholesterol is known to straighten the acyl chains of surrounding lipids which leads to a condensation effect on the membrane bilayer. This affects the

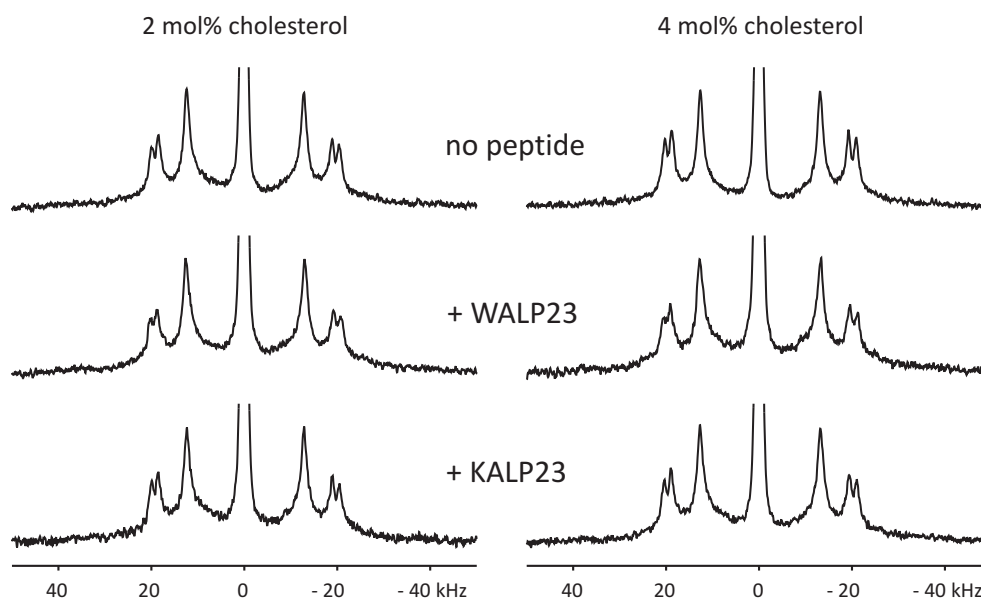


Figure 6: ^2H NMR spectra of β -(d_6 -2,2,3,4,4,6)cholesterol in unoriented bilayers of di-C14:0PC at pH 7.0 and 40°C in the absence and presence of KALP23 or WALP23. The quadrupolar splittings can be assigned to the deuterons in β -(d_6 -2,2,3,4,4,6)cholesterol starting from outside: (3), (2,4)_{ax}, (2,4)_{eq}; position (6) is hidden in the central isotropic peak [43,44].

dynamics of cholesterol itself which leads to the larger quadrupolar splittings [43]. This observation demonstrates that ^2H NMR spectroscopy employing deuterated cholesterol is a sensitive tool to observe very small changes in the behavior of cholesterol.

The presence of WALP23 peptides in the bilayer leads to a small but significant increase of 0.4 - 0.6 kHz in the quadrupolar splittings at both cholesterol concentrations used. Control experiments using 1 mol% of KALP23 show no significant increase in the quadrupolar splittings in the presence of a lysine-flanked peptide. This could suggest an interaction between cholesterol and tryptophan. However, it was shown before that WALP23 also has a stretching effect on the bilayer similar to cholesterol [18] which could cause an increase in quadrupolar splittings. Therefore, the increase in quadrupolar splittings could also be due to the membrane stretching effect of WALP23.

Table 2: Quadrupolar splittings from ^2H NMR spectra of unoriented samples containing deuterated cholesterol.

Peptide	Cholesterol (mol%)	Quadrupolar splittings (kHz)		
		(3)	(2,4) _{ax}	(2,4) _{eq}
no peptide	2	40.4	37.4	25.2
	4	41.2	38.1	25.8
WALP23	2	41.0	38.0	25.6
	4	41.8	38.7	26.2
KALP23	2	40.4	37.5	25.2
	4	41.3	38.3	25.9
WLP23	2	42.3	39.4	26.5
KLP23	2	40.7	37.8	25.4

To discriminate between these possibilities we investigated how membrane stretching due to the presence of peptides in the membrane influences the quadrupolar splittings. For this purpose we used WLP23 and KLP23 which have the same length as WALP23 and KALP23 but have a more hydrophobic stretch of only leucines. Previously, it was found that a lysine-flanked transmembrane peptide having a hydrophobic core of polyleucines exerts a larger ordering effect on lipid acyl chains than an analogous peptide with a core of alternating leucines and alanines [45]. Preliminary experiments in our laboratory indicated that this is also the case for WLP23 and KLP23. If membrane stretching due to the peptides in the bilayer would be the only factor responsible for the increase in quadrupolar splittings of deuterated cholesterol, then we should expect an increase in the quadrupolar splittings for WLP23 compared to WALP23 and for KLP23 compared to KALP23. Evaluation of the quadrupolar splittings for WLP23 and KLP23 listed in Table 2 (^2H NMR spectra not shown) shows that the presence of the polyleucine peptides in the membrane indeed leads to a significant increase in the quadrupolar splittings as compared to the leucine-alanine peptides. Thus, the difference in the quadrupolar splittings in the presence of WALP23 and KALP23 in the bilayer can most likely be attributed to differences in the stretching effect of the peptides.

It is important to note that all ^2H NMR spectra compared show only one component upon addition of WALP23 peptides to the bilayer. This absence of a second component points towards one major population of cholesterol in the bilayer. Therefore, the ^2H NMR experiments using deuterated cholesterol provide no indication for an effect on the dynamics and/or orientation of cholesterol caused by an interaction with interfacial tryptophans.

Influence of cholesterol on deuterated tryptophan side chains

Next, in a complementary approach we investigated whether the presence of cholesterol changes the orientation and/or dynamics of the interfacial tryptophans. We performed ^2H NMR experiments using tryptophan deuterated WALP23 peptides. The peptides were synthesized with tryptophans containing a deuterated indole ring in one position at a time (for amino acid sequences see Table 1). Oriented samples with a peptide/lipid ratio of 1:25 containing either no or 4 mol% of cholesterol in the lipid fraction were prepared. ^{31}P NMR measurements on all oriented samples confirmed a good alignment of the bilayers along the glass platelets (^{31}P NMR spectra not shown). The ^2H NMR spectra of samples containing WALP23- d_5 -Trp2 and WALP23- d_5 -Trp3 in the presence and the absence of cholesterol are shown in Figure 7. The measurements were performed at two different orientations of the bilayers: at 0° with the membrane normal aligned to the magnetic field and at 90° with the membrane normal perpendicular to the magnetic field.

The indole ring contains five deuterons where two deuterons (positions 4 and 7) are equivalent in view of the geometry of the indole ring and therefore bear the same quadrupolar splitting [21]. Thus four quadrupolar splittings are expected for WALP23 with indole ring deuterated tryptophans. Previous ^2H NMR experiments on oriented samples containing the tryptophan-flanked Gramicidin A [21,46,47] or WALP peptides [48,49] showed that not all splittings are always detected for either orientation of the bilayers with respect to the magnetic field. Looking at the ^2H NMR spectra for WALP23- d_5 -Trp2 four splittings can be distinguished for the 90° orientation (Figure 7A, right column) compared to only three splittings for the 0° orientation (Figure 7A, left column). The size of the quadrupolar

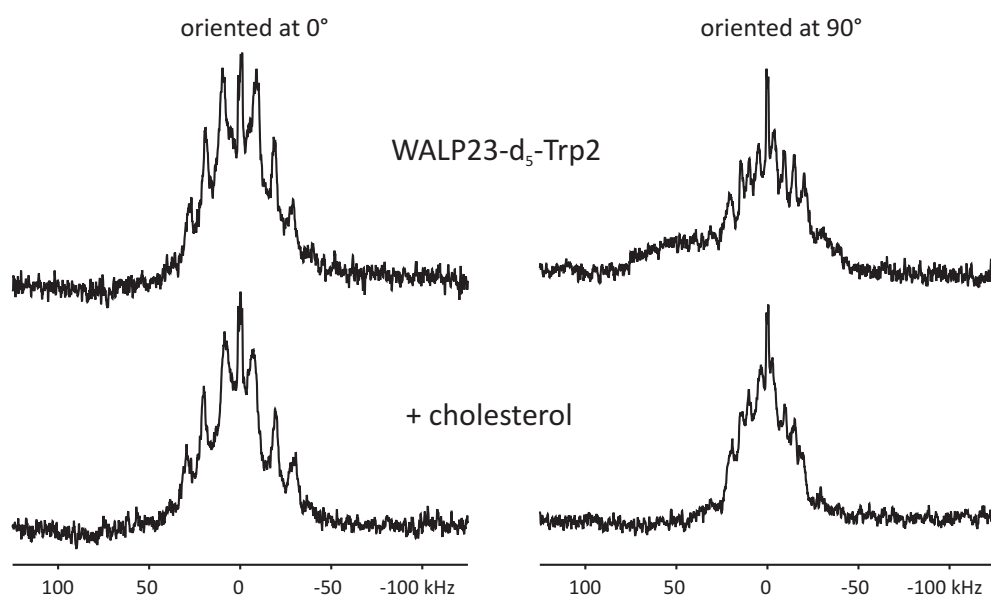


Figure 7: ^2H NMR spectra of WALP23- d_5 -Trp2 (A) and WALP23- d_5 -Trp3 (B) in oriented bilayers of di-C14:0PC at pH 7.0 in the absence and presence of 4 mol% cholesterol added to the lipid fraction at 40% hydration (w/w) and measured at 40°C.

splittings in the 90° orientation can be expected to be halved compared to the 0° orientation due to the fast axial reorientation of the peptides about the bilayer normal [36]. Comparison of the values for WALP23- d_5 -Trp2 in Table 3 shows that this is indeed the case. From these values it can furthermore be concluded that the largest splitting in the 0° orientation is not detected. This is probably due to insufficient sensitivity caused by the magnitude of the quadrupolar splittings in combination with the relatively low peptide/lipid ratio.

The assignments of the quadrupolar splittings to the deuterons of the indole ring cannot be done unambiguously without further experiments e.g. ^2H NMR experiments with partly deuterated indole rings [21] or NMR experiments employing other labels. Nevertheless, the quadrupolar splittings can be considered as fingerprints for the orientational and motional properties of the tryptophan side chains. The shape of the ^2H NMR spectrum of WALP23- d_5 -Trp2 does not change upon addition of cholesterol (compare Figure 7A, top row and bottom row), and there is no significant increase or decrease in the visible quadrupolar splittings (see Table 3). For WALP23- d_5 -Trp3 it is more difficult to distinguish (all) the quadrupolar splittings (data not listed) but also for this peptide the same findings hold (Figure 7B). The results therefore suggest that the orientation and dynamics of the indole rings are not influenced by cholesterol (on the ^2H NMR time scale). Hence also these experiments indicate that there is no specific interaction between cholesterol and interfacial tryptophans.

Table 3: Quadrupolar splittings from ^2H NMR spectra of unoriented samples containing WALP- d_5 -Trp2 in the absence and presence of cholesterol.

Orientation	Cholesterol (mol%)	Quadrupolar splittings* (kHz)			
0°	-	18	38	57	-
90°	-	9	19	29	41
0°	4	15	40	60	-
90°	4	6	20	30	39

* The quadrupolar splittings are estimated to have an experimental error of 1-2 kHz (compare [49])

Discussion

The main objective of the present study was to investigate how cholesterol and interfacial tryptophans of transmembrane peptides or proteins interact in a bilayer and what the possible consequences are for the organization and distribution of these molecules in membranes. For our study we chose a well-defined model system of tryptophan-flanked transmembrane peptides incorporated into cholesterol containing bilayers, sampling a biologically relevant system for such an interaction. To gain insight into the interaction between cholesterol and interfacial tryptophans, we employed a two-fold approach including FRET experiments and solid-state ^2H NMR measurements.

Choice for a low cholesterol concentration in the bilayer

All experiments were performed on bilayers containing only small amounts of cholesterol in the lipid fraction. One reason for this was the consideration that if indeed preferential interactions would occur, they would most easily be observed at low cholesterol concentrations where random contacts between the peptide and the sterol are only few. Even more important however was the consideration that a low cholesterol content is essential to ensure a homogeneous system. It is well known that higher cholesterol concentrations in a phospholipid bilayer can lead to the formation of coexistent phases in the bilayer [50,51]. The onset of phase separation into liquid-ordered (L_o) and liquid-disordered (L_d) domains is strongly dependent on temperature and cholesterol content. For the two-component system di-C14:OPC/cholesterol used in this study, at 30°C the phase separation starts at 8 mol% cholesterol in the bilayer and for 40°C at 14 mol% cholesterol [52], generating a laterally heterogeneous composition of the bilayer. The liquid-ordered domains contain a higher cholesterol concentration and have an increased membrane thickness compared to the liquid-disordered domains. The resulting heterogeneous system would complicate, if not prohibit the interpretation of the experimental data.

This holds in particular for the FRET experiments where data analysis is based on the comparison of experimental FRET efficiencies with theoretical FRET efficiencies where the values are calculated based on a random distribution of donor and acceptor in the bilayer. In the case of a phase separation in the bilayer more cumbersome models would have to be used, which would have to account, among other complexities, for the partitioning of both peptide and DHE between the different phases [41]. For these various reasons we decided to use only small cholesterol concentrations of less than 8 mol% of cholesterol in di-C14:OPC bilayers for our experiments.

Cholesterol does not preferentially localize next to tryptophan-flanked peptides

In case of a preferential interaction with interfacial tryptophans, one would expect a nonrandom distribution of cholesterol in the bilayer when a tryptophan-flanked peptide is included. The sterol would be preferentially localized in the vicinity of the peptide and hence would be depleted from the bulk lipid. To analyze the distribution of cholesterol in the bilayer FRET experiments were performed in which we used the tryptophans of the WALP23 peptides as donor and the fluorescent cholesterol analogue DHE as acceptor. We found that DHE is randomly distributed in the presence of interfacial tryptophans, suggesting that there is no preferential interaction between DHE and interfacial tryptophans.

In these experiments DHE was used because cholesterol does not possess a chromophore with absorption overlapping the emission of tryptophan and because DHE was shown to be suitable for investigation of sterol behavior in the membrane [25]. Similar studies employing the cholesterol analogue DHE as acceptor for FRET experiments have been done on e.g. melittin [53] and the γ M4 segment of the nicotinic acetylcholine receptor AChR [40]. Although cholestatrienol, another fluorescent cholesterol analogue, mimics the properties of cholesterol in the membrane better [54], this analogue has some disadvantages compared to DHE. It degrades rapidly and requires diligent sample handling [55]. Concerning the special properties of cholesterol in the membrane, both analogues do mimic cholesterol only to a limited extent and have poorer condensation effects on the bilayer [54,56]. This emerges from two extra double bonds in the complex ring structure of DHE and cholestatrienol, which cause the fluorescent character but also change the three-dimensional shape of the analogues in comparison to cholesterol.

In principle, it is possible that the difference in three-dimensional structure between DHE and cholesterol could change the behavior with respect to a possible (stacking) interaction with interfacial tryptophans. To gain information on the distribution of cholesterol itself in bilayers containing tryptophan-flanked peptides, we performed a competition experiment in which both the fluorescent cholesterol analogue DHE and cholesterol were incorporated into the bilayers at the same concentration. Cholesterol was found not to compete with DHE for sites next to the tryptophans which strongly suggests that cholesterol is randomly distributed in the bilayer. This finding points towards no preferential interaction between cholesterol and interfacial tryptophans, suggesting that it is equally favorable for cholesterol to be adjacent to WALP23 peptides as to be in contact with the lipid acyl chains.

Cholesterol and interfacial tryptophans do not affect each others orientation and/or dynamics

Even for a random distribution of cholesterol in the bilayer it is still possible that cholesterol and interfacial tryptophans affect each other in a specific way, possibly mediated by adjacent lipids. Since any interaction between two molecules is associated with changes in the dynamics and/or orientation of the molecules involved, we used solid-state ^2H NMR spectroscopy to test this hypothesis. This technique is a sensitive tool to observe small changes in dynamics and/or orientation of deuterium labeled compounds in a lipid bilayer.

We performed ^2H NMR measurements employing either deuterated cholesterol or tryptophan deuterated WALP23 peptides. We found that the magnitudes of the quadrupolar splittings yielded by the deuterated tryptophans do not change after addition of cholesterol to the bilayer. In case of deuterated cholesterol small changes in the sizes of the quadrupolar splittings were observed, which could be attributed to small differences in effects of the peptides on lipid chain order in the bilayer. These findings suggest that there is no change in average orientation or in dynamics for either cholesterol or the tryptophan side chains of WALP23, and therefore that these molecules have neither a direct nor a lipid mediated influence on each other. Another important observation was that for all ^2H NMR spectra recorded in the presence of either deuterated cholesterol or deuterated tryptophan-flanked peptides in the bilayer, only one component could be distinguished. This absence of a second population is another indication for the absence of specific interactions resulting in preferential surrounding of the peptide by cholesterol. Hence, these findings are in good agreement with the results from the FRET experiments.

Nature of interaction between cholesterol and interfacial tryptophans

Looking at the molecular structures of cholesterol and tryptophan, it is very well conceivable that the complex ring structure of cholesterol directly interacts with the tryptophan indole ring. Indeed, molecular modeling studies suggested favorable stacking interactions between cholesterol and tryptophan where the face of the complex ring system of cholesterol and the indole ring of tryptophan build the interaction interface (personal communication with R. Brasseur, CBMN in Gembloux, Belgium). In a phospholipid bilayer, the long axis and therefore also the flat face of the complex ring system of cholesterol is oriented almost parallel to the bilayer normal [44,57]. It is possible to calculate the orientation of the tryptophan side chain with respect to the bilayer from the quadrupolar splittings of a deuterated indole ring if the spectral assignments are known [21,47].

Preliminary attempts to calculate the orientations of the deuterated tryptophans of WALP23-*d*₅-Trp2 and WALP23-*d*₅-Trp3 using an automatic assignment procedure yielded for both tryptophan positions a reliable minimum for a single orientation. The best fits to the sets of quadrupolar splittings summarized in Table 3 yielded very similar orientations both in the absence and presence of cholesterol in the bilayer. For both WALP23-*d*₅-Trp2 and WALP23-*d*₅-Trp3 the flat face of the tryptophan indole ring adopts an angle of approximately 30° with respect to the bilayer normal which is comparable to the orientations determined for the tryptophan side chains in gramicidin A [21]. Such an orientation of the tryptophan indole ring would imply that for a stacking interaction either the indole ring or the cholesterol would need to turn about 30° with respect to the bilayer normal. ²H NMR experiments clearly show that the orientations of both the indole ring and cholesterol remain unchanged in the presence of the respective other molecule in the bilayer. In view of the considerations above this suggests that no direct stacking interaction occurs between tryptophan and cholesterol.

In general, two molecules will preferentially interact if this interaction leads to a decrease of the free energy of the system. Apparently the energy cost for changing the orientation of interfacial tryptophans and/or cholesterol to facilitate a preferential interaction in combination with the loss of entropy resulting from such an interaction is higher than the energy gain from a specific interaction between the two molecules. By itself this is not surprising. The orientation of cholesterol in the bilayer is governed by its amphiphilic properties whereby the small hydroxyl headgroup of cholesterol preferably resides between the phospholipid headgroups. A change in the orientation of cholesterol, e.g. of 30° with respect to the bilayer normal, can be expected to result in a large energy cost due to its preferable alignment alongside the lipid acyl chains. The side chain of tryptophan is small compared to cholesterol, but it is connected to a larger peptide backbone, which restricts the number of possible and energetically favorable orientations. Statistical analysis of side chain conformations in α -helices of known structures of (membrane) proteins show that only certain combinations of ϕ and ψ torsion angles for tryptophans are feasible and favorable [58,59]. These constraints may prevent a preferential interaction between tryptophans and cholesterol in the bilayer.

The results of the present study seem in contradiction with all earlier indications found for a specific interaction between cholesterol and tryptophans located in the bilayer. How can we explain this? It is important to note here, that all experiments indicating such a preferential interaction were carried out in bilayer systems with a relatively high cholesterol content. Either the protein resides in a membrane that (natively) has a very high cholesterol content, as is the case of the acetylcholine receptor enriched membranes from the neuro-muscular junction [14], or the membrane contains cholesterol-rich domains, as for caveolae [13] or lipid rafts [1], into which the protein partitions favorably.

High cholesterol concentrations in a bilayer change the behavior of the cholesterol in the bilayer itself as well as the material properties of the bilayers compared to a bilayer containing no or only low concentrations of cholesterol [60]. Thus, it is possible that the two situations may not be comparable and that our findings may not be applicable to proteins in caveolae and rafts. Furthermore, in the case that a tryptophan containing peptide or protein is present in a cholesterol-rich environment, this will increase the probability for their interaction. Together with the changed bilayer properties this may result in a modulation of membrane and protein structure and dynamics, which in the studies mentioned above has been explained to possibly involve a preferential interaction between cholesterol and tryptophans.

The suggested specificity for cholesterol and tryptophan in these studies may also be related to the anchoring properties of tryptophans in membrane proteins. Previously it has been observed that tryptophans are preferably located in the lipid-water interface [7,9,61]. Higher cholesterol concentrations are known to lead to a laterally heterogeneous bilayer containing cholesterol enriched domains which have an increased thickness compared to the cholesterol depleted domains. Depending on its hydrophobic length the peptide/protein can be driven towards the thicker and thus cholesterol enriched domains of the bilayer to relieve the hydrophobic mismatch. Since tryptophans have been shown to be essential for proper positioning of proteins in (biological) membranes [62-65] a mutation in this residue may place it out of cholesterol-rich domains even when there is no specific interaction between cholesterol and interfacial tryptophans. Hence there would be only an apparent specificity.

In any case, our study on model systems with relatively low cholesterol concentrations has clearly demonstrated that cholesterol and tryptophan do not have a *general* tendency to preferentially interact with one another. This is an important result, because it helps understanding the basic principles behind organization of proteins and lipids in membranes, here in particular between interfacial tryptophans abundant in membrane proteins and cholesterol, a membrane constituent in many types of biological membranes.

Acknowledgements

This research project has been supported by a Marie Curie Early Stage Research Training Fellowship from the European Community's Sixth Framework Program for A.H. (Biomem-MEST-CT 2004-007931). We thank R. Brasseur and A. Thomas (Centre de Biophysique Moléculaire Numérique, Faculté Universitaire des Sciences Agronomiques de Gembloux, Gembloux, Belgium), and B. de Kruijff (Utrecht University) for stimulating discussions, and A. Fedorov (Instituto Superior Técnico, Lisbon) for help with the time-resolved fluorescence spectroscopy measurements.

References

1. Epand RM (2006) Cholesterol and the interaction of proteins with membrane domains. *Prog Lipid Res*, 45:279–294.
2. Pike LJ (2004) Lipid rafts: heterogeneity on the high seas. *Biochem J*, 378:281–292.
3. Hancock JF (2006) Lipid rafts: contentious only from simplistic standpoints. *Nat Rev Mol Cell Biol*, 7:456–462.
4. Ohvo-Rekilä H, Ramstedt B, Leppimäki P, and Slotte JP (2002) Cholesterol interactions with phospholipids in membranes. *Prog Lipid Res*, 41:66–97.
5. van Duyl BY, Meeldijk H, Verkleij AJ, Rijkers DTS, Chupin V, de Kruijff B, and Killian JA (2005) A synergistic effect between cholesterol and tryptophan-flanked transmembrane helices modulates membrane curvature. *Biochemistry*, 44:4526–4532.
6. Yau WM, Wimley WC, Gawrisch K, and White SH (1998) The preference of tryptophan for membrane interfaces. *Biochemistry*, 37:14713–14718.
7. Schiffer M, Chang CH, and Stevens FJ (1992) The functions of tryptophan residues in membrane proteins. *Protein Engineering*, 5:213–214.
8. Braun P and von Heijne G (1999) The aromatic residues Trp and Phe have different effects on the positioning of a transmembrane helix in the microsomal membrane. *Biochemistry*, 38:9778–9782.
9. de Planque MRR, Bonev BB, Demmers JAA, Greathouse DV, Koeppe II RE, Separovic F, Watts A, and Killian JA (2003) Interfacial anchor properties of tryptophan residues in transmembrane peptides can dominate over hydrophobic matching effects in peptide-lipid interactions. *Biochemistry*, 42:5341–5348.
10. White SH and Wimley WC (1998) Hydrophobic interactions of peptides with membrane interfaces. *Biochim Biophys Acta*, 1376:339–352.
11. Dougherty DA (1996) Cation- π interactions in chemistry and biology: a new view of benzene, Phe, Tyr, and Trp. *Science*, 271:163–168.
12. Gasset M, Killian JA, Tournois H, and de Kruijff B (1988) Influence of cholesterol on gramicidin-induced H_{II} phase formation in phosphatidylcholine model membranes. *Biochim Biophys Acta*, 939:79–88.
13. Carozzi AJ, Roy S, Morrow IC, Pol A, Wyse B, Clyde-Smith J, Prior IA, Nixon SJ, Hancock JF, and Parton RG (2002) Inhibition of lipid raft-dependent signaling by a dystrophy-associated mutant of caveolin-3. *J Biol Chem*, 277(20):17944–17949.
14. Santiago J, Guzmán GR, Rojas LV, Marti R, Asmar-Rovira GA, Santana LF, McNamee M, and Lasalde-Dominicci JA (2001) Probing the effects of membrane cholesterol in the *Torpedo californica* acetylcholine receptor and the novel lipid-exposed mutation alphaC418W in *Xenopus* oocytes. *J Biol Chem*, 276:46523–46532.
15. Killian JA and von Heijne G (2000) How proteins adapt to a membrane-water interface. *Trends Biochem Sci*, 25:429–434.
16. Killian JA (2003) Synthetic peptides as models for intrinsic membrane proteins. *FEBS Lett*, 555:134–138.
17. Killian JA and Nyholm TKM (2006) Peptides in lipid bilayers: the power of simple models. *Curr Opin Struct Biol*, 16:473–479.
18. de Planque MRR, Kruijtzter JAW, Liskamp RMJ, Marsh D, Greathouse DV, Koeppe II RE, de Kruijff B, and Killian JA (1999) Different membrane anchoring positions of tryptophan and lysine in synthetic transmembrane alpha-helical peptides. *J Biol Chem*, 274(30):20839–20846.
19. ten Kortenaar PBW, van Dijk BG, Peeters JM, Raaben BJ, Adams PJHM, and Tesser GI (1986) Rapid and efficient method for the preparation of Fmoc-amino acids starting from 9-fluorenylmethanol. *Int J Pept Prot Res*, 27:398–400.
20. Greathouse DV, Koeppe II RE, Providence LL, Shobana S, and Andersen OS (1999) Design and characterization of gramicidin channels. *Methods Enzymol*, 294:525–550.
21. Koeppe II RE, Sun H, van der Wel PCA, Scherer EM, Pulay P, and Greathouse DV (2003) Combined experimental/theoretical refinement of indole ring geometry using deuterium magnetic resonance and ab initio calculations. *J Am Chem Soc*, 125:12268–12276.
22. Rijkers DTS, Kruijtzter JAW, Killian JA, and Liskamp RMJ (2005) A convenient solid phase synthesis of S-palmitoyl transmembrane peptides. *Tetrahedron Lett*, 46:3341–3345.

23. Rouser G, Fleischer S, and Yamamoto A (1970) Two-dimensional thin layer chromatographic separation of polar lipids and determination of phospholipids by phosphorus analysis of spots. *Lipids*, 5:494–496.
24. Sparr E, Ganchev DN, Snel MME, Ridder ANJA, Kroon-Batenburg LMJ, Chupin V, Rijkers DTS, Killian JA, and de Kruijff B (2005) Molecular organization in striated domains induced by transmembrane alpha-helical peptides in dipalmitoyl phosphatidylcholine bilayers. *Biochemistry*, 44:2–10.
25. Smutzer G, Crawford BF, and Yeagle PL (1986) Physical properties of the fluorescent sterol probe dehydroergosterol. *Biochim Biophys Acta*, 862:361–371.
26. Gardecki JA and Maroncelli M (1998) Set of secondary emission standards for calibration of the spectral responsivity in emission spectroscopy. *Appl Spectrosc*, 52(9):1179–1189.
27. Loura LMS, Fedorov A, and Prieto M (1996) Resonance energy transfer in a model system of membranes: application to gel and liquid crystalline phases. *Biophys J*, 71:1823–1836.
28. Loura LMS, Fedorov A, and Prieto M (2000) Membrane probe distribution heterogeneity: a resonance energy transfer study. *J Phys Chem B*, 104(29):6920–6931.
29. Marquardt DW (1963) An algorithm for least-squares estimation of nonlinear parameters. *Journal of the Society for Industrial and Applied Mathematics*, 11:431–441.
30. Lakowicz JR (1999) Principles of Fluorescence Spectroscopy. Kluwer Academic / Plenum Publishers.
31. Davenport L, Dale RE, Bisby RH, and Cundall RB (1985) Transverse location of the fluorescent probe 1,6-diphenyl- 1,3,5-hexatriene in model lipid bilayer membrane systems by resonance excitation energy transfer. *Biochemistry*, 24:4097–4108.
32. Salamon Z, Lindblom G, Rilfors L, Linde K, and Tollin G (2000) Interaction of phosphatidylserine synthase from *E. coli* with lipid bilayers: coupled plasmon-waveguide resonance spectroscopy studies. *Biophys J*, 78:1400–1412.
33. Stryer L (1978) Fluorescence energy transfer as a spectroscopic ruler. *Annu Rev Biochem*, 47:819–846.
34. Vos WL, Koehorst RBM, Spruijt RB, and Hemminga MA (2005) Membrane-bound conformation of M13 major coat protein - a structure validation through FRET-derived constraints. *J Biol Chem*, 280:38522–38527.
35. Wolber PK and Hudson BS (1979) An analytic solution to the Förster energy transfer problem in two dimensions. *Biophys J*, 28:197–210.
36. Strandberg E, Özdirekcan S, Rijkers DTS, van der Wel PCA, Koeppe II RE, Liskamp RMJ, and Killian JA (2004) Tilt angles of transmembrane model peptides in oriented and non-oriented lipid bilayers as determined by 2H solid-state NMR. *Biophys J*, 86:3709–3721.
37. Davis JH (1983) The description of membrane lipid conformation, order and dynamics by 2H-NMR. *Biochim Biophys Acta*, 737(1):117–171.
38. Koenig BW, Strey HH, and Gawrisch K (1997) Membrane lateral compressibility determined by NMR and X-ray diffraction: effect of acyl chain polyunsaturation. *Biophys J*, 73:1954–1966.
39. Smaby JM, Momsen MM, Brockman HL, and Brown RE (1997) Phosphatidylcholine acyl unsaturation modulates the decrease in interfacial elasticity induced by cholesterol. *Biophys J*, 73:1492–1505.
40. de Almeida RFM, Loura LMS, Prieto M, Watts A, Fedorov A, and Barrantes FJ (2004) Cholesterol modulates the organization of the gammaM4 transmembrane domain of the muscle nicotinic acetylcholine receptor. *Biophys J*, 86:2261–2272.
41. Loura LMS, de Almeida RFM, and Prieto M (2001) Detection and characterization of membrane microheterogeneity by resonance energy transfer. *J Fluoresc*, 11:197–209.
42. de Almeida RFM, Loura LMS, Prieto M, Watts A, Fedorov A, and Barrantes FJ (2006) Structure and dynamics of the gammaM4 transmembrane domain of the acetylcholine receptor in lipid bilayers: insights into receptor assembly and function. *Mol Membr Biol*, 23:305–315.
43. Léonard A and Dufourc E (1991) Interactions of cholesterol with the membrane lipid matrix. A solid state NMR approach. *Biochimie*, 73:1295–1302.
44. Marsan MP, Muller I, Ramos C, Rodriguez F, Dufourc EJ, Czaplicki J, and Milon A (1999) Cholesterol orientation and dynamics in dimyristoylphosphatidylcholine bilayers: a solid state deuterium NMR analysis. *Biophys J*, 76:351–359.

45. Paré C, Lafleur M, Liu F, Lewis RN, and McElhane RN (2001) Differential scanning calorimetry and ²H nuclear magnetic resonance and fourier transform infrared spectroscopy studies of the effects of transmembrane alpha-helical peptides on the organization of phosphatidylcholine bilayers. *Biochim Biophys Acta*, 1511:60–73.
46. Killian JA, Taylor MJ, and Koeppe II RE (1992) Orientation of the valine-1 side chain of the gramicidin transmembrane channel and implications for channel functioning. A ²H NMR study. *Biochemistry*, 31:11283–11290.
47. Koeppe II RE, Killian JA, and Greathouse DV (1994) Orientations of the tryptophan 9 and 11 side chains of the gramicidin channel based on deuterium nuclear magnetic resonance spectroscopy. *Biophys J*, 66:14–24.
48. van der Wel PCA, Strandberg E, Killian JA, and Koeppe II RE (2002) Geometry and intrinsic tilt of a tryptophan-anchored transmembrane alpha-helix determined by ²H NMR. *Biophys J*, 83:1479–1488.
49. van der Wel PCA, Reed ND, Greathouse DV, and Koeppe II RE (2007) Orientation and motion of tryptophan interfacial anchors in membrane-spanning peptides. *Biochemistry*, 46:7514–7524.
50. Ipsen JH, Mouritsen OG, and Bloom M (1990) Relationships between lipid membrane area, hydrophobic thickness, and acyl-chain orientational order: the effects of cholesterol. *Biophys J*, 57:405–412.
51. Silvius JR (2003) Role of cholesterol in lipid raft formation: lessons from lipid model systems. *Biochim Biophys Acta*, 1610:174–183.
52. Almeida PFF, Vaz WLC, and Thompson TE (1992) Lateral diffusion in the liquid phases of dimyristoylphosphatidylcholine/cholesterol lipid bilayers: a free volume analysis. *Biochemistry*, 31:6739–6747.
53. Raghuraman H and Chattopadhyay A (2004) Interaction of melittin with membrane cholesterol: a fluorescence approach. *Biophys J*, 87:2419–2432.
54. Scheidt HA, Müller P, Herrmann A, and Huster D (2003) The potential of fluorescent and spin-labeled steroid analogs to mimic natural cholesterol. *J Biol Chem*, 278(46):45563–45569.
55. Fischer RT, Stephenson FA, Shafiee A, and Schroeder F (1984) Delta5,7,9(11)-cholestatrien-3beta-ol: a fluorescent cholesterol analogue. *Chem Phys Lipids*, 36:1–14.
56. Ohvo-Rekilä H, Akerlund B, and Slotte JP (2000) Cyclodextrin-catalyzed extraction of fluorescent sterols from monolayer membranes and small unilamellar vesicles. *Chem Phys Lipids*, 105:167–178.
57. Dufourc EJ, Parish EJ, Chitrakorn S, and Smith ICP (1984) Structural and dynamical details of cholesterol-lipid interaction as revealed by deuterium NMR. *Biochemistry*, 23:6062–6071.
58. Chamberlain AK and Bowie JU (2004) Analysis of side-chain rotamers in transmembrane proteins. *Biophys J*, 87:3460–3469.
59. Dunbrack RL (2002) Rotamer libraries in the 21st century. *Curr Opin Struct Biol*, 12:431–440.
60. McIntosh TJ and Simon SA (2006) Roles of bilayer material properties in function and distribution of membrane proteins. *Annu Rev Biophys Biomol Struct*, 35:177–198.
61. Demmers JAA, van Duijn E, Haverkamp J, Greathouse DV, Koeppe II RE, Heck AJR, and Killian JA (2001) Interfacial positioning and stability of transmembrane peptides in lipid bilayers studied by combining hydrogen/deuterium exchange and mass spectrometry. *J Biol Chem*, 276:34501–34508.
62. Lookene A, Groot NB, Kastelein JJP, Olivecrona G, and Bruin T (1997) Mutation of tryptophan residues in lipoprotein lipase - effects on stability, immunoreactivity, and catalytic properties. *J Biol Chem*, 272:766–772.
63. Ridder ANJA, Morein S, Stam JG, Kuhn A, de Kruijff B, and Killian JA (2000) Analysis of the role of interfacial tryptophan residues in controlling the topology of membrane proteins. *Biochemistry*, 39:6521–6528.
64. Draheim RR, Bormans AF, Lai RZ, and Manson MD (2005) Tryptophan residues flanking the second transmembrane helix (TM2) set the signaling state of the tar chemoreceptor. *Biochemistry*, 44:1268–1277.
65. Draheim RR, Bormans AF, Lai RZ, and Manson MD (2006) Tuning a bacterial chemoreceptor with protein-membrane interactions. *Biochemistry*, 45:14655–14664.

Chapter 3

Orientation and Dynamical Properties of a Transmembrane Model Peptide as Studied by a New Strategy Based on Solid-State NMR Methods

Andrea Holt,[‡] Léa Rougier,[§] Valérie Réat,[#] Olivier Saurel,[#] Jerzy Czaplicki,[#]
Franck Jolibois,[§] J. Antoinette Killian[‡] and Alain Milon[#]

[‡]Chemical Biology & Organic Chemistry, Bijvoet Center for Biomolecular Research, Utrecht University, Utrecht, The Netherlands; and [§]LCPNO, Université de Toulouse-UPS, INSA, CNRS, UMR 5215, Toulouse, France; and [#]Institut de Pharmacologie et de Biologie Structurale, Université de Toulouse-UPS, CNRS, UMR 5089, Toulouse, France.

This chapter is an adapted and extended version of:

Order Parameters of a Transmembrane Helix in a Fluid Bilayer: Case Study of a WALP Peptide
Submitted to *Journal of the American Chemical Society* (2009)

Abstract

In the present work, we establish a new strategy based on solid-state NMR methods, called Multiple Anisotropic Constraints and Dynamic Analysis of Membrane peptides (MACADAM) method, for precise and efficient analysis of orientation and dynamics of transmembrane peptides. For this purpose, we determined ^{13}C and ^{15}N chemical shift anisotropies as well ^{13}C - ^{15}N dipolar couplings on two different isotope labeled WALP23 peptides (Acetyl-GWWLALALALALALALALWWA-amide) which were incorporated into model membranes. This set of dynamically averaged anisotropic constraints was combined with previously published quadrupolar splittings, and the complete set of constraints was analyzed using a generalized, 4-parameter dynamic peptide model. For WALP23 in bilayers of dimyristoylphosphatidylcholine (DMPC), we obtained a tilt angle of 20.5° and rotation angle of around 150° . The peptide was found to exhibit large oscillation amplitudes around the helical axis, in agreement with observations of earlier molecular dynamics simulations (Özdirekcan *et al.* (2007), *J Am Chem Soc*, 129:15174-15181). From extensive analysis of various subsets of experimental constraints we identified a minimal set of constraints required to analyze the orientation and dynamical properties of transmembrane peptides, which now allows efficient exploration of the structure and dynamics of peptide-lipid complexes.

Introduction

Membrane proteins perform a wide range of vital functions in the cell, including signaling, transduction of energy and transport of ions and solutes over the cell membrane. In spite of their obvious importance knowledge on the structural properties of membrane proteins is relatively sparse. Even less is known about the dynamical processes that are essential for functioning and that include internal motions like tilting and rotation of helices. The lack of general knowledge on membrane proteins is for a large part due to the lack of convenient methods to study the structure and dynamics of these hydrophobic proteins in a lipid environment. Adding to the complexity is the notion that the surrounding lipids can influence both membrane protein structure and dynamics. These difficulties initiated the design of simplified model systems of artificial transmembrane α -helical peptides, reconstituted into synthetic lipid bilayers. Such simple peptide/lipid model systems offer several advantages. Most importantly, suitable labels can easily be incorporated that allow the use of a wide range of biophysical approaches to study the detailed molecular organization of these systems. Moreover, both lipid and peptide composition can be easily and systematically varied, allowing to elucidate basic principles of membrane protein organization and dynamics.

Examples of designed α -helical transmembrane peptides are the so-called WALP peptides which consist of a sequence of variable length of alternating leucine and alanine residues, flanked on both sides by tryptophans to mimic the composition of natural membrane proteins. WALP containing model systems have been extensively characterized with a variety of biophysical approaches, including solid-state NMR methods and MD simulations. Solid-state NMR approaches are particularly suitable to obtain detailed information on the structural properties of transmembrane peptides in lipid bilayers. For example, helix tilt and rotation angles [1-3] as well as deviations from α -helical structure [2,4] can be investigated by analysis of a set of quadrupolar splittings obtained from peptides that include a

deuterium labeled alanine with the GALA (Geometric Analysis of Labeled Alanines) method, or from PISEMA experiments on uniformly ^{15}N labeled peptides by analysis of characteristic wheel-like patterns [5-7]. However, with both these methods assumptions have to be made regarding the dynamics of the peptides. Importantly, a high mobility results in difficulties in interpretation of the results and can lead to underestimation of the tilt angle [8,9].

The importance of obtaining knowledge on motional properties of peptides is illustrated by comparison of results obtained by solid-state NMR and MD simulations on WALP peptides. NMR experiments, applying the GALA method, indicated that WALP peptides have a relatively small tilt angle ($< 10^\circ$) in different types of bilayers [3]. In contrast, MD studies on the same systems suggested much larger tilt angles, fluctuating from around 20° to 40° [8]. As a potential explanation for the discrepancy between NMR and MD results, it was suggested that the WALP peptide can adopt different rotational angles but that there is an energy barrier between these rotational states, such that 'hopping' occurs. From the MD trajectories the authors back-calculated the NMR quadrupolar splittings and they concluded that if such motion indeed would occur, this would lead to an underestimation of the tilt angles determined by NMR. However, it is clear that also MD simulations have important limitations, such as relatively short timescales and the requirement for many input parameters which need to be validated by experimental results. So far, MD simulations have not succeeded in reproducing the experimentally observed splittings.

To solve the observed discrepancy between the two approaches information on the dynamics of transmembrane peptides is required. WALP peptides in PC bilayers seem like an ideal test case for this, because these systems have been characterized extensively already by many different techniques [10,11]. Moreover, there is a general need for simple and well characterized model systems to validate new techniques and to calibrate existing methods. Since WALP/PC systems are in fact already being used for this purpose, it is of paramount importance that they indeed are reliably characterized.

The aim of this study was to develop a solid-state NMR approach that allows the determination of the orientation as well as of dynamical properties of transmembrane peptides. We devised a new technique that extends the model used with the GALA method by two parameters that take into account oscillations around the helical axis of the peptide and wobble-like off-axis motions in a cone affecting the tilt angle of the helix. By combining the set of quadrupolar splittings from earlier ^2H NMR experiments with additional experimental data from solid-state NMR experiments on peptides including ^{13}C labeled alanine and ^{15}N labeled leucine, the Multiple Anisotropic Constraints and Dynamic Analysis of Membrane peptides (MACADAM) method is able to determine both orientation and motional properties of peptides in a lipid bilayer.

We obtained a tilt angle of 20.5° which is much larger than the tilt angle of 5.2° obtained from the previous ^2H NMR study [3], and agrees well with the results obtained recently from fluorescence experiments [12]. Furthermore, by reduction and permutation of experimental constraints a minimal set of constraints needed for reliable analysis was found. This paves the way for this new technique to determine orientational and dynamical parameters of systems in which the peptide and/or lipid composition can be varied, allowing the use of these systems to further explore basic principles that determine the structure and dynamics of lipid/protein complexes.

Material and Methods

Materials

Triple-labeled WALP23 peptides (for amino acid sequences see Table 1) were synthesized using Fmoc/tBu solid-phase synthesis as described elsewhere for related KALP peptides [13]. Deuterium labeled L-alanine (3,3,3- d_3 or 2,3,3,3- d_4), $^{13}\text{C}_1$ labeled L-alanine (1- ^{13}C , 99%) and ^{15}N labeled L-leucine (^{15}N , 98%) were purchased from Cambridge Isotopes Laboratories Inc. (Andover, MA, USA). Fmoc (9-fluorenylmethyloxycarbonyl) was used to protect its amino functionality as described by ten Kortenaar *et al.* [14] before being used in the peptide synthesis. 1,2-dimyristoyl-sn-glycero-3-phosphocholine (di-C14:0PC) were purchased from Avanti Polar Lipids Inc. (Alabaster, AL, USA) and used without further purification. The identity of the synthesized peptides was verified by mass spectrometry and the purity was analyzed by HPLC using a C4 reverse phase HPLC column. For analytical and, if necessary preparative, HPLC a solvent system with solvent A composed of 95% water, 5% acetonitrile and 0.1% TFA, and solvent B composed of 80% acetonitrile, 20% iso-propanol and 0.1% TFA was used. The purity of the peptides used in this study was generally better than 95%.

Methods

Simulations using the dynamic model

Both quadrupolar and dipolar splittings can be calculated from

$$(1) \quad g(\vartheta) = K \cdot \frac{3\cos^2\vartheta - 1}{2},$$

where K is a constant that depends on the type of interaction and ϑ the angle between the membrane normal and the vector for the interaction.

For the generalized dynamic model the following relations apply

$$(2a) \quad \cos \vartheta = \cos \tau \cdot \cos \varepsilon_p - \sin \tau \cdot \sin \varepsilon_p \cdot \cos \vartheta,$$

$$(2b) \quad \cos \tau = \cos \tau \cdot \cos \Delta\tau - \sin \tau \cdot \sin \Delta\tau \cdot \cos \zeta,$$

where τ is the tilt angle of the α -helix and the angle between the vector of the interaction and the helix axis is given by ε_p . In the equations above, φ is defined as $\varphi = \psi + \rho$, where ψ is depending on the geometry and ρ is the rotation angle of the helix. In the generalized model, the tilt angle is given by τ , and the wobbling cone of the helix is given by $\Delta\tau$. The angle ζ is later used to integrate over the oscillation motions $\Delta\rho$.

Table 1: Amino acid sequence of the triple-isotope labeled WALP23 peptides synthesized for this study.

peptide	amino acid sequence
WALP23- $^2\text{H}_4$ -Ala7- $^{13}\text{C}_1$ -Ala13- ^{15}N -Leu14	Acetyl-GWWLALA ^a LALA ^b L ^c ALALALWWA-amide
WALP23- $^{13}\text{C}_1$ -Ala11- ^{15}N -Leu12- $^2\text{H}_3$ -Ala13	Acetyl-GWWLALALALA ^b L ^c A ^d LALALWWA-amide

^a alanine contains [$\text{C}_{\alpha}^2\text{H}_4$]; ^b leucine contains [^{15}N]; ^c alanine contains [$^{13}\text{C}_1$], ^d alanine contains [$\text{C}_{\alpha}^2\text{H}_3$].

Substituting equation 2a into the expression $(3 \cos^2 \vartheta - 1) / 2$ leads to the equation

$$(3) \quad \frac{3 \cos^2 \vartheta - 1}{2} = \left(\frac{3 \cos^2 \tau - 1}{2} \right) \cdot \left(\frac{3 \cos^2 \varepsilon_p - 1}{2} \right) + \frac{3}{4} (\sin^2 \tau \cdot \sin^2 \varepsilon_p \cdot \cos 2\vartheta - \sin 2\tau \cdot \sin 2\varepsilon_p \cdot \cos \vartheta).$$

This equation describes the quadrupolar and dipolar interactions in the quasi-static model introduced by Strandberg *et al.* [2], which can be used to analyze experimental data in terms of two parameters to retrieve the tilt angle τ and the rotation angle ρ .

For the generalized dynamic model defined by the four parameters tilt τ , wobble $\Delta\tau$, rotation ρ and oscillation $\Delta\rho$, equation 2b is substituted into equation 3 and $\langle \cos^2 \vartheta \rangle$ is calculated by integration of

$$(4) \quad \langle \cos^2 \vartheta \rangle = \frac{\int_0^{2\pi} \int_{\vartheta_1}^{\vartheta_2} \int_0^{\tau_1} \cos^2 \vartheta \sin \tau_1 d\tau_1 d\vartheta d\zeta}{\int_0^{2\pi} \int_{\vartheta_1}^{\vartheta_2} \int_0^{\tau_1} \sin \tau_1 d\tau_1 d\vartheta d\zeta},$$

where $\vartheta_1 = \psi + \rho - \Delta\rho$ and $\vartheta_2 = \psi + \rho + \Delta\rho$.

The CSA (chemical shift anisotropy) effects depend on the polar coordinates of the external magnetic field B_o in the principal axis frame of the CSA tensor

$$(5) \quad h(\vartheta, \varphi) = -K'_{CSA} \left[\left(\frac{3 \cos^2 \vartheta - 1}{2} \right) + \frac{1}{2} \eta (\sin^2 \vartheta \cdot \cos 2\varphi) \right],$$

where η is the asymmetry parameter. For the generalized model which includes wobble and oscillation movements, integration is performed analogous to what was described above.

Quantum chemistry calculations

All quantum chemical calculations were performed using the Gaussian 03 suite [15]. The molecular geometry of WALP23 was optimized using the ONIOM hybrid approach [16,17]. For this purpose, the peptide was divided into an active and inactive part. The active part consisting of 7 residues centered either on Ala11-Leu12 or on Ala13-Leu14 was optimized using the hybrid Density Functional Theory B3LYP method [18,19] associated with a Pople type double ξ basis set augmented by polarization functions on all atoms i.e. 6-31G(d,p) (a description of basis sets can be found in [20]). The inactive part of the peptide i.e. the rest of the peptide has been optimized using a semi-empirical (AM1) approach [21-23]. The chemical shielding tensors were computed at B3LYP/6-31G(d,p) level on the whole peptide using the Gauge Including Atomic Orbital (GIAO) method [24-28].

NMR sample preparation

Stock solutions of ca. 20 mM di-C14:OPC in chloroform were prepared, and the lipid concentration was determined by a phosphorus assay [29]. Stock solutions of WALP23 were prepared with a concentration of ca. 500 μ M in TFE and the concentration of WALP23 was determined by absorption spectroscopy using an extinction coefficient of 22400 $M^{-1}cm^{-1}$ at 280 nm for WALP23. For unoriented samples, typically 0.5 μ mol of WALP23 peptides and 50 μ mol di-C14:OPC were mixed in solution. The organic solvents were evaporated under a nitrogen flow and further removed under vacuum overnight (ca. $1 \cdot 10^{-2}$ mbar). Subsequently,

the samples were hydrated with Milli-Q water and lyophilized to yield a fluffy powder, facilitating a thorough hydration at the low hydration levels needed. The unoriented samples were hydrated with deuterium-depleted water to 33% (water/{water+lipid+peptide}, w/w) and incubated overnight at 37°C to equilibrate the hydration throughout the sample. For the MAS (magic angle spinning) NMR experiments, the samples were transferred to a MAS rotor by centrifugation.

For oriented samples, small sheets with dimensions 4.2 x 14 mm² were cut from polycarbonate film with a thickness of 20 µm and cleaned with pure ethanol. Appropriate amounts of peptides and lipids were mixed at a molar ratio of 1:100 and organic solvents were removed as described above. The peptide/lipid mixture was redissolved in methanol at 30 mg/ml and spread on the polycarbonate sheets to reach typically 0.5 mg lipid/cm². After evaporation of the solvent, the sheets were put to vacuum overnight to further remove any organic solvent present. Then, the sheets covered with the dry peptide/lipid mixture were stacked with 0.3 µl deuterium-depleted water added on each sheet, and after every 10 sheets the complete stack was very gently pressed with the help of glass plates to achieve straight stacking planes. To support the flimsy polycarbonate sheets, finally a thin glass platelet cut from microscopy cover slides was placed on the top and the bottom of the complete stack. Then, the stack of pre-hydrated sheets was incubated at 37°C in presence of a reservoir of deuterium-depleted water for several days to promote alignment of the lipid bilayers along the polycarbonate surface.

NMR spectroscopy

Static NMR experiments were carried out on a narrow bore Bruker Avance NMR spectrometer operating at 500.13 MHz for ¹H. For ²H and ¹⁵N NMR experiments, a Bruker 5 mm single resonance probe head and a Bruker 7 mm double resonance probe head were used, respectively. Both probe heads were equipped with a solenoid coil oriented at 90° with respect to the magnetic field. All MAS NMR experiments were performed on a 700.13 MHz Bruker Avance narrow bore NMR spectrometer using a Bruker 3.2mm MAS triple-tuned solenoid coil. The ¹H radio frequency field strength for hetero nuclear two-pulse phase-modulation decoupling was 86 kHz for all experiments. The spectra were acquired with a repetition delay of 3 s to avoid sample heating. The carbonyl ¹³C line widths were equal to 0.3 ppm, indicating a good structural homogeneity. CP (cross-polarization) MAS spectra were acquired using a ¹H excitation pulse length of 2.9 µs and a CP spin-lock field-strength of 50 kHz. The CP contact time was 4.5 ms for ¹³C experiments and 1.5 ms for ¹⁵N experiments. For calibration ¹³C spectra were referenced to DSS and ¹⁵N spectra to liquid ammonia, and, in both cases, the ¹H methyl peak of lipid acyl chains was set to 0.85 ppm and used as internal reference for calibration of the ¹³C and ¹⁵N CP MAS spectra.

All measurements were performed at 40°C and the samples were allowed to equilibrate for at least 10 minutes before the start of the measurements. ³¹P NMR experiments were performed to confirm the formation of bilayers in the case of unoriented samples, and to determine the quality of alignment of the bilayers in case of oriented samples. The experiments were carried out at 202.5 MHz using a single 90° pulse sequence with a relaxation delay time of 1 s and proton decoupling. All previous ²H NMR experiments have been performed on samples with a peptide/lipid ratio of 1:100 and a hydration level of ca. 60% (w/w). The limited space in the MAS rotor samples tubes with diameter 3.2 mm utilized for the MAS NMR experiments required using a lowered hydration level of 33% (w/w) to achieve sufficient sensitivity.

The compatibility of new and old experimental data was ensured with ^2H NMR experiments performed at the same conditions than used in the previous studies [2,3]. Static ^2H NMR experiments were performed at 76.78 MHz using a standard quadrupolar echo pulse sequence with $3.9 \mu\text{s}$ 90° pulses, an echo delay time of $40 \mu\text{s}$, and a 1 s relaxation delay time. The possible effects of the relatively low hydration in the oriented bilayers on the properties of the peptide were checked by comparison of the quadrupolar splittings of deuterated alanines in oriented bilayers and in non-oriented bilayers at excess water. The quadrupolar splittings observed were close to the values reported in earlier ^2H NMR studies [2,3], suggesting that the bilayers are fully hydrated at the lower hydration level of 33% (w/w) used for the MAS NMR experiments in the present study.

Rotational-echo double resonance experiments

The dynamically averaged ^{15}N - ^{13}C dipolar coupling was determined using a conventional REDOR (rotational-echo double resonance) experiment [30]. The evolution of the ^{13}C signal with and without dipolar coupling between the heteronuclei ^{13}C and ^{15}N was monitored with the help of an interleaved two-dimensional REDOR experiment at a spinning frequency of 10 kHz, with and without reintroduction of the ^{13}C and ^{15}N dipolar coupling and with mixing times ranging from 0 to 5 ms, incrementing in steps of $400 \mu\text{s}$. The ^{15}N π pulse length was $10 \mu\text{s}$ and the pulses were phased according to the xy-4 scheme [31]. The ^{13}C π pulse length was $10 \mu\text{s}$. CW (continuous wave) and TPPM (two-pulse phase-modulation) ^1H decoupling were applied during the evolution time and acquisition, respectively.

For analysis, the ^{13}C signals were integrated and the evolution of the dipolar coupling was calculated by

$$(6) \quad \text{REDOR}(\tau_e) = 1 - \frac{S(\tau_e)}{S_0(\tau_e)} = \frac{\Delta S(\tau_e)}{S_0(\tau_e)},$$

where τ_e is the evolution time of the dipolar interaction (cf. pulse sequence). $S(\tau_e)$ and $S_0(\tau_e)$ are the experimental ^{13}C peak intensities for the evolution time τ_e with and without reintroduction of the ^{13}C - ^{15}N dipolar interaction, respectively.

The experimental data points for the evolution of the dipolar coupling were fitted using the theoretical REDOR function [32]:

$$(7) \quad F(\tau, dnc) = 1 - \frac{\int_0^{\frac{\pi}{2}} \int_0^{\pi} \cos(-dnc \cdot 2\tau \sqrt{2} \cdot \sin(2\theta) \cdot \sin\gamma) \sin\theta \, d\theta \, d\gamma}{\int_0^{\frac{\pi}{2}} \int_0^{\pi} \sin\theta \, d\theta \, d\gamma},$$

where τ is the evolution time of the dipolar interaction, dnc is the dynamically averaged ^{13}C - ^{15}N dipolar coupling and (θ, γ) are the Euler angles relating the principal axis system of the dipolar interaction to the rotor-fixed reference frame.

Results and Discussion

Simulation of the motional effects

First, we performed simulations to investigate the effects of dedicated peptide motions on the quadrupolar splittings. In the quasi-static model employed for analysis using the GALA method only two parameters were employed to describe the orientation of the peptide helix within the membrane: a tilt angle τ between the helix axis and the membrane normal, and a rotation angle ρ between the direction of tilt and an arbitrarily chosen reference point i.e. an amino acid position (see Figure 1A). In the new dynamic model dedicated peptide motions were included by extending the previous model with a parameter $\Delta\rho$ describing oscillations around the helix axis superimposed on the initial rotation of the helix, and a parameter $\Delta\tau$ describing wobbling-in-a-cone motions of the α -helix superimposed on the initial helix tilt (see Figure 1B).

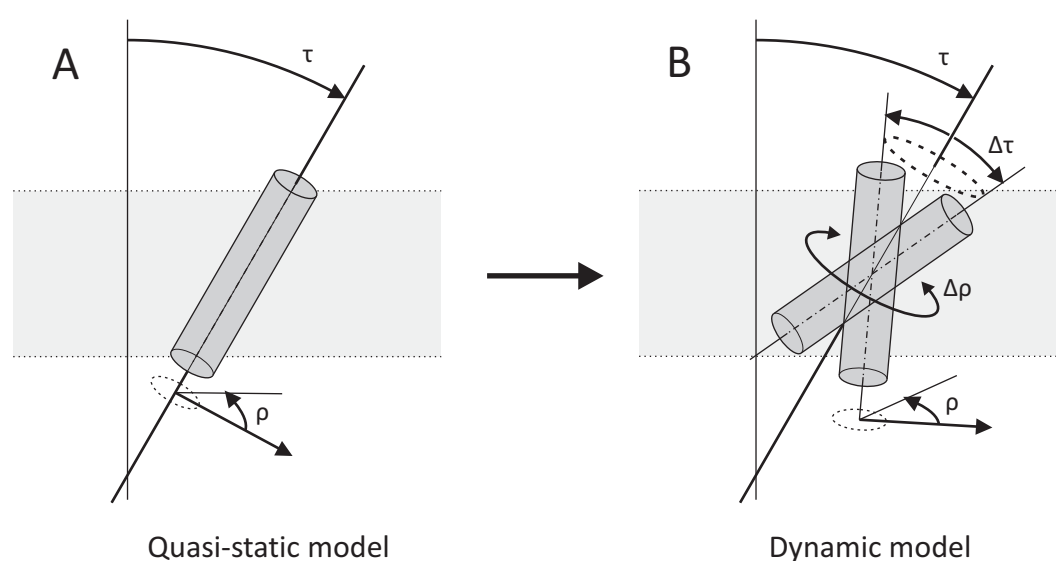


Figure 1: (A) The quasi-static model describes the orientation of the peptide by a tilt angle τ and a rotation angle ρ . (B) In the dynamic model the previous model is extended by an oscillation $\Delta\rho$ around the helix axis and by a wobbling-in-a-cone motion $\Delta\tau$.

To begin with, we calculated quadrupolar splittings for different tilt angles using the quasi-static model, and the curves obtained show larger modulation of the quadrupolar splittings as the tilt angles of the peptide in the membrane increase (Figure 2A). For convenience, the reference rotation angle defining the phase of the curve for the quadrupolar splittings was set to 0° for all simulations. Next, we explored the effect of dedicated peptide motions on the quadrupolar splittings. With increasing peptide oscillations the quadrupolar splittings are more averaged i.e. the modulation becomes smaller (Figure 2B). From these calculations we observed that decreasing the tilt angle in the quasi-static model and increasing the extent of peptide oscillations in the dynamic model has similar effects on the calculated quadrupolar splittings. Figure 2C illustrates that the quadrupolar splittings calculated for a peptide with a tilt angle of 12° using the quasi-static model and calculated for a peptide with a tilt angle of 18° exhibiting oscillations of 46° using the dynamic model are almost indistinguishable. A similar result could be obtained when calculating the quadrupolar splittings for a smaller tilt angle of 6° and a wobbling of 10° , instead of oscillations.

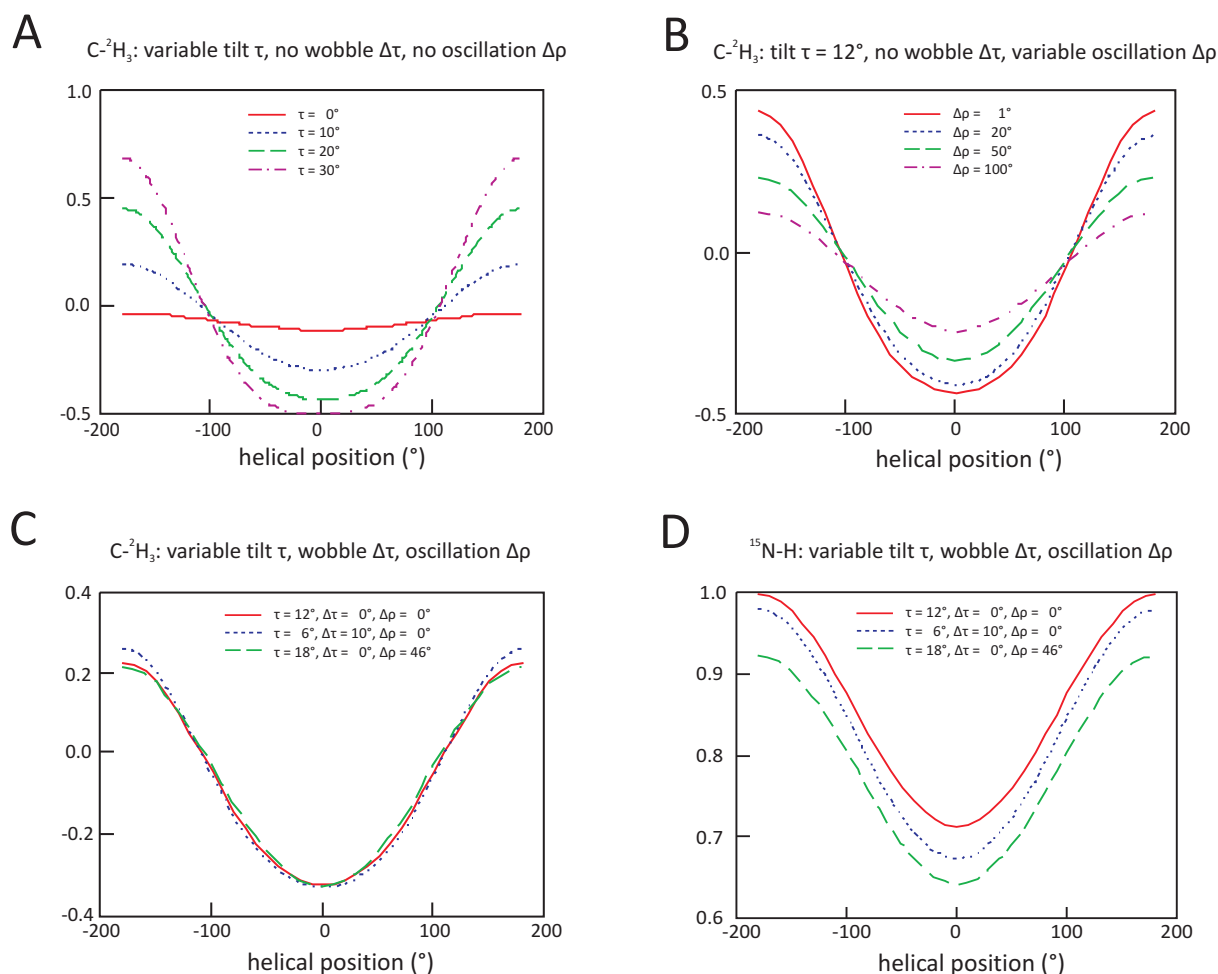


Figure 2: Top: Simulations of quadrupolar/dipolar couplings (relative intensities) obtained for transmembrane peptides containing a methyl-deuterated alanine/ ^{15}N labeled amino acid using (A) the quasi-static model for different tilt angles and (B) the dynamic model for different extents of oscillation at a fixed tilt angle of 12° . Bottom: Simulations of quadrupolar splittings (C) and ^{15}N -H dipolar couplings (D) using the dynamic model for the same combinations of tilt τ , wobble $\Delta\tau$ and oscillation $\Delta\rho$ to show the effect of different orientation with respect to the helix axis.

From the simulations above it is clear that peptide motions like oscillations around the helix axis and wobbling-in-a-cone motions affect the experimentally determined quadrupolar splittings and that using the quasi-static model for analysis in particular in case of increased oscillations may lead to too small tilt angles. Indeed, fitting the original set of four experimentally determined quadrupolar splittings reported in [3] using the quasi-static model yielded a relatively small tilt angle of 5.2° (see fit results depicted in Figure 3A). Next, we fitted the original set of four quadrupolar splittings reported in [3] using the dynamic model. To avoid an underdetermined system, the number of free parameters was reduced by fixing $\Delta\tau = 0^\circ$ i.e. wobbling is neglected. With this restriction we find a global minimum, yielding a tilt angle of 9.2° and an oscillation amplitude around the helix axis of ca. 100° (fit depicted in Figure 3B). A second local minimum yields a larger tilt angle of ca. 20.5° and an oscillation amplitude of ca. 135° . Both fits are in reasonable agreement with the experimental data.

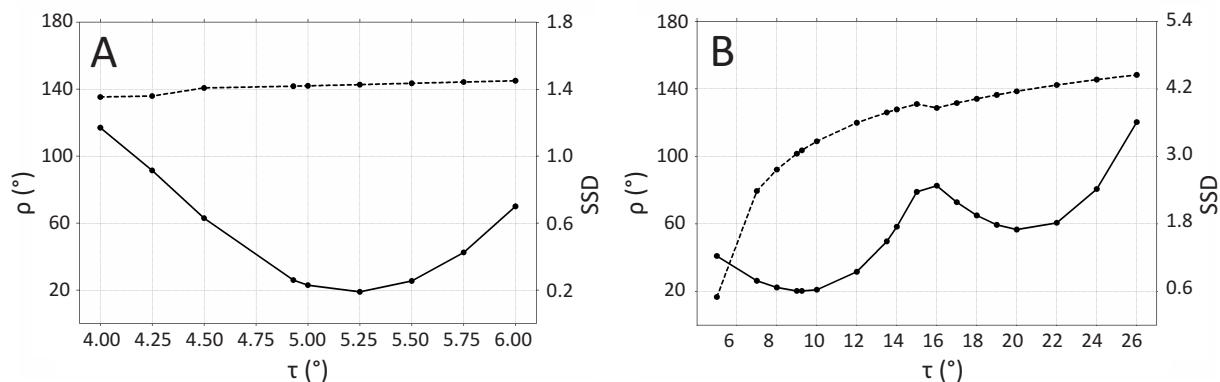


Figure 3: Fit to the set of four quadrupolar splittings reported in [3] (A) using the quasi-static, 2-parameter model described by a tilt angle τ and a rotation angle ρ (dotted), and (B) using the dynamic, 4-parameter model that was extended by 2 parameters describing oscillation $\Delta\rho$ (dotted) and wobbling $\Delta\tau$ (here $\Delta\tau = 0^\circ$ was imposed to avoid under-determination). The sum of squared deviation is given as solid line.

A solution to avoid an underdetermined system is to increase the number of constraints i.e. the number of experimental data points. As experimental constraints accessible to NMR methods we chose ^{13}C - ^{15}N and ^{15}N -H dipolar couplings, and ^{15}N and ^{13}C chemical shift tensors of peptides that contain ^{15}N and ^{13}C isotope labels in backbone positions. Since the main tensor elements have different orientations with respect to the helix axis, dedicated peptide motions will have a different averaging effect on these nuclear interactions. We demonstrate this by comparison of averaging effects on the quadrupolar interaction of a deuterium labeled alanine with an angle of typically 58° for the C- $^2\text{H}_3$ bond (Figure 2C) and on a backbone amide ^{15}N -H dipolar interaction with an angle of typically 15° to the helix axis (Figure 2D). The curves show the (relative) sizes of the ^{15}N -H dipolar and quadrupolar interactions, which were calculated for the same combinations of parameters and clearly illustrate the weaker influence of averaging for the ^{15}N -H dipolar interaction.

Additional experimental constraints

Both ^{13}C and ^{15}N nuclei can easily and selectively be introduced in different positions of the peptide during peptide synthesis by isotope labeled amino acids. For this study, we have synthesized two WALP23 peptides with a ^{13}C labeled alanine and ^{15}N labeled leucine in different consecutive positions, and, for control purposes, also deuterium labeled alanines were introduced in both WALP23 peptides. Both peptides were incorporated into di-C14:0PC bilayers and NMR samples were prepared as described in the Materials and Methods section.

^{13}C and ^{15}N isotropic chemical shifts

First, high speed ^{13}C CP MAS spectra were recorded at a spinning rate of 10 kHz to confirm the α -helical conformation of the WALP23 peptides incorporated in di-C14:0PC bilayers (see Figure 4). The ^{13}C CP MAS spectra include signals from the ^{13}C labeled alanines in the WALP23 peptides and, due to the natural abundance of ^{13}C in the lipids, also from different chemical groups of the lipids. Residual ^{13}C in the lipid carbonyls is observed at 176 ppm. The isotropic chemical shift of the ^{13}C in the carbonyls of the alanine in both triple-labeled WALP23 peptides labeled in position 11 (Figure 4B) or 13 (Figure 4A) is located at 178.9 ppm.

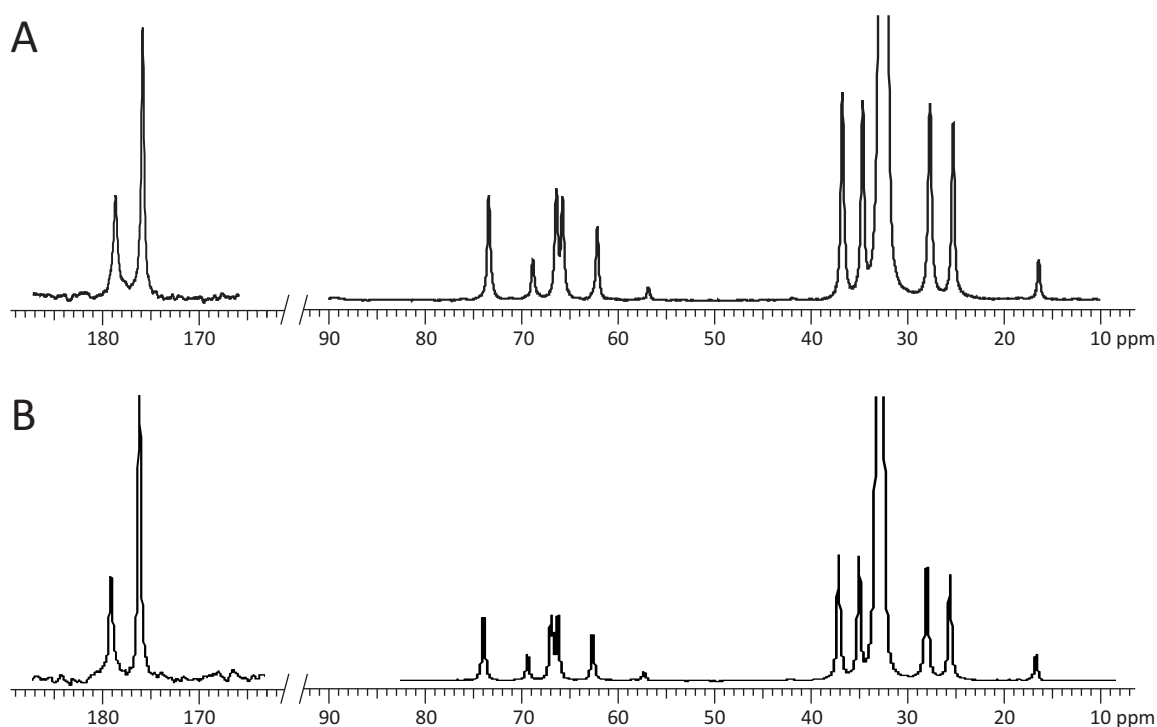


Figure 4: ^{13}C CP MAS spectrum of (A) WALP23- $^2\text{H}_4$ -Ala7- $^{13}\text{C}_1$ -Ala13- ^{15}N -Leu14 and (B) WALP23- $^{13}\text{C}_1$ -Ala11- ^{15}N -Leu12- $^2\text{H}_3$ -Ala13 incorporated into non-oriented bilayers of di-C14:0PC at a peptide/lipid ratio of 1:100 hydrated to 33% (w/w) and recorded at a rotation speed of 10 kHz at 40 °C.

The secondary structure of the peptides is reflected in the isotropic chemical shift of labeled backbone carbonyls, with values of 178.5 ppm for an α -helical conformation and 175.0 ppm for a beta sheet confirmation being reported for alanines including ^{13}C labeled carbonyls after correction for the primary sequence effect [33-35].

Then, high speed ^{15}N CP MAS spectra were recorded for both triple-labeled WALP23 peptides to determine the ^{15}N isotropic chemical shift (see Figure 5). In general, the lower sensitivity of the ^{15}N nucleus compared to the ^{13}C nucleus causes a lower signal/noise ratio of the spectra. Furthermore, only the signal of the ^{15}N labeled peptide is observed which is due to the lower abundance of ^{15}N in the choline groups of the lipids. The ^{15}N isotropic chemical shift for the peptides with ^{15}N labeled leucine in position 12 (Figure 5B) and 14 (Figure 5A) was determined to 116.6 ppm and 116.5 ppm, respectively. These values are typical for α -helical peptides.

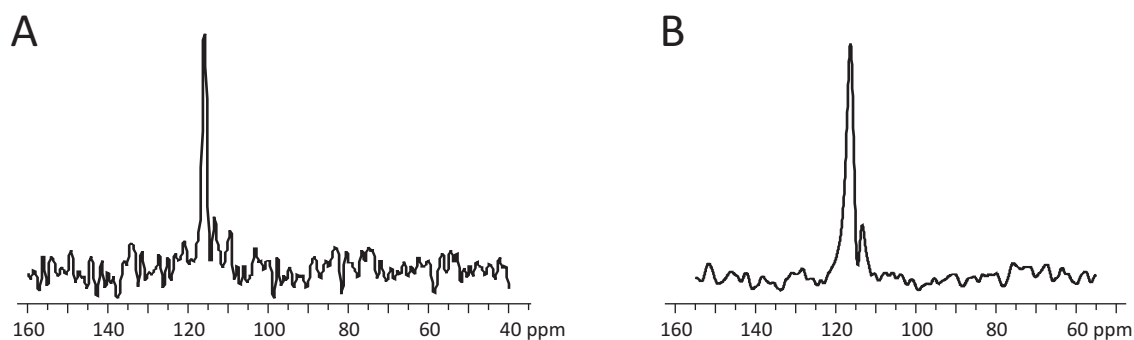


Figure 5: ^{15}N CP MAS spectrum of (A) WALP23- $^2\text{H}_4$ -Ala7- $^{13}\text{C}_1$ -Ala13- ^{15}N -Leu14 and (B) WALP23- $^{13}\text{C}_1$ -Ala11- ^{15}N -Leu12- $^2\text{H}_3$ -Ala13 incorporated into non-oriented bilayers of di-C14:0PC at a peptide/lipid ratio of 1:100 hydrated to 33% (w/w) and recorded at a rotation speed of 10 kHz at 40 °C.

Next, we analyzed the various dynamically averaged parameters in order to obtain sufficient information for a complete description of the dynamical model. The experiments and their results are described below and the values obtained for the different experiments are summarized in Table 2.

Dynamically averaged $^{13}\text{C}_1$ chemical shift anisotropies

To determine the dynamically averaged $\Delta\nu_{\text{CS}}$ and the asymmetry parameter η_{CS} for $[^{13}\text{C}_1]$ -Ala, we performed ^{13}C CP MAS NMR experiments at a low spinning speed of 1 kHz to obtain the rotational side band patterns for $[^{13}\text{C}_1]$ -Ala (Figure 6). The rotational side band patterns were analyzed with the freeware *dmfit* (<http://crmht-europe.cnrs-orleans.fr/dmfit>). The best fits to the experimental spectra are shown in Figure 6 as a red line. The dynamically averaged chemical shift anisotropy $\Delta\nu_{\text{CS}}$ found was -16.4 ppm for $[^{13}\text{C}_1]$ -Ala11 (Figure 6B) and -20.1 ppm for $[^{13}\text{C}_1]$ -Ala11 (Figure 6A) (summarized in Table 2). In both cases, the sideband pattern analysis yielded an asymmetry parameter η_{CS} of zero which corresponds to a CSA tensor with an axial symmetry (not shown), suggesting that the α -helical peptides inserted into the bilayer undergo fast diffusion motions. This is consistent with the rapid axial reorientation motions around the bilayer normal observed from ^2H NMR experiments [1].

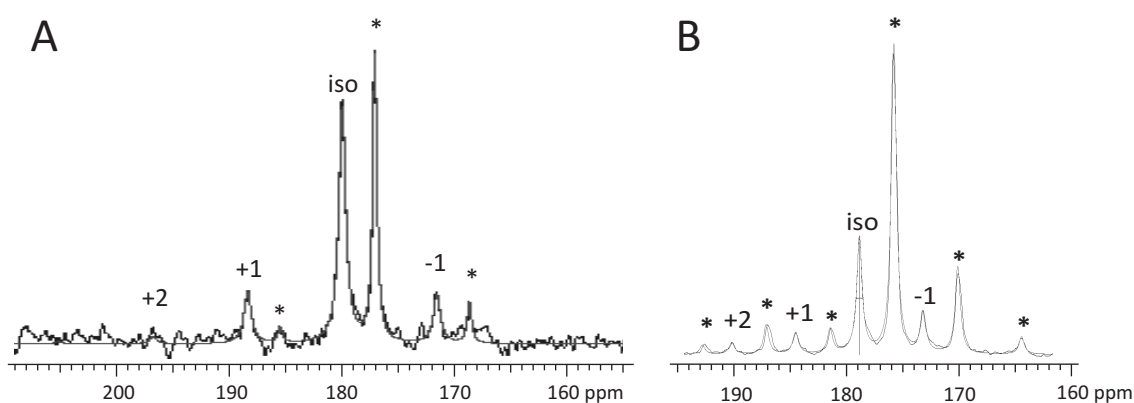


Figure 6: Spinning side band patterns for (A) WALP23- $[^2\text{H}_4]$ -Ala7- $[^{13}\text{C}_1]$ -Ala13- $[^{15}\text{N}]$ -Leu14 and (B) WALP23- $[^{13}\text{C}_1]$ -Ala11- $[^{15}\text{N}]$ -Leu12- $[^2\text{H}_3]$ -Ala13 incorporated into non-oriented bilayers of di-C14:0PC, hydration 33% (w/w) at 40°C, obtained with a ^{13}C CP MAS NMR experiment at a spinning rate of 1 kHz. The thin solid line shows the best fit obtained from spinning side band analysis using *dmfit*. The peptide carbonyl spinning side bands are indicated with numbers and the lipid carbonyl band with stars.

Dynamically averaged ^{15}N chemical shift anisotropies

The dynamically averaged ^{15}N CSA was obtained from oriented samples of both triple labeled peptides, which were measured at 90° orientation and 0° of the bilayers to the magnetic field (Figure 7A). The dynamically averaged CSA can then be calculated from the spectral shoulders at 0° and 90° orientation using $\Delta\nu_{\text{CS}} = \delta_{0^\circ} - \delta_{90^\circ}$. The dynamically averaged chemical shift anisotropies $\Delta\nu_{\text{CS}}$ found were -105.6 ppm for ^{15}N -Leu14 (NMR spectrum not shown) and -114.6 ppm for ^{15}N -Leu12 (summarized in Table 2). Similar to the dynamically averaged ^{13}C spectra, the asymmetry parameter η_{CS} can be assumed to be zero, due to diffusion motions of the peptide.

For comparison, we determined the dynamically averaged ^{15}N CSAs of both peptides also on non-oriented samples hydrated with an excess of water. Using non-oriented bilayers, the signal originating from peptides in bilayers with 90° orientation to the magnetic field

accumulates much faster and directly yields the chemical shift for the 90° orientation (Figure 7B). In case of axially symmetric interaction tensors i.e. an asymmetry parameter η_{CS} of zero, the chemical shift anisotropy can be calculated from $\Delta\nu_{CS} = \delta_{0^\circ} - \delta_{90^\circ} = -3(\delta_{90^\circ} - \delta_{iso})$. Using this equation we obtained a dynamically averaged CSA of -74.7 ppm for ^{15}N -Leu12 (spectrum not shown) and of -85.2 ppm for ^{15}N -Leu14. These values are significantly smaller than the ones determined in oriented bilayers, the reason for this is not known. Maybe the difference in hydration levels plays a role, or the choice of the bilayer system i.e. oriented or non-oriented bilayers, may influence the peptide orientation and/or types and effect of peptide motions.

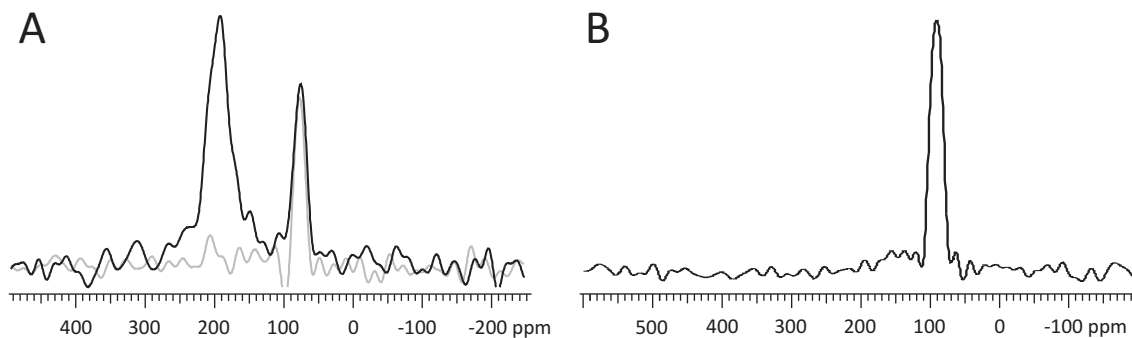


Figure 7: (A) ^{15}N NMR spectrum for WALP23- $^{13}\text{C}_1$ -Ala11- ^{15}N -Leu12- $^2\text{H}_3$ -Ala13 incorporated into oriented bilayers of di-C14:OPC at 0° (black line) and 90° orientation (grey line), fully hydrated (ca. 40%, w/w) at 40°C, obtained with a ^{15}N CP NMR experiment. (B) ^{15}N NMR spectrum for WALP23- $^2\text{H}_4$ -Ala7- $^{13}\text{C}_1$ -Ala13- ^{15}N -Leu14 incorporated into non-oriented bilayers of di-C14:OPC, hydration 33% (w/w) at 40°C, obtained with a ^{15}N CP NMR experiment.

Dynamically averaged ^{13}C - ^{15}N dipolar couplings

For both triple-labeled WALP23 peptides the dynamically averaged dipolar coupling between the heteronuclei $^{13}\text{C}_1$ in the alanines and ^{15}N in the leucines was determined using a conventional REDOR experiment. The experimentally determined evolution of the $^{13}\text{C}_1$ signal was calculated according to equation 6 for both triple-labeled peptides (depicted in Figure 8) and analyzed with the theoretical REDOR function given in equation 7. The best fits to the experimental data are shown in Figure 8 as a solid line. The dynamically averaged dipolar couplings found were 313 Hz for $^{13}\text{C}_1$ -Ala11- ^{15}N -Leu12 and 286 Hz for $^{13}\text{C}_1$ -Ala13- ^{15}N -Leu14. However, the reliability of the dipolar couplings obtained is low (± 100 Hz). The low signal/noise ratio prevented recordings of $S(\tau)$ and $S_0(\tau)$ data over long evolution periods, i.e. until the first minimum in the evolution of the dipolar interaction was distinguishable.

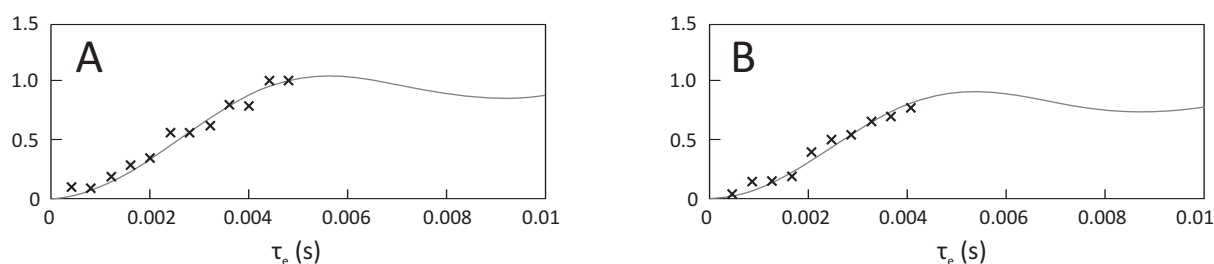


Figure 8: Evolution of the $^{13}\text{C}_1$ - ^{15}N dipolar coupling for (A) WALP23- $^2\text{H}_4$ -Ala7- $^{13}\text{C}_1$ -Ala13- ^{15}N -Leu14 and (B) WALP23- $^{13}\text{C}_1$ -Ala11- ^{15}N -Leu12- $^2\text{H}_3$ -Ala13 as a function of the evolution time τ_e used for the REDOR experiment. The crosses denote values determined from REDOR experiment and the solid line the fitted curve.

Static values for ^{13}C and ^{15}N chemical shift anisotropies

For interpretation of the dynamically averaged chemical shifts it is important to know the static values of the ^{13}C and ^{15}N chemical shift anisotropies. For both triple-labeled WALP23 peptides, we determined the static values from ^{13}C and ^{15}N CP MAS NMR experiments at low spinning speeds on dry powders of the peptides. The spinning side band patterns for ^{13}C and ^{15}N nuclei are shown in Figure 9. The best fits obtained from *dmfit* are shown as a thin solid line, the corresponding parameters of the [$^{13}\text{C}_1$]-Ala13 and [$^{13}\text{C}_1$]-Ala11 static chemical shift anisotropies are given in Table 2.

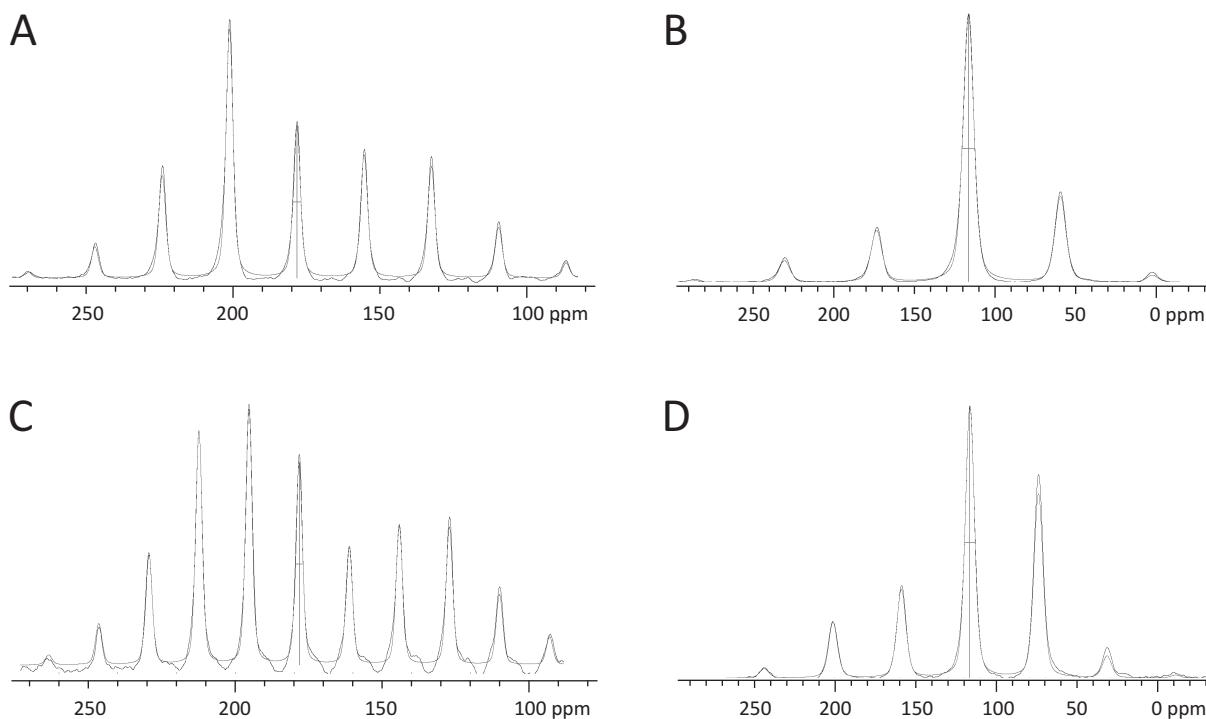


Figure 9: Top row: ^{13}C spinning side band patterns for (A) WALP23- $^{2}\text{H}_4$ -Ala7- $^{13}\text{C}_1$ -Ala13- ^{15}N -Leu14 and (C) WALP23- $^{13}\text{C}_1$ -Ala11- ^{15}N -Leu12- $^{2}\text{H}_3$ -Ala13 obtained from a ^{13}C CP MAS NMR experiment at a spinning rate of 4 kHz respectively 3 kHz. Bottom row: ^{15}N spinning side band patterns for (B) WALP23- $^{2}\text{H}_4$ -Ala7- $^{13}\text{C}_1$ -Ala13- ^{15}N -Leu14 and (D) WALP23- $^{13}\text{C}_1$ -Ala11- ^{15}N -Leu12- $^{2}\text{H}_3$ -Ala13 obtained from a ^{15}N CP MAS NMR experiment at a spinning rate of 4 kHz respectively 3 kHz. The best fit obtained from spinning side band analysis using *dmfit* is denoted by a thin solid line.

Peptide model & quantum chemistry calculations

To analyze the dynamically averaged NMR parameters, we require the principal values and principal axis orientations of the selected interaction tensors i.e. the isotope labeled amino acids incorporated in the WALP23 peptide. The ^{15}N and ^{13}C CSA static tensor components were determined using quantum chemistry (Euler angles are given in Table 3). The computed principal values of the ^{15}N and ^{13}C static tensors are in close agreement with the experimental values determined on the dry peptide powders by spinning side band analysis of the powder peptide (standard deviation of 2.5 ppm for ^{13}C and of 1.5 ppm for ^{15}N).

Table 2: Experimental NMR Parameters determined for the WALP23 peptides including a [¹³C₁]-Ala, [¹⁵N]-Leu and [C_α-²H₃]-Ala in different positions.

Bilayer system	non-oriented	Dynamically averaged		Static	
		non-oriented	oriented	dry peptide powder	
Chemical shift anisotropy [§]	ν_{iso} (ppm)	$\Delta\nu_{\text{CS}}$ (ppm)	$\Delta\nu_{\text{CS}}$ (ppm)	$\Delta\nu_{\text{CS}}$ (ppm)	η_{CS} (ppm)
[¹³ C ₁]-Ala11	178.3	-16.4 ± 1.6		-84.2	0.59
[¹³ C ₁]-Ala13	177.5	-20.1 ± 2.0		-85.1	0.62
[¹⁵ N]-Leu12	116.6	-105.6 ± 5.0	-74.7 ± 4.8	104.6	0.20
[¹⁵ N]-Leu14	116.2	-114.6 ± 5.0	-85.2 ± 4.8	104.5	0.19
Dipolar interactions		$\Delta\nu_{\text{DC}}$ (Hz)		$\Delta\nu_{\text{DC}}$ (Hz)	
[¹³ C ₁]-Ala11-[¹⁵ N]-Leu12		313 ± 100		1010	
[¹³ C ₁]-Ala13-[¹⁵ N]-Leu14		286 ± 100		1010	
Quadrupolar interactions		$\Delta\nu_{\text{Q}}$ (Hz)	$\Delta\nu_{\text{Q}}$ (Hz)	$\Delta\nu_{\text{Q}}$ (Hz)	
[C _α - ² H ₃]-Ala7		500 ± 500*	500 ± 500*	37700	
[C _α - ² H ₃]-Ala9		6600 ± 500*	5725 ± 500*	37700	
[C _α - ² H ₃]-Ala11		2300 ± 500*	1000 ± 500*	37700	
[C _α - ² H ₃]-Ala13		7750 ± 500*	6025 ± 500*	37700	
[C _α - ² H ₃]-Ala15		500 ± 500*	500 ± 500*	37700	
[C _α - ² H ₃]-Ala17		6500 ± 500*	6075 ± 500*	37700	

* Experimental data from [2].
[§] The chemical shift anisotropy is defined as $\Delta\nu_{\text{CS}} = (\delta_{333} - \delta_{\text{iso}}) = (\delta_{90^\circ} - \delta_{0^\circ})$, and the asymmetry parameter as $\eta_{\text{CS}} = (\delta_{222} - \delta_{111}) / (\delta_{333} - \delta_{\text{iso}})$.
The principal values are sorted according $|\delta_{333} - \delta_{\text{iso}}| > |\delta_{111} - \delta_{\text{iso}}| > |\delta_{222} - \delta_{\text{iso}}|$.

The analysis using the extended dynamic peptide model was based on the optimized geometry of the peptide model. Inclusion of all 12 experimental constraints obtained on non-oriented, i.e. the previously published ²H results from [2] combined with the ¹⁵N and ¹³C results obtained in this study (listed in Table 2), allowed determination of the orientational and dynamical parameters of the WALP23 peptide incorporated into bilayers of di-C14:0PC with good accuracy (Table 4, A). The good quality of the master solution i.e. the fit to the complete data set of 12 constraints is illustrated in Figure 10. To determine a minimally required set of constraints for dynamic analysis, we repeated the analysis for a number of subsets of the constraints (Table 4, B to H). The tilt and rotation angle were found to be very stable among the various subsets of constraints as long as sufficient constraints of different orientation to the helix axis were included (Table 4, B, D to F). Fitting the experimental data set obtained on oriented bilayer systems yielded very similar results for the tilt angle (Table 4, I), indicating no significant effect of the bilayer system on the peptide orientation. However, the obtained rotation angle is shifted by ca. 180°. This is most likely due to the nature of the fitting functions and will be discussed in more detail below.

Table 3: Calculated interaction tensor orientations of the peptide model used for analysis. The Euler angles are defined with respect to the principal axis frame of the peptide. Since the dipolar and quadrupolar interaction tensors have nearly axial symmetry, two Euler angles are sufficient for description.

Chemical shift tensors	α (°)	β (°)	γ (°)
[¹³ C ₁]-Ala11	-82.0	97.7	323.3
[¹³ C ₁]-Ala13	-77.9	102.7	135.8
[¹⁵ N]-Leu12	-163.3	15.1	20.5
[¹⁵ N]-Leu14	-138.0	15.6	168.0

Dipolar interactions	θ (°)	ϕ (°)
[¹³ C ₁]-Ala11-[¹⁵ N]-Leu12	66.2	302.4
[¹³ C ₁]-Ala13-[¹⁵ N]-Leu14	71.1	128.8

Quadrupolar interactions	θ (°)	ϕ (°)
[C- ² H ₃]-Ala7	58.7	85.5
[C- ² H ₃]-Ala9	57.2	249.4
[C- ² H ₃]-Ala11	62.1	56.4
[C- ² H ₃]-Ala13	55.9	227.5
[C- ² H ₃]-Ala15	61.5	27.9
[C- ² H ₃]-Ala17	58.3	176.9

Table 4: Parameters from analysis with the dynamic model for various (sub)sets of anisotropic NMR constraints. All fits were performed using the experimental data obtained on peptides inserted into non-oriented bilayers, unless otherwise indicated.

	Number and nature of constraints	SSD	τ (°) *	$\Delta\tau$ (°) *	ρ (°) *	$\Delta\rho$ (°) *
A	12 complete data set †	0.36	20.3 ± 5.4	14.1 ± 19	146 [§] ± 13	83 [§] ± 38
B	10 removed 2 ¹⁵ N- ¹³ C DC	0.33	20.5 ± 3.5	14.1 ± 7	150 [§] ± 13	86 [§] ± 41
C	14 added 2 simulated ¹⁵ N-H DC #		20.3 ± 5.4	14.1 ± 19	146 [§] ± 13	83 [§] ± 38
D	6 2 ¹⁵ N CSA, 2 ¹³ C CSA, 2 C- ² H ₃ Δv_Q		22.6 ± 9.0	2.8 ± ∞	149 [§] ± 15	92 [§] ± 48
E	8 6 C- ² H ₃ Δv_Q , 2 ¹⁵ N CSA		20.4 ± 2.7	13 ± 16	146 [§] ± 13	82 [§] ± 57
F	8 2 ¹⁵ N CSA, 2 ¹³ C CSA, 4 C- ² H ₃ Δv_Q		18.9 ± 2.9	19.2 ± 3.1	137 [§] ± 28	83 [§] ± 38
G1	6 6 C- ² H ₃ Δv_Q alone; solution a	0.3	0 ± ∞	32 ± 9	147 [§] ± 16	80 [§] ± 89
G2	6 6 C- ² H ₃ Δv_Q alone; solution b	0.6	21.0 ± 16	1 ± ∞	145 [§] ± 16	69 [§] ± 164
H	4 2 ¹⁵ N CSA, 2 simulated ¹⁵ N-H DC		16.5 ± ∞	23 ± ∞	142 [§] ± 136	40 [§] ± ∞
I	8 6 C- ² H ₃ Δv_Q , 2 ¹⁵ N CSA ^		23.4 ± 1.6	34.4 ± 2.4	147 ± 8	143 ± 4

*The uncertainties were computed with the GOSA software [36] taking into account the experimental accuracy of the each experimental parameter, and is a quantification of the under-determination of some parameters (due to a flat surface potential).

† A second acceptable solution is $\tau = 22.5^\circ$, $\rho = 151^\circ$ and $\Delta\rho = 153^\circ$ (SSD = 1.25).

§ The rotation and oscillation angles were corrected by subtraction of 180°, since the extent of the oscillation $\Delta\rho$ exceeds 180° and therefore samples the full circle (see text for further explanations).

The ¹⁵N-H dipolar couplings were calculated based on the parameters of solution A.

^ Experimental values determined on peptides inserted in oriented bilayers.

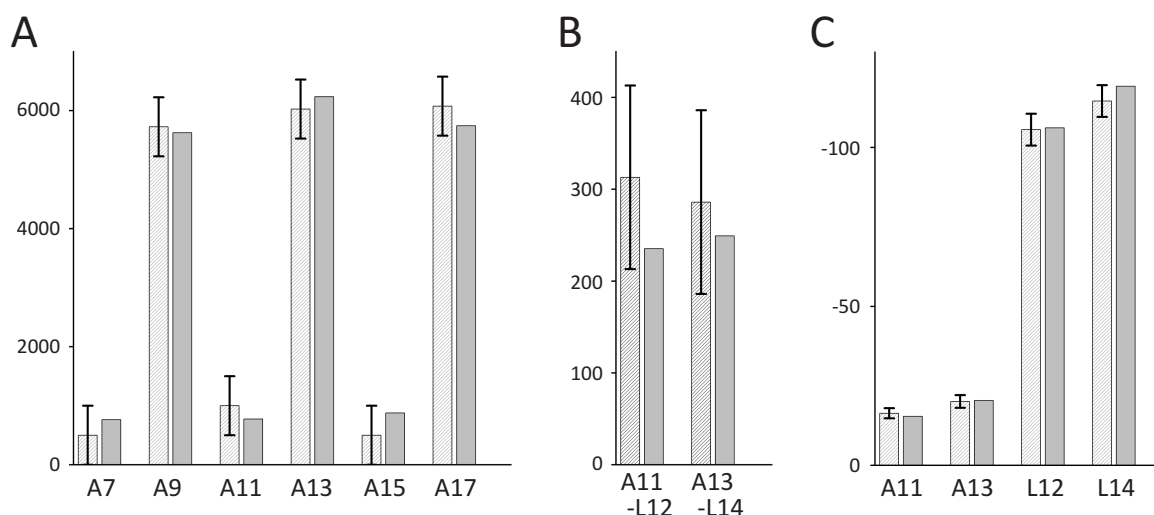


Figure 10: Best fit (light grey bars) to the complete set of 12 experimental constraints obtained at a relative hydration of 33% (dark grey bars): (A) $C_{\alpha}-^2H_3$ quadrupolar couplings (in Hz) of labeled Ala7, Ala9, Ala11, Ala13, Ala15, Ala17; (B) $^{15}N-^{13}C_1$ dipolar couplings (in Hz) of $[^{13}C_1]$ -Ala11- $[^{15}N]$ -Leu12 and $[^{13}C_1]$ -Ala13- $[^{15}N]$ -Leu14; and (C) Chemical shift anisotropies (in ppm) of $[^{13}C_1]$ -Ala11 and $[^{13}C_1]$ -Ala13 and $[^{15}N]$ -Leu12 and $[^{15}N]$ -Leu14. The experimental values are summarized in Table 2 and the fits results are given in row A of Table 4.

WALP peptides are highly dynamic

The analysis using the dynamic model yielded two in terms of SSD acceptable solutions with similar tilt angles, but very different rotation angles (see Figure 11). When comparing both solutions, we note that the rotation angles are displaced by ca. 180° , and that the oscillation amplitude $\Delta\rho$ of the best solution (A) is much larger than for the second best solution (B). For the best solution (A) numerical integration is performed over the rotation angles in the range $\rho = 326^\circ \pm 263^\circ$ to include motional averaging around the helical axis. In this case the oscillation amplitude of the peptide is larger than 180° , which means that the rotation angles are sampled over more than the full turn of 360° , with a maximum probability occurring in the range $\rho = 146^\circ \pm 83^\circ$; while for the second best solution (B) the averaging over rotation angles is performed only in the range $\rho = 151^\circ \pm 153^\circ$. In fact, both solutions represent the same preferred helix rotation angle ρ of ca. 150° . Most likely, the observation of these two, in principle identical solutions is due to the fact that averaging is included into the fit procedures using delta-functions. Within the sampled range the probability of the delta function is one, whereas outside the range it is zero. In this particular case, the actual distribution of rotation angles may be slightly better sampled by a delta function with the parameters of solution A. Instead of the delta function, the more intuitive Gaussian function could be used for sampling, but this would require time-consuming numerical integration of the fitting functions.

When sampling the distribution using delta functions, we obtained a tilt angle τ of ca. 20.5° for WALP23 peptides incorporated into bilayers of di-C14:0PC, which agrees well with the results obtained recently from fluorescence experiments [12] and confirms the trends indicated in MD simulations [8]. The rotation angle of ca. 150° agrees well with the rotation angle of 155° reported from previous 2H NMR studies [2,3], and also with the rotation angle of 136° reported for WALP23 in di-C18:1PC from a recent fluorescence study [12]. The wobbling amplitude $\Delta\tau$ was determined to ca. 14° and the oscillation amplitude $\Delta\rho$ to more than 150° , indicating that WALP peptides are highly dynamic when incorporated into membranes.

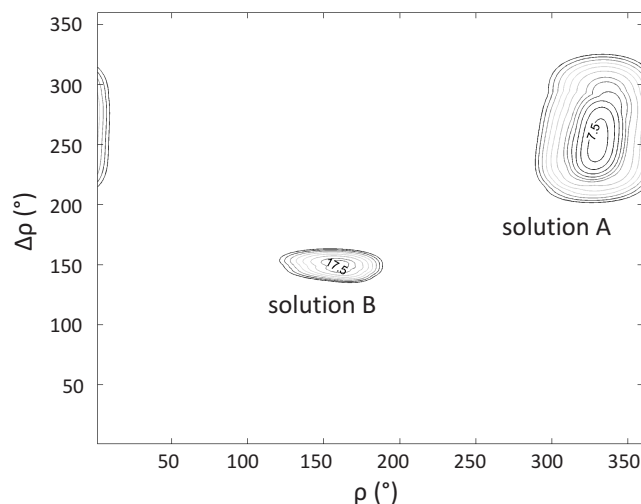


Figure 11: SSD from fits to the complete set of 12 experimental constraints as a function of the rotation angle ρ and the oscillation amplitude $\Delta\rho$. Two acceptable solutions were found i.e. solution A: $\tau = 20.3^\circ$, $\rho = 326^\circ$, $\Delta\rho = 263^\circ$ with SSD = 0.36; and solution B: $\tau = 22.5^\circ$, $\rho = 151^\circ$, $\Delta\rho = 153^\circ$ with SSD = 1.25.

It should be noted here that the wobbling amplitude is still loosely determined, and that a reasonable fit can be found even by imposing an wobbling amplitude $\Delta\tau = 0^\circ$. In contrast, the oscillation amplitude $\Delta\rho$ was found to be very large, which confirms that data analysis based on the quasi-static model previously used is insufficient, as previously suggested from two independent molecular dynamics simulations studies [8,9].

Using the complete set of experimental constraints we were able to extract an unambiguous solution for the orientational and motional parameters of the peptide. Qualitatively, the ^{15}N - ^{13}C dipolar couplings obtained for WALP23 were found to be weak (~ 300 Hz) and of relatively low accuracy (compare Figure 14). Removing these constraints did not significantly change the outcome of the fit (Table 4, B), but led to a slightly improved SSD. This finding suggests to proceed without the fairly time-consuming REDOR experiments. Similarly, addition of (simulated) ^{15}N -H dipolar couplings, which can be obtained experimentally from (also time consuming) PISEMA experiments, did not improve the result of the fit (Table 4, C). This can be understood from the fact that the main tensor orientations of ^{15}N -H dipolar couplings and ^{15}N CSA interactions have a very similar orientation and therefore duplicate each other.

If only constraints with very similar orientation to the peptide helix were used, the system was found to be underdetermined, which is reflected in the fit parameter with undetermined accuracy (i.e. $\pm \infty$). When including only quadrupolar splittings, two solutions with reasonable agreement to the experimental data can be found (Table 4, G1 and G2). Both solutions give a very similar rotation angle that agrees well with the master solution (Table 4, A), indicating that a data set of only quadrupolar splittings still allows reliable determination of the rotation angle. The system was also found to be underdetermined if only ^{15}N CSAs and (simulated) ^{15}N -H dipolar couplings were included in the analysis (Table 4, H).

Summary

Generalization of the model for analysis

In previous ^2H NMR studies of Strandberg *et al.* [2] and Özdirekcan *et al.* [3] the orientation of WALP23 peptides in lipid bilayers was determined from analysis of a set of quadrupolar splittings obtained from WALP23 peptides including a single deuterium labeled alanine with the GALA method. The model underlying this approach describes the orientation of the peptide with respect to the bilayer by two parameters, a tilt angle τ of the α -helix with respect to the membrane normal and a rotation angle ρ around the long axis of the α -helix (Figure 1A). Peptide motions were included into the approach by a global order parameter S , which mainly accounts for motions about the membrane normal. This model can be seen as a quasi-static model since it neglects dedicated peptide motions about the helix axis.

To overcome these limitations, we extended the conventional peptide model by wobbling-in-a-cone motions about the short axes of the α -helix and by oscillations around the long axis, which are superimposed on the initial rotation. For this purpose, two motional parameters were introduced into the model, $\Delta\tau$ describing the wobbling and $\Delta\rho$ describing the oscillations. This new dynamic model describes the topology of the peptide in the bilayer by now four parameters, a tilt angle τ , a wobbling $\Delta\tau$, a rotation angle ρ and an oscillation $\Delta\rho$ (Figure 1B). No other/additional motions (e.g. in form of a global order parameter) were included. Due to the increased number of parameters in the generalized, dynamic model more independent experimental constraints are required. A larger number of quadrupolar splittings can not satisfy this demand since peptide motions can be expected to affect all quadrupolar splittings in a similar way, and effectively, the system will still be underdetermined. Thus, a better and more elegant solution is the acquisition of additional experimental constraints with different orientation to the helix axis.

In the present study, we determined the chemical shift anisotropies of ^{13}C labeled backbone carbonyls and of ^{15}N labeled backbone amides as well as ^{13}C - ^{15}N dipolar couplings along the backbone of the peptide, introduced by an amino acid with a ^{15}N labeled amide connected to the ^{13}C labeled carbonyl of the preceding amino acid. These anisotropic interactions were selected because they have very different orientations of their principal axis system with respect to the helix axis. The ^{15}N CSA (and ^{15}N -H dipolar couplings) can be expected to be most sensitive to the tilt angle and wobbling motions, whereas the other anisotropic constraints (including the quadrupolar splittings) will be sensitive to all orientational and motional parameters.

Minimal set of constraints

We explored the space of solutions for various subsets of the 12 experimental constraints to identify a minimal set of constraints required for dynamical analysis. When doing the analysis using a set of only 4 constraints including the 2 (simulated) ^{15}N -H dipolar couplings and 2 ^{15}N CSAs, the system was found to be underdetermined (Table 4, H). Both interactions are oriented almost parallel to the helix axis and therefore report very sensitive on the tilt angle and wobbling, and much less sensitive on the rotation angle and oscillations.

Similar observations can be made when only the quadrupolar splittings are included into the analysis (Table 4, G1 and G2), underlining the need for constraints with different orientations with respect to the helix axis. However, a dynamic analysis using a very diverse set of constraints including 2 ^{15}N CSAs, 2 ^{13}C CSAs and only 2 quadrupolar splittings yielded quite poor results. The quality of the fit was found to improve significantly with the number of quadrupolar splittings included in the analysis (Table 4, compare B, D and F). Alternatively, a set including the 2 ^{15}N CSAs and 6 quadrupolar splittings allowed determination of all four parameters with very good accuracy (Table 4, E).

In order to efficiently determine the orientation and motional parameters of a transmembrane peptide, we propose to use a set of 6 to 8 constraints including minimally 2 ^{15}N chemical shift anisotropies, and 4 - 6 quadrupolar splittings determined on deuterated alanines; or alternatively, to use 2 ^{15}N chemical shift anisotropies, 2 ^{13}C chemical shift anisotropies and 2 - 4 quadrupolar splittings. These experimental constraints can be measured on two (or three) different synthetic peptides, each including a ^{15}N labeled backbone amide, (a ^{13}C labeled backbone carbonyl), and one or more deuterated alanines, depending on the number of alanines that are present (or introduced) in the transmembrane segment. The quadrupolar splittings can be distinguished if the percentage of labeled alanine is varied among the different positions, which can be achieved by mixing deuterated and unlabeled alanines [37]. The time needed for acquisition of NMR spectra is estimated to ca. 3-4 days on a 500 to 700 MHz solid-state NMR spectrometer.

In conclusion, the presented approach allows a robust, precise and efficient determination of the orientation and dynamical parameters of transmembrane peptides using well-established solid-state NMR techniques. In particular, we succeeded to accurately determine the orientation and dynamics of WALP23 peptides inserted in di-C14:0PC. In future, this achievement will allow proper calibration of lipid-proteins interaction parameters required for MD simulations of membrane proteins, paving the way to further advancement in this field. This technique is now established for WALP peptides but it can be applied to other transmembrane peptides, and thus opens up the way explore the effects of the lipid environment, including hydrophobic mismatch or the presence of cholesterol, on the orientation and dynamics of transmembrane peptides.

Acknowledgements

This research project has been supported by a Marie Curie Early Stage Research Training Fellowship from the European Community's Sixth Framework Program for A.H. (Biomem-MEST-CT 2004-007931). The IPBS NMR equipment was financed by the French research ministry, the Université Paul Sabatier, the Région Midi Pyrénées and European structural funds. We thank Rutger W. H. M. Staffhorst, Lucie P. Khemtémourian-Oosting and Jacques P.F. Doux for peptide synthesis.

References

1. van der Wel PCA, Strandberg E, Killian JA, and Koeppe II RE (2002) Geometry and intrinsic tilt of a tryptophan-anchored transmembrane alpha-helix determined by 2H NMR. *Biophys J*, 83:1479–1488.
2. Strandberg E, Özdirekcan S, Rijkers DTS, van der Wel PCA, Koeppe II RE, Liskamp RMJ, and Killian JA (2004) Tilt angles of transmembrane model peptides in oriented and non-oriented lipid bilayers as determined by 2H solid-state NMR. *Biophys J*, 86:3709–3721.
3. Özdirekcan S, Rijkers DTS, Liskamp RMJ, and Killian JA (2005) Influence of flanking residues on tilt and rotation angles of transmembrane peptides in lipid bilayers. A solid-state 2H NMR study. *Biochemistry*, 44:1004–1012.
4. Daily AE, Greathouse DV, van der Wel PCA, and Koeppe II RE (2008) Helical distortion in tryptophan- and lysine-anchored membrane-spanning alpha-helices as a function of hydrophobic mismatch: a solid-state deuterium NMR investigation using the geometric analysis of labeled alanines method. *Biophys J*, 94:480–491.
5. Traaseth NJ, Buffy JJ, Zamoon J, and Veglia G (2006) Structural dynamics and topology of phospholamban in oriented lipid bilayers using multidimensional solid-state NMR. *Biochemistry*, 45:13827–13834.
6. Park SH and Opella SJ (2005) Tilt angle of a trans-membrane helix is determined by hydrophobic mismatch. *J Mol Biol*, 350:310–318.
7. Marassi FM and Opella SJ (2000) A solid-state NMR index of helical membrane protein structure and topology. *J Magn Reson*, 144:150–155.
8. Özdirekcan S, Etchebest C, Killian JA, and Fuchs PFJ (2007) On the orientation of a designed transmembrane peptide: toward the right tilt angle? *J Am Chem Soc*, 129:15174–15181.
9. Esteban-Martin S and Salgado J (2007) The dynamic orientation of membrane-bound peptides: bridging simulations and experiments. *Biophys J*, 93:4278–4288.
10. Killian JA (2003) Synthetic peptides as models for intrinsic membrane proteins. *FEBS Lett*, 555:134–138.
11. Killian JA and Nyholm TKM (2006) Peptides in lipid bilayers: the power of simple models. *Curr Opin Struct Biol*, 16:473–479.
12. Holt A, Koehorst RBM, Meijneke T, Gelb MH, Rijkers DT, Hemminga MA, and Killian JA (2009) Tilt and rotation angles of a transmembrane model peptide as studied by fluorescence spectroscopy. *Biophys J*, submitted.
13. de Planque MRR, Kruijtz JAW, Liskamp RMJ, Marsh D, Greathouse DV, Koeppe II RE, de Kruijff B, and Killian JA (1999) Different membrane anchoring positions of tryptophan and lysine in synthetic transmembrane alpha-helical peptides. *J Biol Chem*, 274(30):20839–20846.
14. ten Kortenaar PBW, van Dijk BG, Peeters JM, Raaben BJ, Adams PJHM, and Tesser GI (1986) Rapid and efficient method for the preparation of Fmoc-amino acids starting from 9-fluorenylmethanol. *Int J Pept Prot Res*, 27:398–400.
15. Frisch MJ, Trucks GW, Schlegel HB, Scuseria GE, Robb MA, Cheeseman JR, Montgomery JA Jr, Vreven T, Kudin KN, Burant JC, Millam JM, Iyengar SS, Tomasi J, Barone V, Mennucci B, Cossi M, Scalmani G, Rega N, Petersson GA, Nakatsuji H, Hada M, Ehara M, Toyota K, Fukuda R, Hasegawa J, Ishida M, Nakajima T, Honda Y, Kitao O, Nakai H, Klene M, Li X, Knox JE, Hratchian HP, Cross JB, Bakken V, Adamo C, Jaramillo J, Gomperts R, Stratmann RE, Yazyev O, Austin AJ, Cammi R, Pomelli C, Ochterski JW, Ayala PY, Morokuma K, Voth GA, Salvador P, Dannenberg JJ, Zakrzewski VG, Dapprich S, Daniels AD, Strain MC, Farkas O, Malick DK, Rabuck AD, Raghavachari K, Foresman JB, Ortiz JV, Cui Q, Baboul AG, Clifford S, Cioslowski J, Stefanov BB, Liu G, Liashenko A, Piskorz P, Komaromi I, Martin RL, Fox DJ, Keith T, Al-Laham MA, Peng CY, Nanayakkara A, Challacombe M, Gill PMW, Johnson B, Chen W, Wong MW, Gonzalez C, and Pople JA, Gaussian 03, Revision E.01.1. Gaussian, Inc., Wallingford, CT, 2004.
16. Maseras F and Morokuma K (1995) IMOMM: a new integrated ab initio molecular + mechanics geometry optimization scheme of equilibrium structures and transition states. *J Comput Chem*, 16:1170–1179.
17. Vreven T and Morokuma K (2000) On the application of the IMOMO (integrated molecular orbital + molecular orbital) method. *J Comput Chem*, 21:1419–1432.

18. Lee CT, Yang WT, and Parr RG (1988) Development of the Colle-Salvetti correlation-energy formula into a functional of the electron-density. *Phys Rev B*, 37:785–789.
19. Becke AD (1993) Density-functional thermochemistry .3. The role of exact exchange. *J Chem Phys*, 98:5648–5652.
20. Foresman JB and Frisch A (1996) Exploring Chemistry With Electronic Structure Methods: a Guide to Using Gaussian. Gaussian, Inc., Pittsburgh, PA, 2nd edn.
21. Dewar MJS and Thiel W (1977) MINDO/3 study of the addition of singlet oxygen (1.DELTA.gO2) to 1,3-butadiene. *J Am Chem Soc*, 99:2338–2339.
22. Dewar MJS, McKee ML, and Rzepa HS (1978) MNDO parameters for third period elements. *J Am Chem Soc*, 100:3607–3607.
23. Anders E, Koch R, and Freunsch P (1993) Optimization and application of lithium parameters for PM3. *J Comput Chem*, 14:1301 – 1312.
24. Wolinski K, Hinton JF, and Pulay P (1990) Efficient implementation of the gauge-independent atomic orbital method for NMR chemical shift calculations. *J Am Chem Soc*, 112:8251–8260.
25. Wolinski K and Sadlej AJ (1980) Self-consistent perturbation theory: open-shell states in perturbation-dependent non-orthogonal basis sets. *Mol Phys*, 41:1419–1430.
26. Ditchfield R (1974) Self-consistent perturbation theory of diamagnetism I. A gauge-invariant LCAO method for N.M.R. chemical shifts. *Mol Phys*, 27:789–807.
27. McWeeny R (1962) Perturbation theory for the Fock-Dirac density matrix. *Phys Rev*, 126:1028–1034.
28. London F (1937) Théorie quantique des courants interatomiques dans les combinaisons aromatiques. *J Phys Radium*, 8:397–409.
29. Rouser G, Fleischer S, and Yamamoto A (1970) Two-dimensional thin layer chromatographic separation of polar lipids and determination of phospholipids by phosphorus analysis of spots. *Lipids*, 5:494–496.
30. Gullion T and Schaefer J (1989) Rotational-echo double-resonance NMR. *J Magn Reson*, 81:196–200.
31. Gullion T, Baker DB, and Conradi MS (1990) New, compensated Carr-Purcell sequences. *J Magn Reson*, 89:479–484.
32. Gullion T and Schaefer J (1989) Detection of weak heteronuclear dipolar coupling by rotational-echo double-resonance nuclear magnetic resonance. *Adv Magn Reson*, 13:57–83.
33. Saito H (1986) Conformation-dependent carbon-13 chemical shifts: a new means of conformational characterization as obtained by high-resolution solid-state carbon-13 NMR. *Mag Res Chem*, 24:835–852.
34. Wishart DS, Sykes BD, and Richards FM (1991) Relationship between nuclear magnetic resonance chemical shift and protein secondary structure. *J Mol Biol*, 222:311–333.
35. Wishart DS and Sykes BD (1994) The 13C chemical-shift index: a simple method for the identification of protein secondary structure using 13C chemical-shift data. *J Biomol NMR*, 4:171–180.
36. Czaplicki J, Cornélissen G, and Halberg F (2006) GOSA, a simulated annealing-based program for global optimization of nonlinear problems, also reveals transyears. *J Appl Biomed*, 4:87–94.
37. Vostrikov VV, Grant CV, Daily AE, Opella SJ, and Koeppe II RE (2008) Comparison of “polarization inversion with spin exchange at magic angle” and “geometric analysis of labeled alanines” methods for transmembrane helix alignment. *J Am Chem Soc*, 130:12584–12585.

Chapter 4

Tilt and Rotation Angles of a Transmembrane Model Peptide as Studied by Fluorescence Spectroscopy

Andrea Holt,[‡] Rob B. M. Koehorst,[§] Tania Rutters-Meijneke,[‡] Michael H. Gelb,[¶]
Dirk T.S. Rijkers,[†] Marcus A. Hemminga,[§] and J. Antoinette Killian[‡]

[‡]Chemical Biology & Organic Chemistry, Bijvoet Center for Biomolecular Research, Utrecht University, Utrecht, The Netherlands; and [†]Medicinal Chemistry & Chemical Biology, Utrecht Institute of Pharmaceutical Sciences, Utrecht University, Utrecht, The Netherlands; and [§]Laboratory of Biophysics, Wageningen University, Wageningen, The Netherlands; and [¶]Departments of Chemistry and Biochemistry, University of Washington, Washington, Seattle, USA.

Accepted for publication in *Biophysical Journal* (2009)

Abstract

In this study the membrane orientation of a tryptophan-flanked model peptide, WALP23, was determined by using peptides that were labeled at different positions along the sequence with the environment-sensitive fluorescent label BADAN. The fluorescence properties, reflecting the local polarity, were used to determine the tilt and rotation angles of the peptide based on an ideal α -helix model. For WALP23 inserted in dioleoylphosphatidylcholine (DOPC), an estimated tilt angle of the helix with respect to the bilayer normal was obtained of $24 \pm 5^\circ$. When the peptides were inserted into bilayers with different acyl chain length or containing different concentrations of cholesterol, small changes in tilt angle were observed as response to hydrophobic mismatch, while the rotation angle appeared to be independent of lipid composition. In all cases the tilt angles were significantly larger as those previously determined from ^2H NMR experiments, supporting recent suggestions that the relatively long time-scale of ^2H NMR measurements may result in an underestimation of tilt angles due to partial motional averaging. The observation that the adaptations of the tilt angles to mismatch are relatively small is consistent with the simultaneous occurrence of additional mechanisms to compensate for hydrophobic mismatch of these tryptophan-flanked peptides.

Introduction

Membrane proteins fulfill many essential functions for the survival of the cell. These functions include signaling, transport of molecules across the membrane and transduction of energy which by definition all require at least a temporal change in the conformation of the membrane protein. For a number of membrane proteins it has been suggested that their function, and therefore most probably also their conformation, depends on membrane properties such as bilayer thickness, lipid packing, or the presence of microdomains (e.g. [1-3]). In many cases the underlying mechanism of the interaction between membrane proteins and the lipid environment is still far from being elucidated, which is partly due to the difficulties to study these complex hydrophobic systems.

To avoid some of the problems, simple model systems composed of artificial or natural peptides in synthetic lipid bilayers have been utilized to get deeper insight into the basic principles of peptide-lipid interactions. One example of a frequently used natural model peptide is the M13 coat protein [4]. For this peptide it was shown that the transmembrane part responds to decreasing bilayer thickness by increasing its tilt angle [5], similar to what has been reported for other small membrane peptides/proteins like the transmembrane segment of Vpu [6], cell-signaling peptides [7] or alamethicin [8].

In addition to natural peptides, synthetic model peptides with well-defined structures are being used for experimental and modeling studies to understand basic principles of peptide/lipid interactions [9-13]. These peptides offer the advantage that they allow systematic variation of peptide parameters, like hydrophobic length or hydrophobicity, and easy incorporation of labels via peptide synthesis. An example is the family of WALP peptides, which consist of a hydrophobic stretch of alternating leucines and alanines flanked by a pair of tryptophans at the N/C-termini. These and other transmembrane model peptides are now widely used in systematic approaches to investigate consequences of hydrophobic mismatch such as helix tilting.

For WALP peptides measurement of tilt angles appeared to be not straightforward. A recently developed approach using ^2H NMR spectroscopy on alanine deuterated peptides showed for WALP23 peptides a very small but systematic increase in tilt angle with decreasing bilayer thickness [14,15]. However, recent MD (molecular dynamics) studies predict much larger tilt angles for WALP23 [16] and related model peptides [17,18]. This discrepancy may be due to the fact that only limited motion was included in the models used for analysis of the ^2H NMR data, which may not have been sufficient to account for averaging effects and could lead to an underestimation of the tilt angle [16,17,19]. Alternatively, the MD simulations may need improvement, for example the use of longer time scales. Clearly, solving this issue is important since accurate determination of the tilt angle is essential for understanding the basic principles of peptide/lipid interactions.

One approach towards obtaining accurate tilt angles would be to include different types of NMR labels combined with different dynamic models. PISEMA methods [20,21] are one step towards this direction. Alternatively one could use methods with shorter timescales, reducing signal averaging due to peptide motions. Here, we chose the latter approach by using steady-state fluorescence spectroscopy. For this purpose, a set of WALP23 peptides with single cysteine replacements at different positions in the peptide sequence was labeled with the fluorescent label BADAN which reports about the polarity of the local environment [22]. Analysis of the fluorescence results for WALP23 peptides in bilayers yielded similar rotation angles, but much larger tilt angles than determined from ^2H NMR experiments, suggesting indeed an underestimation of the tilt angle due to motional averaging. Furthermore, WALP23 was found to respond to changes in the thickness of the bilayers by only partly adapting its tilt angle. This is in agreement with the observation that tilting is not the only response of WALP peptides to mismatch, but that other responses can occur simultaneously, such as stretching or disordering of the lipids and an increased tendency to self-associate [9].

Materials and Methods

Materials

1,2-dimyristoleoyl-sn-glycero-3-phosphocholine (di-C14:1PC), 1,2-dipalmitoleoyl-sn-glycero-3-phosphocholine (di-C16:1PC), 1,2-dioleoyl-sn-glycero-3-phosphocholine (di-C18:1PC), 1,2-dieicosenoyl-sn-glycero-3-phosphocholine (di-C20:1PC) and 1,2-dierucoyl-sn-glycero-3-phosphocholine (di-C22:1PC), and cholesterol were purchased as lyophilized powders from Avanti Polar Lipids Inc. (Alabaster, AL, USA) and used without further purification. All other chemicals used were of analytical grade; the water used was deionized and purified with a Milli-Q Gradient water purification system from Millipore Corp. (Billerica, MA, USA).

The peptides WALP23-C0, WALP23-A11C, WALP23-L12C, WALP23-A13C and WALP23-C24 were synthesized using Fmoc/tBu solid-phase peptide synthesis as described elsewhere for related KALP peptides [23]. All other peptides were synthesized using manual solid phase synthesis protocols by SynPep Inc. (Dublin, CA, USA). The peptide sequences are given in Table 1.

Table 1: Sequences of the BADAN labeled WALP23 peptides and masses determined using MALDI-TOF mass spectrometry characterization.

Pos.	Peptide	Sequence	Theor. mass	Observed mass
0	WALP23-C0	Acetyl-C*GWWLALALALALALALALWVA-amide	2831.6	2855.4, M+Na
2	WALP23-W2C	Acetyl-GC*WLALALALALALALALWVA-amide	2645.5	2669.4, M+Na
4	WALP23-L4C	Acetyl-GWWC*ALALALALALALALWVA-amide	2718.5	2741.7, M+Na
6	WALP23-L6C	Acetyl-GWWLAC*ALALALALALALALWVA-amide	2718.5	2742.3, M+Na
8	WALP23-L8C	Acetyl-GWWLALAC*ALALALALALALALWVA-amide	2718.5	2742.3, M+Na
10	WALP23-L10C	Acetyl-GWWLALALAC*ALALALALALALALWVA-amide	2718.5	2742.0, M+Na
11	WALP23-A11C [†]	Acetyl-GWWLALALALC*LALALALALWVA-amide	2764.6	2786.7, M+Na
12	WALP23-L12C [†]	Acetyl-GWWLALALALAC*ALALALALWVA-amide	2722.5	2746.0, M+Na
13	WALP23-A13C [†]	Acetyl-GWWLALALALALC*LALALALWVA-amide	2764.6	2788.3, M+Na
14	WALP23-L14C	Acetyl-GWWLALALALALAC*ALALALWVA-amide	2718.5	2742.3, M+Na
16	WALP23-L16C	Acetyl-GWWLALALALALALAC*ALALWVA-amide	2718.5	2741.7, M+Na
18	WALP23-L18C	Acetyl-GWWLALALALALALALAC*ALWVA-amide	2718.5	2742.7, M+Na
20	WALP23-L20C	Acetyl-GWWLALALALALALALALAC*WVA-amide	2718.5	2742.4, M+Na
22	WALP23-W22C	Acetyl-GWWLALALALALALALALALWC*A-amide	2645.5	2768.7, M+Na
24	WALP23-C24	Acetyl-GWWLALALALALALALALALWVGC*-amide	2817.6	2841.6, M+Na

* Cysteine labeled with BADAN.

[†] Peptide includes a d₄-alanine.

Methods

Labeling of peptides with BADAN

To label the peptides with BADAN (6-bromoacetyl-2-dimethylaminonaphthalene; Molecular Probes, Invitrogen Corp., Carlsbad, CA, USA), ca. 1 mg of each peptide was weighed into an Eppendorf tube and dissolved in 200 µl TFE (trifluoroethanol). Subsequently, 10 µl H₂O was added. Then, the peptide solution was deoxygenized by bubbling with N₂ gas for several minutes. While keeping the peptide solution under N₂ atmosphere, 2 µl of triethylamine and 1.5 equivalents of BADAN label, dissolved in methanol and purged with N₂, were added. After stirring the reaction mixture in the dark during 3 days at 4°C, the peptides were precipitated in 10 ml of cold methyl *tert*-butyl ether/*n*-hexane (1:1; stored at -20°C) to remove unbound BADAN label. The precipitate was collected by centrifugation, the supernatant containing the unreacted BADAN label was decanted and the precipitate was washed once again with methyl *tert*-butyl ether/*n*-hexane (1:1). Removal of unbound BADAN label was confirmed by TLC using chloroform/methanol/water (65:25:4) as running solvent since no free BADAN label was visible under UV light.

The purity of the peptides was analyzed with analytical HPLC using a C4 reverse phase column (Reprosil 300 C4 5 µm, 250 x 4.6 mm) using a linear solvent gradient from 10 - 100% methanol containing 0.1% TFA (trifluoroacetic acid) over 30 minutes. Prior to injection, the peptides were dissolved in TFE. If the purity was less than 90%, the labeled peptides were purified using a solvent gradient from 60-100% methanol containing 0.1% TFA over 40 minutes. For the purified peptides, the HPLC solvents were evaporated and residual TFA was removed by repeated cycles of dissolving the peptides in TFE followed by evaporation under high vacuum. The identity of all BADAN labeled WALP23 peptides was verified by MALDI-TOF mass spectrometry using α-cyano-4-hydroxycinnamic acid as matrix. The observed peptide masses are listed in Table 1.

Sample preparation

Stock solutions of ca. 5 mM lipids in chloroform were prepared by weight. The phospholipid concentrations were determined using the Rouser phosphorus assay. Stock solutions of BADAN labeled WALP23 peptides were prepared with a concentration of ca. 25 μM in TFE. The peptide concentration was determined by absorption spectroscopy using an extinction coefficient of $22400 \text{ M}^{-1}\text{cm}^{-1}$ at 280 nm for WALP23. The main absorption band of the BADAN label attached to the WALP peptides has a maximum at 387 nm, but also low absorbance at 280 nm. We corrected for this by subtraction of a pure BADAN absorption spectrum of equal intensity. From the peptide absorption spectra a typical labeling efficiency was estimated to be 80-90%.

After mixing solutions with appropriate amounts of peptide and phospholipids/cholesterol, the organic solvents were evaporated under a stream of N_2 gas and were further removed under vacuum overnight (ca. $1 \cdot 10^{-2}$ mbar). All fluorescence experiments were performed with a peptide/lipid molar ratio of 1/500 and a final peptide concentration of ca. 1 μM . The samples were hydrated with buffer (25 mM HEPES, 100 mM NaCl, pH 7.0) and vortexed. Large Unilamellar Vesicles (LUVs) were produced by extrusion through inorganic membrane filters with 200 nm pore size (Anotop 10; Whatman International Ltd., Maidstone, England).

Fluorescence measurements

After preparation, the samples (1.2 ml) were directly transferred to a 10 mm quartz cuvette and measured at room temperature on a Fluorolog 3.22 fluorimeter (Jobin Yvon-Spex, Edison, NJ, USA), using excitation light at 380 nm and a band pass of 2 nm in both excitation and detection light paths. The emission spectra were corrected for wavelength dependent deviations in the detection system using the instrument-specific correction file. All spectra were also corrected for background signals using a blank sample containing unlabeled WALP23 peptides with the same peptide/lipid ratio. Inner filter effects were negligible since all samples measured had an absorbance of less than 0.025.

Analysis of the fluorescence spectra

Fluorescent labels containing a DAN moiety like BADAN exhibit a dual fluorescence behavior with two different excited states, the LE (locally excited or Franck Condon) state and the ICT (intramolecular charge transfer) states evolving from the short-lived LE state [24]. The complex line shape of BADAN emission spectra can be explained by the presence of different emitting ICT states, i.e., a non-hydrogen-bonded ICT state, and hydrogen-bonded HICT states in an immobilized environment (HICT_i) and in a mobile environment (HICT_m), all possessing different energy levels and therefore emitting at different wavelengths (see [25] for an energy level scheme). The fraction of each emission state on the total emission depends on the local environment of the label.

For a quantitative analysis, the fluorescence spectra were decomposed into the different spectral components described above using three Gaussians, each characterized by a width, intensity and a peak position. The fraction of each spectral component is then calculated from the product of width and intensity, relative to the total of all spectral components. The fraction of total hydrogen-bonded labels f_{HB} is found by addition of the spectral fractions of mobile and immobile hydrogen-bonded BADAN labels. While the peak position of the HICT_m component highly depends on the local polarity at the label position, the HICT_i and

ICT components were found to be relatively independent in case of BADAN [25]. This allows simplification of the spectral decomposition by fixing the peak position of the ICT state and the HICT_i state at 23400 cm⁻¹ and 22140 cm⁻¹, respectively. These numbers were determined from emission spectra with a large fraction of the respective spectral component.

Calculation of the tilt and rotation angles

The geometry of a regular α -helix is defined by an increment along the helix axis of $d_{helix} = 1.5 \text{ \AA}$ per amino acid and a turn around the helix axis of $\rho_{helix} = 100^\circ$ per amino acid. The position x_{pos} of the labeled cysteine at position n_{label} with respect to the reference residue at position n_{ref} along the helix axis can then be calculated by

$$(1) \quad x_{pos} = d_{helix} (n_{ref} - n_{label}).$$

The orientation of a tilted transmembrane peptide is described by the angle τ between the membrane normal and the helix axis and the rotation angle ρ describes the angle between the direction of tilt and the C $_{\alpha}$ -atom of the reference residue with respect to the helix axis along the helix axis (see Figure 1). The position of a the label in a tilted transmembrane peptide is then calculated by

$$(2) \quad x_{label} = x_{pos} \cos \tau - d_{label} \sin \tau \cdot \cos((n_{label} - n_{ref}) \rho_{helix} - \rho),$$

where d_{label} the distance between the label and the helix axis.

The peak positions of the HICT_m state and the total hydrogen-bonded fractions were fitted using a Gaussian function

$$(3) \quad y = y_0 + a \cdot \exp \left\{ -\frac{1}{2} \left(\frac{(x_{label} - x)}{b} \right)^2 \right\},$$

where y_0 is the emission peak position of HICT_m state of a cysteine-bound BADAN label in aqueous environment ($y_0 = 19200 \text{ cm}^{-1}$ [25]), a is a scaling factor representing the shift in emission peak position between the membrane center and the aqueous environment, x denotes the distance parallel to the membrane normal between membrane center and the reference residue Gly1 ($n_{ref} = 1$), and b represents the width of the Gaussian distribution.

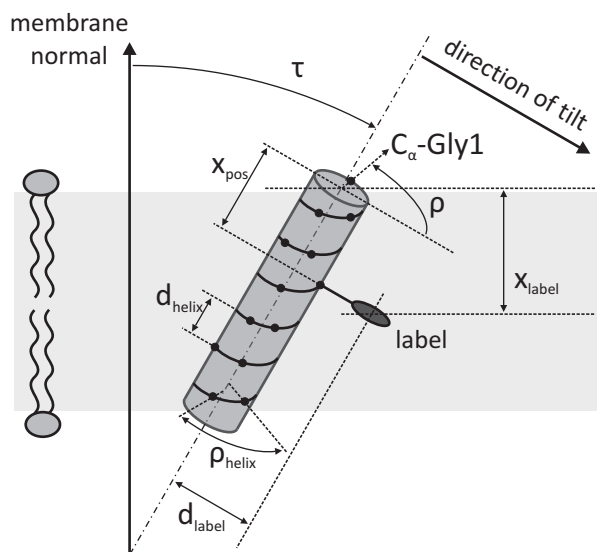


Figure 1: Schematic drawing of the angles describing the orientation of a tilted transmembrane peptide in the membrane. The tilt angle τ describes the angle between the membrane normal and the helix axis and the rotation angle ρ describes the angle between the direction of tilt and the C $_{\alpha}$ -atom of Gly1 in WALP23 with respect to the helix axis.

Results

Spectral shape depends on label position

A series of WALP23 peptides with cysteine replacements in different positions along the α -helix was labeled with the environment-sensitive fluorophore BADAN. The labeled peptides were inserted in di-C18:1PC and fluorescence spectra were recorded (Figure 2). The spectra for WALP23 peptides labeled at positions close to the peptide termini are clearly different from spectra from peptides labeled at positions in the hydrophobic stretch, and show abrupt changes in polarity between position 4 and 6, and between positions 18 and 20. The differences in spectral shape are due to the sensitivity of BADAN to the polarity of the local environment. Across a lipid bilayer, the polarity of the environment changes from very polar for the water phase and lipid head groups to apolar for the lipid acyl chain region with a steep gradient across the interfacial region [26]. The emission maximum exhibits a large red shift of 80 nm for labels positioned close to the peptide termini, indicating a more polar environment for labels at the N- or C-terminus of the peptide. These findings confirm the transmembrane insertion of the WALP23 peptide in di-C18:1PC bilayers.

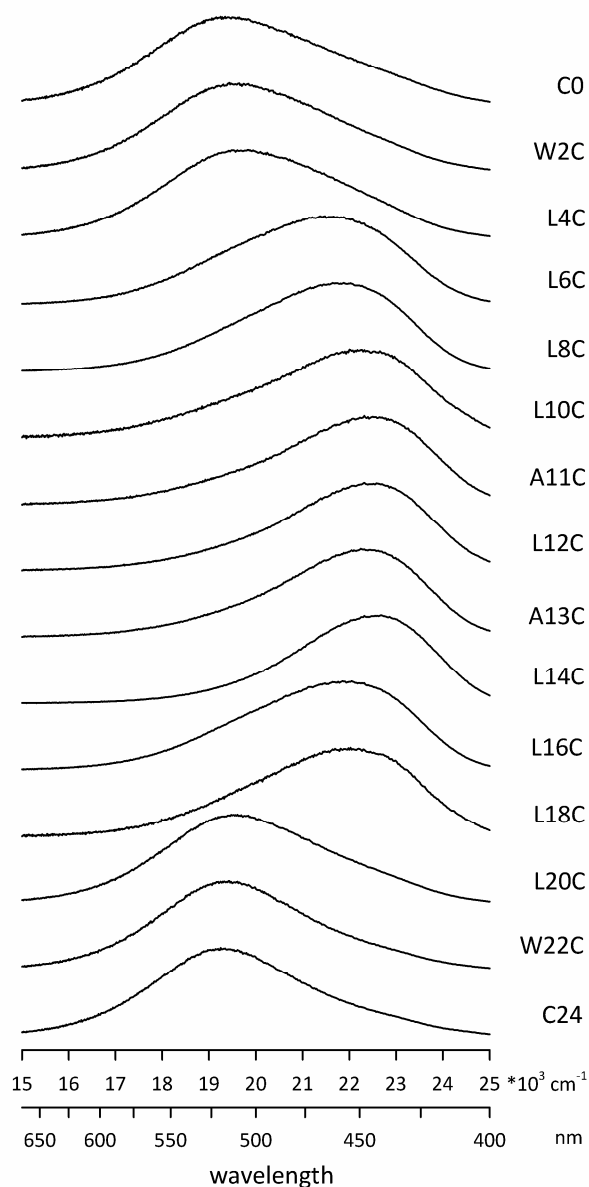


Figure 2: Emission spectra for a series of BADAN labeled WALP23 peptides incorporated in di-C18:1PC using a peptide/lipid ratio of 1:500. The final concentration of peptide was ca. 1 μ M. All samples were measured at room temperature.

Quantification of the spectral effects

Next, the effects were quantified by spectral decomposition of the emission spectra, yielding different types of information, as described previously [25]. In Figure 3, the decomposition is illustrated for a label positioned in the bilayer interior (upper panel) and a label located at the lipid-water interface (bottom panel). Closer inspection reveals striking differences in spectral components. For position 14 all components are almost equally present (Figure 3A), whereas for a label at position 0 (N-terminus) a large fraction of mobile hydrogen-bonded labels is observed (Figure 3B). Furthermore, the emission maximum of the mobile hydrogen-bonded labels shifts (from 20690 cm^{-1} at position 14 to 19470 cm^{-1} at the N-terminus), which reflects changes in the polarity of the local label environment [25]. The fraction of immobilized labels emitting with a maximum of 22140 cm^{-1} is larger for position 14, which indicates that labels located in the bilayer interior are more restricted in their motion. Finally, the spectral fraction of non hydrogen-bonded labels emitting with a maximum of 23400 cm^{-1} is much larger for the label positioned in the interior of the bilayer, as expected because there are less water molecules in the interior of the bilayer compared to the membrane-water interface.

Determination of the peptide orientation

For further analysis, we utilize the peak position P_m of the mobile hydrogen-bonded fraction of labels. In principle, also the total fraction of hydrogen-bonded labels f_{HB} can be used to retrieve the tilt angle. Here, we focused on P_m because it is more sensitive to changes across the membrane.

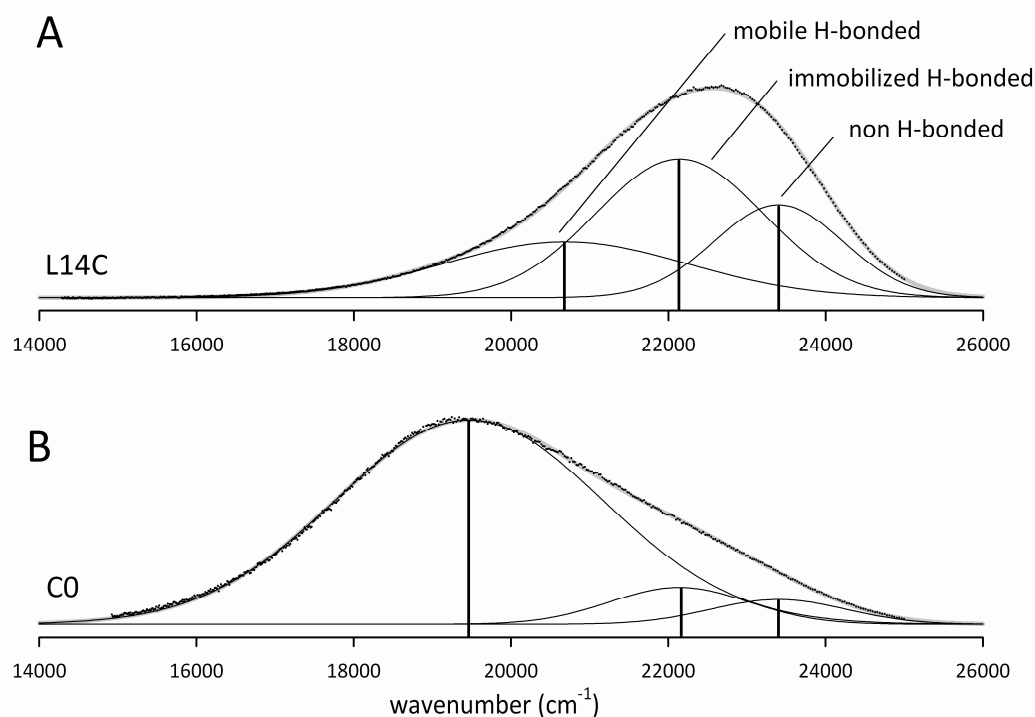


Figure 3: Spectral decomposition for emission spectra (dots) for a BADAN label in position L14C (A) and at the N-terminus (B). For both fits (thick grey line), the peak positions of the spectral components were allowed to vary for the HICT_m state (between 18000 and 22000 cm^{-1}) and were fixed for the HICT_i and ICT states at 22140 cm^{-1} and 23400 cm^{-1} , respectively (thin lines).

The polarity profile as sensed by the BADAN labels roughly follows a sigmoidal shaped curve (see data points in Figure 4A), as expected for the polarity profile of a bilayer [26]. Thus, the emission spectrum of a BADAN label attached to the WALP23 peptide strongly reflects the location, i.e. the depth of insertion in the bilayer. If the peptide is tilted with respect to the membrane normal, the location of any label in the bilayer will depend on the extent of tilting and the rotation of the helix. Tilt introduces a periodicity on the depth of insertion into the bilayer, and the phase of the periodicity is determined by the rotation of the helix. Closer inspection of the P_m data set for WALP23 peptides in di-C18:1PC suggests indeed such a periodicity (black line in Figure 4A), superimposed on a sigmoidal curve (grey line in Figure 4A, representing the expected profile for a non-tilted helix). From this, quantitative information can be retrieved about the orientation of the WALP23 peptide, similar to an approach that has been used to determine the tilt angle for M13 coat protein [5].

To obtain the tilt and rotation angles, the WALP23 peptide is modeled as an ideal α -helix. We also assume that the peptide tilt and rotation angle are not biased by the presence of the label. The validity of these assumptions will be discussed later. In addition, an estimation of the distance between label and the helix axis is needed to calculate the depth of insertion of the label in the bilayer. The label is connected to the peptide via a flexible linker chain, leading to a distance distribution. As a first approximation, we estimated the average orthogonal distance of the label to the helix axis to 7.5 Å. The fit procedures are further detailed and discussed in more detail later. In brief, choosing a larger distance will result in a smaller tilt angle, and vice versa.

Using the model described above, the insertion depths of labels attached to different positions can be calculated for any given combination of tilt angle τ and rotation angle ρ (for details see supplementary material). These depths of insertion can be translated to a polarity, i.e. wavenumber peak position using a polarity profile for the bilayer. In literature the sigmoidal function has been used for this [5,27]. Here, we used a Gaussian to describe the polarity profile of the bilayer because it requires one fit parameter less, and hence

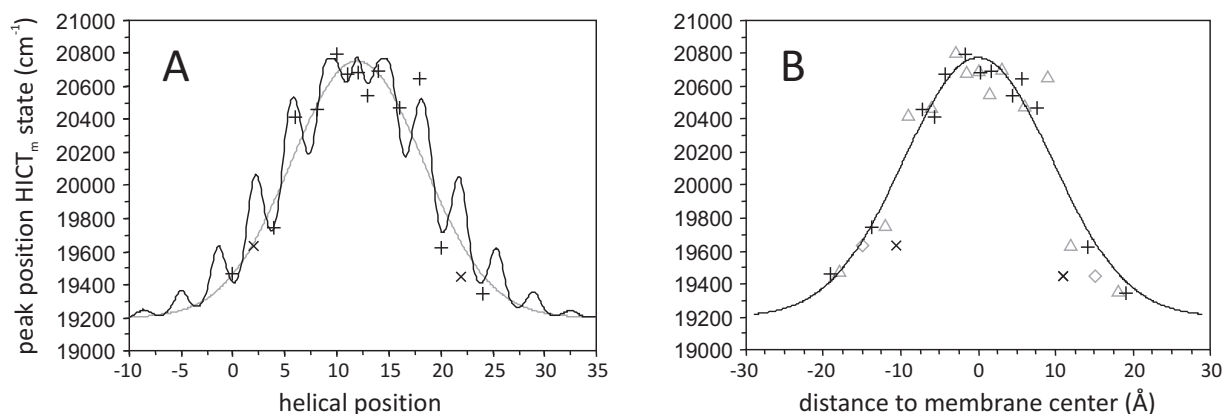


Figure 4: Fits to the peak positions of the HICT_m state of BADAN labeled WALP23 peptides in di-C18:1PC depending on the helical position of the label (A) and on the distance of the label to the center of the membrane (B). The best solution ($\tau = 23.6^\circ$, $\rho = 107^\circ$) is indicated with a black line in (A) and with black symbols in (B) (position of Trp by (x), other positions by (+)). For comparison, the result with an imposed tilt angle $\tau = 0^\circ$ is depicted in (A) with a grey line and in (B) with grey symbols (position of Trp by (\diamond), other positions by (Δ)).

allows more reliable comparison. However, very similar results were obtained when the results were fitted with a sigmoidal function (data not shown). The calculated polarities were fitted to the polarity data sets using least square minimization to retrieve the best solution for tilt and rotation angles.

Figure 4A (black line) shows the best fit (tilt angle $\tau = 23.6^\circ$ and a rotation angle $\rho = 107^\circ$) to the P_m data set of WALP23 peptides incorporated into bilayers of di-C18:1PC as function of the helical position, while Figure 4B shows the fit dependent on the insertion depths of labels. To obtain this fit, the data points for position 2 and 22 where interfacial tryptophans were replaced by cysteines labeled with BADAN were omitted (Figure 4, x), as these points showed large deviations compared to all other data points. We believe that this is a direct result of substituting tryptophans, because these may be a dominant factor in determining the global orientation of the peptide [28]. The contour plot of the SSD (sum of squared deviations) for fits with different combinations of tilt and rotation angles shown in Figure 5 illustrates the overall quality of the fit.

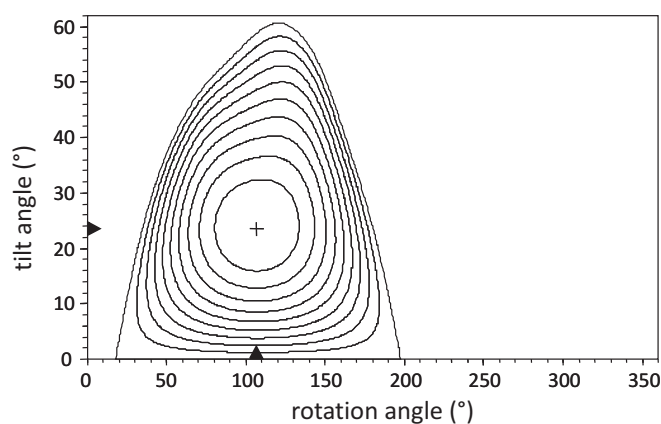


Figure 5: Contour plot of the SSD resulting from fits to the peak position of the HICT_m state of BADAN labeled WALP23 peptides in di-C18:1PC. The global minimum is marked by (+) and denotes the best solution. The isolines represent linearly spaced intervals based on the SSD of the best solution and the SSD of the solution with an imposed tilt angle $\tau = 0^\circ$, i.e. the helix oriented parallel to the membrane normal. The combinations of tilt and rotation angles not enclosed by the isolines give SSD's larger than the SSD obtained for $\tau = 0^\circ$.

Effects of hydrophobic mismatch

To investigate the effects of hydrophobic mismatch, fluorescence spectra were recorded for BADAN labeled WALP23 peptides inserted into bilayers of unsaturated phospholipids with varying thickness. The results of the spectral decomposition are depicted in Figure 6. A lower value of the wavenumber peak position P_m corresponds to a more polar environment, and vice versa. For the thinner bilayers, the local polarity sensed by the BADAN labels is higher in the bilayer interior, which can be explained by a lower water content in thicker hydrocarbon layers. However, for the thickest bilayer, di-C22:1PC, we observed a relatively high polarity for some labels positioned in the middle of the α -helix. This is possibly due to water molecules trapped in the center of the bilayer as a consequence of peptide-induced bilayer distortions under conditions of large negative mismatch.

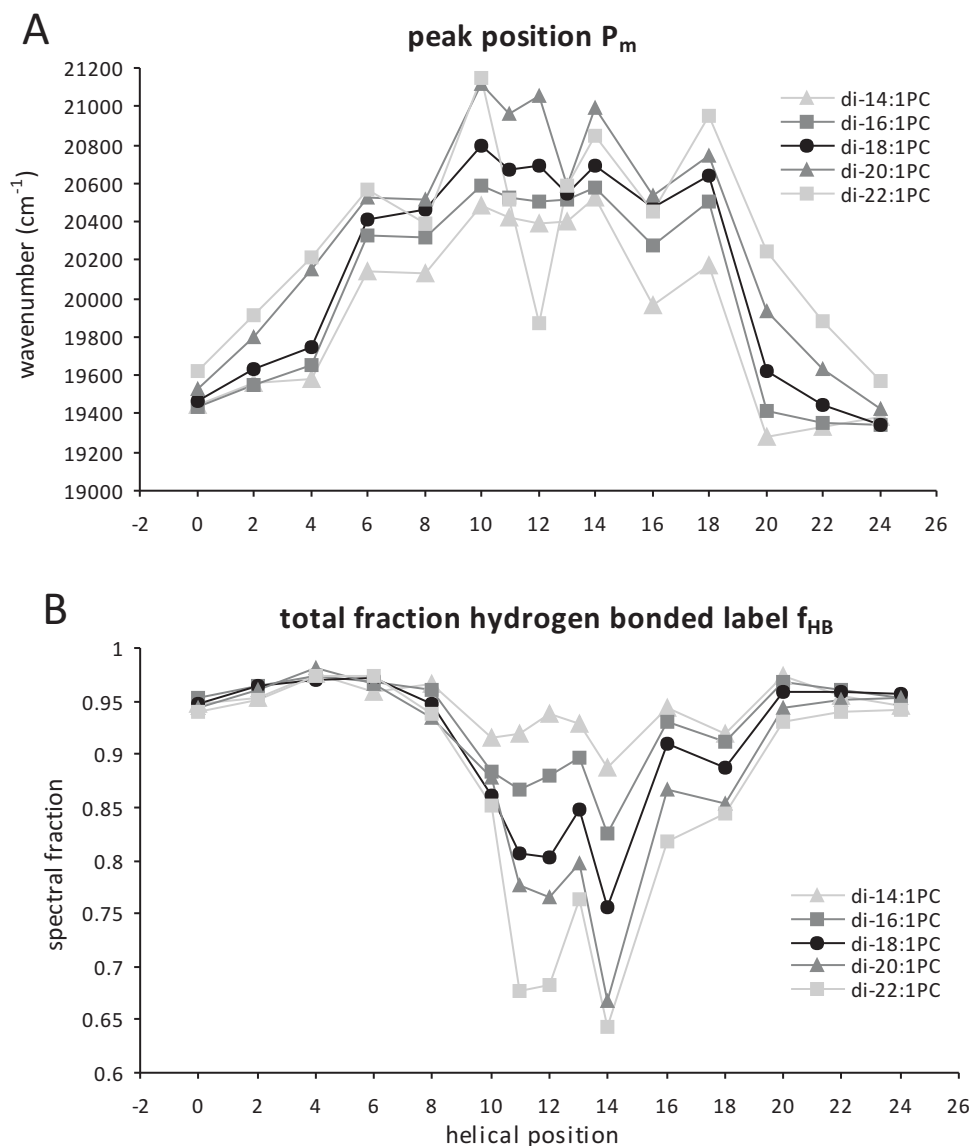


Figure 6: Wavenumber position P_m of the mobile hydrogen-bonded fraction of labels (A) and total fraction of hydrogen-bonded labels f_{HB} (B) obtained from spectral decomposition of emission spectra of BADAN labeled WALP23 peptides incorporated in bilayers of unsaturated phospholipids with different thickness. The lines are drawn to guide the eyes, as only a selection of positions in the WALP23 peptide was labeled with BADAN.

Similar trends were observed for the total hydrogen-bonded fraction of labels f_{HB} (Figure 6B). f_{HB} not only depends on the position of the label in the α -helix but also on the thickness of bilayer. For all bilayer thicknesses used, f_{HB} is largest for the label positions close to the ends of the α -helix and decreases for positions in the interior of the bilayer (see Figure 6B). The decrease of f_{HB} in the bilayer interior is more pronounced for thicker bilayers, indicating that less hydrogen bond donors are present in thicker bilayers. In principle, both data sets for f_{HB} and P_m can be used to retrieve the tilt angle, but P_m was found to be more sensitive to changes across the membrane.

The P_m profiles for the different bilayers were fitted to determine tilt and rotation angles for WALP23 peptides incorporated in bilayers of different thickness (results listed in Table 2). For the thinnest and the thickest bilayer (di-C14:1PC and di-C22:1PC) no reliable fits could be obtained which may be due to distortions in the local lipid environment or in the peptide structure under these extreme mismatch conditions. The tilt angles slightly decrease with increasing bilayer thickness, whereas the rotation angle remains about the same. This suggests a preferred orientation of the peptide, which is independent of the tilt. The adaptations of tilt angle are much less than expected for a complete adaptation to mismatch based on geometrical considerations. Indeed, if the peptide has a tilt angle of 23.6° in di-C18:1PC and it would completely adapt to the thickness of the thinner bilayer in di-C16:1PC by further tilting, one would expect a tilt angle of 34.9° in this latter bilayer. Similarly, if the tilt angle of 24.8° that we observed in di-C16:1PC would be a result of adaptation to mismatch, than one would expect zero tilt in di-C18:1PC.

The general error of the tilt angles is quite large since the precise distance between the label and the helix axis is not known (see supplementary material). Nevertheless, we believe the small changes in tilt angle to be significant, because the ‘relative values’ of the tilt angles are estimated to be accurate within less than a degree when comparing the values for bilayers with different thicknesses.

Table 2: Tilt and rotation angles estimated for WALP23 peptides in bilayers of different thickness.

Bilayer	Exp. τ ($^\circ$)	Exp. ρ ($^\circ$)	d_c^* (\AA)	Calc. τ ($^\circ$) [§]	
				Initial $\tau(\text{di-C18:1PC}) = 0^\circ$	Initial $\tau(\text{di-C18:1PC}) = 23.6^\circ$
di-C16:1PC	24.8	96	26.5	26.5	34.9
di-C18:1PC	23.6	107	29.6	0	23.6
di-C20:1PC	19.8	108	33.1	bilayer too thick	bilayer too thick

* Thickness of the bilayer hydrophobic core derived from [29].

§ For full compensation of hydrophobic mismatch.

Effect of cholesterol

Addition of cholesterol is known to increase the bilayer thickness due to its ordering effect on the surrounding lipid acyl chains. This effect is most pronounced for saturated lipids but also unsaturated lipids are slightly ordered and therefore thickened [29]. BADAN labeled peptides were incorporated into di-C18:1PC bilayers containing cholesterol concentrations of up to 40 mol%. The emission spectra showed only minor changes for increasing cholesterol concentrations (spectra not shown). It was found that the polarity sensed by the BADAN labels decreases slightly with increasing cholesterol concentration (Figure 7A), suggesting that the more ordered bilayer contains less water molecules in the hydrocarbon region. The changes in the local polarity and hydrogen-bonding capacity as sensed by the BADAN labels are much smaller for changes in cholesterol concentrations than for changes in bilayer thickness (compare Figure 6 and Figure 7).

The polarity data sets for the different cholesterol concentrations were fitted according to the procedure above and yielded reliable fits for all cholesterol concentrations used. As summarized in Table 3, the tilt angles show a slight decrease with increasing cholesterol concentration, whereas the rotation angle remains almost unchanged. The results suggest that the effect of cholesterol can be attributed to its effect on bilayer thickness and that the presence of cholesterol by itself does not affect the behavior of the peptide in the bilayer.

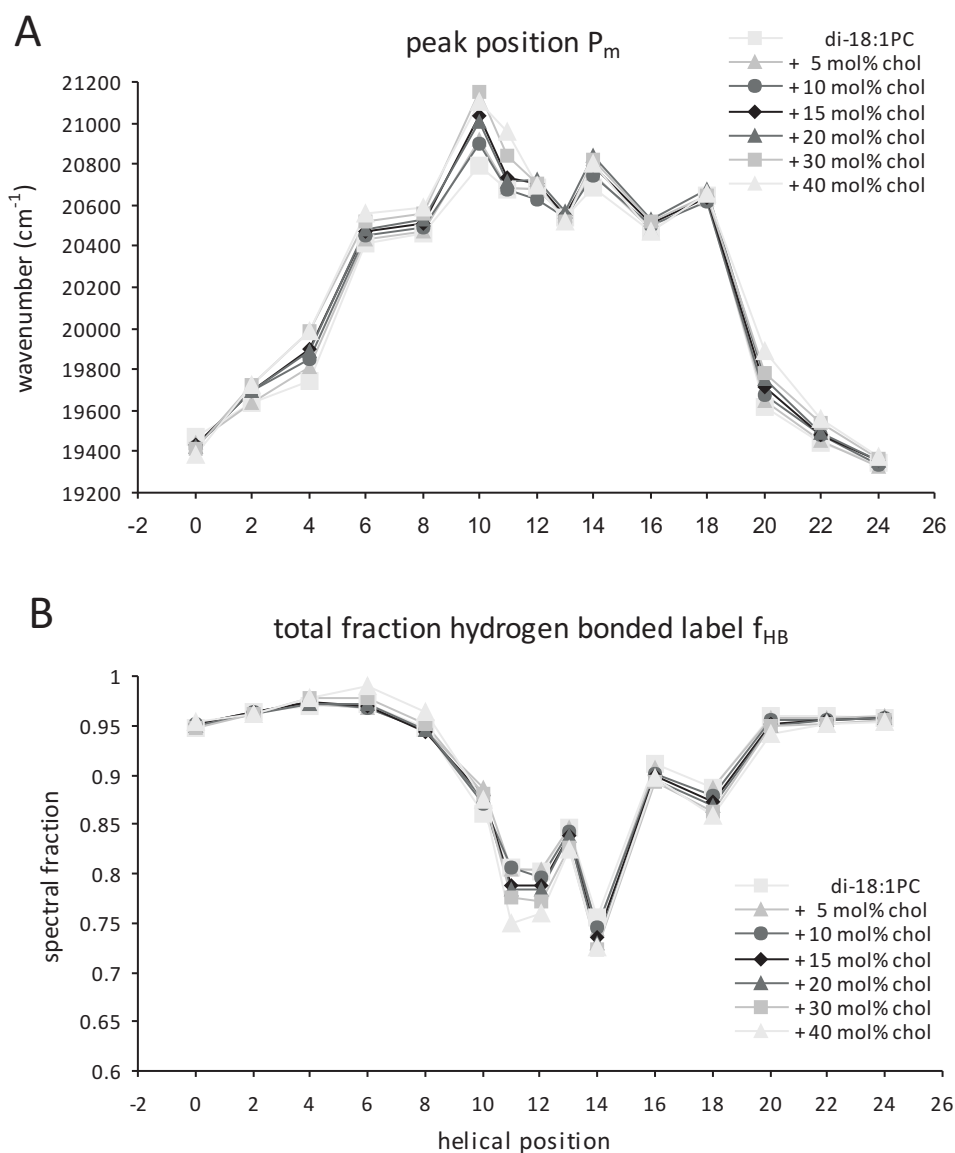


Figure 7: Wavenumber position P_m of the mobile hydrogen-bonded fraction of labels (A) and total fraction of hydrogen-bonded labels f_{HB} (B) obtained from spectral decomposition of emission spectra of BADAN labeled WALP23 peptides incorporated in di-C18:1PC containing different cholesterol concentrations.

Table 3: Tilt and rotation angles estimated for WALP23 peptides in di-C18:1PC bilayers containing different concentrations of cholesterol.

Cholesterol (mol%)	τ ($^\circ$)	ρ ($^\circ$)	d_c^* (\AA)
0	23.6	107	29.6
5	23.3	110	29.9
10	23.1	109	30.2
15	22.3	111	30.7
20	23.0	108	31.3
30	20.7	111	32.7
40	18.4	108	34.6

* Thickness of the bilayer hydrophobic core derived from [29].

Discussion

The main objective of the present study was to investigate the tilt and rotation angles of the transmembrane model peptide WALP23 in a lipid bilayer. A series of WALP peptides was labeled with the environment-sensitive fluorescent label BADAN in different positions and incorporated into bilayers with different thickness and cholesterol content. Spectral decomposition of the emission spectra yielded information regarding the polarity and hydrogen bonding capacities in the local vicinity of positions along the α -helix. These data profiles were used to retrieve the orientation of the transmembrane helix.

Analysis using the ideal α -helix model

The model used to fit the data profiles is based on a canonical α -helix. Circular dichroism and FTIR spectroscopy experiments showed that WALP peptides adopt a regular α -helical conformation in various types of bilayers [23,30]. In addition, MD simulation studies indicated that WALP23 in a matching bilayer of di-C14:0PC adopts a highly regular α -helical structure for the hydrophobic core region, and that unordered structures only occur for the residues at the N- and C-termini [16]. In agreement with this, fits excluding the data points from the potentially unordered residues at the N and C-termini of the helix yield small SSD values. Furthermore, leaving out any data point within the hydrophobic region yielded very similar values of tilt and rotation angles (not shown), supporting the notion that the BADAN label does not interfere with the regularity of the α -helix.

The quality of the fits to the polarity profiles was best for WALP23 peptides incorporated into bilayers of di-C18:1PC, representing the situation of hydrophobic matching. For WALP23 peptides in bilayers of di-C16:1PC and di-C20:1PC, where the lipids may have slightly adapted, the fit was still good as judged by the SSD. However, in bilayers of di-C14:1PC and di-C22:1PC the quality of the fits was poor, even yielding local minima. This observation can be explained by the possible responses of the peptide and lipids to these extreme mismatch situations [9]. In case of di-C14:1PC, the hydrophobic region of the bilayer is much too thin for a WALP23 peptide, which may lead to a distortion of the peptide backbone, as suggested for WALP23 peptide in di-C12:0PC [15,31]. Similarly, for WALP23 peptides in much too thick bilayers of di-C22:1PC the α -helix may become partly unwound. Such distortions would prohibit the use of the ideal α -helix model for data analysis. The analysis could be further complicated by local distortions of the bilayer as a consequence of mismatch. Finally, it is possible that only a limited amount of peptides may be incorporated into the bilayer at extreme mismatch situations [11,30]. Also this would hamper data analysis since it is not possible to separate spectral fractions originating from such a non-incorporated population from those of the transmembrane population. However, at the low peptide/lipid ratio's used in the present study, we do not expect this latter effect to be significant.

Advantages & disadvantages of using fluorescent labels

Our approach based on fluorescence spectroscopy complements the well-established NMR methods to investigate the orientation of membrane-associated peptides, and involves several advantages as well as disadvantages. The most important advantage here is that fluorescence spectroscopy operates on much shorter time scales than NMR spectroscopy, preventing any influence due to (global) peptide motions. In our analysis, the instantaneous distributions of tilt and rotation angles are accounted for by fitting the spectral components with Gaussians, yielding a value for the mean orientation. Another advantage is that fluorescence spectroscopy is a sensitive method and requires only low concentrations of fluorescent molecules. This allows performing experiments at low peptide/lipid ratios and under physiologically relevant hydration conditions. However, a major disadvantage of the technique is the need for fluorescent labels that could interfere with the orientation or conformation of the peptide.

In this study we used BADAN as environment-sensitive label. Like the more frequently used IAEDANS probe, it belongs to the family labels containing a fluorescent DAN moiety (see Figure 8 for structures). Whereas IAEDANS has a single emission state, BADAN has relatively complex fluorescence properties, which provide additional information but also complicate the interpretation of the results. Advantages of the BADAN label are that it is uncharged and has a shorter linker chain than IAEDANS, which can be expected to introduce less bias for the orientation of the label in the hydrophobic environment of the membrane. For studies on natural peptides containing charged residues that strongly influence the local polarity, the longer linker chain of IAEDANS can be advantageous because it allows probing the more distant membrane environment. Recently, the membrane topology of the M13 coat protein was successfully investigated using IAEDANS [5].

WALP23 has a very regular amino acid sequence of alternating leucines and alanines in the hydrophobic stretch and does not contain any charged residues. Thus, the influence of the amino acid sequence can be expected to be negligible, which allows using the BADAN label. For all labeled positions, we assumed a homogeneous spatial distribution of label orientations due to the flexible linker chain, although we cannot exclude the possibility that its average orientation may be biased by the lipid environment. Like for any other label, we also cannot exclude the possibility that the orientation of the peptide may be biased by the label. However, for WALP23 we expect that any influence of the label on the orientation of the peptide is small, as long as the label is positioned within the hydrophobic stretch flanked by the tryptophans. These tryptophans have been shown to strongly anchor to the membrane-water interface [32], thereby most likely determining preferred tilt and rotation angles, and dominating any effect of the label.

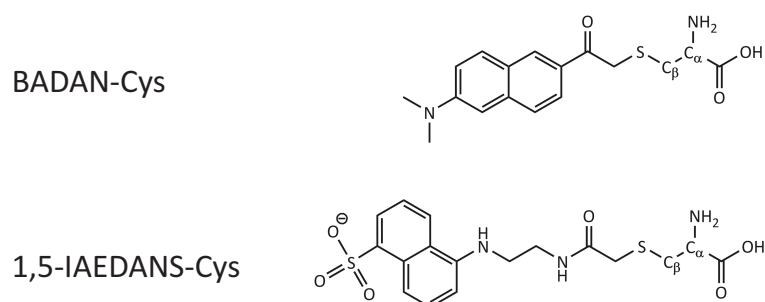


Figure 8: Structures of the fluorescent labels BADAN and 1,5-IAEDANS, both coupled to a cysteine.

Accuracy of the estimated tilt angle

To fit the polarity data sets, we used an estimated distance of 7.5 Å for the distance of the label to the axis of the α -helix. A similar study employing a related fluorescent label indicated a direct relationship between the tilt angles obtained and this distance [5]. The BADAN label is connected to the α -helix via a linker chain including five single bonds (see Figure 8), allowing for a large ensemble of spatial conformations. This leads to a distribution of distances for the label connected to the peptide helix. To get insight into the relationship between tilt angle and the distance of the label to the helix axis, we performed fits to the polarity data sets for a range of distances. Figure 9A shows that the tilt angles strongly depend on the distance of the label to the helix axis and have smaller values the larger the distance used for the fit.

Let us now consider some extreme conformational situations for a BADAN label attached to a cysteine in the peptide helix (inset in Figure 9A). The largest distance can be found for a label with a completely extended linker chain (ca. 13 Å), and the shortest distance is estimated by the limitations due to steric hindrance near the α -helix (ca. 4 Å), leading to tilt angles of 13° and 39° from the polarity data, respectively (see Figure 9A, dashed arrows). Thus, the tilt angle of 23.6° obtained using 7.5 Å has a large uncertainty, and it is evident that to determine the correct tilt angle, we need a good estimate of the distance of the label to the helix axis.

It is possible to somewhat narrow down the uncertainty by including fits to the total fraction of hydrogen-bonded labels. This reflects the hydrogen-bonding capacity in the local vicinity of the BADAN label, which, based on the results depicted in Figure 6B and 7B, can be expected to follow a more or less similar profile as the polarity. At first sight surprisingly, the fits to the hydrogen bonding data yielded much smaller tilt angles (see Figure 9B, grey line). However, this difference can be explained by the fact that the local polarity is sensed from the naphthalene unit while the carbonyl in the linker chain senses the hydrogen bonding capacity. Looking at the chemical structure of the BADAN label linked to a peptide, for most conformations in the spatial ensemble the hydrogen bond accepting carbonyl in the linker will be located much closer to the helix axis than the naphthalene unit (inset in Figure 9B). Based on the chemical structure of the label, these two moieties have a fixed distance of 4.5 Å to each other. Therefore, in the most extended conformation of the label the carbonyl can be located up to 4.5 Å closer to the helix axis, allowing the determination of a lower limit for the tilt angle.

Inspection of the curves in Figure 9B shows that when the tilt angle gets smaller, the distance between carbonyl and naphthalene unit increases. At a tilt angle of ca. 16°, the distances used to fit the different data sets have a difference of 4.5 Å (indicated in Figure 9B), which corresponds to the largest distance for the naphthalene unit to the helix axis of ca. 11.5 Å. Similarly, the upper limit for the tilt angle is confined by the geometry of the α -helix. The C_{α} -atoms have an average distance of 2.7 Å to the helix axis. This implies a distance of at least 3 Å for the carbonyl of the BADAN to the helix axis, which yields an upper limit of 33° for the tilt angle.

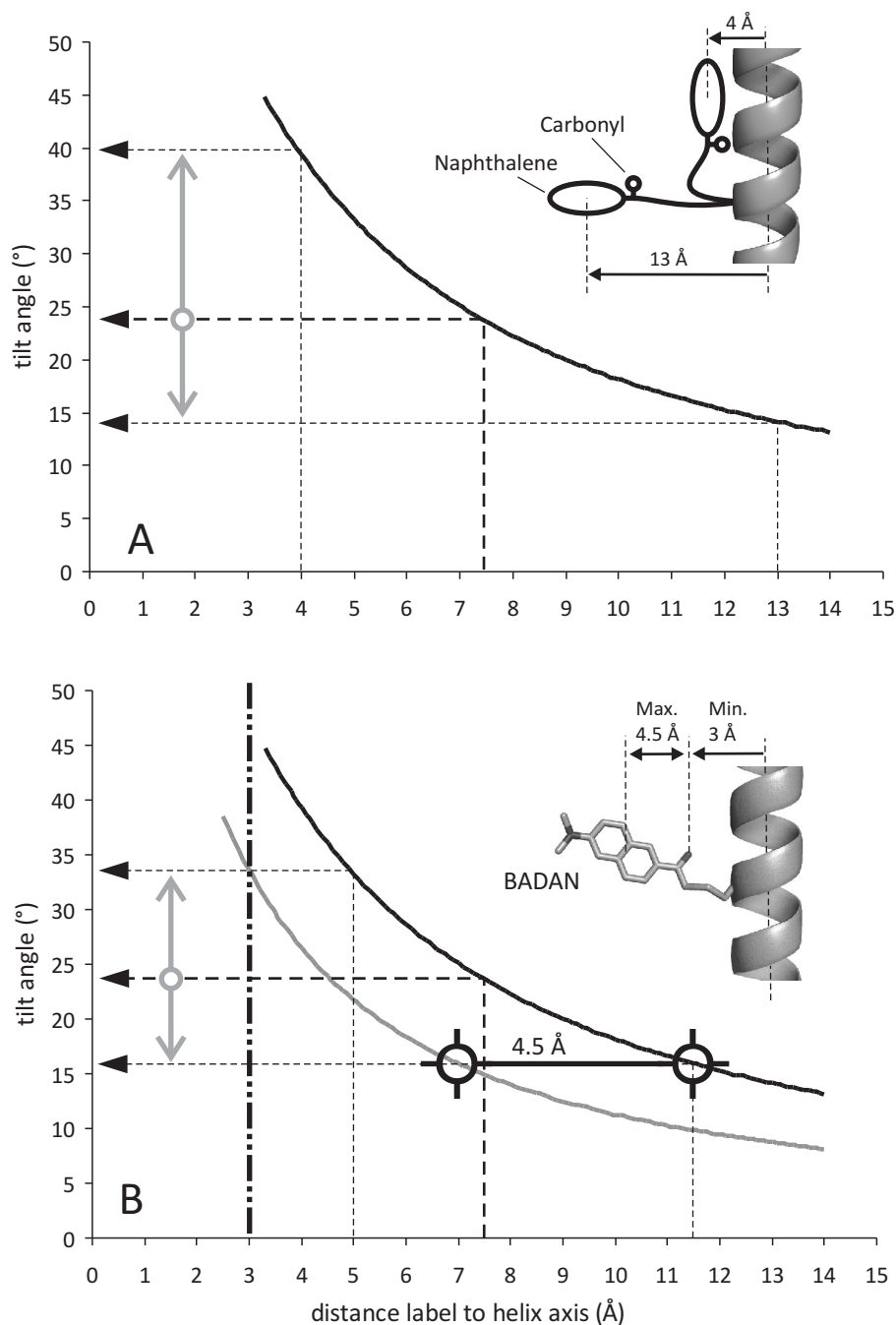


Figure 9: Dependence of the tilt angles obtained for WALP23 peptides in di-C18:1PC on the distance of the label to the helix axis. (A) Fit to the polarity data. The distance between naphthalene and helix axis can be minimal 4 Å and maximal 13 Å, corresponding to tilt angles of 13° and 39° (follow thin dashed lines). The grey arrows indicate the uncertainty in tilt angle. (B) Fit to the polarity data (solid black line) and to the total fraction of hydrogen-bonded labels (solid grey line). The possible distances can be further narrowed down by consideration of steric hindrances imposed from the peptide helix, which limits the carbonyl to minimal 3 Å distance, corresponding to a tilt angle of maximal 33° and of the geometry of the label, which allows the carbonyl and naphthalene maximal 4.5 Å apart, corresponding to a tilt angle of minimal 16° (for further explanations see text).

Thus, we were able to determine a reliable upper and lower limit for the tilt angle by simple consideration of the geometry of a regular α -helix and the chemical structure of the BADAN label. For a spatial ensemble, the mean value of the distance between naphthalene unit and the helix axis can be found between these extreme values and was fixed to 7.5 Å in our analysis. The values for all tilt angles obtained using this distance are estimated to be correct within 5°. If the actual average distance of the label to the helix axis is smaller, this will lead to larger tilt angles, and vice versa. However, in case that the actual distance differs from the one chosen, a systematic error is introduced in the tilt angles obtained for peptides inserted in different types of bilayers. Hence, the conclusions drawn with respect to effects of mismatch situations on the peptide orientation still remain valid. The range of possible values for the distances of the sensing locations of the BADAN label with respect to the helix axis could be further narrowed down by molecular modeling or MD simulations of a WALP23 peptide labeled with BADAN. Another possibility is the use of ALADAN, a fluorescent amino acid including a DAN moiety with an even shorter linker chain, requiring specialized synthesis work [33].

Membrane orientation of WALP peptides

In the present study, we found tilt angles of $24 \pm 5^\circ$ for WALP23 peptides in di-C18:1PC bilayers, which is much larger than the angles found in previous ^2H NMR studies [14,15]. In these studies, analysis of a set of quadrupolar splittings of WALP23 peptides including a single deuterium labeled alanine with the Geometric Analysis of Labeled Alanines method yielded relatively small tilt angles of 4.8 and 5.2° for WALP23 peptides incorporated into matching bilayers of di-C18:1PC and di-C14:0PC, respectively [14]. In di-C12:0PC, representing a positive mismatch situation, only a small increase to 8.1° was observed [14]. Similar small tilt angles were reported using a different solid-state NMR method, PISEMA, on related peptides [20].

Recently, it was suggested that the observation of relatively small tilt angles determined from ^2H NMR experiments may have been due to additional signal averaging, leading to an underestimation of the observed tilt angle [16,19,28]. The larger tilt angles obtained in the present study using fluorescence methods are in line with the larger tilt angles (33.5°) suggested from MD simulation studies [16,17]. If partial motional averaging would be caused mainly by large amplitude fluctuations around the helix axis, one would expect that the rotation angles calculated from the ^2H NMR experiments would not be significantly influenced by this motion. To compare the rotation angles obtained with the fluorescence experiments to those from previous ^2H NMR results, we need to correct the rotation angle for method inherent offsets. Due to the preferred orientation of the BADAN label along the C_α - C_β bond, the fitted rotation angle differs from the rotation angle referenced to the C_α -atom. We estimated the angle offset to 29° using a distance of 7.5 Å of the label to the helix axis and an angle of 43.3° between C_α orthogonally connected to the helix axis and the C_α - C_β bond. The corrected rotation angle of 136° agrees well with the rotation angle of 146° obtained from previous ^2H NMR experiments [14].

Our fluorescence experiments indicate that the response of the tilt angle of WALP23 to changing bilayer thickness is insufficient to compensate for effects of hydrophobic mismatch. This points towards additional mismatch responses of these peptides and agrees with the observation that under conditions of positive hydrophobic mismatch tryptophan-flanked peptides locally stretch the bilayer [32] and have an increased tendency to self-associate [34]. This is in contrast to results from solid-state NMR studies on a peptide derived from Vpu, for which a complete compensation of hydrophobic mismatch by tilting has been observed [6]. Apparently, there is an energetic cost for tilting of the WALP peptides. This may be due to the presence of the tryptophan residues and is in line with the suggestion that interfacially localized tryptophans may 'buffer' a transmembrane helix from changes in orientation due to changes in bilayer thickness [35]. Such an effect may also explain the absence of interfacial tryptophans in the mechanosensitive channel MscL. This channel protein undergoes large changes in tilt of α -helices upon opening, which was shown to be interfered with by the introduction of interfacial tryptophan residues [36].

To gain more information on the role of interfacial tryptophans for determining tilt and rotation angles, it would be interesting to study the KALP peptides, which are analogous to the WALP peptides, but which have a pair of lysines at both sides of the lipid-water interface instead of tryptophans. Indeed these peptides do not seem to have strong anchoring interactions, as no complementary adaptation of the lipids was observed upon introducing mismatch [32]. Previous ^2H NMR experiments suggested that WALP and KALP peptides both adopt small tilt angles [14]. However, as discussed above, for correct determination of tilt angles using ^2H NMR information about motional averaging is required, and this may not be the same for KALP peptides as for WALP peptides. By using the approach presented above one could in principle circumvent these problems, but unfortunately this method is most likely not suitable for determination of the tilt angles of KALP peptides. One reason is that the lack of strong interfacial anchoring may result in a larger influence of the label on the orientation of KALP than for WALP peptides. In addition, the charged lysine side chains in the KALP peptides may interfere with data analysis because they may have a large effect on the local polarity that is sensed by the BADAN label. Thus, further development of complementary methods, such as solid-state NMR techniques that take into account different types of possible motions or further development of MD approaches is necessary to fully understand the principles of how lipids affect the orientation of transmembrane helices.

Acknowledgements

This work was supported by a Marie Curie Early Stage Research Training Fellowship from the European Community's Sixth Framework Program for A.H. (Biomem-MEST-CT 2004-007931), and by a NIH grant for M. G. (1S10RR023065-01).

References

1. Albanesi D, Mansilla MC, and de Mendoza D (2004) The membrane fluidity sensor desk of *bacillus subtilis* controls the signal decay of its cognate response regulator. *J Bacteriol*, 186:2655–2663.
2. Booth PJ (2005) Sane in the membrane: designing systems to modulate membrane proteins. *Curr Opin Struct Biol*, 15:435–440.
3. Nyholm TKM, Özdirekcan S, and Killian JA (2007) How protein transmembrane segments sense the lipid environment. *Biochemistry*, 46(6):1457–1465.
4. Stopar D, Spruijt RB, and Hemminga MA (2006) Anchoring mechanisms of membrane-associated M13 major coat protein. *Chem Phys Lipids*, 141:83–93.
5. Koehorst RBM, Spruijt RB, Vergeldt FJ, and Hemminga MA (2004) Lipid bilayer topology of the transmembrane alpha-helix of M13 major coat protein and bilayer polarity profile by site-directed fluorescence spectroscopy. *Biophys J*, 87:1445–1455.
6. Park SH and Opella SJ (2005) Tilt angle of a trans-membrane helix is determined by hydrophobic mismatch. *J Mol Biol*, 350:310–318.
7. Ramamoorthy A, Kandasamy SK, Lee DK, Kidambi S, and Larson RG (2007) Structure, topology, and tilt of cell-signaling peptides containing nuclear localization sequences in membrane bilayers determined by solid-state NMR and molecular dynamics simulation studies. *Biochemistry*, 46:965–975.
8. Marsh D, Jost M, Peggion C, and Toniolo C (2007) Lipid chain-length dependence for incorporation of alamethicin in membranes: electron paramagnetic resonance studies on TOAC-spin labeled analogs. *Biophys J*, 92:4002–4011.
9. Killian JA and Nyholm TKM (2006) Peptides in lipid bilayers: the power of simple models. *Curr Opin Struct Biol*, 16:473–479.
10. Shahidullah K and London E (2008) Effect of lipid composition on the topography of membrane-associated hydrophobic helices: stabilization of transmembrane topography by anionic lipids. *J Mol Biol*, 379:704–718.
11. Mall S, Broadbridge R, Sharma RP, Lee AG, and East JM (2000) Effects of aromatic residues at the ends of transmembrane alpha-helices on helix interactions with lipid bilayers. *Biochemistry*, 39:2071–2078.
12. Yano Y, Takemoto T, Kobayashi S, Yasui H, Sakurai H, Ohashi W, Niwa M, Futaki S, Sugiura Y, and Matsuzaki K (2002) Topological stability and self-association of a completely hydrophobic model transmembrane helix in lipid bilayers. *Biochemistry*, 41:3073–3080.
13. Liu F, Lewis RNAH, Hodges RS, and McElhaney RN (2002) Effect of variations in the structure of a polyleucine-based alpha-helical transmembrane peptide on its interaction with phosphatidylcholine bilayers. *Biochemistry*, 41:9197–9207.
14. Özdirekcan S, Rijkers DTS, Liskamp RMJ, and Killian JA (2005) Influence of flanking residues on tilt and rotation angles of transmembrane peptides in lipid bilayers. A solid-state 2H NMR study. *Biochemistry*, 44:1004–1012.
15. Strandberg E, Özdirekcan S, Rijkers DTS, van der Wel PCA, Koeppe II RE, Liskamp RMJ, and Killian JA (2004) Tilt angles of transmembrane model peptides in oriented and non-oriented lipid bilayers as determined by 2H solid-state NMR. *Biophys J*, 86:3709–3721.
16. Özdirekcan S, Etchebest C, Killian JA, and Fuchs PFJ (2007) On the orientation of a designed transmembrane peptide: toward the right tilt angle? *J Am Chem Soc*, 129:15174–15181.
17. Esteban-Martin S and Salgado J (2007) Self-assembling of peptide/membrane complexes by atomistic molecular dynamics simulations. *Biophys J*, 92:903–912.
18. Kandasamy SK and Larson RG (2006) Molecular dynamics simulations of model trans-membrane peptides in lipid bilayers: a systematic investigation of hydrophobic mismatch. *Biophys J*, 90:2326–2343.
19. Strandberg E, Esteban-Martin S, Salgado J, and Ulrich AS (2009) Orientation and dynamics of peptides in membranes calculated from 2H-NMR data. *Biophys J*, 96:3223–3232.
20. Vostrikov VV, Grant CV, Daily AE, Opella SJ, and Koeppe II RE (2008) Comparison of “polarization inversion with spin exchange at magic angle” and “geometric analysis of labeled alanines” methods for transmembrane helix alignment. *J Am Chem Soc*, 130:12584–12585.

21. Esteban-Martin S, Strandberg E, Fuertes G, Ulrich AS, and Salgado J (2009) Influence of whole-body dynamics on 15N PISEMA NMR spectra of membrane proteins: a theoretical analysis. *Biophys J*, 96:3233–3241.
22. Weber G and Farris FJ (1979) Synthesis and spectral properties of a hydrophobic fluorescent probe: 6-propionyl-2-(dimethylamino)naphthalene. *Biochemistry*, 18:3075–3078.
23. de Planque MRR, Kruijtz JAW, Liskamp RMJ, Marsh D, Greathouse DV, Koeppe II RE, de Kruijff B, and Killian JA (1999) Different membrane anchoring positions of tryptophan and lysine in synthetic transmembrane alpha-helical peptides. *J Biol Chem*, 274(30):20839–20846.
24. Józefowicz M, Kozyra KA, Heldt JR, and Heldt J (2005) Effect of hydrogen bonding on the intramolecular charge transfer fluorescence of 6-dodecanoyl-2-dimethylaminonaphthalene. *Chem Phys*, 320:45–53.
25. Koehorst RBM, Spruijt RB, and Hemminga MA (2008) Site-directed fluorescence labeling of a membrane protein with BADAN: probing protein topology and local environment. *Biophys J*, 94:3945–3955.
26. White SH and Wimley WC (1998) Hydrophobic interactions of peptides with membrane interfaces. *Biochim Biophys Acta*, 1376:339–352.
27. Marsh D (2001) Polarity and permeation profiles in lipid membranes. *Proc Natl Acad Sci U S A*, 98:7777–7782.
28. Esteban-Martin S and Salgado J (2007) The dynamic orientation of membrane-bound peptides: bridging simulations and experiments. *Biophys J*, 93:4278–4288.
29. Kucerka N, Pencser J, Nieh MP, and Katsaras J (2007) Influence of cholesterol on the bilayer properties of monounsaturated phosphatidylcholine unilamellar vesicles. *Eur Phys J E*, 23:247–254.
30. de Planque MRR, Goormaghtigh E, Greathouse DV, Koeppe II RE, Kruijtz JAW, Liskamp RMJ, de Kruijff B, and Killian JA (2001) Sensitivity of single membrane-spanning alpha-helical peptides to hydrophobic mismatch with a lipid bilayer: effects on backbone structure, orientation, and extent of membrane incorporation. *Biochemistry*, 40:5000–5010.
31. Daily AE, Greathouse DV, van der Wel PCA, and Koeppe II RE (2008) Helical distortion in tryptophan- and lysine-anchored membrane-spanning alpha-helices as a function of hydrophobic mismatch: a solid-state deuterium NMR investigation using the geometric analysis of labeled alanines method. *Biophys J*, 94:480–491.
32. de Planque MRR, Bonev BB, Demmers JAA, Greathouse DV, Koeppe II RE, Separovic F, Watts A, and Killian JA (2003) Interfacial anchor properties of tryptophan residues in transmembrane peptides can dominate over hydrophobic matching effects in peptide-lipid interactions. *Biochemistry*, 42:5341–5348.
33. Cohen BE, McAnaney TB, Park ES, Jan YN, Boxer SG, and Jan LY (2002) Probing protein electrostatics with a synthetic fluorescent amino acid. *Science*, 296:1700–1703.
34. Sparr E, Ash WL, Nazarov PV, Rijkers DTS, Hemminga MA, Tieleman DP, and Killian JA (2005) Self-association of transmembrane alpha-helices in model membranes - importance of helix orientation and role of hydrophobic mismatch. *J Biol Chem*, 280:39324–39331.
35. Webb RJ, East JM, Sharma RP, and Lee AG (1998) Hydrophobic mismatch and the incorporation of peptides into lipid bilayers: a possible mechanism for retention in the Golgi. *Biochemistry*, 37:673–679.
36. Chiang CS, Shirinian L, and Sukharev S (2005) Capping transmembrane helices of MscL with aromatic residues changes channel response to membrane stretch. *Biochemistry*, 44:12589–12597.

Chapter 5

Influence of Hydrophobic Mismatch and Peptide Composition on the Diffusion of Transmembrane Model Peptides

Andrea Holt,[‡] Sivaramakrishnan Ramadurai,[†] Viktor V. Krasnikov,[†] Dirk T.S. Rijkers,[§]
Bert Poolman[†] and J. Antoinette Killian[‡]

[‡]Chemical Biology & Organic Chemistry, Bijvoet Center for Biomolecular Research, Utrecht University, Utrecht, The Netherlands; and [§]Medicinal Chemistry & Chemical Biology, Utrecht Institute of Pharmaceutical Sciences, Utrecht University, Utrecht, The Netherlands; and [†]Department of Biochemistry, Groningen Biomolecular Sciences and Biotechnology Institute & Zernike Institute for Advanced Materials, University of Groningen, The Netherlands.

Manuscript in preparation

Abstract

In this study, we investigated the effect of amino acid composition and hydrophobic length on the lateral diffusion of helical transmembrane segments in membranes using fluorescence correlation spectroscopy (FCS). For this purpose, we synthesized model peptides with varying length and composition of the hydrophobic stretch, and either tryptophans or lysines, respectively, as flanking residues. The peptides were labeled with the fluorescent label Alexa 488 and incorporated into phospholipid bilayers of different hydrophobic thickness and composition. Giant unilamellar vesicles (GUVs) were formed by Electroformation using a flow chamber covered with transparent, indium-tin oxide (ITO) coated microscope glasses. Measurements on the different peptides showed only minor effects of the peptide composition on the diffusion coefficients. We observed that the lateral diffusion was slowed down for peptides experiencing hydrophobic mismatch as compared to hydrophobic matching conditions. Furthermore, we found that peptides incorporated into a ternary lipid system exhibiting phase separation (i.e. unsaturated phospholipids/sphingolipids/cholesterol) remain in liquid-disordered membrane microdomains even under conditions of extreme positive hydrophobic mismatch. Based on the results obtained we propose a model explaining the diffusion behavior of transmembrane peptides in bilayers of different hydrophobic thickness.

Introduction

Biological membranes are composed of a large variety of lipid species and membrane proteins with diverse functions and structures. The diversity in molecular species also results in lateral heterogeneity. The presence of membrane microdomains exhibiting a lipid (and protein) composition different from that of the bulk membrane was suggested to have functional importance [1-3]. Due to their divergent lipid composition membrane microdomains can have (completely) different properties than the bulk membrane and can serve as assembling platforms and/or workspaces for some membrane proteins.

It was suggested that membrane microdomains favor specific protein-protein interactions by concentrating certain proteins in these microdomains while excluding others (reviewed in [4]). Membrane microdomains are believed to be highly dynamic structures that change in time and localization [5]. A prominent candidate for such membrane microdomains are liquid-ordered domains enriched in cholesterol, so-called lipid rafts. Both assembly and disassembly of such local domains requires diffusion of individual molecules entering or leaving the membrane microdomains [6,7].

The aim of the present work is to understand the basic principles of membrane diffusion behavior and the peptide-lipid interactions involved. Our approach was to use designed model peptides, which are incorporated into model membranes. This approach allows systematic variation of the peptide properties such as hydrophobic length, structure of the hydrophobic stretch and nature of flanking residues, as well as variation of the lipid properties such as bilayer thickness, sterol content and phase behavior. A recent study on the diffusion of transmembrane peptides with different hydrophobic lengths inserted into an artificial bilayer system reported a maximum for the diffusion coefficient for hydrophobic matching conditions [8]. A complicating factor in this case was that the bilayer system consisted of a cubic phase of surfactant, and that the hydrophobic thickness was modulated by addition of dodecane which incorporates in-between the layers of surfactant.

Here, we investigated the influence of hydrophobic mismatch on the diffusion of transmembrane peptides in bilayers of unsaturated phospholipids with different thickness, representing a biologically more relevant system. For our study, we used the well-characterized WALP and KALP peptides composed of a hydrophobic stretch of alternating leucines and alanines flanked at both ends by a pair of tryptophans and lysines, respectively, and a tryptophan-flanked peptide with a hydrophobic stretch of only leucines, called WLP peptide. Using fluorescence correlation spectroscopy, we determined the diffusion coefficients of Alexa 488 labeled peptides with hydrophobic stretches of 17 or 21 amino acids lengths, which were inserted into phospholipid bilayers. We found maximal diffusion for hydrophobic matching conditions, and hindered lateral mobility for positive and negative mismatch situations. Furthermore, our experiments show only minor effects of peptide composition on the lateral diffusion of the molecules in the membrane.

Hydrophobic mismatch could also play a role as driving force for partitioning of membrane proteins to the liquid-ordered, cholesterol-rich domains. We used the fluorescently labeled peptides to investigate the partitioning behavior of tryptophan-flanked peptides with different hydrophobic lengths incorporated into bilayers known to exhibit phase separation. Our results suggest that WALP peptides do not partition into cholesterol-rich, liquid-ordered domains even under extreme hydrophobic mismatch conditions.

Materials and Methods

Materials

1,2-dimyristoleoyl-*sn*-glycero-3-phosphocholine (di-C14:1PC), 1,2-dipalmitoleoyl-*sn*-glycero-3-phosphocholine (di-C16:1PC), 1,2-dioleoyl-*sn*-glycero-3-phosphocholine (di-C18:1PC), 1,2-dieicosenoyl-*sn*-glycero-3-phosphocholine (di-C20:1PC), 1,2-dierucoyl-*sn*-glycero-3-phosphocholine (di-C22:1PC), cholesterol, and sphingomyelin extracted from egg-yolk were purchased from Avanti Polar Lipids Inc. (Alabaster, AL, USA) as lyophilized powders and used without further purification. The peptides Cys-WALP23, Cys-WALP27, Cys-KALP23, Cys-KALP27, and Gly-Cys-WLP23 were synthesized using Fmoc/tBu peptide solid-phase synthesis as described elsewhere for related KALP peptides [9]. The peptide sequences are given in Table 1.

The fluorescent probes Alexa 488 (Alexa Fluor 488 C5-maleimide) and DiD-C18:0 (DiI_{C18}(5) solid1,1'-dioctadecyl-3,3,3',3'-tetramethylindodicarbocyanine, 4-chlorobenzene-sulfonate salt) were bought from Molecular Probes, Invitrogen Corp. (Carlsbad, CA, USA). All other chemicals used were of analytical grade; the water used was deionized and purified with a Milli-Q Gradient water purification system from Millipore Corp. (Billerica, MA, USA). ITO (indium-tin oxide) coated microscope cover slides (thickness #1, 0.13-0.16 mm; 15-30 ohms) were bought from SPI supplies / Structure Probes Inc. (West Chester, PA, USA).

Table 1: Amino acid sequences of peptides labeled with Alexa 488.

Peptide	Sequence
Cys-WALP23	Acetyl-C*GWWLALALALALALALALWVA-amide
Cys-WALP27	Acetyl-C*GWWLALALALALALALALALWVA-amide
Cys-KALP23	Acetyl-C*GKKLALALALALALALALWVA-amide
Cys-KALP27	Acetyl-C*GKKLALALALALALALALALWVA-amide
Gly-Cys-WLP23	Acetyl-GC*GWWLLLLLLLLLLLLLLLLLWVA-amide

* Cysteine labeled with Alexa 488 C₅-maleimide.

Methods

Peptide labeling with Alexa 488

To label the peptides with Alexa 488, ca. 0.5 mg of each peptide was weighed into an Eppendorf tube and dissolved in 200 μ l trifluoroethanol. Subsequently, 10 μ l H₂O was added. Then, the peptide solution was deoxygenized by bubbling with gaseous N₂ gas for several minutes. While keeping the peptide solution under N₂ atmosphere, 2 μ l of triethylamine and 1.25 (peptide) equivalents of Alexa 488 label, dissolved in methanol and purged with N₂, were added. After stirring the reaction mixture in the dark during 3 days at 4°C, the peptides were precipitated in 10 ml of cold methyl *tert*-butyl ether/*n*-hexane (1:1; stored at -20°C) to remove unbound Alexa 488 label. The precipitate was collected by centrifugation, the supernatant containing the unreacted Alexa 488 label was decanted and the precipitate was washed once again with methyl *tert*-butyl ether/*n*-hexane (1:1). The Alexa 488-labeling of all peptides was verified by MALDI/TOF mass spectrometry using α -cyano-4-hydroxycinnamic acid as matrix.

Sample preparation

Stock solutions of ca. 5 mM lipids in chloroform were prepared by weight and subsequently diluted to reach 0.5 mM concentration. The phospholipid stock solutions were characterized using the Rouser phosphorus assay [10]. Stock solutions of Alexa 488 labeled WALP23 peptides were prepared at a concentration of ca. 10 μ M in TFE. The peptide concentration was determined by absorption spectroscopy using an extinction coefficient of 22,400 M⁻¹cm⁻¹ at 280 nm for WALP23. Peptide-bound Alexa 488 absorption at 280 nm was corrected for by subtraction of the 280 nm absorbance of free label, which was scaled to equal intensity at the main absorbance band around 488 nm. From the peptide absorption spectra a typical labeling efficiency of 80-90% was estimated.

For each tested bilayer composition, samples containing ca. 200 nmol of lipids were prepared by mixing appropriate amounts of phospholipids, (and cholesterol and sphingomyelin, if present) and Alexa 488 labeled peptides at a peptide/lipid ratio of 1:100,000. Additionally, the fluorescent lipid dye DiD-C18:0, dissolved in methanol, was added at a ratio of 1:100,000 to the bulk lipids. After thorough mixing, the organic solvents were evaporated under a stream of N₂ gas and were further removed under vacuum overnight (ca. 1*10⁻² mbar). The sample was redissolved in 40 μ l of chloroform/methanol (1:1, v:v) and ca. 4 μ l of the mixture was applied in small droplets onto an ITO coated microscope slide stored on a warm plate of ca. 50°C. The solvents were allowed to evaporate for 5-10 minutes on the warm plate.

The home-made electroformation setup (see Figure 1) was assembled using a second ITO coated cover slip, and the electroformation chamber was filled with buffer (10 mM KP_i, pH 7.0) warmed to 50°C. Subsequently, an alternating current with frequency 10 Hz of 2 V (corresponding to ca. 400 V/m) was applied using a function generator (FG 100, Digimess). Electroformation was allowed for at least 2 hours, while keeping the chamber on the warm plate to prepare sufficient numbers of homogeneous and equally-sized GUVs without inclusions. For the FCS measurements, the electroformation setups were directly mounted on the sample stage of the laser scanning confocal microscope.

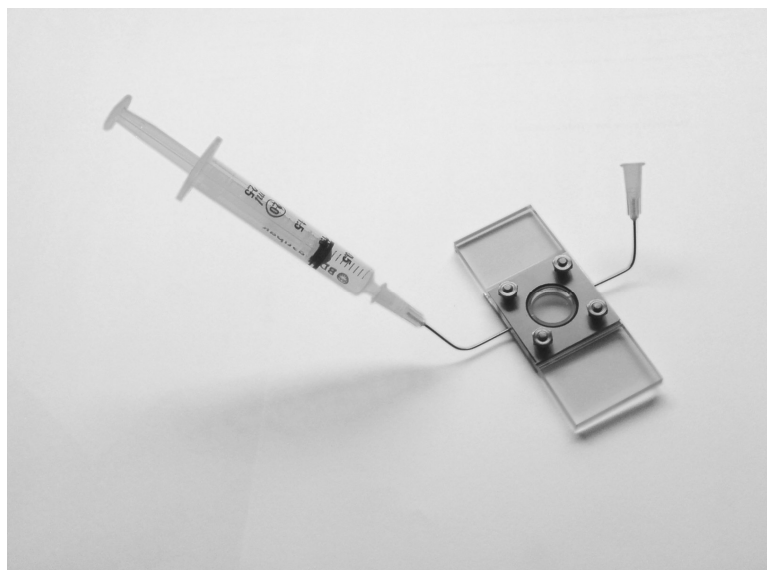


Figure 1: Home-made setup to produce GUVs using electroformation.

The use of the conducting microscope slides has the additional advantage of growing GUVs in reach of the short focus of the objective of the laser scanning microscope. This allowed measuring the fluorescence intensity fluctuations on GUVs that are still attached to the microscope slide at the bottom, minimizing movements within the long observation of 8 s for each measurement. Furthermore, we observed a noticeable reduction of the often occurring low-frequency oscillations on the membrane if more GUVs were growing in direct proximity, probably due to a backing effect of the surrounding GUVs to micro-flows in the sample chamber.

FCS measurements

FCS measurements were performed on a scanning confocal microscope equipped with two lasers of different wavelength. The laser scanning confocal microscope is based on an inverted microscope Axiovert S 100 TV (Zeiss, Jena, Germany) in combination with a galvanometer optical scanner (model 6860, Cambridge Technology, Watertown, MA) and a microscope objective nanofocusing device (P-721, Physik Instrumente, Karlsruhe/Palmbach, Germany). The laser beams were focused by a Zeiss C-Apochromat infinity-corrected 1.2 NA 63x water immersion objective. A blue laser (488 nm, argon ion laser, Spectra Physics) and a red laser (633 nm He-Ne laser, JDS Uniphase) were used to excite the Alexa 488 fluorophore and the lipid dye DiD-C18:0, respectively.

The fluorescence was collected through the same objective, separated from the excitation beams by a beam-pick off plate (BSP20-A1, Thor-Labs) and directed through emission filters (HQ 535/50 and HQ675/50, Chroma technology) and pinholes (diameter of 30 μm) onto two avalanche photodiodes (SPCM-AQR-14, EG&G). The fluorescence signal was digitized, and the autocorrelation curve was calculated using a multiple τ algorithm. The autocorrelation curves were fitted with a model for two-dimensional Brownian motion [11]. The setup was calibrated using an averaged diffusion coefficient $D = 380 \mu\text{m}^2/\text{s}$ for Alexa 488 and Alexa 633 in water [12]. The lateral radius w_{xy} of the detection volume depends on the wavelengths of the light and was estimated to be 195 nm for Alexa 488, and 264 nm for DiD-C18:0.

For the FCS measurements, the focal volume was usually positioned at the upper pole of a GUV. For this purpose, the samples were examined under the microscope for qualified GUVs using white light or a fluorescence lamp. A xy-scan was performed and the focus was centered to a suitable GUV, followed by a z-scan that was used to position the focus to the membrane. For each tested condition, the fluorescence intensity fluctuations of ca. 10 different GUVs were recorded for up to 10 periods each lasting 8 s. For each combination of peptide and bilayer, FCS measurements were performed on at least 10 selected GUVs with a diameter between 5-20 μm . The diffusion times obtained for Alexa 488 labeled peptides and the lipid marker DiD-C18:0 were translated into diffusion coefficients, using the estimated lateral radii of 195 nm and 264 nm for the detection volume, respectively.

Results

First, we investigated the influence of peptide composition on the diffusion of transmembrane model peptides mimicking transmembrane segments of membrane proteins. For this purpose, we synthesized transmembrane peptides with different length and sequence of the hydrophobic stretch, and with different flanking residues (for peptide sequences see Table 1). The flanking residues chosen were the aromatic residues tryptophan and the positively charged amino acid lysine, which were both found to have a preference for locations at the membrane-water interface [13]. A cysteine was added to the N-terminus of each peptide to attach an Alexa 488 label functionalized with a maleimide moiety. The Alexa 488 labeled peptides were inserted into bilayers made of unsaturated phospholipids with hydrocarbon chain lengths varying from 14 to 22 carbons.

The diffusion coefficients obtained for the different peptides in different types of bilayers are plotted against bilayer thickness in Figure 2. In general, the diffusion coefficients of the peptides decreased with increasing thickness of the bilayer. A similar relationship between the diffusion coefficients and the thickness of the bilayer has been observed for diffusion of lipid probes in pure lipid bilayers [14], which can be explained by an increased viscosity of thicker bilayers due to an increased number of van-der-Waals interactions between the lipid hydrocarbon chains. The larger viscosity of thicker bilayers would limit the diffusion of inserted transmembrane peptides.

Influence of the peptide composition

Closer inspection of the diffusion coefficients suggests some interesting trends. For example, for the peptides WALP23 and WALP27, we observed in all bilayers slower diffusion for the peptides with the longer hydrophobic stretch (see values summarized in Table 2). The same trend was observed for the KALP23 and the KALP27 peptide, but with a smaller difference in diffusion coefficients. These results may be explained by a larger number of van-der-Waals interactions between the longer hydrophobic stretch of the peptide and the hydrocarbon chains of the lipids, or other mismatch related effects.

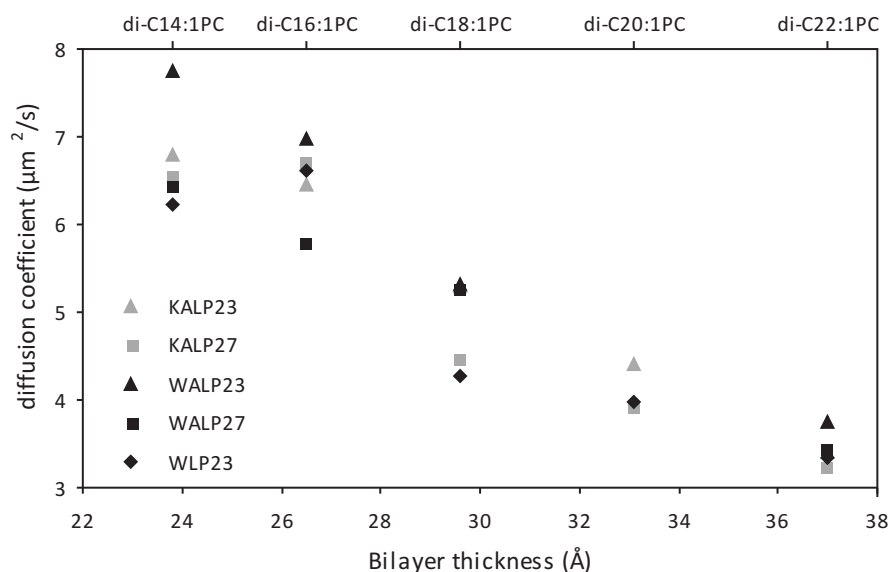


Figure 2: Diffusion coefficients of different Alexa 488 labeled model peptides inserted into bilayers of different thickness (the bilayer thickness was derived from [15]).

Another trend is observed when comparing peptides only differing in the flanking residues. Here, the diffusion coefficients were generally slightly larger for the tryptophan-flanked WALP than for the lysine-flanked KALP peptides, even though KALP peptides are effectively shorter than WALP peptides with the same length of the leucine-alanine stretch. Although tryptophans have large aromatic side chains, which have been suggested to anchor membrane proteins to the membrane interface, the bulky side chain apparently hinders the diffusion less than the long and flexible lysine side chain. One possible explanation may be that the cationic side chains of lysines slow down the diffusion by interacting with the (partial) charges of the zwitter-ionic phospholipids.

Finally, for all types of bilayers investigated, the diffusion coefficients of the WLP23 peptides with a hydrophobic stretch of leucines only were smaller than for the WALP23 peptides with alternating leucines and alanines. The hydrophobic radius of the peptides with leucines only is slightly larger than that of peptides with alternating leucines and alanines, and the peptides have a more regular outer contour. However, these small differences on their own are not expected to be reflected in a significant difference in the diffusion speed. The most likely explanation for the small differences observed in diffusion would be that the hydrophobicity of transmembrane segments plays a role in the strength and/or frequency of van-der-Waals type peptide-lipid interactions.

Table 2: Diffusion coefficients of different Alexa 488 labeled peptides in bilayers of different thickness.

Peptide incorporated in	WALP23 D (μm/s ²) [§]	WALP27 D (μm/s ²) [§]	KALP23 D (μm/s ²) [§]	KALP27 D (μm/s ²) [§]	WLP23 D (μm/s ²) [§]	thickness (Å) *
di-C14:1PC	7.76 ± 0.25	6.47 ± 0.24	6.80 ± 0.24	6.58 ± 0.18	6.22 ± 0.21	23.8
di-C16:1PC	6.97 ± 0.24	5.80 ± 0.10	6.46 ± 0.22	6.72 ± 0.11	6.61 ± 0.17	26.5
di-C18:1PC	5.33 ± 0.11	5.28 ± 0.20	5.30 ± 0.08	4.48 ± 0.11	4.26 ± 0.12	29.6
di-C20:1PC			4.40 ± 0.14	3.92 ± 0.20	3.97 ± 0.23	33.1
di-C22:1PC	3.75 ± 0.09	3.46 ± 0.09	3.40 ± 0.18	3.26 ± 0.04	3.35 ± 0.09	37.0

* Bilayer thickness derived from [15].

[§] Standard error of the mean is given; the standard deviation is ca. 10% of the absolute value.

Influence of cholesterol concentration

Cholesterol is known to thicken lipid bilayers due to its ordering effect on the lipid acyl chains. This effect is most pronounced for saturated lipids but was also observed for unsaturated lipids [15]. The ordering effect of cholesterol also renders the bilayers more rigid, which can be expected to slow down the diffusion of peptides. Here, we investigated the influence of cholesterol concentrations up to 40 mol%, added to bilayers of di-C18:1PC, on the diffusion of WALP23 and the fluorescent lipid dye DiD-C18:0. DiD-C18:0 reports on the diffusion of bulk lipids. Inspection of the diffusion coefficients plotted in Figure 3 shows that the diffusion coefficients of both the peptide and lipid analogue decrease with increasing cholesterol concentrations (data summarized in Table 3).

In the presence of cholesterol GUV formation was generally less efficient, which was compensated for by prolonged electroformation. Compared to the GUVs obtained from pure phospholipids, the GUVs containing cholesterol were smaller in size and less homogeneous in terms of fluorescence, i.e. varied in brightness. The latter observation could reflect differences in the lipid composition for different GUVs, which would also explain the larger standard deviations in the diffusion coefficients when cholesterol was present (see Figure 3).

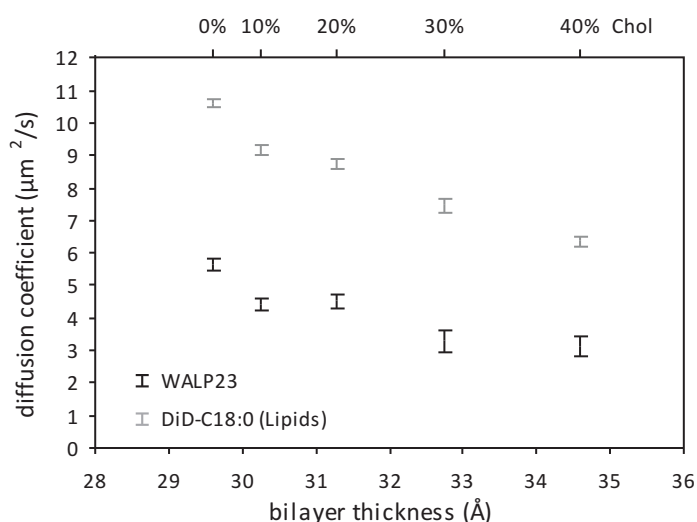


Figure 3: Diffusion coefficients of DiD-C18:0 (grey symbols) and Alexa 488 labeled WALP23 peptides (black symbols) inserted into bilayers of di-C18:1PC and varying concentrations of cholesterol (the bilayer thickness was derived from [15]). The error bars give the standard error of the mean (SEM).

Table 3: Diffusion coefficients of Alexa 488 labeled WALP23 peptides and the fluorescent lipid marker DiD, incorporated into bilayers of di-C18:1PC that contain varying amounts of cholesterol.

Peptide/Lipid marker incorporated in di-C18:1PC + cholesterol (mol%)	WALP23 D (μm/s ²) [§]	DiD D (μm/s ²) [§]	thickness (Å) [*]
0	5.65 ± 0.12	10.61 ± 0.16	29.6
10	4.44 ± 0.14	9.16 ± 0.18	30.2
20	4.52 ± 0.18	8.74 ± 0.22	31.3
30	3.29 ± 0.22	7.46 ± 0.32	32.7
40	3.13 ± 0.17	6.35 ± 0.29	34.6

^{*} Bilayer thickness derived from [15].

[§] Standard error of the mean (SEM) is given; the standard deviation is ca. 10% of the absolute value.

Preliminary experiments for KALP23 peptides inserted into bilayers containing 10 mol% of cholesterol indicated a much lower influence of cholesterol on the diffusion of KALP23 peptides compared to WALP23 peptides (results not listed/shown). However, the number of peptides in the detection volume was found to be very low compared to samples containing WALP23 peptides prepared with the same peptide/lipid ratio. Closer inspection using a fluorescence lamp showed bright irregular structures for samples containing KALP23 peptides, suggesting that a large fraction of the labeled peptide was not incorporated in the membrane in the presence of cholesterol. The reason for this is not understood.

Peptide partitioning in bilayers exhibiting liquid-ordered & liquid-disordered phases

The binary lipid systems composed of unsaturated phospholipids and cholesterol used above do not exhibit phase separation on the macroscopic scales accessible with light microscopy. If, on the other hand, saturated (long chain) lipids or sphingomyelin are also added, macroscopic phase separation into a liquid-ordered, cholesterol-rich phase and a liquid-disordered phase can be observed. From experiments with cell membranes exhibiting membrane microdomains, it is known that some membrane proteins can be found preferably in the liquid-ordered domains, whereas others are solely found in the liquid-disordered domains. Frequently, a ternary lipid system composed of equal molar fractions of cholesterol, unsaturated phospholipids and sphingomyelin is used to model lipid rafts [6,16,17]. Due to the ordering effect of cholesterol, the liquid-ordered phase has an increased thickness compared to the liquid-disordered phase. To investigate whether tryptophan-flanked peptides have any preference for liquid-ordered or liquid-disordered phases, we incorporated WALP peptides into GUVs composed of a ternary lipid system.

First, we incorporated Alexa 488 labeled WALP23 peptides into GUVs composed of equal molar fractions of cholesterol, di-C18:1PC and egg-sphingomyelin. The fluorescent lipid dye, DiD-C18:0, was also incorporated into the bilayers. This dye has a very similar structure to DiI-C18:0, which was found to partition into the liquid-disordered phases at this lipid composition [18-20]. The confocal image showing the fluorescence of DiD-C18:0 (Figure 4, right panel) confirms the phase separation into liquid-ordered and liquid-disordered domains. The fluorescence of the Alexa 488 labeled WALP23 peptides (Figure 4, left panel) showed a very similar distribution in the GUVs, indicating that the WALP23 peptides partition into the liquid-disordered domains. The liquid-disordered domains contain mainly di-C18:1PC, which matches the hydrophobic thickness of the hydrophobic stretch of WALP23 peptides.

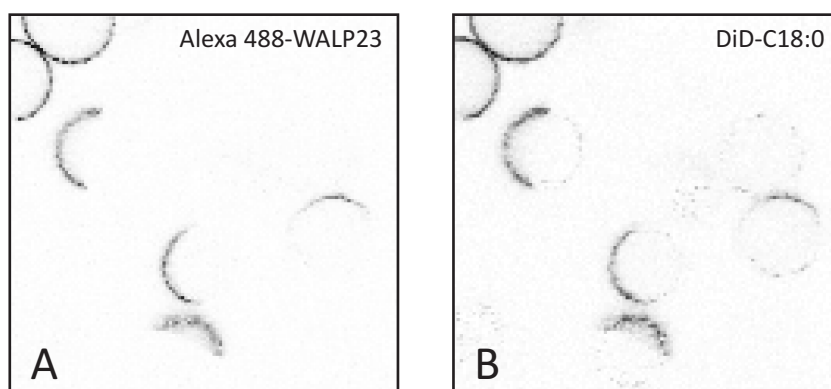


Figure 4: Confocal images of GUVs composed of di-C18:1PC/cholesterol/egg-sphingomyelin (1:1:1) containing Alexa 488 labeled WALP23. (A) Fluorescence from Alexa 488 labeled peptides and (B) from DiD-C18:0.

In the next step, we investigated whether extreme hydrophobic mismatch could drive the WALP peptides into a better matching liquid-ordered phase. For this purpose, we replaced di-C18:1PC by di-C14:1PC, yielding a thinner liquid-disordered phase with the hydrophobic thickness decreased by ca. 6 Å. To maximize the hydrophobic mismatch, we incorporated the longer WALP27 peptide of which the hydrophobic length is 6 Å longer than that of a WALP23 peptide when assuming a canonical α -helical structure. For this combination, the peptide may partition into the liquid-ordered phase to relieve the large hydrophobic mismatch. The liquid-ordered phase composed of mainly cholesterol and egg-sphingomyelin (about 84% of C16:0-sphingomyelin) matches the hydrophobic length of WALP27 much better than the thinner liquid-disordered phase containing mainly di-C14:1PC. The confocal images shown in Figure 5 reveal that Alexa 488 labeled peptides and DiD-C18:0 still colocalize in the membrane, suggesting that, in spite of the extreme hydrophobic mismatch, WALP27 peptides still prefer the liquid-disordered phase over the cholesterol-rich, liquid-ordered phase.

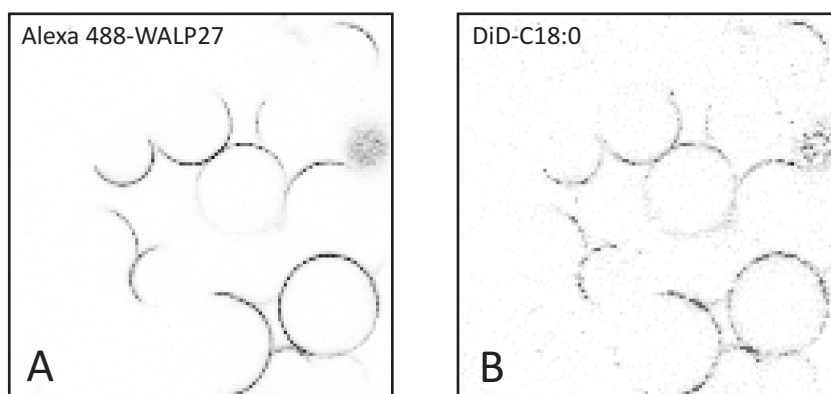


Figure 5: Confocal images of GUVs composed of di-C14:1PC/cholesterol/egg-sphingomyelin (1:1:1) containing Alexa 488 labeled WALP27. (A) Fluorescence from Alexa 488 labeled peptides and (B) from DiD-C18:0.

Discussion

The aim of this study was to elucidate whether differences in the structure of transmembrane peptides influence the lateral diffusion of the molecules in lipid bilayers. For this purpose, we synthesized different transmembrane model peptides with variations in the hydrophobic length, the composition of the hydrophobic stretch and the flanking residues. Fluorescence correlation spectroscopy was used to investigate the effect of peptide compositions on the diffusion of the Alexa 488 labeled peptides, which were incorporated in bilayers of unsaturated phospholipids with different acyl chain lengths. In addition, we investigated the effect of cholesterol addition on the diffusion of transmembrane model peptides, and the partitioning behavior of tryptophan-flanked peptides in a bilayer system exhibiting phase separation.

As anticipated, the lateral diffusion was slowed down in thicker bilayers due to stronger van-der-Waals interactions between the lipid acyl chains, similar to what has been observed by Kahya *et al.* [14]. Furthermore, we found that an increase in hydrophobic length of the transmembrane peptides led to a small but significant slowing down of the diffusion, especially in thin bilayers. Before trying to explain these data, let us first consider which factors determine the diffusion speed. According to the widely accepted hydrodynamic

model of Saffman & Delbrück, the diffusion coefficients of transmembrane proteins or peptides moving along the bilayer plane decrease with increasing hydrodynamic radius of the diffusing object and also with increasing bilayer thickness [21]. The exact relationship between hydrodynamic radius and the diffusion coefficients is still a matter of debate [8]. Our recent work (published elsewhere) indicates that the diffusion coefficients of integral membrane proteins scale with $\ln(1/R)$ rather than with $1/R$ [22], which means that diffusion is only weakly dependent on (an increase in) hydrodynamic radius.

Effects of hydrophobic mismatch

Several adaptations can occur as response to increasing hydrophobic mismatch including tilting (in positive mismatch situations), peptide aggregation, and bilayer distortion (illustrated in Figure 6). Most likely, all these possible adaptation will have a more or less pronounced effect on the hydrodynamic radius of the transmembrane peptide, and hence on the diffusion coefficient of the peptide. It can be expected that transmembrane peptides can tolerate a certain extent of hydrophobic mismatch, and that any adaptations to a small extent of hydrophobic mismatch will have only small effects on the diffusion coefficient. With increasing hydrophobic mismatch such effects will progressively become larger since more extensive adaptations will be required to still accommodate the peptide in the membrane. In the following, several possible adaptations to hydrophobic mismatch and their potential consequences on hydrodynamic radius are discussed in more detail.

First, the lipids surrounding the peptide may adapt. Up to a certain extent, the dynamic character of bilayers in combination with the inherent flexibility of the lipid acyl chain allows local thickening or thinning of the bilayer in vicinity of the peptide (Figure 6B and 6D). This most likely leads to a small increase of the effective hydrodynamic radius of the peptide.

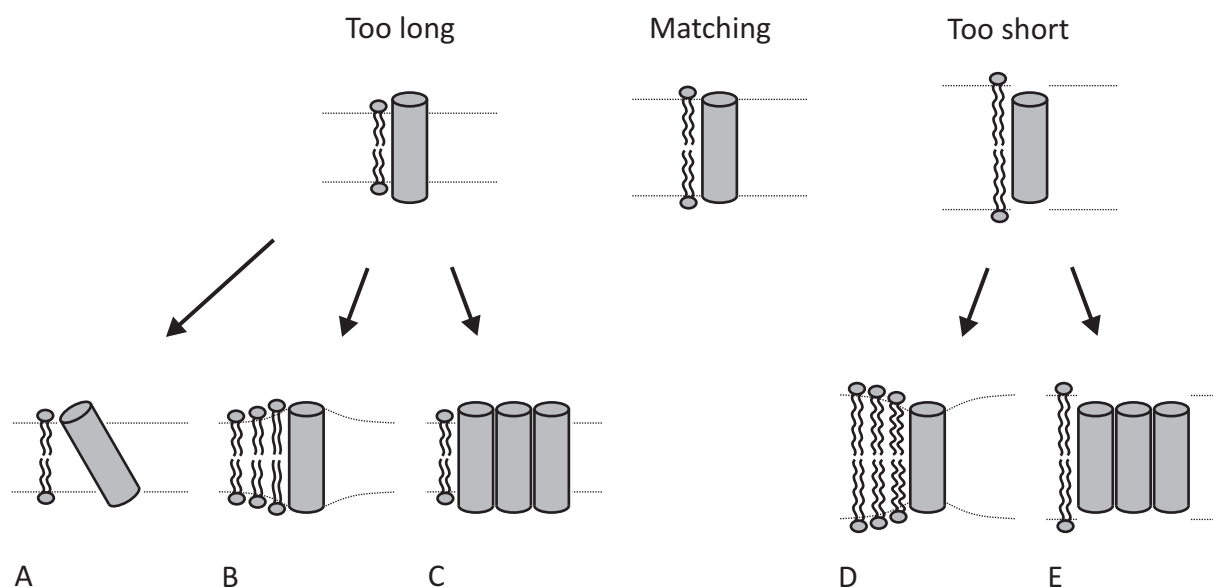


Figure 6: Possible adaptations to hydrophobic mismatch in case of too short transmembrane peptides: (A) peptide tilting, (B) bilayer distortion, and/or (C) peptide aggregation; in case of too long transmembrane peptides: (D) bilayer distortion, and/or (E) peptide aggregation.

Under conditions of large hydrophobic mismatch also more distant lipid layers around the peptide may need to adapt to still accommodate the peptide, which again would increase the effective hydrodynamic radius. Second, transmembrane peptides may tilt (more) when experiencing positive hydrophobic mismatch (Figure 6A), with the same effect on the hydrodynamic radius. For WALP peptides inserted into bilayers of different thickness, only small changes in the tilt angle have been observed [23,24]. Finally, the peptides may dimerize or even oligomerize to relieve the hydrophobic mismatch (Figure 6C and 6E). In matching or nearly matching situations WALP peptides were found to have no tendency to self-associate and can thus be expected to exist as monomers [25].

Therefore, especially at the low peptide/lipid ratios used in this study the hydrodynamic radius can be assumed to stay approximately the same for matching and nearly matching situations, and hence the diffusion coefficients of the peptides would be mainly determined by the properties of the membrane, i.e. would decrease monotonously as a function of bilayer thickness (solid line in Figure 7). However, if the hydrophobic mismatch would become too large, transmembrane peptides could aggregate even at low peptide/lipid ratios. The larger hydrodynamic radius of the peptide clusters would consequently lead to a slower diffusion both in case of large positive and negative hydrophobic mismatch (dashed lines in Figure 7). Such an effect has been observed in a study using selectively aggregated peptides of different cluster size [26].

The experimentally determined diffusion coefficients (depicted in Figure 2) would be consistent with such a diffusion behavior as illustrated in Figure 8. For example, for WLP23 the diffusion coefficients roughly follow a reciprocal relationship with membrane thickness ($1/h$) in di-C16:1PC, di-C18:1PC and di-C20:1PC, whereas the diffusion coefficients observed for di-C14:1PC and di-C22:1PC show (much) smaller values than expected from extrapolation of the matching and nearly matching situations (see Figure 8A). For the other peptides investigated a similar trend in the diffusion behavior for different bilayer thicknesses can be observed.

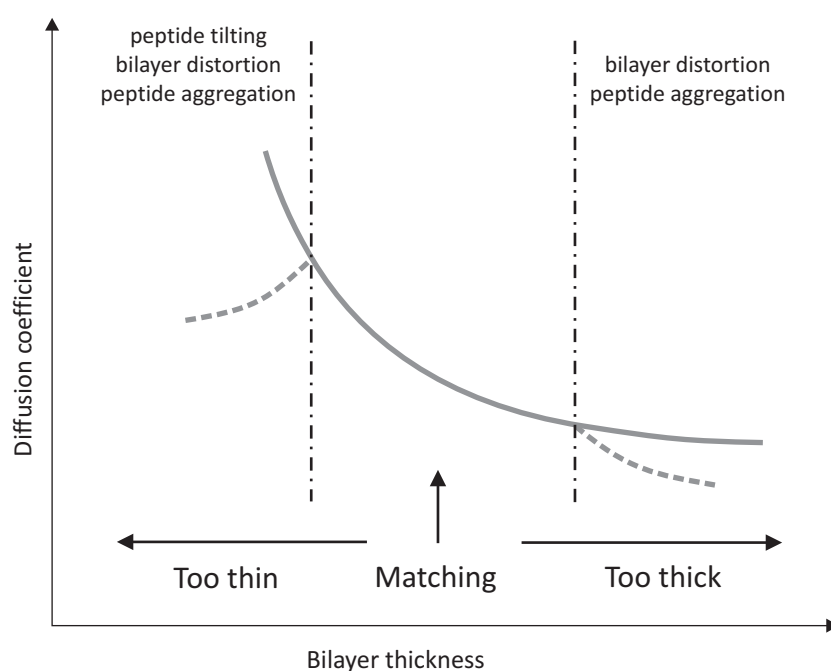


Figure 7: Schematic drawing of the trends in diffusion coefficient of a transmembrane peptide as a function of hydrophobic mismatch.

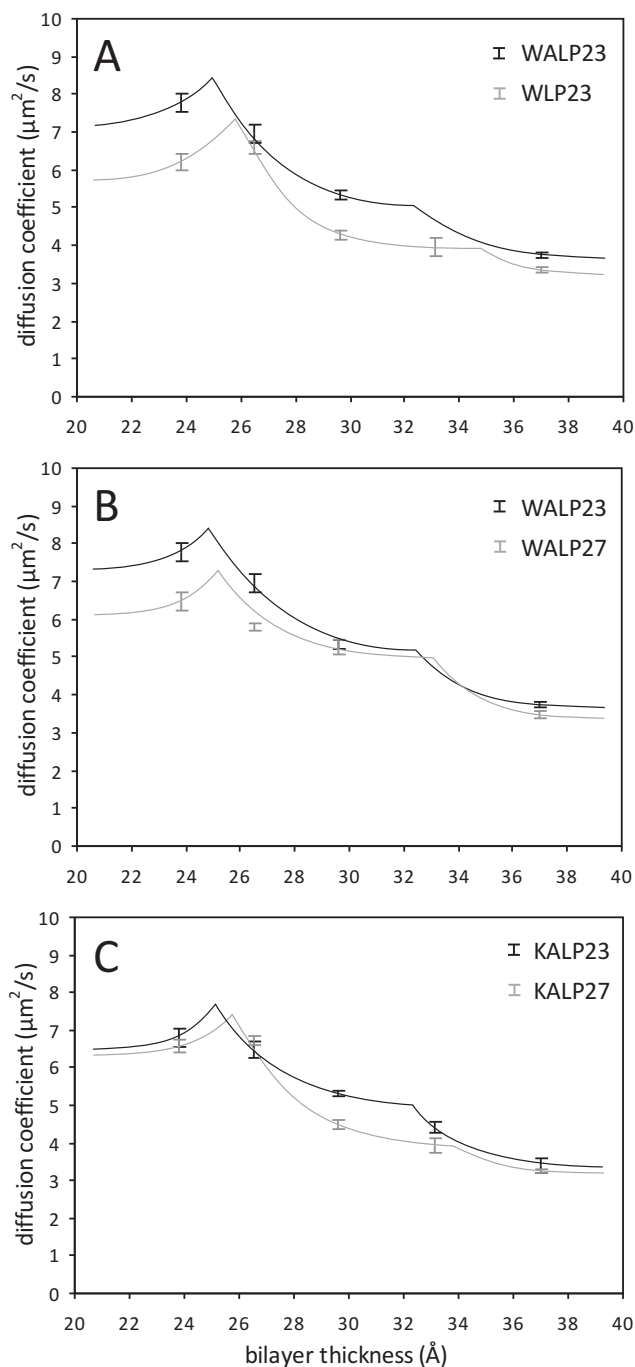


Figure 8: Diffusion coefficients of Alexa 488 labeled peptides including a hydrophobic stretch of different lengths either flanked by tryptophans (A, B) or lysines (C). The hydrophobic stretch is composed of either alternating leucines and alanines (B,C), or only leucines (A, WLP23), which were inserted into bilayers of different thickness of the hydrophobic core region (the bilayer thickness was derived from [15]). The lines are hypothetical curves drawn by eye to the experimentally determined diffusion coefficients.

A recent study on the diffusion of transmembrane peptides with different hydrophobic lengths inserted into an artificial bilayer system with tunable thickness reported a maximal diffusion coefficient for hydrophobic matching conditions [8]. In agreement with this study, our data also shows a maximum in the diffusion coefficients. However, we believe that the maximum in the diffusion coefficients is not related to hydrophobic matching, but to the transition from small positive mismatch that still can be tolerated to larger positive mismatch where additional compensation mechanisms start to dominate. This transition may also be accompanied with formation of peptide dimers (or even oligomers) and/or other effects like bilayer distortion and peptide tilting. The transition from small negative mismatch to large negative hydrophobic mismatch is not covered in the study by Gambin *et al.* [8].

In fact, the artificial bilayer system used in this latter study may bear some problems when monitoring consequences of hydrophobic mismatch. First, the surfactants used form cubic phases, also known as “sponge phase”, with unknown effects on the diffusion coefficients of the transmembrane peptides. Second, to adjust the hydrophobic thickness dodecane was added, which is expected to incorporate in-between the leaflets of surfactant. It is likely that the dodecane will be distributed unevenly under negative and positive mismatch conditions. In case that the artificial bilayer system swollen with dodecane is too thick, the peptides may promote a cushion effect, where the transmembrane peptides constitute interconnected buttons on both sides of the surfactant bilayer. Such behavior would hamper the interpretation of results obtained for negative hydrophobic mismatch.

Effects of cholesterol

Some types of eukaryotic membranes contain major amounts of cholesterol, which is known to play a special role in biological membranes. Cholesterol was shown to be a major constituent in lipid rafts, and thickens the membrane due to its ordering effect on lipid acyl chains. Earlier studies on the lateral diffusion in binary lipid systems showed that the lateral diffusion of the lipids is almost linearly decreasing with increasing cholesterol concentration [14]. In agreement with this study, we observed that the diffusion coefficients of WALP23 peptides in cholesterol containing bilayers decrease with increasing cholesterol concentration. The diffusion coefficients of the peptides are even smaller in the presence of cholesterol than would be expected from the increase in bilayer thickness upon incorporation of cholesterol (Figure 9). Thus, lateral diffusion in membranes is not only influenced by the hydrophobic thickness of the bilayer but also by the presence of cholesterol. Cholesterol is known to order surrounding lipid acyl chains, which leads to a more condensed and thicker bilayer. As a consequence, the inherent flexibility of the lipid acyl chains is reduced and it may be more difficult to accommodate peptides in cholesterol-rich (regions of) membranes.

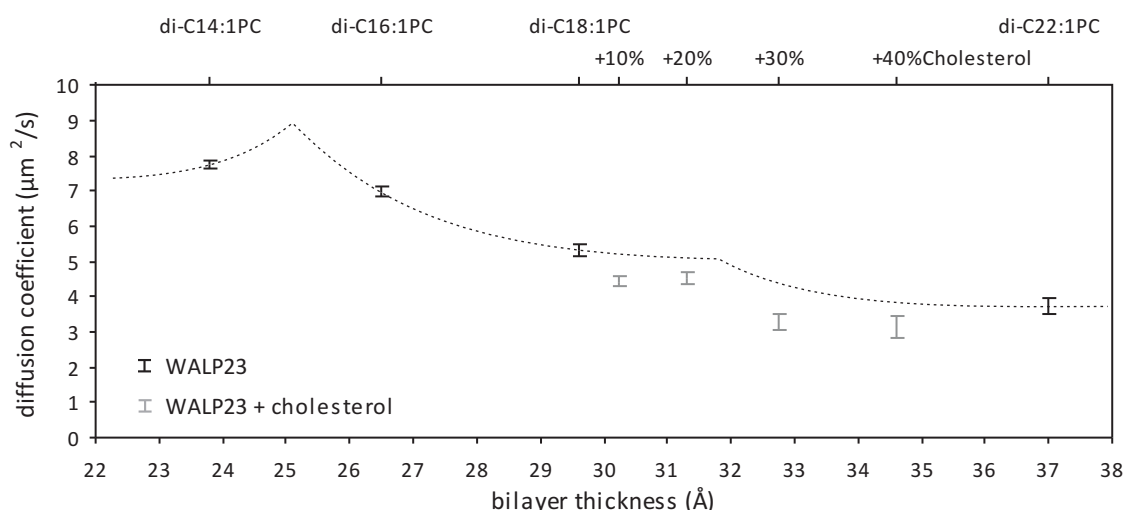


Figure 9: Diffusion coefficients of Alexa 488 labeled WALP23 peptides, which were inserted into bilayers of different thickness or bilayers of di-C18:1PC containing different amounts of cholesterol (bilayer thickness derived from [15]). The error bars give the standard error of the mean (SEM).

Finally, when incorporating WALP peptides in membranes exhibiting phase separation, we observed that WALP peptides remain in the liquid-disordered phase even when experiencing large hydrophobic mismatch. In an earlier study of Fastenberg *et al.* using fluorescence quenching techniques it was reported that the related peptide acetyl-KKWWL₈AL₈WWKK-amide also preferred the liquid-disordered phase over the liquid-ordered cholesterol containing phase [27], similar to what was found for transmembrane peptides of type acetyl-KKG(LA)_{4/5}W(LA)_{4/5}KKA-amide [28]. To our best knowledge, to date there is no single-pass transmembrane helical peptide known to partition into the cholesterol-rich, liquid-ordered phase. In such model membrane systems transmembrane peptides introduce disorder in the ordered membrane domains which may entail a larger energetic cost than the adaptations needed to accommodate the peptide in too thin liquid-disordered domain. Thus, simple consideration of hydrophobic length of transmembrane segments and the membrane is not sufficient as determinant for partitioning behavior. However, the extent of hydrophobic matching between transmembrane segments and membrane will contribute to the total energy of the system, and may together with other, more dominating factors play a decisive role for the partitioning behavior of transmembrane peptides and proteins in membranes.

Acknowledgements

This work was supported by a Marie Curie Early Stage Research Training Fellowship from the European Community's Sixth Framework Program for A.H. (Biomem-MEST-CT 2004-007931). Funding was obtained from the Zernike Institute for Advanced Materials and a NWO-Top subsidy grant for B.P. (Top-subsidy grant 700.56.302). We thank Nicoletta Kahya for initiating part of this project and for helpful discussions at early stages of the project.

References

1. Sorice M, Molinari S, Marzio LD, Mattei V, Tasciotti V, Ciarlo L, Hiraiwa M, Garofalo T, and Misasi R (2008) Neurotrophic signalling pathway triggered by prosaposin in PC12 cells occurs through lipid rafts. *FEBS J*, 275:4903–4912.
2. Brady JD, Rich TC, Le X, Stafford K, Fowler CJ, Lynch L, Karpen JW, Brown RL, and Martens JR (2004) Functional role of lipid raft microdomains in cyclic nucleotide-gated channel activation. *Mol Pharmacol*, 65:503–511.
3. Lacalle RA, Mira E, Gómez-Moutón C, Jiménez-Baranda S, Martínez-A C, and Mañes S (2002) Specific SHP-2 partitioning in raft domains triggers integrin-mediated signaling via Rho activation. *J Cell Biol*, 157:277–289.
4. Simons K and Toomre D (2000) Lipid rafts and signal transduction. *Nat Rev Mol Cell Biol*, 1:31–39.
5. Vereb G, Szöllösi J, Matkó J, Nagy P, Farkas T, Vígh L, Mátyus L, Waldmann TA, and Damjanovich S (2003) Dynamic, yet structured: the cell membrane three decades after the Singer-Nicolson model. *Proc Natl Acad Sci U S A*, 100:8053–8058.
6. Kahya N, Scherfeld D, Bacia K, Poolman B, and Schwille P (2003) Probing lipid mobility of raft-exhibiting model membranes by fluorescence correlation spectroscopy. *J Biol Chem*, 278:28109–28115.
7. Risselada HJ and Marrink SJ (2008) The molecular face of lipid rafts in model membranes. *Proc Natl Acad Sci U S A*, 105:17367–17372.
8. Gambin Y, Lopez-Esparza R, Reffay M, Sierrecki E, Gov NS, Genest M, Hodges RS, and Urbach W (2006) Lateral mobility of proteins in liquid membranes revisited. *Proc Natl Acad Sci U S A*, 103:2098–2102.
9. de Planque MRR, Kruijtz JAW, Liskamp RMJ, Marsh D, Greathouse DV, Koeppe II RE, de Kruijff B, and Killian JA (1999) Different membrane anchoring positions of tryptophan and lysine in synthetic transmembrane alpha-helical peptides. *J Biol Chem*, 274(30):20839–20846.

10. Rouser G, Fleischer S, and Yamamoto A (1970) Two-dimensional thin layer chromatographic separation of polar lipids and determination of phospholipids by phosphorus analysis of spots. *Lipids*, 5:494–496.
11. Elson EL and Magde D (1974) Fluorescence correlation spectroscopy. i. Conceptual basis and theory. *Biopolymers*, 13:1–27.
12. Petrášek Z and Schwille P (2008) Precise measurement of diffusion coefficients using scanning fluorescence correlation spectroscopy. *Biophys J*, 94:1437–1448.
13. Landolt-Marticorena C, Williams KA, Deber CM, and Reithmeier RAF (1993) Nonrandom distribution of amino-acids in the transmembrane segments of human type I single span membrane proteins. *J Mol Biol*, 229:602–608.
14. Kahya N and Schwille P (2006) How phospholipid-cholesterol interactions modulate lipid lateral diffusion, as revealed by fluorescence correlation spectroscopy. *J Fluoresc*, 16:671–678.
15. Kucerka N, Pencer J, Nieh MP, and Katsaras J (2007) Influence of cholesterol on the bilayer properties of monounsaturated phosphatidylcholine unilamellar vesicles. *Eur Phys J E*, 23:247–254.
16. Goñi FM, Alonso A, Bagatolli LA, Brown RE, Marsh D, Prieto M, and Thewalt JL (2008) Phase diagrams of lipid mixtures relevant to the study of membrane rafts. *Biochim Biophys Acta*, 1781:665–684.
17. Veatch SL and Keller SL (2005) Miscibility phase diagrams of giant vesicles containing sphingomyelin. *Phys Rev Lett*, 94:148101.
18. Bacia K, Scherfeld D, Kahya N, and Schwille P (2004) Fluorescence correlation spectroscopy relates rafts in model and native membranes. *Biophys J*, 87:1034–1043.
19. Kahya N, Scherfeld D, Bacia K, and Schwille P (2004) Lipid domain formation and dynamics in giant unilamellar vesicles explored by fluorescence correlation spectroscopy. *J Struct Biol*, 147:77–89.
20. Baumgart T, Hunt G, Farkas ER, Webb WW, and Feigenson GW (2007) Fluorescence probe partitioning between lo/l_d phases in lipid membranes. *Biochim Biophys Acta*, 1768:2182–2194.
21. Saffman PG and Delbrück M (1975) Brownian motion in biological membranes. *Proc Natl Acad Sci U S A*, 72:3111–3113.
22. Ramadurai S, Holt A, Krasnikov VV, van den Bogaart G, Killian JA, and Poolman B (2009) Lateral diffusion of membrane proteins. *J Am Chem Soc*, submitted.
23. Özdirekcan S, Rijkers DTS, Liskamp RMJ, and Killian JA (2005) Influence of flanking residues on tilt and rotation angles of transmembrane peptides in lipid bilayers. A solid-state 2H NMR study. *Biochemistry*, 44:1004–1012.
24. Holt A, Koehorst RBM, Meijneke T, Gelb MH, Rijkers DT, Hemminga MA, and Killian JA (2009) Tilt and rotation angles of a transmembrane model peptide as studied by fluorescence spectroscopy. *Biophys J*, submitted.
25. Sparr E, Ash WL, Nazarov PV, Rijkers DTS, Hemminga MA, Tieleman DP, and Killian JA (2005) Self-association of transmembrane alpha-helices in model membranes - importance of helix orientation and role of hydrophobic mismatch. *J Biol Chem*, 280:39324–39331.
26. Lee CC and Petersen NO (2003) The lateral diffusion of selectively aggregated peptides in giant unilamellar vesicles. *Biophys J*, 84:1756–1764.
27. Fastenberg ME, Shogomori H, Xu X, Brown DA, and London E (2003) Exclusion of a transmembrane-type peptide from ordered-lipid domains (rafts) detected by fluorescence quenching: extension of quenching analysis to account for the effects of domain size and domain boundaries. *Biochemistry*, 42:12376–12390.
28. Vidal A and McIntosh TJ (2005) Transbilayer peptide sorting between raft and nonraft bilayers: comparisons of detergent extraction and confocal microscopy. *Biophys J*, 89:1102–1108.

Chapter 6

Summarizing Discussion

In the present thesis, several aspects of peptide-lipid interactions were investigated with the help of designed model peptides that were incorporated into model membranes. Synthetic model peptides offer the advantage that their amino acid sequence can be varied easily, allowing systematic investigation of peptide-lipid interactions. In particular, model peptides composed of a hydrophobic stretch of alternating leucines and alanines flanked by a pair of tryptophans, called WALP peptides, were employed for these studies. These peptides are useful to study the role of aromatic residues located at the membrane-water interface. There is great interest in the specific role of these residues since aromatic residues like tryptophan and tyrosine are frequently found at the membrane-water interface of membrane proteins [1].

These aromatic residues were suggested to anchor membrane proteins in the membrane, which may help them to adopt the correct orientation in the membrane [2-4]. The anchoring function of interfacial tryptophans could be due to an unspecific interaction with phospholipid headgroups [5]. But also more specific interactions with certain lipids could occur, which may involve interactions of the aromatic tryptophan side chain. One interesting candidate for specific tryptophan-lipid interactions is cholesterol. Below we will first discuss our studies on the specificity of WALP-cholesterol interactions. Thereafter, we will discuss the role of tryptophan on tilting of WALP peptides and how tilting depends on the lipid environment discussed, and finally, some aspects of lateral diffusion of transmembrane peptides will be covered.

Specificity of interactions between WALP peptides and cholesterol

Several studies have indicated an interaction between tryptophans in transmembrane segments of membrane proteins and cholesterol [6-9]. In some types of membranes cholesterol is an abundant lipid and therefore, it is important to know whether such an interaction with interfacial tryptophans really occurs. In **chapter 2**, we present an investigation of the proposed preferential interaction between cholesterol and interfacial tryptophans using the tryptophan-flanked model peptide WALP23. We performed ^2H NMR experiments using deuterium-labeled cholesterol or WALP23 including a deuterium-labeled tryptophan, which were inserted into membranes of saturated phospholipids. These experiments showed that there was no change in orientation and dynamics of either molecule in the presence of the putative interaction partner. In addition, competition experiments using the fluorescent cholesterol analogue dehydroergosterol showed that cholesterol remains randomly distributed also in the presence of peptides with interfacial tryptophans in the bilayer. Both findings suggested that there is no general tendency for an interaction between cholesterol and tryptophans located at the membrane-water interface.

Before, van Duyl *et al.* had reported a synergistic effect when both cholesterol and tryptophan-flanked model peptides were present in the membrane, and proposed a preferential interaction between cholesterol and interfacial tryptophans [9]. The authors performed ^{31}P NMR experiments on model membranes composed of unsaturated phospholipids containing high concentrations of cholesterol and observed the formation of an isotropic phase when also tryptophan-flanked WALP peptides were present in the membrane above a certain concentration threshold. This effect was not observed in presence of the same concentration of the structurally similar lysine-flanked KALP peptides.

How can we explain this apparent discrepancy between the study of van Duyl *et al.* [9] and our study presented in **chapter 2**, where no preferential interaction was observed? In the following, we propose that this observation is related to differences in acyl chain saturation, probably resulting in different miscibility of cholesterol in these bilayers.

Studies on the phase behavior of ternary lipids systems suggested that in mixtures of long-chain saturated lipids and short-chain saturated lipids cholesterol exhibits essentially similar solubility in phases of long-chain lipids and short-chain lipids [10]. To some extent the same holds for lipids including only one mono-unsaturated acyl chain. However, in mixtures containing saturated lipids and lipids with two mono-unsaturated acyl chains cholesterol was found to be much less well accommodated in phases containing mainly unsaturated lipids, i.e. the liquid-disordered phases. Apparently, from the energetic point of view, integration of cholesterol in bilayers of lipids with fully saturated acyl chains is much more favorable. It is well known that cholesterol increases the order of neighboring lipid acyl chains, which condenses and therefore thickens the bilayer.

This ordering effect is most pronounced for saturated fatty acid chains with lengths similar to the long axis of cholesterol [11]. In atomistic molecular dynamics simulations using mono-unsaturated lipids with double bonds at different positions in the acyl chain it was found that the ordering effect on the lipid acyl chains was smallest when the double bond was located in the middle of the acyl chain, i.e. at the height of the cholesterol ring system [12]. Therefore, integration of cholesterol in unsaturated bilayers with double bonds in the middle of both acyl chains, as valid for the commonly employed di-C18:1(Δ 9-*cis*)PC (also often abbreviated as DOPC), seems to be particularly unfavorable. We propose that it is this impaired miscibility of cholesterol in bilayers of unsaturated lipids that might explain the previously observed synergistic effect between tryptophan-flanked peptides and cholesterol in the study by van Duyl *et al.* [9].

Like cholesterol, also transmembrane peptides including a relatively long hydrophobic stretch flanked with aromatic residues were found to induce significant ordering of (saturated) lipid acyl chains [13]. This could be due to the fact that the bulky side chains of tryptophans can impose important steric restrictions for integration into the membrane-water interface. This is in contrast to peptides flanked by charged residues like lysine, where the long, flexible side chains of lysines allow much more freedom. Therefore, lipid ordering in the vicinity of the lysine-flanked peptides may not be necessary since the flexible lysine side chains can adapt to the membrane over quite some range.

These differences in behavior of the flanking residues may have large consequences. Most probably, the ordering effect of WALP peptides is most pronounced for the lipids residing in direct vicinity of the peptides, e.g. for WALP23 inserted in bilayers of di-C18:1(Δ 9-*cis*)PC. In bilayers composed of unsaturated lipids this ordering effect may attract the cholesterol molecules next to the peptides, since it can be expected that it is less favorable for cholesterol to integrate with the completely unordered, unsaturated lipids in the bulk membrane. As a consequence, cholesterol molecules may be concentrated around the peptides, giving rise to an apparent preferential interaction. If the concentration of cholesterol and tryptophan-flanked peptides is then increased above a certain limit, this could lead to the observed synergistic effect between cholesterol and interfacial tryptophans.

However, in case of lysine-flanked KALP peptides the lipid acyl chains are not ordered and therefore, cholesterol would remain in random distribution in the bilayer and no isotropic phase would be induced, in agreement with the findings of van Duyl *et al.* [9]. A new series of ^{31}P NMR experiments in bilayers of saturated lipids could be performed to explore the validity of these hypotheses.

In our study presented in **chapter 2**, we used bilayers of saturated lipids, i.e. di-C14:0PC, to investigate the proposed preferential interaction between cholesterol and interfacial tryptophans. Cholesterol is nicely miscible in saturated lipids and exhibits largest ordering capacities for acyl chains including 14 - 18 carbons [11]. Therefore, (any) additional ordering of lipid acyl chains in the vicinity of WALP flanked peptides can be expected to be small and would most probably not induce a redistribution of cholesterol in bilayers of saturated lipids, as we indeed observed. New experiments on bilayers containing unsaturated lipids could be performed to investigate the distribution behavior of cholesterol in the presence of tryptophan-flanked peptides in the bilayer.

Another indication for the absence of specific interactions between cholesterol and tryptophans located at the membrane-water interface has been found from recent studies on perfringolysin O. This protein is a member of the large family of pore-forming toxins produced by Gram-positive bacteria. Several years ago, the tryptophan-rich undecapeptide of this protein was suggested to interact with cholesterol-rich membranes because of its highly conserved structure and the fact that the tryptophan residues were shown to insert into the membrane surface [14]. However, a more recent study suggested that binding of perfringolysin O to cholesterol containing membranes was independent of the insertion of the tryptophan-rich undecapeptide into cholesterol containing membranes, but instead involves a specific interaction of cholesterol to another loop of the protein [15]. This observation also contra-indicates a general tendency for tryptophans to interact with membrane-bound cholesterol.

Tilt angles of WALP peptides

The anchoring properties of interfacial tryptophans in membrane proteins were suggested to play an important role for their function. Another important parameter in the same context of membrane protein function involves the tilt angle of the transmembrane segments. Typically, the transmembrane segments in membrane proteins were found to have a tilt angle of $24 \pm 14^\circ$ [16]. ^2H NMR studies on transmembrane model peptides, which are frequently used to mimic transmembrane segments of such membrane proteins, yielded relatively small tilt angles of only $4 - 12^\circ$ [17]. In contrast to this, recent molecular dynamics (MD) simulations of the WALP23 peptide [18] and on related model peptides [19] yielded tilt angles in the range of $30 - 40^\circ$.

To explain the discrepancy the authors of both studies suggested that motional averaging of the quadrupolar splittings could have led to an underestimation of the helix tilt angle. The GALA method that is used to analyze a set of quadrupolar splittings is based on a quasi-static peptide model, where the orientation of the peptides is described by a tilt and rotation angle, and peptide motions are only accounted for by a global order parameter. It was found that the large fluctuations in rotation angles observed in both MD simulation studies

led to a reduction of the back-calculated ^2H -NMR splittings, and that analysis of such averaged quadrupolar splittings using the GALA method would yield too small tilt angles. As a consequence, such an averaging effect could also camouflage the effects of the different flanking residues.

In **chapter 3**, we present a new solid-state NMR approach, called MACADAM, which allows the investigation of orientational and motional properties of transmembrane peptides at the same time. This advanced NMR approach is based on the fact that nuclear interactions with different main tensor orientations with respect to the helix axis and therefore to the membrane normal are dynamically averaged to different extent. For this purpose, we determined dynamically averaged ^{13}C and ^{15}N chemical shift anisotropies and dynamically averaged ^{13}C - ^{15}N dipolar interactions of WALP23 peptides including isotope-labeled amino acids at different positions in the peptide backbone. The NMR results were analyzed using a dynamical model, which extended the previous quasi-static model by oscillations around the helix axis and wobbling-in-a-cone motions. A tilt angle of 21° was found, which is much larger than the tilt angle of around 5° determined from ^2H NMR experiments in combination with the GALA method. The rotation angle of 150° agrees well with the results reported previously from ^2H NMR experiments [17].

Frequently, the PISEMA (polarization inversion with spin exchange at the magic angle) technique is used to determine the orientation of transmembrane segments [20]. The characteristic wheel-like PISEMA patterns reflect projections of the residues in helices and provide direct information on the orientation of the transmembrane helices in bilayers. The two-dimensional ^1H - ^{15}N dipolar coupling/ ^{15}N chemical shift PISEMA spectra of uniformly ^{15}N -labeled peptides are recorded on oriented bilayers. To achieve sufficient sensitivity high peptide/lipid ratios of 1:16 [21] or 1:20 [22] have been used, which could have undesirable side effects on the orientation of the transmembrane peptides if one wants to study the effects of the lipid environment on single transmembrane peptides. The new MACADAM technique does not rely on the use of oriented samples, which consequently permits the use of unoriented samples with peptide/lipid ratios of 1:100. However, the major advance of the MACADAM technique is that it also gives detailed and accurate information on motional properties of the transmembrane segments.

Very recently, Strandberg *et al.* re-analyzed experimental ^2H NMR data published for WALP23 peptides [23] using different peptide models with increasing complexity of peptide dynamics. Different peptide models were found to match the data with similar deviations in terms of *rsm*, but yielded very different tilt angles [24]. These findings agree well with our simulations based on the conventional, quasi-static and the extended, dynamic peptide model presented in **chapter 3**. In an accompanying publication, the same authors investigated the effect of peptide dynamics on PISEMA experiments [25]. For this purpose, PISEMA spectra were generated from trajectories of an earlier MD study on WLP23 [19]. Analysis of this data with the different peptide models yielded similar tilt angles for both the quasi-static and the dynamic peptide models. However, the virtual PISEMA data could be fitted best with a peptide model including explicit oscillations and wobbling, which is identical to the dynamic peptide model we have used in **chapter 3**.

In an attempt to explore the differences between the established solid-state NMR methods Vostrikov *et al.* compared the results of ^2H NMR and PISEMA experiments obtained on a related model peptide, a GWALP peptide [22]. In this study, the experimental data sets were separately analyzed using the conventional quasi-static peptide model. In first instance not surprising, both the ^2H NMR and PISEMA data sets yielded very similar tilt angles of 12.6° and 10.8° , respectively. Closer inspection of the fits to the experimental data shows that the fit to the experimental quadrupolar splittings is of good quality, whereas the experimental ^{15}N data show some deviations from the fitted PISEMA wheel. Especially to the higher dipolar couplings the PISEMA data points do not show good matching with the fitted PISEMA wheel, which may suggest an underestimation of the tilt angle (compare discussion in [25]). The GWALP peptide is a close relative of the WALP peptides, which is flanked at both ends by only a single tryptophan and may also exhibit important motions around the helical axis. Together with the notion that analysis of only ^2H NMR data does not yield reliable tilt angles due to motional averaging, it is very well possible that the use of the conventional, quasi-static peptide model may not be sufficient in this case.

Most of the natural transmembrane peptides investigated with solid-state NMR methods are believed to exist as homo-oligomers in the functional unit; good examples are the influenza A M2 channel [21,26], phospholemman [27] or phospholamban [28]. Interactions between the subunits of these helical bundles can be expected to largely restrict the motions of the transmembrane segments. Especially oscillations around the helix axis will be small since such motions would alter the position of contact interfaces to neighboring helices. Thus, the orientation parameters of transmembrane segments participating in oligomers will be much less affected by motional averaging when investigated with solid-state NMR methods. WALP peptides may behave completely different. In matching and nearly matching situations WALP peptides were shown to have no tendency to self-associate even at high peptide/lipid ratio, and only under large mismatch conditions a slightly higher tendency to self-associate was found [29]. Therefore, for WALP peptides in matching bilayer large peptide motions i.e. oscillations around the helix axis are much more probable which would lead to averaging of the quadrupolar splittings.

The major advancement of the new MACADAM technique is that it combines nuclear interactions with different orientations with respect to the helix axis, which allows the accurate determination of both orientation and dynamics of transmembrane segments in membranes. This technique is now established for WALP peptides and these peptides can now be studied in bilayers of different thickness to further investigate the effects of hydrophobic mismatch on the orientation and now also the dynamical properties of these transmembrane model peptides. Before, ^2H NMR experiments on WALP peptides yielded only small differences in tilt angles when inserted into bilayers of different hydrophobic thickness, these findings can now be validated using the new MACADAM approach. In future, it can be applied to other transmembrane peptides with different structures, i.e., different flanking residues, structure of the hydrophobic stretch, or hydrophobic lengths. Once a set of 2-3 triple-isotope labeled peptides has been synthesized, the effects of different lipid environments including bilayers with different thickness, (phospho)lipid composition and cholesterol content on the orientation and dynamics of these peptides can be studied systematically. Thus, this new technique paves the way to a better understanding of the basic principles underlying structural organization of peptide-lipid complexes.

In **chapter 4**, an alternative, complementary approach for the investigation of the orientation of transmembrane peptides in membranes based on steady-state fluorescence spectroscopy is presented. For this purpose, WALP23 peptides with cysteine replacements in different positions along the helix were labeled with the environment-sensitive label BADAN, and fluorescence spectra were recorded for bilayers with varying thickness. The fluorescence spectra of BADAN reflect the local polarity at the position of the label, which was used to determine the orientation of the peptide in the bilayer. For WALP23 inserted in di-C18:1PC we found a tilt angle of ca. 24° and a rotation angle of 136° , which agrees well with the results of the NMR study presented in **chapter 3**. Furthermore, we observed only small changes in tilt angle upon changing the hydrophobic thickness of the bilayer, i.e. 24.8° and 19.8° in bilayers of di-C16:1PC and di-C20:1PC, respectively. These findings suggest that WALP23 peptides do not fully compensate for hydrophobic mismatch by tilting, which agrees well with the results of a previous ^2H NMR study [17]. Indeed, full compensation is not expected since other/additional adaptations like lipid stretching or disordering [3], or an increased tendency to self-associate [29] were shown to occur.

As already mentioned above, tryptophans in interfacial positions of membrane proteins are thought to couple transmembrane segments to the membrane in a very particular manner; on the one hand interfacial tryptophans prefer a distinct location at the membrane-water interface [30,31], but on the other hand tryptophans in interfacial positions were also shown to inhibit tilting of transmembrane segments [32]. This at first sight controversial behavior of tryptophan-flanked transmembrane segments may have two reasons. First, interfacial tryptophans were shown to order lipid acyl chains in the vicinity of transmembrane segments when experiencing positive hydrophobic mismatch, which may also involve a more or less pronounced concerted response of lipids in more remote lipid layers around the transmembrane segments [13]. Such a stretching of the lipids leads to a more ordered and condensed bilayer around the transmembrane peptide, which in turn may hinder tilting. Second, tilting may entail a different and more unfavorable rotamer conformation and/or localization of the tryptophan side chain in the membrane. It was found before that tryptophans prefer certain rotameric conformations and locations at the membrane interface [30,31,33]. The latter may be important for maintaining the correct localization and orientation of tryptophans at the membrane-water interface, assuring the proper orientation and insertion of membrane proteins.

In contrast, the charged residue lysine has completely different properties. This amino acid has a long flexible side chain, which may allow the membrane proteins to readily adapt to varying membrane thickness. Furthermore, lysines in interfacial positions were suggested to be able to relieve negative hydrophobic mismatch situations by snorkeling to the membrane-water interface [34,35]. This particular behavior may have the function to alleviate distortion of the surrounding lipids and thus, to maintain constant local bilayer properties, which could be important for the function of the membrane protein. Further investigation of differences in behavior of lysine-flanked peptides as compared to tryptophan-flanked peptides may lead to a better understanding of the complex interaction mechanisms of membrane proteins and peptides with the membrane.

Diffusion properties of WALP peptides

In **chapter 5**, we present a study on the influence of the amino acid structure on the lateral diffusion of transmembrane peptides. For this purpose, fluorescence correlation spectroscopy experiments were performed on Alexa 488 labeled model peptides. In particular, we compared peptides with different lengths of the hydrophobic stretch (i.e. 17 or 21 amino acids in length), with different types of flanking residues (i.e. tryptophans or lysines), and with different structure of the hydrophobic stretch (i.e. alternating leucines and alanines or only leucines). These peptides were incorporated into bilayers of different thickness, i.e. lipids with different acyl chain length, and composition, i.e. concentration of cholesterol and sphingomyelin. Maximal lateral diffusion was observed for peptides in matching and nearly matching hydrophobic conditions. For peptides experiencing positive or negative mismatch lateral diffusion was found to be slowed down.

We developed a model that explains these observations in view of possible adaptations to mismatch situations including peptide tilting, bilayer distortions and peptide aggregation. To further test this model, it may be worthwhile to extend the present work by diffusion measurements on model peptides with shorter hydrophobic stretches, i.e. WALP19 and KALP19 peptides, and/or longer hydrophobic stretches, i.e. WALP31 and KALP31 peptides. Furthermore, it may be useful to investigate in more detail if aggregation of peptides under large hydrophobic mismatch occurs. For this purpose, dual-color FCS experiments could be performed on samples containing peptides with different labels, i.e. containing a fraction of peptides labeled with Alexa 488 and a fraction labeled with Alexa 633. In case that the peptides indeed dimerize or even oligomerize under large mismatch conditions, the pairs or clusters including peptides with labels of both colors can be detected by cross-correlation between the fluorescence emissions of the two populations of peptides.

Furthermore, FCS experiments using WALP23 peptides inserted into bilayers containing different concentrations of cholesterol showed that the lateral diffusion of the peptides is slowed down even more than we would expect from the increase in bilayer thickness in presence of cholesterol. This again illustrates the bilayer condensing effect of cholesterol, leading to a more viscous bilayer. Preliminary experiments using KALP23 suggested a much weaker influence on the diffusion of lysine-flanked peptides in presence of cholesterol in the bilayer. However, also much less peptides was found to be incorporated in presence of cholesterol, which could indicate that bilayers of unsaturated lipids also containing cholesterol may exclude lysine-flanked peptides due to an unfavorable interaction between these molecules. This observation could constitute an alternative explanation for the observations of van Duyl *et al.* discussed in the beginning of this chapter, i.e. the absence of a phase change when replacing WALP peptides with KALP peptides in bilayers of unsaturated lipids containing large amounts of cholesterol [9]. The transmembrane incorporation of KALP peptides into the cholesterol containing bilayers was not verified in these particular experiments.

Future prospects

The work presented in this thesis predominantly aims at characterization of the properties and behavior of the tryptophan-flanked model peptide WALP23 in bilayers of different thickness and cholesterol content. A new solid-state NMR approach for the investigation of the orientation and dynamics of transmembrane peptide was established, which opens up the way to explore the effects of peptide composition and of bilayer composition on the

orientation and dynamics of transmembrane segments in great detail. In future, this achievement will allow proper calibration of lipid-proteins interaction parameters required for MD simulations of membrane proteins, paving the way to further advancement in this field. In addition, much new data was collected on the orientation and dynamics of WALP (and KALP) peptides, giving a clearer view on the properties of these model peptides. WALP peptides are now better characterized model peptides which can be used to test and develop new techniques for the investigation of transmembrane proteins and peptides. In addition, WALP peptides have been shown to represent powerful tools for the investigation of the basic principles of peptide-lipid interactions. To conclude, the results presented in this thesis open interesting possibilities for future studies of peptide-lipid interactions.

References

1. Landolt-Marticorena C, Williams KA, Deber CM, and Reithmeier RAF (1993) Nonrandom distribution of amino-acids in the transmembrane segments of human type I single span membrane proteins. *J Mol Biol*, 229:602–608.
2. Stopar D, Spruijt RB, and Hemminga MA (2006) Anchoring mechanisms of membrane-associated M13 major coat protein. *Chem Phys Lipids*, 141:83–93.
3. de Planque MRR, Bonev BB, Demmers JAA, Greathouse DV, Koeppe II RE, Separovic F, Watts A, and Killian JA (2003) Interfacial anchor properties of tryptophan residues in transmembrane peptides can dominate over hydrophobic matching effects in peptide-lipid interactions. *Biochemistry*, 42:5341–5348.
4. Braun P and von Heijne G (1999) The aromatic residues Trp and Phe have different effects on the positioning of a transmembrane helix in the microsomal membrane. *Biochemistry*, 38:9778–9782.
5. Sanderson JM and Whelan EJ (2004) Characterisation of the interactions of aromatic amino acids with diacetyl phosphatidylcholine. *Phys Chem Chem Phys*, 6:1012–1017.
6. Gasset M, Killian JA, Tournois H, and de Kruijff B (1988) Influence of cholesterol on gramicidin-induced H_{II} phase formation in phosphatidylcholine model membranes. *Biochim Biophys Acta*, 939:79–88.
7. Santiago J, Guzmán GR, Rojas LV, Marti R, Asmar-Rovira GA, Santana LF, McNamee M, and Lasalde-Dominicci JA (2001) Probing the effects of membrane cholesterol in the *Torpedo californica* acetylcholine receptor and the novel lipid-exposed mutation alphaC418W in *Xenopus* oocytes. *J Biol Chem*, 276:46523–46532.
8. Carozzi AJ, Roy S, Morrow IC, Pol A, Wyse B, Clyde-Smith J, Prior IA, Nixon SJ, Hancock JF, and Parton RG (2002) Inhibition of lipid raft-dependent signaling by a dystrophy-associated mutant of caveolin-3. *J Biol Chem*, 277(20):17944–17949.
9. van Duyl BY, Meeldijk H, Verkleij AJ, Rijkers DTS, Chupin V, de Kruijff B, and Killian JA (2005) A synergistic effect between cholesterol and tryptophan-flanked transmembrane helices modulates membrane curvature. *Biochemistry*, 44:4526–4532.
10. Feigenson GW (2007) Phase boundaries and biological membranes. *Annu Rev Biophys Biomol Struct*, 36:63–77.
11. Ouimet J and Lafleur M (2004) Hydrophobic match between cholesterol and saturated fatty acid is required for the formation of lamellar liquid ordered phases. *Langmuir*, 20:7474–7481.
12. Martinez-Seara H, Róg T, Pasenkiewicz-Gierula M, Vattulainen I, Karttunen M, and Reigada R (2008) Interplay of unsaturated phospholipids and cholesterol in membranes: effect of the double-bond position. *Biophys J*, 95:3295–3305.
13. de Planque MRR, Boots JWP, Rijkers DTS, Liskamp RMJ, Greathouse DV, and Killian JA (2002) The effects of hydrophobic mismatch between phosphatidylcholine bilayers and transmembrane alpha-helical peptides depend on the nature of interfacially exposed aromatic and charged residues. *Biochemistry*, 41:8396–8404.
14. Nakamura M, Sekino N, Iwamoto M, and Ohno-Iwashita Y (1995) Interaction of theta-toxin (perfringolysin o), a cholesterol-binding cytolysin, with liposomal membranes: change in the aromatic side chains upon binding and insertion. *Biochemistry*, 34:6513–6520.

15. Soltani CE, Hotze EM, Johnson AE, and Tweten RK (2007) Structural elements of the cholesterol-dependent cytolysins that are responsible for their cholesterol-sensitive membrane interactions. *Proc Natl Acad Sci U S A*, 104:20226–20231.
16. Ulmschneider MB, Sansom MS, and Di Nola A (2005) Properties of integral membrane protein structures: derivation of an implicit membrane potential. *Proteins: Struct, Funct, Bioinf*, 59:252–265.
17. Özdirekcan S, Rijkers DTS, Liskamp RMJ, and Killian JA (2005) Influence of flanking residues on tilt and rotation angles of transmembrane peptides in lipid bilayers. A solid-state 2H NMR study. *Biochemistry*, 44:1004–1012.
18. Özdirekcan S, Etchebest C, Killian JA, and Fuchs PFJ (2007) On the orientation of a designed transmembrane peptide: toward the right tilt angle? *J Am Chem Soc*, 129:15174–15181.
19. Esteban-Martin S and Salgado J (2007) The dynamic orientation of membrane-bound peptides: bridging simulations and experiments. *Biophys J*, 93:4278–4288.
20. Marassi FM and Opella SJ (2000) A solid-state NMR index of helical membrane protein structure and topology. *J Magn Reson*, 144:150–155.
21. Wang J, Kim S, Kovacs F, and Cross TA (2001) Structure of the transmembrane region of the M2 protein H+ channel. *Protein Sci*, 10:2241–2250.
22. Vostrikov VV, Grant CV, Daily AE, Opella SJ, and Koeppe II RE (2008) Comparison of “polarization inversion with spin exchange at magic angle” and “geometric analysis of labeled alanines” methods for transmembrane helix alignment. *J Am Chem Soc*, 130:12584–12585.
23. Strandberg E, Özdirekcan S, Rijkers DTS, van der Wel PCA, Koeppe II RE, Liskamp RMJ, and Killian JA (2004) Tilt angles of transmembrane model peptides in oriented and non-oriented lipid bilayers as determined by 2H solid-state NMR. *Biophys J*, 86:3709–3721.
24. Strandberg E, Esteban-Martin S, Salgado J, and Ulrich AS (2009) Orientation and dynamics of peptides in membranes calculated from 2H-NMR data. *Biophys J*, 96:3223–3232.
25. Esteban-Martin S, Strandberg E, Fuertes G, Ulrich AS, and Salgado J (2009) Influence of whole-body dynamics on 15N PISEMA NMR spectra of membrane proteins: a theoretical analysis. *Biophys J*, 96:3233–3241.
26. Cady SD, Goodman C, Tatko CD, DeGrado WF, and Hong M (2007) Determining the orientation of uniaxially rotating membrane proteins using unoriented samples: a 2H, 13C, and 15N solid-state NMR investigation of the dynamics and orientation of a transmembrane helical bundle. *J Am Chem Soc*, 129:5719–5729.
27. Wong A, Beevers AJ, Kukol A, Dupree R, and Smith ME (2008) Solid-state 17O NMR spectroscopy of a phospholemmann transmembrane domain protein: implications for the limits of detecting dilute 17O sites in biomaterials. *Solid State Nucl Magn Reson*, 33:72–75.
28. Abu-Baker S, Lu JX, Chu S, Shetty KK, Gor'kov PL, and Lorigan GA (2007) The structural topology of wild-type phospholamban in oriented lipid bilayers using 15N solid-state NMR spectroscopy. *Protein Sci*, 16:2345–2349.
29. Sparr E, Ash WL, Nazarov PV, Rijkers DTS, Hemminga MA, Tieleman DP, and Killian JA (2005) Self-association of transmembrane alpha-helices in model membranes - importance of helix orientation and role of hydrophobic mismatch. *J Biol Chem*, 280:39324–39331.
30. Yau WM, Wimley WC, Gawrisch K, and White SH (1998) The preference of tryptophan for membrane interfaces. *Biochemistry*, 37:14713–14718.
31. Persson S, Killian JA, and Lindblom G (1998) Molecular ordering of interfacially localized tryptophan analogs in ester- and ether-lipid bilayers studied by 2H-NMR. *Biophys J*, 75:1365–1371.
32. Chiang CS, Shirinian L, and Sukharev S (2005) Capping transmembrane helices of MscL with aromatic residues changes channel response to membrane stretch. *Biochemistry*, 44:12589–12597.
33. Chamberlain AK and Bowie JU (2004) Analysis of side-chain rotamers in transmembrane proteins. *Biophys J*, 87:3460–3469.
34. Kandasamy SK and Larson RG (2006) Molecular dynamics simulations of model trans-membrane peptides in lipid bilayers: a systematic investigation of hydrophobic mismatch. *Biophys J*, 90:2326–2343.
35. Strandberg E and Killian JA (2003) Snorkeling of lysine side chains in transmembrane helices: how easy can it get? *FEBS Lett*, 544:69–73.

Nederlandstalige samenvatting

Alle levende organismen bestaan uit cellen, beginnend van maar een enkele cel voor bacteriën tot meer dan miljarden cellen in het organisme mens. Al deze cellen zijn omhuld door een celmembraan bestaand uit een dubbele laag van lipiden, dat zijn vetachtige moleculen met een waterminnend en een waterafstotend uiteinde. De meeste in membranen voorkomende lipiden vormen in water spontaan een bilaag door de waterafstotende uiteinden naast elkaar te plaatsen. Zo wordt een ondoordringbare barrière voor wateroplosbare stoffen gevormd en worden ongewenste stoffen buiten de cel en voeding en andere nuttige stoffen binnen de cel gehouden. Naast een veeltal van verschillende lipiden bevat een celmembraan ook een veeltal verschillende membraaneiwwitten. Een grote groep van deze membraaneiwwitten, de transmembraaneiwwitten, steekt door de membraan heen en is voor een groot gedeelte aan de buitenkant waterafstotend om goed contact met de membraan te kunnen maken. Alle natuurlijke eiwwitten bestaan uit lange, gevouwen ketens van aan elkaar geknoopte aminozuren, waarvan er 20 verschillende soorten zijn met allemaal verschillen in de zijketens. Sommige aminozuren zijn waterafstotend zoals alanines en leucines, andere zijn waterminnend en soms zelfs geladen zoals lysines, of bezitten een grote aromatische ringstructuur zoals tryptofaan. De volgorde van de aminozuren in de keten bepaald de driedimensionale structuur van het eiwit, en deze structuur bepaald de functie van het eiwit. In veel gevallen bestaan transmembraaneiwwitten uit een bundel van meerdere transmembrane α -helices.

Membraaneiwwitten verzorgen heel diverse functies voor de cel, onder ander transport van voeding- en afvalstoffen over de membraan, doorgeven van signalen en enzymatische activiteiten. Afwezigheid of niet goed functioneren van een membraaneiwit kan het overleven van de cel ernstig belemmeren en daardoor ook ziektes veroorzaken. In veel gevallen is de functie van membraaneiwwitten afhankelijk van de eigenschappen van de omgevende membraan, en zijn onder andere de bilaagdikte, samenstelling en vloeibaarheid van de membraan belangrijke parameters. Nog steeds is er maar beperkt inzicht in hoe de werkwijze van membraaneiwwitten wordt beïnvloed door de omgevende membraan omdat membraaneiwwitten heel hydrofobe systemen zijn en daardoor moeilijk te bestuderen. Deze problemen kunnen deels worden omzeild door het gebruik van transmembraan modelpeptiden die transmembraan segmenten van membraaneiwwitten nabootsen. Veel gebruikte modelpeptiden zijn de WALP en KALP modelpeptiden die bestaan uit een reeks van afwisselend alanines en leucines met een paar tryptofanen of lysines aan beide uiteinden. Tegenwoordig worden deze modelpeptiden veel voor systematische studies over het gedrag van transmembrane segmenten gebruikt, zoals de interactie met afzonderlijke lipiden, de oriëntatie en diffusiesnelheid van peptiden met verschillende structuur in membranen met gevarieerde samenstelling. Uiteraard zijn modelpeptiden ook belangrijk voor de ontwikkeling en verbetering van methodes ter bestudering van de structuur van membraaneiwwitten.

In het kader van dit proefschrift zijn de boven beschreven transmembraan modelpeptiden gebruikt om het gedrag van transmembraanpeptiden in membranen van verschillende dikte en samenstelling te onderzoeken. In het verleden zijn er aanwijzingen gevonden voor een voorkeursinteractie tussen cholesterol en tryptofanen die in het membraan/water grensvlak geplaatst waren. In **hoofdstuk 2** wordt beschreven hoe deze interactie is onderzocht met

behelp van het WALP peptide. Daarvoor zijn peptiden met ^2H , een isotoop van waterstof, bevattende tryptofaan gemaakt en met ^2H NMR experimenten onderzocht in wel en geen cholesterol bevattende modelmembranen. De resultaten van deze experimenten toonden aan dat noch de oriëntatie noch de dynamiek van de tryptofaan zijketen wordt beïnvloed door toevoeging van cholesterol in de membraan, wat betekent dat er geen interactie plaatsvindt. Daarnaast is een soortgelijk experiment uitgevoerd met ^2H bevattend cholesterol en ook hier is gevonden dat de oriëntatie en dynamiek van cholesterol niet verandert door het aanwezig zijn van het tryptofaan bevattende peptide. Verder toonden fluorescentie experimenten met een fluorescerend analoog van cholesterol aan dat cholesterol ook in aanwezigheid van het tryptofaan bevattende peptide gelijkmatig in de membraan verdeeld blijft. De conclusie van dit onderzoek is dat er geen algemene voorkeur bestaat voor een interactie tussen cholesterol en tryptofanen in het membraan.

Ook belangrijk voor het goed functioneren van membraaneiwitten is de juiste oriëntatie van de α -helices. In **hoofdstuk 3** wordt een verfijnde methode ter bepaling van de oriëntatie en dynamiek van transmembraanpeptiden op basis van nucleaire magnetische resonantie, de zogenaamde MACADAM methode, beschreven. Aanleiding voor het ontwikkelen van de nieuwe methode was de vinding dat experimentele data, bestaande uit alleen ^2H NMR resultaten, even goed verklaard konden worden met een complex bewegingsmodel voor het peptide als met het eenvoudige conventionele model. Het probleem is opgelost door aanvullende data van NMR metingen aan ^{13}C en ^{15}N gelabelde peptiden te verzamelen. Analyse van de NMR data met het nieuwe complexe bewegingsmodel leverde veel grotere tilthoeken van het WALP peptide op ten opzichte van de membraan dan de benadering met het eenvoudige bewegingsmodel. De vinding van een grotere tilthoek wordt bevestigd door de experimenten beschreven in **hoofdstuk 4**. Hier wordt een alternatieve methode voor de bepaling van tilthoeken toegepast op basis van fluorescentie metingen aan peptiden met fluorescerende labels in verschillende posities. De gebruikte label rapporteert heel gevoelig over de polariteit in de directe omgeving van de label. Membranen zijn in het midden veel minder polair dan naar buiten toe en dit bijzondere polariteitsprofiel kan benut worden voor de berekening van de oriëntatie van het peptide in de membraan. Verder is met deze methode gevonden dat WALP peptiden verschillen in de dikte van de bilaag niet volledig compenseren door een grotere tilthoek, wat op een bijzonder rol van tryptofanen in het lipide/water grensvlak zou kunnen duiden.

Het gedrag van peptiden in de membraan is afhankelijk van de structuur van het peptide. In **hoofdstuk 5** is met fluorescentie correlatie spectroscopie de diffusiesnelheid van peptiden met verschillende lengtes en met verschillende aminozuren aan de uiteinden gemeten. Experimenten in membranen met verschillende dikten toonden aan dat de peptiden in een membraan met passende en bijna passende dikte goed kunnen bewegen en dat veel te dikke en te dunne membranen de beweging van de peptiden in de membraan belemmeren. Blijkbaar zijn grote aanpassingen nodig om aan deze extreme omstandigheden te voldoen.

Het in dit proefschrift beschreven onderzoek heeft belangrijke inzichten geleverd in het gedrag van transmembraanpeptiden. Daarnaast is een nieuwe methode voor de bepaling van de oriëntatie en dynamiek van transmembraanpeptiden ontwikkeld. Het WALP peptide is nu een goed gekarakteriseerd modelpeptide dat in de toekomst gebruikt kan worden voor de ontwikkeling van nieuwe methodes voor het bestuderen van membraaneiwitten en ook voor de calibratie van bestaande technieken zoals moleculaire dynamica simulaties.

Zusammenfassung in deutscher Sprache

Alle lebenden Organismen bestehen aus Zellen, angefangen von nur einer einzigen Zelle bei Bakterien bis hin zu mehr als Milliarden Zellen im Organismus Mensch. All diese Zellen sind umhüllt von einer Zellmembran bestehend aus einer Doppelschicht von Lipiden, das sind fettartige Moleküle bestehend aus einem Wasser liebenden und einem Wasser abstoßenden Ende. Die meisten in Zellmembranen vorkommenden Lipide formen in Wasser spontan eine Lipiddoppelschicht, indem sich die Wasser abstoßenden Enden aneinanderlagern. Dadurch wird eine undurchdringbare Barriere für wasserlösliche Stoffe gebildet, wodurch unerwünschte Substanzen außerhalb der Zelle, und Nahrung und andere nützliche Stoffe innerhalb der Zelle verbleiben. Neben einer Fülle von verschiedenen Lipiden enthält eine Zellmembran auch eine Vielzahl verschiedener Membranproteine. Eine große Gruppe dieser Membranproteine, die Transmembranproteine, erstreckt sich durch die Membran hindurch und ist darum an der Außenseite größtenteils Wasser abstoßend, um sich gut in die Membran integrieren zu können. Alle Proteine, umgangssprachlich auch Eiweiße genannt, bestehen aus langen, gefalteten Ketten von miteinander verknüpften Aminosäuren, wovon es in der Natur 20 verschiedene gibt und die sich nur in den Seitenketten unterscheiden. Manche dieser Aminosäuren sind Wasser abstoßend wie zum Beispiel Alanin und Leucin, andere sind Wasser liebend und manche sogar geladen wie zum Beispiel Lysin, und wieder andere besitzen große, aromatische Ringstrukturen wie zum Beispiel Tryptophan. Die Reihenfolge dieser Aminosäuren in der Kette bestimmt die dreidimensionale Struktur des Proteins, und diese Struktur wiederum bestimmt die Funktion eines Proteins. Transmembranproteine bestehen in vielen Fällen aus Bündeln von aneinander gelagerten, transmembranen Segmenten, den α -Helices.

Transmembranproteine erledigen sehr vielfältige Funktionen für die Zelle, unter anderem Transport von Nahrungssubstanzen und Abfallstoffen über die Membran, Übertragung von Signalen und auch enzymatische Funktionen. Fehlende oder nicht gut funktionierende Membranproteine können das Überleben der Zelle ernsthaft beeinträchtigen und dadurch auch Krankheiten verursachen. In vielen Fällen ist die Funktion von Membranproteinen abhängig von den Eigenschaften der umliegenden Membran, wichtige Parameter sind hier unter anderem die Dicke, Zusammenstellung und die Viskosität der Membran. Noch immer haben wir nur begrenztes Wissen darüber, wie die Funktion von Membranproteinen von der umliegenden Membran beeinflusst wird. Ein Grund dafür ist, dass Membranproteine sehr Wasser abstoßende Gebilde sind und dadurch schwierig zu untersuchen. Zum Teil können diese Probleme umgangen werden durch den Gebrauch von transmembranen Modelpeptiden, welche die transmembranen Segmente nachbilden. Häufig gebrauchte Modelpeptide sind die WALP und KALP Peptide, die aus einer Reihe von abwechselnd Alanin und Leucin mit jeweils einem Paar Tryptophane oder Lysine an beiden Enden bestehen. Gegenwärtig werden diese Modelpeptide viel für systematische Studien über das Verhalten von transmembranen Segmenten mit variierender Aminosäuresequenz eingebettet in Membranen mit unterschiedlicher Zusammenstellung, wie zum Beispiel für Studien über die Wechselbeziehungen von Peptiden zu besonderen Lipiden oder über die Orientierung und Bewegungsgeschwindigkeit von Peptiden, genutzt. Außerdem sind Modelpeptide außerordentlich nützlich für die Entwicklung und Verbesserung von Methoden zur Untersuchung der Struktur von Membranproteinen.

Im Rahmen dieser Doktorarbeit wurden die oben beschriebenen transmembranen Modelpeptide zur Untersuchung des Verhaltens von transmembranen Peptiden in Membranen mit unterschiedlicher Dicke und Zusammenstellung benutzt. In der Vergangenheit wurden Hinweise auf eine bevorzugte Wechselwirkung zwischen Cholesterol, einem Membranlipid mit speziellen Eigenschaften, und Tryptophane an der Wasser-Membran Grenzfläche gefunden.

In **Kapitel 2** wird beschrieben, wie diese Wechselwirkung mit Hilfe des WALP Peptids untersucht wurde. Zu diesem Zweck wurden WALP Peptide, die das Wasserstoffisotop Deuterium (^2H) enthalten, synthetisiert und mit Kernspinresonanzexperimenten in Membranen mit und ohne Cholesterolgehalt untersucht. Die Ergebnisse dieser Experimente zeigten, dass sich weder die Orientierung noch die Dynamik der Seitenketten der Tryptophane durch das Zufügen von Cholesterol veränderten, was bedeutet, dass keine Wechselwirkung stattfindet. Außerdem wurden noch ähnliche Experimente mit Deuterium enthaltendem Cholesterol durchgeführt, und auch hier wurden keine Veränderungen der Orientierung und der Dynamik von Cholesterol in Anwesenheit von Tryptophan enthaltenden Peptiden gefunden. Weiterhin zeigten Fluoreszenzexperimente mit einem fluoreszierendem Analog von Cholesterol, dass Cholesterol auch in Anwesenheit von Tryptophan enthaltenden Peptiden gleichmäßig in der Membran verteilt bleibt. Das Fazit dieser Experimente ist, dass keine allgemeine Tendenz zur Wechselwirkung von Cholesterol mit Tryptophanen in der Membran besteht.

Ebenso wichtig für eine korrekte Funktion von Membranproteinen ist die richtige Orientierung der transmembranen Segmente, der α -Helices, in der Membran. In **Kapitel 3** wird eine neue, verfeinerte Methode, die sogenannte MACADAM Methode, zur Bestimmung der Orientierung und Dynamik von transmembranen Peptiden basierend auf Kernspinresonanzspektroskopie (NMR Spektroskopie) beschrieben. Anlass zur Entwicklung dieser neuen Methode war die Erkenntnis, dass experimentelle Daten, bestehend aus nur Deuterium NMR Daten, mit einem verbesserten komplexen Bewegungsmodell für ein Peptid eingebettet in eine Membran ebenso gut interpretiert werden konnten wie mit dem einfachen herkömmlichen Bewegungsmodell. Ansatz zur Lösung des Problems war die Gewinnung zusätzlicher NMR Messdaten aus Experimente an Peptiden, in die gezielt Aminosäuren mit ^{13}C und ^{15}N Isotopen eingebaut wurden. Die Analyse des kompletten NMR Datensatzes, bestehend aus alten und neuen Daten, mit dem verbesserten komplexen Bewegungsmodell ergab einen viel größeren Neigungswinkel des Peptids in der Membran als bei Analyse mit dem einfachen herkömmlichen Modell. Der Befund der viel größeren Neigung wurde bestätigt durch die in **Kapitel 4** beschriebene Studie. Hier wurde eine alternative Methode basierend auf Fluoreszenzexperimenten für die Bestimmung des Neigungswinkels angewendet auf Peptide, die mit fluoreszierenden Markern in verschiedenen Positionen entlang der α -Helix versehen wurden. Dieser fluoreszierende Marker berichtet sehr sensibel über die Polarität in der direkten Umgebung des Markers. Da Membranen in der Mitte sehr viel weniger polar sind als weiter außen, kann auf Grundlage dieses besonderen Polaritätsprofils die Orientierung des Peptids in der Membran berechnet werden. Außerdem wurde mit dieser Methode gefunden, dass WALP Peptide unterschiedliche Membrandicken nicht komplett durch einen größeren Neigungswinkel ausgleichen, was auch eine besondere Rolle der Tryptophane an der Wasser-Membran Grenzfläche hinweisen könnte.

Zudem ist das Verhalten von Peptiden in der Membran auch abhängig von der Peptidstruktur. In **Kapitel 5** wurde mit Fluoreszenzkorrelationsspektroskopie die Bewegungsgeschwindigkeit von Peptiden mit verschiedenen Längen und mit unterschiedlichen Aminosäuren an den Enden gemessen. Experimente in Membranen mit unterschiedlicher Dicke ergaben, dass sich Peptide in einer Membran mit passender Dicke gut bewegen können, wohingegen viel zu dünne und viel zu dicke Membranen die Beweglichkeit der Peptide erheblich beeinträchtigen. Wahrscheinlich sind in diesem Fall große Anpassungen nötig, um die extremen Unterschiede auszugleichen.

Die in dieser Doktorarbeit beschriebenen Studien haben wichtige Einsichten in das Verhalten von Transmembranpeptiden in der Membran geliefert. Darüber hinaus wurde eine neue, verbesserte Methode zur Bestimmung der Orientierung und Dynamik von Transmembranpeptiden entwickelt. Das WALP Peptid ist jetzt ein gut erforschtes Modellopeptid, das in Zukunft für die Entwicklung von neuen Methoden zur Erforschung von Membranproteinen und zur Kalibrierung von bestehenden Techniken wie Molekulardynamiksimulationstechniken benutzt werden kann.

Dankwoord – Danksagung – Acknowledgments

Promoveren doe je niet alleen... zo begint het dankwoord in veel proefschriften en er zit ook wel een stukje waarheid in. Zonder al de mensen om me heen was ik er misschien nooit gekomen. Bijna vier jaar geleden ben ik naar Nederland verhuisd om in Utrecht aan het avontuur promotie te beginnen, tijd vliegt als je het leuk hebt... Alles begann mit einem Hinweis von Herrn Heinz-Jürgen Steinhoff auf die Marie Curie Stipendien der EU für eine Promotion im europäischen Ausland. Herr Steinhoff, ich möchte Ihnen an dieser Stelle noch einmal herzlich danken für den Hinweis, der mir so einzigartige Möglichkeiten für meine Promotionszeit eröffnet hat.

Ik wil graag ten eerste mijn begeleider en promotor Antoinette Killian bedanken. Antoinette, hartelijk dank voor je voortdurende inzet om mij tot een goede onderzoeker te vormen en mijn promotietijd een succes te laten worden; ik heb veel van je geleerd. Ook in moeilijke tijden wist je mij te motiveren en dankzij je altijd constructieve kritiek is dit proefschrift geworden tot wat nu voor je ligt. Ook Ben de Kruijff, oud-hoogleraar in de groep, wil ik graag bedanken. Ben, het was een plezier om met jou over mijn onderzoek te kunnen discussiëren. Het is opmerkelijk hoe snel je soms de zwakke plek in mijn onderzoeksstrategieën wist te ontdekken.

Large parts of the research described in this thesis were performed in collaborations with research groups throughout Europe and elsewhere. First, I would like to thank Alain Milon for being my secondary supervisor and for the successful long-range collaboration aiming at determination of the 'real' tilt angle of the WALP peptides. Valerie and Olivier, many thanks for performing the many NMR experiments and explaining these advanced NMR techniques to me. Jerzy, you did a gorgeous job on analyzing the NMR results, your lesson on how to calculate the error of a fit has been very useful. Many thanks to all the members of the lab in Toulouse for the nice time that I spent in your lab. Louic, hartelijk dank dat ik tijdens mijn eerste lange verblijf in Toulouse in jouw appartementje mocht logeren. In this context, I also would like to thank all the members of the Marie Curie network for the many inspiring meetings during the last years. Especially Mari, Renske and Louic, we had a great time at the Summer school in Rovinj in 2006.

Furthermore, I would like to thank Manuel Prieto for giving me the opportunity to perform the time-resolved FRET measurements in his lab. Manuel, you always took the time to explain the difficult bits of fluorescence spectroscopy. In addition, I would like to thank the members of his lab at that time, especially Rodrigo for helping me with the preparation of the samples and the interpretation of the results, and Alexander for help with these sophisticated fluorescence measurements. Next, I would like to thank Robert Brasseur and Annick Thomas for introducing me to the world of molecular modeling. Then, I want to thank Bert Poolman and his group for the fruitful collaboration on the diffusion of transmembrane peptides. Siva, Geert and Viktor, many thanks for your help with these sometimes tricky FCS experiments. Armagan, thank you for teaching me how to make GUVs using ITO coated plates. En, last but not least, wil ik graag Marcus Hemminga en Rob Koehorst bedanken voor de leuke samenwerking in het BADAN project. Rob, heel erg bedankt voor je tomeloze inzet voor ons project, je enthousiasme is zondermeer besmettelijk.

Next, I would like to thank Thomas and Suat for giving me a good start into my projects by teaching me how to handle lipids and the model peptides, and how to perform ^2H NMR experiments. Dirk (from Medicinal Chemistry), Rutger, Ruud (from Membrane Enzymology), Anna (from Roger Koeppe's lab), Lucie en Jacques, many thanks for (the help with) the not always straightforward synthesis of the many different peptides. Dirk, bedankt voor het mij leren hoe peptiden gelabeld worden en voor het nauwkeurig lezen van ons gezamenlijke publicaties om ook de kleine, verstopte fouten eruit te halen.

Ook de stafleden van Biochemie van Membranen groep mogen niet missen in deze lijst: Irene v. D., hartelijk dank voor je ondersteuning in bureaucratische aangelegenheden en dat wij ook voor stiften, nietjes en andere benodigdheden bij je langs konden komen. Het lab draait en dat is vooral te danken aan de analisten: Martijn, Mandy en Marlies, bedankt voor jullie hulp en het een en ander scheikundig kneepje. Wat er ook mis was met de apparaten, je kon er altijd op rekenen dat Dick het weer gaande kreeg. Dick, bedankt voor het maken van onderdelen voor mijn experimenten in Groningen, geniet van je welverdiende pension.

Verder mogen ook mijn collega AiO's van de toenmalige kamer Zuid 601 niet ongenoemd blijven: Erica, Tania, Jacob, Vincent, Nick en in het begin nog Edgar, het is aan jullie te danken dat ik het dankwoord nu (deels) in jullie moedertaal kan schrijven. Zodra jullie in het begin doorhadden dat ik best wat Nederlands begreep, weigerden jullie verder in het Engels met mij te communiceren en dat was goed zo. Mede AiO's Tania en Erica, we zijn bijna tegelijk begonnen met het promotieonderzoek. Het was erg leuk om met jullie de grote en kleine successen en natuurlijk ook frustraties betreffende het onderzoek te kunnen delen, hartelijk dank dat jullie mijn paranimfen wilden zijn. Erica, roze is jouw kleur maar een roze rokje heb je niet in je bezit, toch? Tania, het is wel aan jou te danken dat de planten nog groen en de guppy's nog steeds in leven zijn (of de ongetelde nakomelingen ervan). Daarnaast herinner ik me nog aan een schitterende bruiloft; wat een leuk gezicht, Tania en Jochem in een paardenkoets. Jammer genoeg heb ik het feestje 's avonds moeten missen. En dan Jacob, met vragen van wat voor aard dan ook kon ik altijd bij jouw terecht en, verbazend genoeg, wist jij meestal ook het antwoord nog (of waar het te vinden was). Ik ben blij dat je na een lange zoektocht Karin hebt ontmoet. Vincent, je hebt een waardevolle bijdrage aan mijn culturele integratie geleverd, je liefde voor Bingo.fm en je fotomuur met de meest diverse, vooraanstaande Nederlandse figuren zullen me nog lang bijblijven.

In de afgelopen jaren heb ik met nog meer mensen mijn kamer mogen delen: Robert, Diana, en later Tami, bedankt voor de altijd goede sfeer. Diana, es war wunderbar zwischendurch ab und an mal Deutsch sprechen zu können, ook al antwoordde jij meestal toch in het Nederlands. Nicht den Gummibaum vergessen zu gießen! En Robert, je doet me denken aan een altijd opgeruimd bureau, waarlijk het tegenovergestelde van de bergen van papier (en voedsel en nog andere dingen waarvan we liever niets willen weten...) op het bureau van Vincent. Dan op de kamer ernaast Yvonne, altijd heb je een glimlachje voor iedereen, dat herinner ik me nog van mijn allereerste bezoek aan Utrecht. And, last but not least, the French fraction Lucie and Jacques. Lucie, congratulations with your little son and all the best for your future! Jacques, you really have your own fashion style, keep it! Also I would like to thank the other (former) PhD students Robin, Pieter and Cedric, Postdoc's Inge, Maarten, Irene H. and Chris, and staff members Eefjan and Toon for any help and advice and the good atmosphere in the group during these years in Utrecht. Zeker ben ik nog iemand vergeten te noemen, ook jullie bedankt.

Na nu bijna vier jaar voel ik me best wel thuis in Nederland. En toch, ondanks Vincents pogingen blijf ik Nederlandse kroketten nog steeds niet lekker vinden. Maar Nederland heeft culinair meer te bieden dan kroketten, en dat mocht ik samen met mijn collega's tijdens vele gezellige uitstapjes naar diverse restaurants in Utrecht beproeven. Niet te vergeten de ongetelde, meestal spontaan georganiseerde gezellige kookavonden samen met Tania, Erica, Jacob, Silvia en Monika toen ik nog aan de Lombokstraat woonde. Achteraf gezien was het een verschrikkelijk studentenhuus, maar de tientallen Marokkaanse en Turkse groente- en fruitwinkels in de buurt waren wel zo handig. Het was een belevenis om met zoveel verschillende nationaliteiten onder een dak te wonen: Scott from Down Under, Adriano the Italian macho and Monika from Poland, it was a great time.

Dann möchte ich mich noch bei meinen Freunden bedanken fürs Dasein und Zuhören. Besonders bei Matthias, Danke fürs immer wieder anrufen und ermuntern! Und bei Silvia, Dein unerschütterlicher Optimismus ist immer wieder eine Wohltat. Jetzt habe ich endlich wieder Zeit, Euch alle mal wieder zu besuchen.

Zu guter Letzt möchte ich mich bei meiner Familie bedanken. Mama, Du hast immer an mich geglaubt und alle meine ambitionierten Vorhaben im In- und Ausland unterstützt. Papa, Du hast mich schon früh gefordert. Nicht zu vergessen meine beiden Brüder Ingo und Uwe, die meine zahllosen Umzüge immer tatkräftig unterstützt haben und sich jetzt anscheinend immer noch nicht daran gewöhnen können, dass ich doch in Holland bleibe. Auch möchte ich an dieser Stelle noch mal meiner Tante Maria und meinem Patenonkel Friedrich danken, Ihr habt vor nun schon einigen Jahren meine Zukunft entscheidend beeinflusst.

Und natürlich darf auch mein Freund Tim in dieser Liste nicht fehlen. Lieber Tim, Tausend Dank für Deine Liebe und die bedingungslose Unterstützung während der letzten Jahre. Gerade mal ein paar Wochen nach unserem Kennenlernen hatte ich mir ziemlich unglücklich den linken Fuß gebrochen und Du hast mich wundervoll gepflegt und mich unterstützt, wo Du nur konntest. Genauso wie auch in den letzten Monaten, wo ich manchmal noch bis spät mit der Doktorarbeit beschäftigt war.

Andrea

List of Publications

Holt A, Ramadurai S, Krasnikov VV, Rijkers DTS, Poolman B, and Killian JA. Influence of hydrophobic mismatch and peptide composition on the diffusion of transmembrane model peptides. Manuscript in preparation.

Holt A and Killian JA (2009) Orientation and dynamics of transmembrane peptides: the power of simple models. *Eur Biophys J Biophys Lett*, submitted.

Holt A, Rougier L, Réat V, Saurel O, Czaplicki J, Jolibois F, Killian JA, and Milon A (2009) Order parameters of a transmembrane helix in a fluid bilayer: case study of a WALP peptide. *J Am Chem Soc*, submitted.

Ramadurai S, **Holt A**, Krasnikov VV, van den Bogaart G, Killian JA, and Poolman B (2009) Lateral diffusion of membrane proteins. *J Am Chem Soc*, under revision.

Holt A, Koehorst RBM, Meijneke-Rutters T, Gelb MH, Rijkers DTS, Hemminga MA, and Killian JA (2009) Tilt and rotation angles of a transmembrane model peptide as studied by fluorescence spectroscopy. *Biophys J*, accepted.

Scarpelli F, Drescher M, Meijneke-Rutters T, **Holt A**, Rijkers DTS, Killian JA, and Huber M (2009) Aggregation of transmembrane peptides studied by spin-label EPR. *J Phys Chem B*, in press.

Holt A, de Almeida RFM, Nyholm TKM, Loura LMS, Daily AE, Staffhorst RWHM, Rijkers DTS, Koeppel II RE, Prieto M, and Killian JA (2008) Is there a preferential interaction between cholesterol and tryptophan residues in membrane proteins? *Biochemistry*, 47:2638-2649.

Gagnon DG, **Holt A**, Bourgeois F, Wallendorff B, Coady MJ, and Lapointe JY (2005) Membrane topology of loop 13–14 of the Na⁺/glucose cotransporter (SGLT1): a SCAM and fluorescent labelling study. *Biochim Biophys Acta*, 1712:173-184.

Curriculum Vitae

Andrea Holt was born on 4th August 1977 in Lingen/Ems (Germany), she has two younger brothers. In June 1997 she obtained the Abitur (general certificate for entrance at universities) at the Gymnasium Carolinum in Osnabrück (Germany). Thereafter, she did an internship at OCO-Design in Münster (Germany), a company for industrial design, which in January 1998 was followed by a professional education as a model maker with specialization in demonstration models.

In October 2000 she moved back to Osnabrück and started her academic studies in the bachelor program *Physics and Computer Science* at the University of Osnabrück (Germany). She prepared her bachelor thesis under supervision of Prof. Heinz-Jürgen Steinhoff on distance measurements in membrane proteins using EPR spectroscopy, and graduated with distinction in autumn 2003. Afterwards, she continued in the master program *Physics and Computer Science*. During her studies, she passed in summer 2002 a period of studies abroad at the Central Queensland University in Rockhampton (Australia), and another one in winter/spring 2004 at the Université de Montreal (Quebec, Canada) funded by a scholarship to master students from the DAAD (Deutscher Akademischer Auslandsdienst). In Montreal, she was involved in a research project in the lab of Prof. Jean-Yves Lapointe on the sodium/glucose cotransporter hSGLT1. After return, she prepared her master thesis again under supervision of Prof. Heinz-Jürgen Steinhoff on the simulation of EPR spectra using exact quantum mechanical theory, and she graduated with distinction in spring 2005.

In September 2005 she moved to Utrecht (The Netherlands) and started her Ph.D. research at Utrecht University under supervision of Prof. J. Antoinette Killian in the field of Biomembranes. Her research was funded by a Marie Curie EST fellowship for 36 months granted from the European Community, which enabled her to collaborate with research groups throughout Europe. During her Ph.D. research training she spent time in the labs of Prof. Alain Milon in Toulouse (France), Prof. Bert Poolman in Groningen (The Netherlands), Prof. Marcus Hemminga in Wageningen (The Netherlands), Prof. Robert Brasseur in Gembloux (Belgium), and Prof. Manuel Prieto in Lisbon (Portugal), which allowed her to develop a broad knowledge in biophysics and membrane research.

In February 2009, she migrated to the field of medical physics and works now as postdoctoral researcher at The Netherlands Cancer Institute (NKI-AvL) in Amsterdam (The Netherlands) on improving radiotherapy methods for cancer treatment.

Abbreviations

Alexa 488	Alexa Fluor 488 C5-maleimide; a fluorescent label
ATR-FTIR	Attenuated Total Reflection – Fourier Transform Infrared
BADAN	6-bromoacetyl-2-dimethylaminonaphthalene; a fluorescent label
CD	Circular Dichroism
CP	Cross-Polarization
CSA	Chemical Shift Anisotropy
CW	Continuous Wave
DHE	Dehydroergosterol
DMPC	Dimyristoylphosphatidylcholine, a saturated phospholipid
DOPC	Dioleoylphosphatidylcholine, an unsaturated phospholipid
EPR	Electron Paramagnetic Resonance
FCS	Fluorescence Correlation Spectroscopy
FRET	Förster Resonance Energy Transfer
GALA	Geometric Analysis of Labeled Alanines
GUV	Giant Unilamellar Vesicle
HPLC	High-Pressure Liquid Chromatography
IEADANS	5-(((2-iodoacetyl)amino)ethyl)amino)naphthalene-1-sulfonic acid; a fluorescent label
ITO	indium-Tin Oxide
KALP	Lysine-flanked model peptide including a stretch of leucines and alanines
KLP	Lysine-flanked model peptide including a stretch of only leucines
LUV	Large Unilamellar Vesicle
MACADAM	Multiple Anisotropic Constraints And Dynamic Analysis of Membrane peptides
MALDI-TOF	Matrix-Assisted Laser Desorption/Ionization – Time Of Flight
MAS	Magic Angle Spinning
MD	Molecular Dynamics
NMR	Nuclear Magnetic Resonance
PC	Phosphatidylcholine
PISEMA	Polarization Inversion with Spin Exchange at Magic Angle
REDOR	Rotational-Echo Double Resonance
SEM	Standard Error of the Mean
SSD	Sum of Squared Deviations
SUV	Small Unilamellar Vesicle
TFA	Trifluoroacetic acid
TFE	Trifluoroethanol
TOAC	2,2,6,6-tetramethyl-piperidine-1-oxyl-4-amino-4-carboxyl; a spin labeled amino acid analog
TPPM	Two-Pulse Phase-Modulation
WALP	Tryptophan-flanked model peptide including a stretch of leucines and alanines
WLP	Tryptophan-flanked model peptide including a stretch of only leucines

